# THE DEVELOPMENT OF CONVECTIVE INSTABILITY DURING SESAME, 1979

by

Frank Parker Colby, Jr.

B.S., University of Michigan
(1976)

M.S., Massachusetts Institute of Technology
(1979)

Submitted to the Department of
Meteorology and Physical Oceanography
in Partial Fulfillment of the
Requirements of the Degree of

DOCTORATE OF PHILOSOPHY

at the

MASSACHUSETTS INSTITUTE OF TECHNOLOGY

February, 1983



Signature of Author _____
Department of Meteorology and Physical
Oceanography, 6 January 1983

Certified by _____
Frederick Sanders, Thesis Supervisor

Accepted by _____
Ronald G. Prinn, Chairman, Departmental
Committee on Graduate Students

# DEVELOPMENT OF CONVECTIVE INSTABILITY DURING SESAME, 1979

by

FRANK PARKER COLBY, JR.

Submitted to the Department of
Meteorology and Physical Oceanography
on 25 January 1979 in partial fulfillment of the
requirements for the Degree of Doctorate in Philosophy

## ABSTRACT

Convection in the Central United States is assumed to require the presence of convective instability and a triggering mechanism to release the instability. Often, a stable layer caps the PBL, preventing or delaying the release of convective instability. The development of both convective instability and convective inhibition (from the stable layer) is studied with data from three cases from the SESAME field project of 1979. The cases are: 19-20 April, 9-10 May, 6-7 June. The data are analyzed and both convective instability and inhibition are quantified.

A one-dimensional thermodynamic model which includes radiation, a surface energy balance, and routines to predict soil and boundary layer characteristics is used as a tool to understand the important physical factors involved in the development of convective instability and inhibition.

The results show that some convective instability was present before dawn in all three cases. The boundary layer heating during the day added to the initial instability. Soil moisture, clouds, and changes in atmospheric structure above the PBL were all important factors controlling the PBL evolution.

The modelled convective instability grew during the day as a result of the boundary layer heating. Increased soil moisture sometimes exerted a positive influence on the growth of instability, but in other cases limited the growth by keeping the PBL from heating and deepening. Clouds generally reduced the convective instability growth, but in the June case, clouds had the opposite effect. The influence of changes above the PBL was stronger on the reduction of convective inhibition than on the growth of convective instability. For these cases, the influence on the growth of convective instability from changes above the PBL was stronger than the presence of clouds or the increase of soil moisture, but all of these factors were able to modify the development of convective instability and inhibition.

The results of the modelling and the observations show that the convection occurred where and when the inhibition was reduced to low values. The convection began when the available forcing was sufficient to overcome the remaining inhibition. Therefore, the forecasting of convective outbreaks requires the ability to measure and predict the convective inhibition within the larger region of convective instability.

Thesis Supervisor: Dr. Frederick Sanders

Title: Professor of Meteorology

# TABLE OF CONTENTS

# LIST OF FIGURES

# List of Tables

# INTRODUCTION

The term "convection" is used in meteorology to distinguish overturning motion in the atmosphere from laminar flows. As such, it includes a very broad class of atmospheric motion , which contains both buoyant and non-buoyant motion. For the purpose of this thesis, convection will be much more narrowly defined and will be used to denote only buoyant overturning in the atmosphere. The intent is to include only convection associated with severe weather in the central section of the United States. Although most severe weather is due to buoyant overturning, the association is not strict. Carbone (1982) reported on a case of nearly neutral stratification which produced heavy rain and tornadoes.

Convection in the central U.S. in the spring is assumed to require the following: unstable thermal vertical stratification and an initiating (trigger) mechanism. The expected sequence is approximately as follows: Through large scale or mesoscale motion and/or heating and cooling mechanisms, a section of the atmosphere becomes convectively unstable. This means that air parcels from the planetary boundary layer (PBL), if lifted sufficiently, would become positively buoyant, and would continue to rise in the atmosphere. This requires abundant moisture, as the latent heat of condensation released in the parcel is needed to

maintain the parcel's buoyancy. (The atmospheric lapse rate is almost always more stable than the dry adiabatic lapse rate over any appreciable layer.) There exists a stable layer above the PBL which separates the potentially buoyant air from the rest of the atmosphere. In the central U.S. this stable layer is very often characterized by a temperature inversion. Therefore, for convection to begin, a combination of heating and external dynamic forcing (trigger mechanisms) must act to lift the potentially buoyant air through the stable layer where it will actually be buoyant. In a sense, this expected sequence of events is incorrect. Actually, no parcels are lifted "through" the stable layer. What really happens is that a part of the PBL is destabilized by heating and/or adiabatic cooling of the inversion. This destabilization occurs on a small spatial scale, much smaller than the scale of the observational network. Hence, the appearance of the convection "breaking through" the stable layer is due to differences in scales.

Initiation of this type of convection has been studied for many years with varying emphases. Early work generally focussed on the problems of forecasting this type of weather. Convection is small scale in both space and time, which presents very real forecasting and observational difficulties. Work by Fawbush et al. (1951) sought to characterize large scale patterns which were favorable to convective outbreaks.

Their aids included vertical wind shear, low level temperature and moisture advection, and mid-level vorticity patterns. Darkow et al. (1958) found a convincing statistical correlation between a particular surface temperature pattern and the occurrence of tornadoes. They showed that severe weather often occurred to the east and near the axis of a tongue-shaped warm region. Other work sought to look at vertical stratification, with the development of various indices to quantify instability or potential instability in the atmosphere. Thus, the Showalter Index (Showalter, 1953), the Lifted Index (Galway, 1956), and the Total Totals Index (Miller, 1972) were spawned as forecast aides. This type of analysis continues to the present, with such work as Carlson et al. (1980) and Moore (unpublished) in which new ways of quantifying vertical stratification have been developed which try to take into account more details in the structure. For instance, the Showalter Index simply compares the temperature of air at 850 mb when lifted adiabatically to 500 mb, with the ambient temperature at 500 mb. Carlson et al. (1980) developed an index called Lid Strength Index (LSI) which includes in addition to the Showalter type of buoyancy, a measure of the strength of the inversion which caps the PBL. This index would show a difference between places which have equal amounts of parcel buoyancy but have differing amounts of resistance to initiating the overturning motion.

Much work has focussed on determining what triggering mechanisms are operating in various situations. The result has been the identification of several mechanisms, including ageostrophic frontogenetical convergence, gravity wave triggering, sea breeze convergence, and outflow boundary convergence. As described by Koch and McCarthy (1982), the last of three groups of convection on 8 June 1974 seemed to be forced by frontogenetical motion along a cold front. In this instance the convergence and deformation along the pre-existing front provided the vertical motion to set off the convection.

Work by Uccellini (1975) and later by Miller and Sanders (1980) implicated gravity wave forcing for severe thunderstorms. Uccellini studied data from 18 May 1971 while Miller and Sanders looked at the so-called super-outbreak of tornadoes on 3 April 1974. Both identified wave packets which seemed to have coherent surface signatures through a large section of the east and central United States. They correlated these packets with tornado occurrence and radar echo activity, and showed that the packets seemed to initiate or enhance convective activity as they moved across the country. Koch and McCarthy (1982) also implicated gravity waves in the formation of the second convective outbreak in their study of the 8 June 1974 case. In all of these examples the gravity wave packets triggered convergence in the PBL

which provided the lifting required to trigger the convection.

Sea breeze circulations have been shown to be important in triggering and organizing convection, particularly in Florida. Cooper et al. (1982) showed clearly that peninsula scale convergence due to the daily sea breeze triggered late morning convection. Coastlines are not the only places where sea breeze type circulations can be important. Sun and Ogura (1979) modelled a sea breeze type circulation using data from Oklahoma on 8 June 1966. A very strong temperature gradient formed in the vicinity of Norman, Oklahoma, and a convergence line emerged along this gradient in much the same way as a sea breeze. This "inland sea breeze" was a factor in the triggering of the convection in this case.

Outflow from other storms can act to trigger more convection, through lifting in the manner of a density current bodily pushing the lighter air up. Maddox et al. (1980) examined several cases in which tornadic thunderstorms intensified when they were in the vicinity of thermal boundaries. They theorized that convergence and cyclonic vorticity were enhanced along the boundaries, although they could not show this clearly. Matthews (1981) discussed a case where the outflow from a large convective storm triggered an arc cloud formation in which small convective cells were embedded. Cooper et al. (1982), in their examination of

Florida convection, showed that outflow contributed to convergence on a storm scale which was responsible for new cell growth. A particular case from 1973 in Florida was analyzed by Holle and Maier (1980). They showed that a tornado formed along an intersection of outflows from old cells, with convergence on the order of 10**-3 1/s.

In comparison to the work on dynamic forcing, the creation of the convective instability has received much less attention in the published literature. The mechanisms generally quoted or referred to are differential advection (warm low level, cold upper level) and boundary layer heating (BLH). Of the two, more work on advection has been done. Modahl (1979) studied National Hail Research Experiment data from 1972 - 1974, for the occurrence of hail. He showed that two factors were most important: increased southerly winds to increase moisture and heat in the PBL, and easterly winds to sustain the storms (and perhaps to give upslope triggering). Carlson et al. (1980) attempted to correlate convective outbreaks with the strength of the capping inversion and the amount of potential instability (as discussed with the LSI above). For the case of 10 April 1979, they found good correlation between their fields of LSI and the convection. Davis and Scoggins (1981) used data from Atmospheric Variability Experiment IV (AVE IV, 24-25 April 1975) to examine the creation of convective instability, wind shear,

and vertical motion. They considered all sources of convective instability except BLH. Interestingly, they discovered that all of the other sources (eg. large scale motions) contributed less than the residual, especially in the surface - 850 mb layer. This implies that BLH, part of the residual, could have been the dominant term.

Some studies of convection in mountains suggested that low level advection of moisture was important (as above in Modahl, 1979), but some included BLH as a factor too. Caracena et al. (1979) discussed the Big Thompson Storm in which low level moisture was crucial to the storms sustenance, and upslope winds provided the lifting. Raymond and Wilkening (1980) examined dry convection over an isolated mountain, and found that the mountain was a large source of heat which helped drive an upslope circulation. Although their case was dry, they speculated that an adequate moisture supply would certainly have led to thunderstorm formation over the mountain. Cotton et al. (1982) studied a quasi-steady thunderstorm which formed in the mountains in Colorado on 19 July 1977. They concluded that a combination of BLH, low level moisture advection, and upslope winds initiated the convection.

These studies of convection in mountains have seemed to be more complete than those over the plains, although the BLH

contribution was still not clearly delineated. A study by Ogura et al. (1982) analyzed a convective system on 9-10 May 1979 in the central United States. Their results suggested that BLH, inland sea breeze circulation and perhaps symmetric instability were responsible for the convection, a combination of thermodynamic and dynamic factors.

The above discussion shows that initiation of convection by dynamic forcing occurs in many ways, sometimes many ways in the same place, within a few hours (Koch and McCarthy, 1982). It is apparent that the thermodynamic contribution to the convection sequence has not been well quantified. One can speculate as to the reasons for the lack of work in this area: complex interactions between radiation, surface characteristics, and boundary layer characteristics, plus large spatial variation in the physical constants (such as soil composition, albedo, vegetation, etc.). The problem is certainly difficult from the theoretical standpoint. Additionally, some of the factors are not well observed, such as soil temperature and moisture.

The intent of this thesis is to quantify the relationship between BLH and the development of convective instability. The approach used is a combined observational and modelling study of convective outbreaks occurring in three case studies from the Severe Environmental Storms and Mesoscale Experiment

(SESAME). The cases of 19-20 April, 9-10 May, and 6 June 1979 are examined to determine the role of BLH in the creation of convective instability. For this purpose, convective instability will be measured by the PBL lifted index (PLI). The PBL air is taken as a parcel with the mean potential temperature and mixing ratio of the PBL. The parcel is lifted adiabatically to 500 mb, and its temperature is compared with the ambient 500 mb temperature. When lifted, unstable air will be warmer than the ambient atmosphere. The PLI is positive for instability unlike the operational Lifted Index (Galway, 1956).

The PLI is not the same thing as the surface lifted index (SLI, from Sanders, personal communication) in which parcels are defined by the surface observations. The PLI measures a mean PBL convective instability, above any superadiabatic layers which may be present. For a clear, well-mixed PBL, the PLI can be as much as 4 degrees C lower than the SLI (Fort Sill, Oklahoma sounding at 1800 GMT, 6 June 1979, Fig. 5.20), although generally the difference is closer to 2 degrees C. This difference raises an interesting question: which parcel really measures the cloud-scale convective instability which is responsible for the initiation of convection? Cloud modellers generally need very large perturbations to initiate convection, even with unstable soundings. On the other hand, it is difficult to envision that parcels can rise from the

surface layer through the entire turbulent PBL without dilution. Observations at the top of the clear PBL do not show such large perturbations. I suspect that the answer is that parcels with characteristics in between the two extremes (mean PBL and surface layer), are more representative of the cloud-scale convective instability, being the result of diluted surface layer parcels. Without attempting to settle this question, I shall use the mean PBL parcel definition to measure convective instability in this thesis.

The role of the stable layer is studied as well to determine how much inhibition exists immediately prior to the convection. The inhibition is quantified by integrating the "negative area" on a pseudoadiabatic diagram. This negative area is the region between the parcel's path on the chart, and the ambient sounding, while the parcel is negatively buoyant. The energy equal to this area is found by calculating the work done by the negative buoyancy force per unit mass, = $g \int \frac{T(air) - T(parcel)}{T} dz$ . This can be regarded as an energy well which must be surpassed for the parcel to realize its convective instability. If a PBL parcel were to rise through this negative area, it must have sufficient kinetic energy per unit mass, or an updraft velocity equal to (2*Negative area)**1/2.

The model is used to identify and quantify the role

various physical paramenters have on the BLH. The model is one dimensional, and is designed to model only effects of solar radiation on BLH. Incident radiation on the surface is divided into soil heat, sensible heat and latent heat fluxes. The effect of soil moisture plays a prominent role in this part. The fluxes into the PBL drive turbulent entrainment at the top of the (assumed) well-mixed PBL , and the temperature height and moisture content of the PBL are computed. Above the PBL, atmospheric changes are inferred from observed sounding data and imposed on the model.

The term PBL will be used extensively throughout the rest of this thesis. It is not a well-defined term for the atmosphere. As used in the following, it will refer to the part of the atmosphere which obtains most of its characteristics from its proximity to the ground. Physically, this will mean that part of the atmosphere which is heated during the day by the fluxes from the ground surface. On an adiabatic chart, the well-mixed PBL will be identifiable by a dry adiabatic temperature lapse rate and a nearly constant mixing ratio (q) in the air nearest the ground.

In each of the three cases studied, the conditions prior to convection are analysed, and the location of the outbreak pinpointed. The model is then run using initial data from nearby soundings and varying the important parameters.

Various combinations of physical factors are applied and the effects on convective instability are determined. The physical factors which are varied are ground wetness, presence of clouds, and changes in the atmosphere above the PBL. The factors are tried separately to determine individual importance. Then combinations are tried, with the last runs including all of the relevant factors. If one of these last runs can reproduce the observed surface temperature and PBL moisture content, it will be regarded as a "correct" run in the sense that the included effects are modeled correctly. The model is described in detail in chapter 2. The three case studies follow in chapters 3, 4, and 5. The last chapter, chapter 6, is a summary of the findings.

# THE MODEL

## 2.1: Introduction

One of the tools used in this research is a one-dimensional boundary layer model. The model is primarily used to determine and illustrate the role of boundary layer heating (BLH) in the time evolution of soundings. It is run with and without various physical effects to quantify their importance in generating convective instability and/or removing convective inhibition. The model is also used to determine the vertical structure of the atmosphere at times and locations which did not have real sounding data (i.e. between stations and/or between sounding times). Although SESAME case study days were characterized by 3 hourly soundings on a grid spacing no larger than the normal synoptic grid and often significantly smaller, the convection often broke out "between" soundings in some way (time or space or both). Because of this, it was not possible to make statements about the vertical structure of the atmosphere without some kind of supplementary information.

The convection primarily studied in this thesis occurred after much of the BLH took place. This means that the PBL itself had a simple structure, and the fluxes at the top and

bottom of the PBL could be represented by known structure functions. Although strong horizontal thermal gradients were present by the outbreak time, the initial thermal gradients throughout most of the SESAME area, tended to be small, so that the initial conditions at any point could be specified with some certainty. The model then used these initial conditions and predicted the thermal changes due to BLH for the rest of the model run.

## 2.2: Atmospheric Structure

The PBL is assumed to be well-mixed in heat and moisture. A surface layer of five mb depth is assumed to exist. This is an ad hoc representation of the real structure, but the surface layer is not of crucial importance in affecting the stability of the atmosphere. The PBL above the surface layer is characterized by its potential temperature (well-mixed in heat = constant $\theta$ ), its moisture (well-mixed in moisture = constant q) and its height in meters. The PBL is capped by an inversion which has a strength ( $\Delta\theta$ ) and a depth. The initial inversion depth is taken from the input sounding. The top of the inversion is held constant until the PBL grows enough to absorb all of the inversion layer. The bottom of the inversion rises as the PBL grows by entraining air from the inversion layer into the PBL. The structure above the PBL is taken directly from the data in the original sounding. The

assumed structure is illustrated in Fig. 2.1.

## 2.3: Conceptual Model Run

Detailed later are the various parameterizations used to effect changes in the initial atmospheric structure. They are outlined here. Table 2.1 contains a schedule of the operations in the order actually used by the computer.

Radiative transfer is computed first. The incoming radiation at the top of the atmosphere is a function of time of day and geographic location. Radiation is absorbed by water vapor, $CO_2$, and liquid water (clouds). Some is scattered, some is reflected. The atmosphere and the ground emit infrared radiation, and the net radiation is calculated for each layer in the atmosphere and the ground surface. The net absorbed radiation in the ground is partitioned into three parts: 1) soil heat flux, 2) sensible heat flux to the atmosphere, and 3) latent heat flux to the atmosphere. The soil temperature and moisture are changed to reflect the new surface energy balance. The PBL height and inversion strength change due to surface temperature changes and virtual sensible heat flux. The air temperature in the PBL is determined from the PBL characteristics, and the moisture (q) of the PBL is determined by a budget calculation for the PBL. The last changes made to the sounding are imposed changes above the

PBL. These can be derived from known data (such as three hourly SESAME soundings) or predicted on the basis of current analysis. The model can be stopped and restarted to allow different imposed rates of change or changes in cloud cover. When a whole stable layer is absorbed by the PBL, a new stable layer is incorporated from the next higher level in the sounding.

## 2.4: Radiation

The radiation parameterization is taken from Katayama (1972) and is a routine originally designed for use in the UCLA GCM. The model is described in brief here, and more details are available in Appendix 7.1. The incident radiation and IR emission are calculated separately. The net flux divergence gives a mean temperature change for each model layer. The model incorporates an exponential fit to the data for specific humidity to allow simple integration of water content. $CO_2$ is included in a fixed form based on experimental data of Yamamoto (1952), and its contribution is then a constant.

### A. Incident Radiation

The influx of radiation is computed by starting with the solar constant and modifying it for albedo at the top of the

atmosphere. Scattered and absorbable radiation are computed separately, the fraction being assumed constant (35% available for absorption, 65% scattered to the ground). The scattered part of the incident radiation is corrected for multiple reflection between the atmosphere and the ground.

$$GLW_s = .651\ S_o \cdot ZT \cdot \left(\frac{1-\alpha_s}{1-\alpha_s \cdot \alpha_g}\right) \qquad (2.1)$$

where

$S_o$ = solar constant = f(day of year) -- units of mcal/sqcm min
$ZT$ = zenith angle for time of day and location (radians)
$\alpha_s$ = scattering albedo for atmosphere--if clouds are present they determine the scattering albedo
$\alpha_g$ = albedo of ground surface = f(hour angle)

If a cloud layer is present, its presence is felt by both scattered and absorbable components. If the cloud is thick enough, and covers enough sky, incident radiation can be shut off. The model allows for variable amounts of cloud in each atmospheric layer expressed as a percentage. Only one layer of cloud is allowed, but it may be composed of one or several atmospheric layers of various percentage coverage. The model does not include any feedback mechanism to the cloud amounts, hence these must be manipulated manually whenever the model run is stoppped and restarted. Atmospheric absorption by water vapor is calculated, using the sounding data for specific humidity. Albedo at the surface is parameterized by a method from Wetzel (1978) which allows for the change in

albedo depending on sun angle. The radiation which finally is absorbed in the soil becomes one component of the surface energy balance. The absorbed part of the incident radiation at the ground is

$$GLW_a = .349 \cdot S_o \cdot ZT - \sum_i ABS(i) \qquad (2.2)$$

where ABS(i) = absorption in atmospheric layer i

Total absorption at the ground is then

$$GAB = (1-\alpha_g) \cdot (GLW_s + GLW_a) \qquad (2.3)$$

B. IR Emission

The equation of radiative transfer is solved subject to the boundary conditions that downward infra-red (IR) flux at the top of the atmosphere is zero, and the upward IR flux at the earth's surface is the black body radiation at the surface temperature. Weighted transmission functions are used, corrected for the pressure dependence of absorption by defining an effective amount of an absorber. The total transmission function is assumed to be the product of the individual ones for $CO_2$ and $H_2O$. The following expressions for upward and downward fluxes at a particular height z are obtained (see Appendix 7.1 for details). Downward flux is

$$IR_d = \pi B_z - \pi B_c \tilde{\tau}(u_\infty^* - u_z^*, T_c) - (\pi B_\infty - \pi B_c)\tau(u_\infty^* - u_z^*, \overline{T}) + \int_{\pi B_z}^{\pi B_\infty} \tau(u^* - u_z^*, \overline{T})\, d(\pi B) \qquad (2.4)$$

where $\pi B_i = \sigma T_i^4$

$\sigma$ = Stefan-Boltzmann constant
$\tau$ = mean total transmission function for effective absorber $u^*$ at temperature T
$T_c$ = critical temperature which divides the region of weak temperature dependence of $\tau$ to that of strong dependence of $\tau$.

The weak region is 210 to 320 K for water vapor. So letting $T_c$ = 220 K, the weak dependence region need only have a mean temperature specified = $\overline{T}$. Similarly, the upward flux is

$$IR_u = \pi B_z + \int_{\pi B_z}^{\pi B_g} \tau(u_z^* - u^*, \overline{T})\, d(\pi B) \qquad (2.5)$$

and the net upward flux

$$IR_z = IR_u - IR_d \qquad (2.6)$$

The only difficulty is determining the proper transmission function near the particular level, where tau varies exponentially. The model uses an interpolation factor which is an empirical function of pressure, mixing ratio and layer thickness. This allows proper calculation of tau without a fine vertical mesh. The mean transmission functions are defined by empirical formulae at $T_c$ = 220 K and $\overline{T}$ = 260 K. Temperature dependence of tau for $CO_2$ is neglected, so a mean tau for $CO_2$ is used based on pressure and amount of $CO_2$. The

distribution of $CO_2$ at each pressure level is a constant. The empirical functions for both absorbers were fit to data from Yamamoto (1952). For thick clouds, the top and bottom are assumed to radiate black body radiation at their respective temperatures, with no net flux inside.

## 2.5: Radiation Data Comparison

All of the expressions used for transmission coefficients and atmospheric absorption were derived from empirical data. After the model was assembled, it was run on sounding data to a) allow comparison with radiation measurements, b) allow comparison with other more complex models, and c) allow variation of parameters such as albedo and cloud amount to ensure reasonable behavior.

Data for radiation measurements taken at O'Neill, Nebraska in August and reported in Lettau and Davidson (1957), were available in Wetzel (1978). Fig. 2.2 shows the observations plotted over the radiation calculations from the model. The agreement is quite good, with a slight over forecast near 1200 LST of about eight percent.

Three models were compared with the Katayama radiation routine. Rogers and Walshaw (1966) has been regarded as a classic parameterization for many years, so the IR

calculations were compared with it first. Fig. 2.3 shows the comparison for a sounding taken from Rogers and Walshaw. Notice that the agreement is very close. On Fig. 2.4, three calculations are compared with the model for an equatorial sounding from London (1952). Although differences exist above 8 km, below that level, the present model is nearly in the middle of the scatter of the rest of the calculations. A comparison is also made with a one-dimensional model from Wetzel (1978). Wetzel's parameterization was run on the O'Neill data, and the comparison is shown for net radiation on Fig. 2.2. Again, the agreement is quite satisfactory.

The radiation model's cloud routine was tested for qualitative behavior for thin and thick clouds. The results for the IR cooling only appear on Fig. 2.5. For a very thick cloud, the top of the cloud cools rapidly, while the bottom warms strongly. The cooling occurs because the flux for the top of the cloud only comes from relatively cool layers aloft, while no contribution comes through the thick clouds below. The cloud top radiates strongly to all layers above, so it has a net flux divergence. The opposite is true on the bottom of the cloud, which gives a net warming effect. The clear and partly cloudy cases deviate from the extreme in the expected way, with both the warming and cooling peaks losing intensity. Notice, however, that the sensitivity of the warming peak is much greater than that for the cooling peak. The partly cloud

condition still gives a strong cooling at cloud top, but very little warming below. Presumably, as the cloud barrier is removed, all of the cloud tends to radiate strongly to the layers above. Not shown is the absorption of incident radiation which greatly reduces the extreme values of cooling, giving net cooling at the cloud top of much lower magnitude.

## 2.6: Surface Energy Balance

The surface energy balance at the surface has the form

$$NR = SH + LH + GS \qquad (2.7)$$

where NR is the net radiation incident on the surface, SH is the sensible heat flux upward from the surface, LH is the latent heat flux upward from the surface and GS is the soil heat flux downward into the ground which heats the soil. Fig. 2.1 illustrates the various fluxes and their directions. NR is already known via the radiation routine. The rest are parameterized as follows.

### A. Sensible and Latent Heat Fluxes

The sensible heat flux and latent heat flux (SH, LH) are parameterized using Monin-Obukhov similarity theory for the PBL. The fluxes depend upon the gradients in the surface layer, the depth of the boundary layer, and the incident

radiation . The theory assumes that the structure of temperature and moisture in the PBL have forms which can be described by universal structure functions when scaled equations are used. There are actually two structures involved, since the PBL contains at least two distinct layers: the surface layer and the well-mixed layer. If the functions are required to be matched at their common boundary, the following form results:

$$\frac{\partial \theta}{\partial z} = f_1(h/z_0, h/L) \qquad (2.8)$$

$$\frac{\partial q}{\partial z} = f_2(h/z_0, h/L)$$

where

$z$ = height above the ground
$z_0$ = roughness length
$h$ = the depth of the boundary layer
$L$ = Monin/Obukhov length
$f_1, f_2$ = universal functions

The form of the temperature function is taken from Arya (1975). Details are in Appendix 7.2.

For stable boundary layers, much scatter results when data are compared with theory . However, the present model is used only for unstable, well-mixed conditions. These conditions give quite good agreement between theory and observations (Businger, et al., 1971). Furthermore, the moisture function, $f_2$, is not well defined in the literature, and is usually assumed to be the same as the temperature

structure function. For a well-mixed PBL this is likely a decent assumption, since both $\theta$ and q are nearly constant with height.

B. Soil Heat Flux

The soil heat flux (GS) is parameterized after Bhumralker (1975). Assuming vertical heat flux only, and that the variation of surface soil temperature from an average temperature is sinusoidal, one can solve the heat conduction equation to give eventually an expression for the soil heat flux (see Appendix 7.2 for details). Evaluated at the surface,

$$GS = \left(\frac{\omega c \lambda_k}{2}\right)^{1/2} \left[\frac{1}{\omega}\frac{\partial TG}{\partial t} + TG - TBAR\right] \qquad (2.9)$$

where c = volumetric heat capacity of the soil

TG = ground temperature
TBAR = some suitable average ground temperature
$\lambda_k$ = thermal conductivity of soil
$\omega$ = frequency of oscillation (= $2\pi$ / 1 day)

2.7: Ground Variables

Two parameters are crucial to the calculation of all of the components of radiation: TG and q(ground). These are parameterized by "force-restore" methods from Bhumralker (1975) and Deardorff (1977). Details of the derivations are

in Appendix 7.3. To find TG the heat conduction equation is solved for a layer between 50 cm and 1 cm below ground surface. This gives a prediction equation for TG

$$\frac{\partial TG}{\partial t} = \frac{(NR-SH-LH) - \left(\frac{\omega c \mathbb{K}}{2}\right)^{1/2}\left[TG-TBAR\right]}{c+\left(\frac{c\mathbb{K}}{2\omega}\right)^{1/2}} \qquad (2.10)$$

where $\omega$, c, and $\mathbb{K}$ are as previously defined.

The soil moisture is found by assuming that surface soil moisture responds to three main processes: precipitation, evaporation, and flux from below. The bulk soil moisture (GWB) is assumed to be constant over the period. According to Deardorff (1977) the bulk soil moisture changes over a time scale of a few weeks, so GWB can certainly be assumed constant for a 12 hour period with little loss of accuracy. The surface soil moisture is changed according to:

$$\frac{\partial GW}{\partial t} = \frac{-c_1 LH/\lambda}{\rho_w d_1 WMAX} - c_2\frac{(GW-GWB)}{\tau} \qquad (2.11)$$

where

GWB = % bulk soil saturation (top 50 cm)
GW = % soil saturation
$d_1$ = depth of diurnal cycle (=10 cm)
$\lambda$ = latent heat of evaporation
$\rho_w$ = density of H2O = 1 gm/cc
WMAX = field capacity soil moisture
$\tau$ = period of cycle
$c_1$, $c_2$ are non dimensional constants

Deardorff's values for $c_1$ and $c_2$ were computed from data of Jackson (1973), measurements taken over bare soil near

Phoenix, Arizona in March.

$$c_1 = \begin{cases} 0.5 & GW \geq 75\% \\ 14 - 22.5\,(GW - 0.15) & 15\% < GW < 75\% \\ 14 & GW \leq 15\% \end{cases} \qquad (2.12)$$

$$c_2 = 0.9$$

Notice the middle value of c is a linear interpolation between the two extreme values.

## 2.8: Boundary Layer Variables

The depth of the boundary layer (h) and strength of the inversion ($\Delta\theta$) are predicted according to Zeman and Tennekes (1977). Their method assumes that the PBL depth changes due to turbulent entrainment of air above the inversion into the PBL. No allowance is made for the late afternoon collapse of the PBL, since the convective outbreaks occurred prior to this time. The energy comes from the virtual SH flux at the surface, and the change of depth with time depends upon the strength of the inversion. They use the turbulent kinetic energy budget to develop a simple set of equations to describe this process. The equations which result are:

$$w_*^3 = \frac{g}{T_s} \overline{w\theta_v}_s \, h \qquad (2.13)$$

where

TS = surface temperature (top of surface layer)
h = height of inversion
g = acceleration of gravity
$w_*$ = convective velocity scale

VSH = virtual sensible heat flux at ground

and,

$$w_{bv} = \left(\frac{g\ \gamma}{T_s}\right)^{\frac{1}{2}} \qquad (2.14)$$

where $\gamma$ = temperature gradient above the inversion
$w_{bv}$ = Brunt-Vaisala frequency in the air above the inversion

$$-VSH_h = \frac{VSH\left(c_f - \frac{c_d w_{bv} h}{w_*}\right)}{1 + \frac{c_t w_*^2 T_s}{gh\ \Delta\theta}} \qquad (2.15)$$

where $VSH_h$ = heat flux at the inversion (< 0 to give entrainment from above)
$c_d$, $c_f$, $c_t$ are dimensionless coefficients which are (from Zeman, 1975)

$c_f = 0.50$ $\qquad c_d = 0.024$ $\qquad c_t = 3.55$ $\qquad (2.16)$

$$\frac{\partial h}{\partial t} = \frac{-VSH_h}{\Delta\theta} \qquad (2.17)$$

In the case where $\Delta\theta = 0$, no inversion exists and the atmosphere presents no barrier to inversion rise. In this case, the model assumes a very small value for $\Delta\theta$, since the inversion must rise at a rapid but finite rate due to the turbulent entrainment. Finally,

$$\frac{\partial \Delta\theta}{\partial t} = \gamma \frac{\partial h}{\partial t} - \frac{1}{h}\left(VSH - VSH_h\right) \qquad (2.18)$$

These equations will allow the calculation of the necessary PBL characteristics. See Appendix 7.4 for a discussion of

their derivation.

## 2.9: PBL Temperature and Moisture

The final calculation to be performed is that for PBL values of T( $\Theta$ ) and q. These are found using the simple assumed structure in the PBL, and a budget for $\Theta$ and Q. The pressure level of the top of the inversion is known. The change in the height of the inversion has just been calculated, so the amount of entrainment is known. This entrainment comes from the inversion layer, so the new depth of the inversion layer can be found. Using the new value for $\Delta\theta$, the potential temperature at the top of the inversion, and the lapse rate of potential temperature in the inversion, the potential temperature of the PBL can be calculated. This then gives the new TS value, and the hydrostatic pressure level of the inversion bottom. Since the pressure depth of the surface layer is fixed, the height of the surface layer can be computed hydrostatically. The process is illustrated schematically in Fig. 2.6.

## 2.10: Initialization Procedure

The model requires the initial sounding to have a specific form, to allow the model procedures to operate reasonably. In particular, a thin surface layer and a

well-mixed PBL above are both assumed. Realistically, the atmosphere is unlikely to possess either of these layers until later in the morning, especially in the presence of clouds. Nevertheless, the initial sounding must be forced to conform immediately to the model requirements to prevent model collapse.

The initial sounding is input as available from 400 mb down to near the surface. The data is available from the SESAME tapes at 25mb levels, plus the surface observation. The first data point above the surface on the tapes is always taken at a pressure level which is an integral multiple of 25 mb (ie. 875mb or 950mb). The model cannot handle very thin layers. So if this first data point above the ground is within 10 mb of the surface pressure, it is rejected.

The surface observation is used to determine initial TS and QS in the model. These values are set at the top of the surface layer, 5mb above the ground. The ground temperature is initialized to be 0.1 deg C higher than the surface temperature to produce positive SH flux. The moisture for the PBL is set equal to the surface value. The PBL depth is initialized at 90 m, measured from the ground. The atmosphere above 90 m, up to the first data point, is the first stable layer. If this first stable layer is neutral, the stability is set to a minimal value to allow finite but fast growth.

The delta theta for the first iteration is derived by extending the first data point down to the 90 m level, and calculating its potential temperature. This process is shown on Fig. 2.7. This operation creates an isothermal layer above the initial PBL, and the characteristics of this new layer are used to determine the value for $\Upsilon$ , the lapse rate in the stable air used in the model.

This initialization procedure seems like a major modification to the sounding, but the actual changes are small enough to be barely detectable when plotted on a pseudoadiabatic chart. These changes allow the mixed layer model to work properly. In addition, results from a study by Whiteman (1982) suggest that a small mixed layer appears within 15 minutes of ground illumination, so the errors associated with this initialization procedure should be small. For a typical sounding, the change in the dry static energy of the adjusted portion of the sounding is less than 0.1%.

## 2.11: Sensitivity Tests

There are a number of constants used in this model, many of which are not easily evaluated. A number of sensitivity tests are performed to insure that these arbitrary constants are not controlling the results. The sounding used for this purpose is taken from a PBL field project at O'Neill, Nebraska

on 13 August 1953. (This is the same sounding which has already been mentioned in the radiation comparison discussion above.) The sounding appears in Fig. 2.8. The standard run against which the others are compared uses the following values for the various constants: GWB = 90%, WMAX = 0.80 cc H2O/cc soil, TBAR = 296.5 K, and VS = 1000 cm/s. In addition, initial GW (GWO) is varied, using 55% as the standard value. The results of the standard run appear in Figs. 2.9 through 2.13. No clouds or other changes above the PBL are imposed in this or any of the other sensitivity runs.

The standard run is characterized by strong heating under moderately moist soil conditions. The temperature of the ground (Fig. 2.13) rises rapidly during the day, peaking at 1400 local solar time (LST). The incident solar radiation (Fig. 2.10) is strongest at 1200 and begins to fall off afterwards. The lag between the radiation peak and the ground temperature peak is due to the finite time required for the soil to heat. The soil is not in thermal equilibrium with the incident radiation at noon, and so continues to heat under the decreasing but still strong radiation. The PBL moisture (Fig. 2.11) rises rapidly until near midday, in response to the latent heat flux (Fig. 2.12). The LH flux in this run is sufficient to strongly moisten the PBL. The air above the surface up to about 825 mb is very stable, and the PBL grows slowly, reaching 825 mb very late in the run. The ground

temperature reaches 314 K, while the surface air temperature TS reaches 308 K shortly after. The moisture at this time is nearly 14 g/kg.

A. TBAR Test

TBAR is the diurnal average soil temperature, assumed constant with depth. At a depth equal to the limit of the diurnal variation (about 50 cm), TBAR = T(soil) independent of time. So TBAR can be regarded as a 50 cm soil temperature, assumed constant for the model run. It is varied +/- 4 K from the standard of 296.5 K. The results appear in Table 2.2. The timing of the peak values does not change over the range of TBARs, only the values themselves do. The fluxes show the greatest response, particularly the soil heat flux (almost +/- 20%). Since one of the two factors in the soil heat flux is the quantity TG-TBAR, the model's response to the change in TBAR is expected. Furthermore, the ground temperature responds noticeably, showing a response of +/- 2 to 4%. The other parameters show little response, particularly the value for QS which hardly changes at all (+/- 0.1 g/kg). TBAR does not have a great effect on the model output.

B. VS Test

VS is the magnitude of the wind speed at the top of the

surface layer. It is used in the calculations for the sensible heat flux (SH) and latent heat flux (LH). The standard run uses a value consistent with local observations. The test varied this value from 20% to 150% of the observed speed. The results of the test appear in Table 2.2. As expected, the SH and LH change substantially, about 20% for the VS= 200 run (20% of the observation). However, the soil heat flux (GS) changes more than either LH or SH. The maximum value for GS for the VS=200 run is almost double the VS=1500 (150% of the observation) run. Since GS depends on SH and LH for its calculation, the changes in SH and LH are additive for the soil heat flux.

The ground temperature also responds strongly, since it is linked to the soil heat flux. The changes are pronounced for the weakest wind run, VS=200. The others cluster much closer together. As the wind speed drops, the maximum ground temperature rises rapidly as does the soil heat flux. In a real PBL with weak winds, the effective surface layer in which the eddies remove the heat and moisture from the surface likely becomes smaller (less frictional turbulence), and the eddies less vigorous and efficient. So more incident radiation is left in the soil, both heating it and contributing to a larger soil heat flux. In the model, these effects are part of the parameterization. For moderate changes in wind speed (+/- 50%) the effect is not large. For

a reduction in VS by a factor of 5, the change becomes very important.

The variation in the surface parameters and the PBL depth is significant. The surface temperature is lower by 1 deg C for the VS=200 run, and the surface moisture higher by nearly 1 g/kg. The final PBL depth for the VS=200 run is 851 mb, 30 mb higher in the atmosphere than the standard run. Again this run is anomalous. The other runs are all much closer to each other. It is true, then, that the surface wind speed becomes a critical parameter, but only for very small values. Usually, in strong BLH and deep PBLs, the wind is at least moderate in strength. So the VS parameter does not require extreme care, beyond choosing a value consistent with the observations.

C. WMAX and GWB Test

The effects of the soil moisture capacity (WMAX) and the bulk soil moisture (GWB) are discussed together. Table 2.3 shows the results. As one can see on the table, the variation of these two parameters produces results of similar magnitude. The runs with standard GWB (=90%, the wettest GWB value) show wide variation over the range of WMAX. The runs with standard WMAX (=0.80 cc $H_2O$/cc soil) show nearly the same variation over the GWB values. The only run which is not similar is the

wetter WMAX value (=1.00 cc $H_2O$/cc soil). There is no corresponding wetter GWB value; all the GWB values are dryer than the standard. The general trend for both parameters is cooler and wetter PBLs, and lower inversions for wetter parameter values.

The variation within each of the tests is larger than in the TBAR test. The SH flux almost doubles from wet to dry and the LH flux drops by 30%. The maximum surface temperature change is 2 deg C over the range of WMAX, a difference of more than 10% in the diurnal temperature change. The surface moisture also depends strongly on this parameter, varying by nearly 2 g/kg over the WMAX values. The PBL characteristics change drastically. The dryest WMAX run has a final inversion depth of twice that for the wettest run. These changes are significant and imply a sensitivity in the model to GWB and WMAX. Fortunately, the changes are similar for the two parameters, and hence a range of values for one can be used while holding the other constant. During the case study model runs, the value for WMAX is fixed at 0.50 cc $H_2O$/cc soil, similar to a value used by Deardorff (1977) to model Kansas data. The GWB is then varied over a large range depending on past rainfall. These results are then examined in the case studies to determine which are physically realistic.

D. GWO Test

The results of the test involving the initial surface soil moisture (GWO), can be anticipated from the GWB, WMAX tests. The value of GWO makes a very large difference in the model runs. These results are shown on Table 2.3. Notice that the variation from standard values in GWO runs is +25%, -50% (GWO=70%, 25%), just as for the WMAX tests. This allows simple comparison of the magnitudes of the changes in model results.

The flux variations are similar to the WMAX runs. The SH nearly doubles from wet to dry, while the LH drops by 30%. The change in maximum surface temperature for the GWO runs is almost 4 K, and the surface moisture changes more than 8 g/kg (change from GWO = 25% to 70%). The surface conditions are 2 to 4 times more sensitive to the GWO values than to the GWB or WMAX parameters. The height of the inversion for the dryest run is more than 3 times the height for the wettest run. The initial soil moisture is clearly a crucial parameter in controlling the PBL development in the model. McCumber and Pielke (1981) found that their model was sensitive to soil moisture, and Cooper et al. (1982) also found soil moisture important. In the case studies, a series of runs are made which use a wide range of GWO values. The range is determined in conjunction with the previous day's rainfall, but so many

other unknowns can affect the surface soil moisture (timing of precipitation, plant cover, soil drainage, etc.) that only a range can be specified before the actual runs are made.

## 2.12: Comparison Runs

The model is compared with observations taken during the O'Neill, Nebraska PBL field study, and then with detailed soil modeling by Barnard (1977). The O'Neill run uses the following parameters: TBAR=296.5 K, VS= 1000 cm/s, WMAX = 0.80 cc $H_2O$/cc soil, GWB = 45%, and GWO = 65%. The sounding is shown in Fig. 2.8.

The fluxes are shown in Figs. 2.2, 2.14 and 2.15. Notice the net incident radiation (Fig. 2.2) is over predicted by about 8% (as already noted above), throughout most of the integration. The soil heat flux is plotted just below on the same axes. The observations which are plotted have error bars shown, to give some idea of the scatter in the data. For the first four hours of the run, the model partitions too much radiation to the soil flux. Indeed, judging from the similar figures for SH and LH (Figs. 2.14 and 2.15), it appears that all of the difference in net radiation is given to the soil heat flux. The reason for this model behavior is not clear. The soil heat flux actually has two peaks, one near 800 LST and one near 1200 LST. If the soil is initially very dry at

the surface, the earlier peak disappears. For very high bulk moisture the two peaks merge into one near 1100 LST. This may be evidence that the moisture dependent soil heat capacity is affecting the behavior--depending on the soil moisture, which itself changes rapidly with time in the morning.

The sensible heat flux modeling has difficulties late in the day when the observed flux falls, and the model flux falls much slower (Fig. 2.14). The difference is as big as 50% of the observed flux, and 25% of the nearest error bar value. The latent heat flux (Fig. 2.15) is also much different from the observed value in the afternoon, although it is within the very large error bars. Evidently, the LH was not well observed, and so the observations are imprecise. This anomalous behavior of the fluxes is annoying, but is not as important for this thesis as the effects that these flux errors have on the PBL characteristics themselves.

As the graph of soil temperature shows (Fig. 2.16) these effects are slight. The soil temperature is higher during the morning in the model than the observations, and peaks at a lower temperature. The difference is not large, at most 2 deg C. The effects on surface layer temperature are even smaller (Fig. 2.17). A 2 deg C difference is evident very early in the run (700 LST), but this difference drops to less than 0.5 deg C for the rest of the run until 1800 LST. At this time the

observations show cooling, which Wetzel (1978) attributes to large scale advection, not PBL dynamics. So the surface temperature is very well modeled. The height of the inversion is similarly well handled. Fig. 2.18 shows that the model is within 100 m of the observations until 1400 LST. After this, the O'Neill atmosphere no longer has a well defined PBL, so no data is available after this time.

Barnard Comparison

The model reproduces the fluxes at O'Neill generally well, with certain exceptions. It also models the soil temperature, surface temperature, and PBL height with some accuracy. To test the model further, it is run with data from a detailed soil moisture modeling study. Barnard (1977) uses an 80 layer model to investigate climatic sensitivity of the atmosphere to soil moisture. The sounding used is shown in Fig. 2.19. For the present model, the parameters used are: TBAR = 310.0 K, VS = 1000 cm/s, WMAX = 0.50 cc $H_2O$/cc soil, GWB = 50%, and GWO = 6%. The model results are shown on Figs. 2.20 and 2.21 along with Barnard's results for comparison for two times. Notice that the values of surface moisture compare very well, and the results of the modeling of the well-mixed layer agree quite well too. These results are excellent considering that the present model is so simple in form.

## 2.13: Model Comparison Summary

The model outlined above is simple but effective in reproducing the PBL characteristics as they change with time during a typical spring or summer day. The height of the inversion, surface temperature and surface moisture are the most important parameters for the assessment of convective instability and inhibition to convection. These PBL characteristics depend strongly on soil moisture, and weakly on other model parameters such as surface wind speed or 50 cm soil temperature. The model can successfully reproduce the results of PBL field studies (such as O'Neill, Nebraska) and detailed modeling work (such as Barnard, 1977).

It could be argued that more detail should be included in the model, incorporating perhaps different soil types, multiple soil layers and vegetation. The most telling reason for not doing so is that data to initialize such parameterizations is generally unavilable and would itself require sweeping assumptions rendering the detailed physics meaningless. Secondly, the model does seem able to model the surface energy balance sufficiently well to duplicate more complicated models (e.g. Barnard's 1977 model) and real data. Thirdly, work by McCumber and Pielke (1981) indicates that the details are, in fact, less important than the surface soil moisture. They tested a model of soil characteristics which

included several soil types, and discussed that the soil moisture was much more influential for the fluxes than soil type. Therefore, the model is used in its present, simple form to analyze SESAME, 1979 case study data.

The modeling results for each case are presented in both raw form and in the form of "sensitivity values". The raw numbers for pressure level of the top of the PBL (PH), surface layer temperature (TS), PBL moisture (QS), convective instability (PLI), and convective inhibition (NA) are tabulated for each run in each case.

The sensitivity values are referred to in the discussion and tabulated at the end of the tables. These values are defined by referring to the model run without any modifying physical factors. This run is called the "plain" run. For example, suppose the plain run for 50-50 soil moisture parameters yielded growth of the PBL of 159 mb. When clouds are added to the model, the growth is reduced by 10 mb. The sensitivity value for PBL growth for the addition of clouds is then:

Sensitivity = (Growth with clouds - Plain growth)/ Plain growth = 10 mb / 159 mb = ~6 %.

TS, QS, and PLI are handled similarly. The convective

inhibition cannot be handled in this manner, since the initial NA is undefined, and hence the change in NA is undefined as well. So, the sensitivity values for the convective inhibition are defined by simple comparison of the values at the end of the model runs with those of the plain runs. For example, if the plain run discussed above had an NA of 20 and the run with clouds had a NA of 30, the sensitivity value would be:

Sensitivity = (NA of run with clouds - Plain NA)/ Plain NA

= 10/20 = 50%.

Table 2.1: SCHEDULE OF MODEL CALCULATIONS

After initialization, the model runs as follows for each time step. New values for variables are labeled New (variable). Old values are left plain (variable).

1. Radiation Routine

   A. New IR flux = $f(T_i, p_i, q_i)$ -- sounding data plus geographical location, time, day, etc.

   B. New Incident flux = $f(T_i, p_i, q_i)$ -- sounding data plus same extra items as for IR flux

   Results in $\Delta T$ at each model level due to net radiative flux divergence and the net radiation, NR, absorbed in the soil surface. The $\Delta T$ is not applied to the sounding until the end of the cycle.

2. Soil Heat Flux

   A. New GS = f(TG, TGpast[one time step before], soil characteristics such as heat capacity, thermal conductivity = f[ground wetness] )

   Results in a new value for GS.

3. Surface Sensible Heat Flux and Latent Heat Flux

   A. New SH = f(TG, GW, TS, QS, VS, and constants VK, $Z_0$ )

   B. New LH = $f(u_*$, GW, VS)

   Results in new values for SH, LH.

4. PBL Characteristics

   A. New h = f(New SH, New LH, TS, h, $\Delta\theta$, $\gamma$ )

   B. New $\Delta\theta$ = f($\Delta\theta$, $\gamma$, New SH, New LH, h)

   Results in new values for h, $\Delta\theta$.

5. Ground Variables

   A. New TG = f(TG, New NR, New SH, New LH, TBAR (a

constant), and soil characteristics)

B. New GW = f(GW, New LH, and constants WMAX, $c_1$ = f(GW), and $c_2$)

Results in new values for TG, GW.

6. PBL Variables

A. New TS = f(New h, New $\Delta\theta$, $\Upsilon$ )

B. New QS = f(QS, q[inversion layer], h, New h, New LH)

Results in new values for TS, QS.

7. Change Sounding

A. Change top of PBL -- New T, p = f(New h), q

B. If current inversion is filled, find new stable layer (next layer above) and recompute $\Upsilon$ .

C. Fill in surface (TS, QS) and ground (TG, GW) variables.

D. Compute imposed changes above PBL -- change T, q appropriately. If necessary, change $\Upsilon$ too.

Results in new sounding at end of time step.

8. Output Variables

TABLE 2.2: MODEL RESULTS FOR SENSITIVITY TESTS

TBAR TEST

| TBAR | SH | LH | GS | TG | TS | QS | PH(mb) | PH(m) |
|---|---|---|---|---|---|---|---|---|
| 292.5 | 260 | 583 | 209 | 36.4 | 32.8 | 14.4 | 833 | 1108 |
| 294.5 | 265 | 593 | 193 | 36.7 | 33.0 | 14.3 | 828 | 1161 |
| 296.5* | 270 | 602 | 176 | 37.1 | 33.2 | 14.3 | 822 | 1233 |
| 298.5 | 273 | 614 | 159 | 37.4 | 33.4 | 14.2 | 816 | 1292 |
| 300.5 | 278 | 623 | 142 | 37.8 | 33.6 | 14.3 | 807 | 1388 |

VS TEST

| VS | SH | LH | GS | TG | TS | QS | PH(mb) | PH(m) |
|---|---|---|---|---|---|---|---|---|
| 200 | 224 | 540 | 296 | 44.8 | 32.0 | 15.2 | 851 | 928 |
| 600 | 262 | 582 | 201 | 39.0 | 33.0 | 14.5 | 830 | 1149 |
| 1000* | 270 | 602 | 176 | 37.1 | 33.2 | 14.3 | 822 | 1233 |
| 1200 | 269 | 610 | 168 | 36.5 | 33.2 | 14.2 | 820 | 1247 |
| 1500 | 270 | 618 | 160 | 36.1 | 33.3 | 14.3 | 817 | 1281 |

Fluxes are in mcal/sq cm min. SH = sensible heat flux, LH = latent heat flux, GS = soil heat flux. TG = ground temperature (deg C), TS = surface layer temperature (deg C), QS = PBL mixing ratio (g/kg), PH = level of top of PBL. TBAR = 50 cm soil temperature (K), VS = PBL wind speed (cm/sec), GWB = bulk soil moisture (% of saturation), GWO = surface soil moisture (% of saturation), WMAX = saturation soil moisture (cc H2O/cc soil). * denotes standard run.

TABLE 2.3: MODEL RESULTS FOR SENSITIVITY TESTS (CONT.)

GWB TEST

| GWB | SH | LH | GS | TG | TS | QS | PH(mb) | PH(m) |
|---|---|---|---|---|---|---|---|---|
| 30% | 374 | 464 | 226 | 41.7 | 34.8 | 12.9 | 730 | 2254 |
| 50% | 330 | 511 | 203 | 40.2 | 34.3 | 13.3 | 763 | 1871 |
| 70% | 292 | 558 | 188 | 38.6 | 33.8 | 13.7 | 797 | 1498 |
| 90%* | 270 | 602 | 176 | 37.1 | 33.2 | 14.3 | 822 | 1233 |

WMAX TEST

| WMAX | SH | LH | GS | TG | TS | QS | PH(mb) | PH(m) |
|---|---|---|---|---|---|---|---|---|
| 0.40 | 426 | 455 | 256 | 42.7 | 34.8 | 13.3 | 724 | 2321 |
| 0.60 | 303 | 552 | 191 | 39.1 | 33.9 | 13.7 | 792 | 1552 |
| 0.80* | 270 | 602 | 176 | 37.1 | 33.2 | 14.3 | 822 | 1233 |
| 1.00 | 261 | 633 | 169 | 36.0 | 32.8 | 15.0 | 834 | 1098 |

GWO TEST

| GWO | SH | LH | GS | TG | TS | QS | PH(mb) | PH(m) |
|---|---|---|---|---|---|---|---|---|
| 25% | 405 | 399 | 234 | 42.5 | 35.1 | 10.4 | 703 | 2569 |
| 35% | 359 | 461 | 216 | 41.2 | 34.8 | 11.5 | 737 | 2172 |
| 45% | 311 | 529 | 194 | 39.3 | 34.1 | 12.7 | 779 | 1691 |
| 55%* | 270 | 602 | 176 | 37.1 | 33.1 | 14.3 | 822 | 1233 |
| 70% | 223 | 716 | 146 | 33.4 | 31.3 | 18.7 | 861 | 818 |

See Table 2.2 for caption.

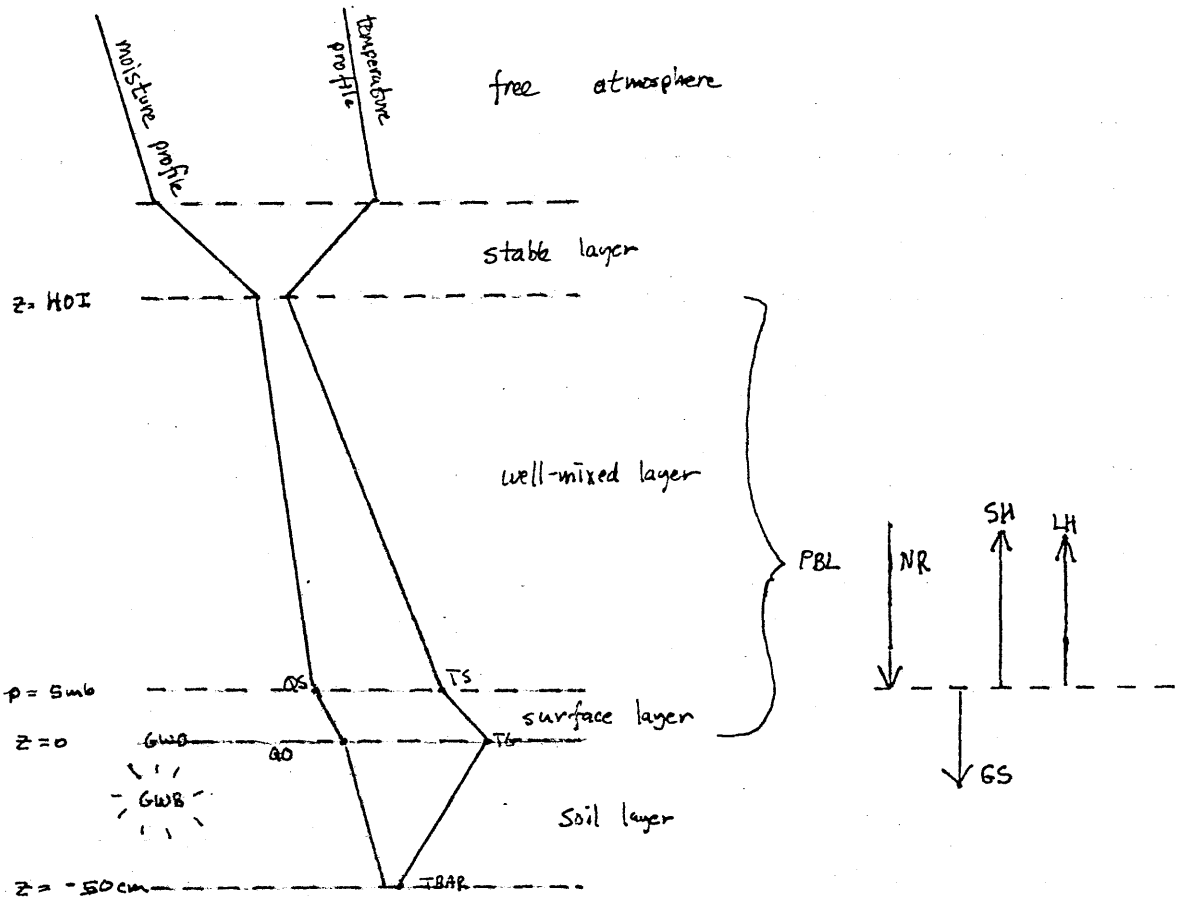


Fig. 2.1 Schematic diagram of model atmosphere. Hypothetical temperatures and dewpoints are shown by upright lines, while model layers are delineated by horizontal lines. Variables are defined in the text. Also shown is flux diagram showing positive direction of fluxes at the surface.

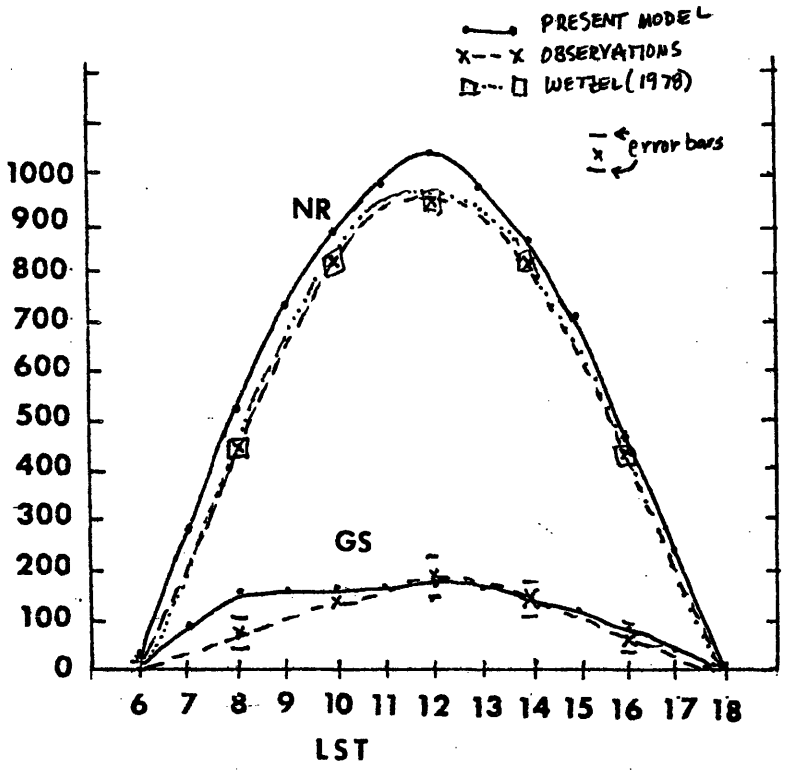


Fig. 2.2 Comparison of model net radiation (NR) and soil (GS) fluxes (mcal/ sq cm min ) with observations and modelling by Wetzel(1978) for O'Neill day number 2.

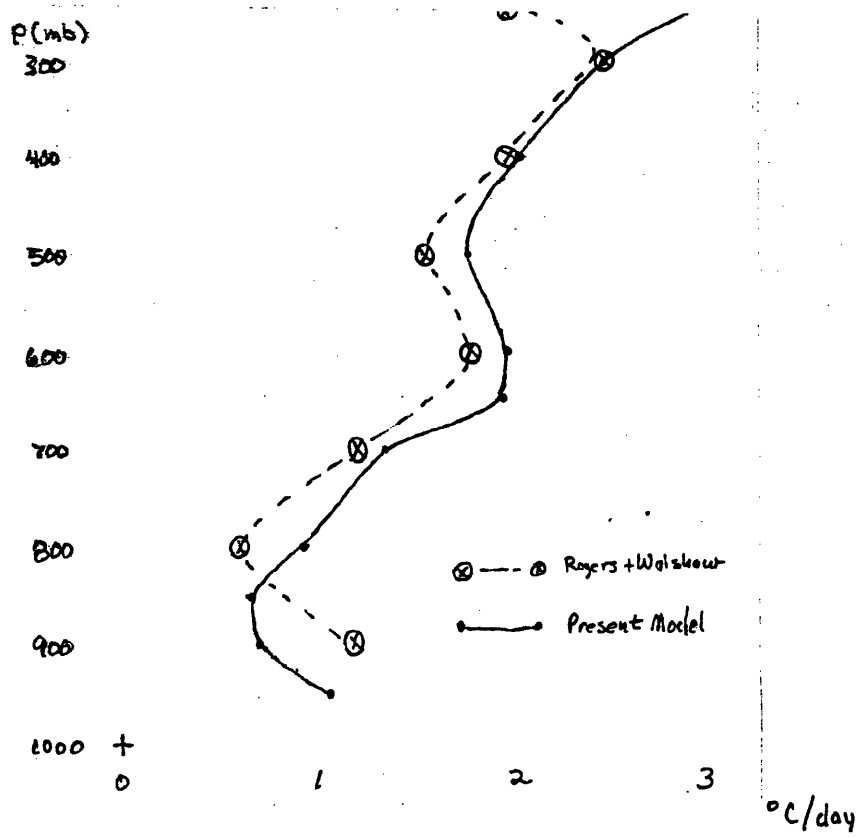


Fig. 2.3 Comparison of model IR cooling rates (solid lines) with calculations of Rogers and Walshaw (1966) (dashed lines).

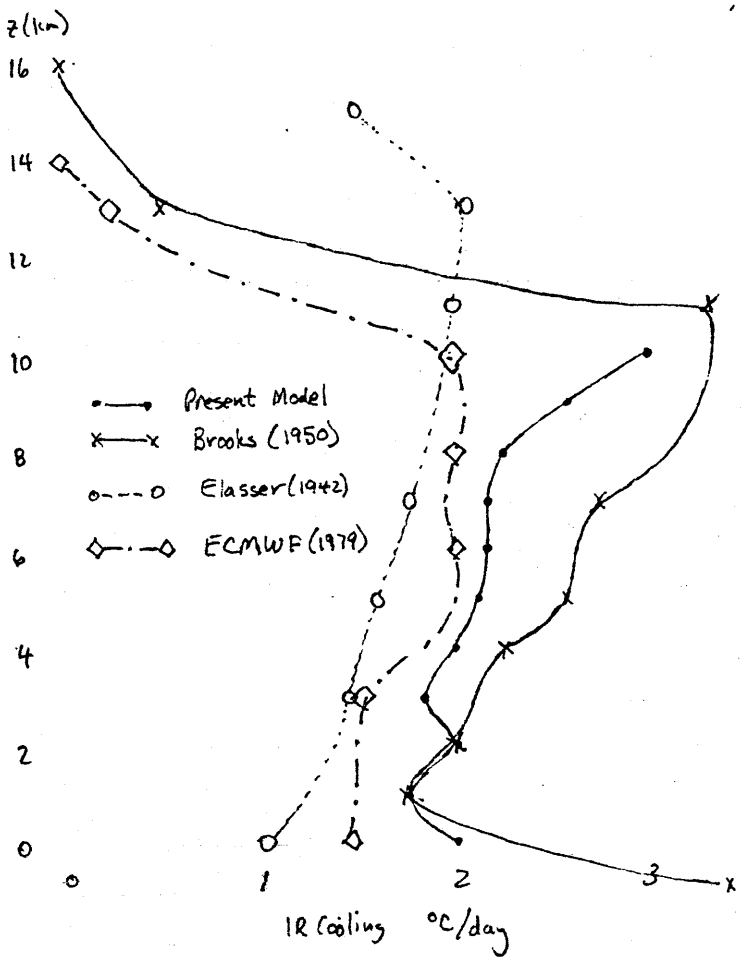


Fig. 2.4 Same as Fig. 2.3 for comparison with Brooks(1950) (solid line connecting *), Elsasser (1942) (dashed line), and ECMWF (1979) (dash-dotted line).

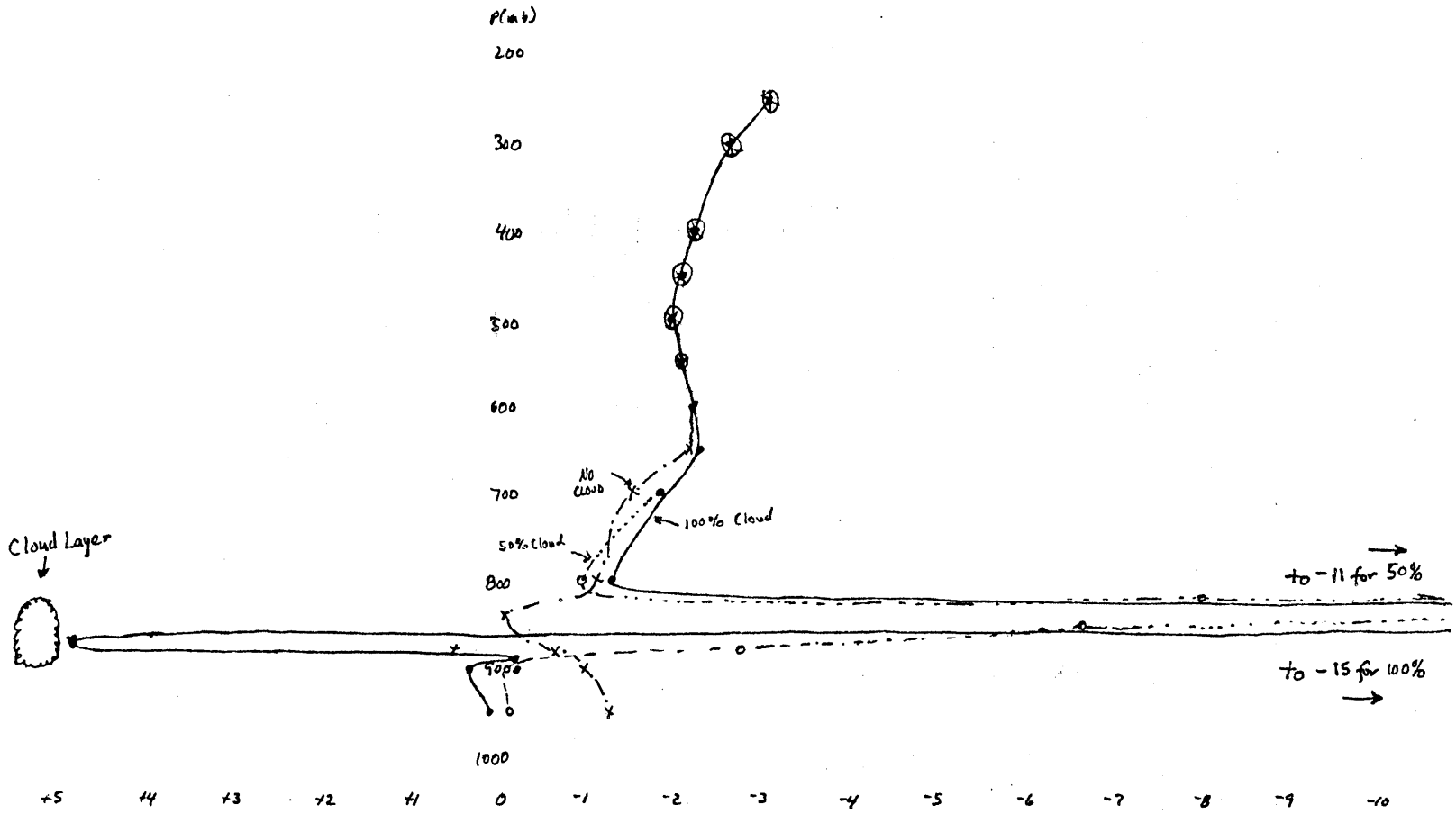


Fig. 2.5 Model IR cooling rates (only) for cloud layer between 880 mb and 820 mb, of 50% coverage (dotted line), 100% coverage (solid line), and no cloud (dash-dotted line).

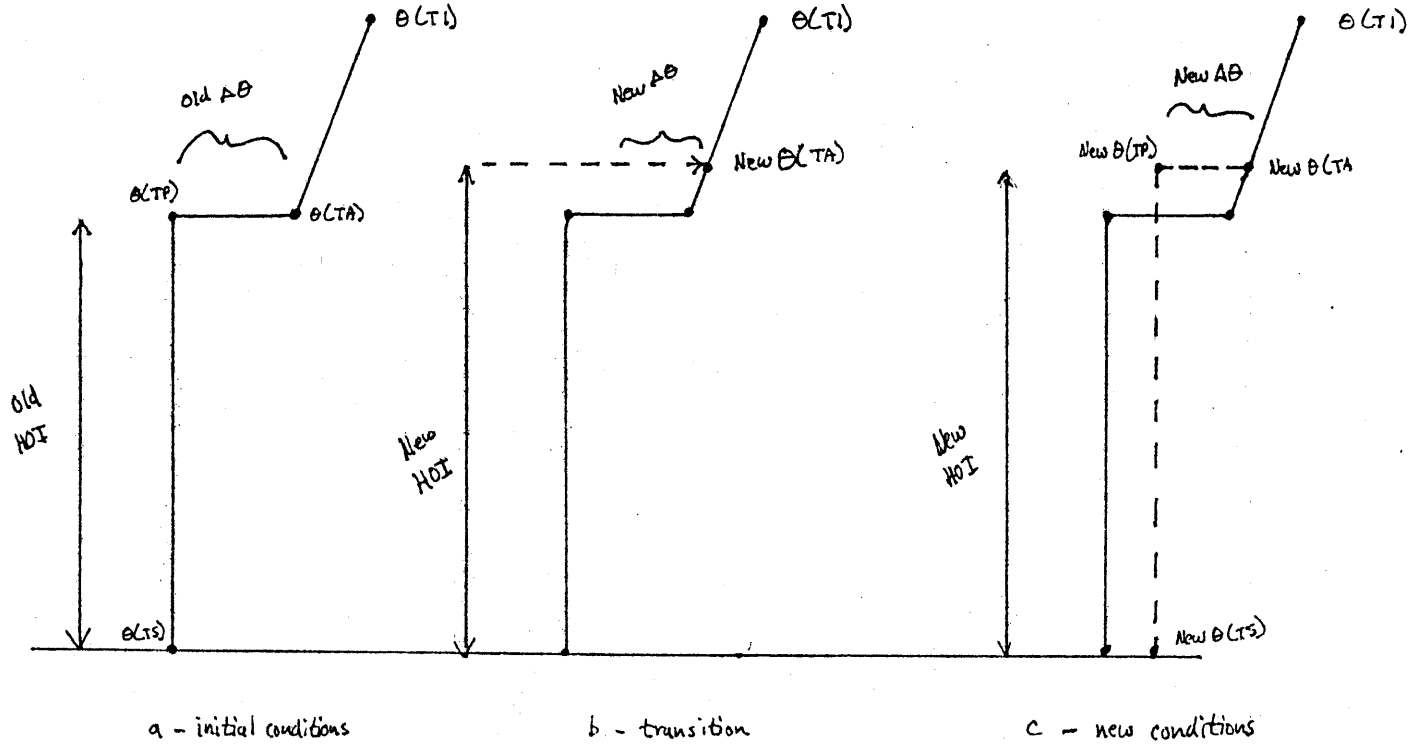


(γ is a constant during this process)

Fig. 2.6 Schematic diagram illustrating process of finding new PBL potential temperature from new inversion calculations. Horizontal axis is potential temperature.

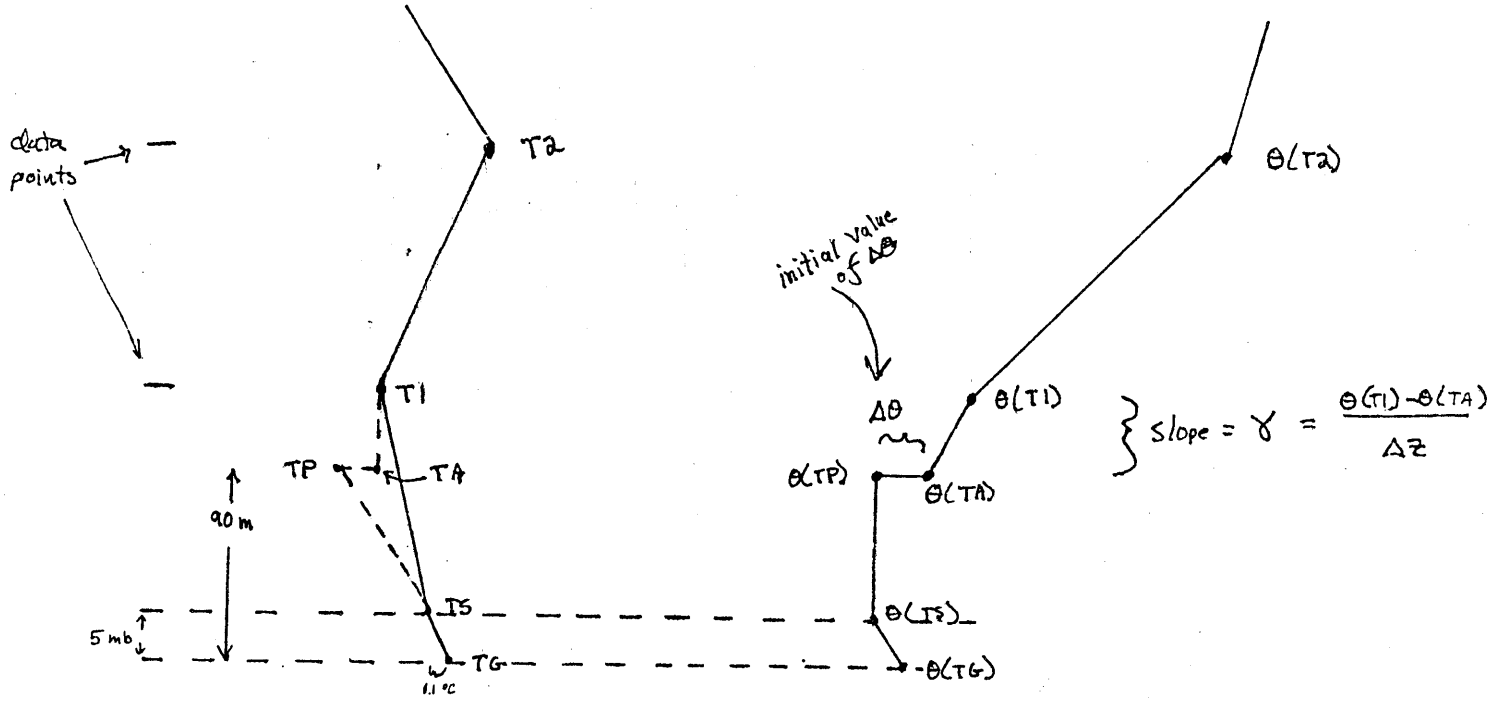


Fig. 2.7 Schematic diagram showing process of initialization of $\Delta\theta$ from initial sounding. Vertical axis is height. Horizontal axis on left side is temperature, and on right side is potential temperature.

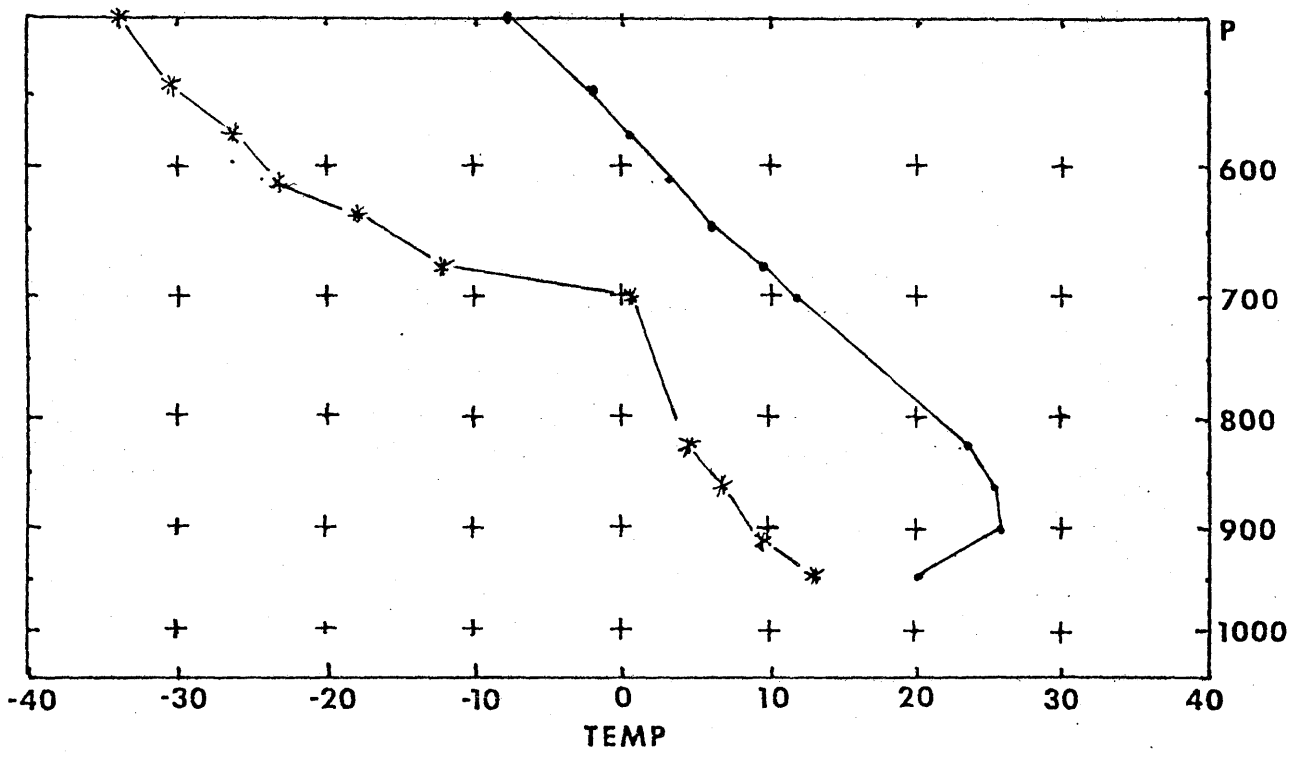


Fig. 2.8 Sounding plotted on a pseudoadiabatic diagram from O'Neill, Nebraska at 1200 GMT. Line connecting dots for temperature (deg C) and line connecting * for dewpoint (deg C).

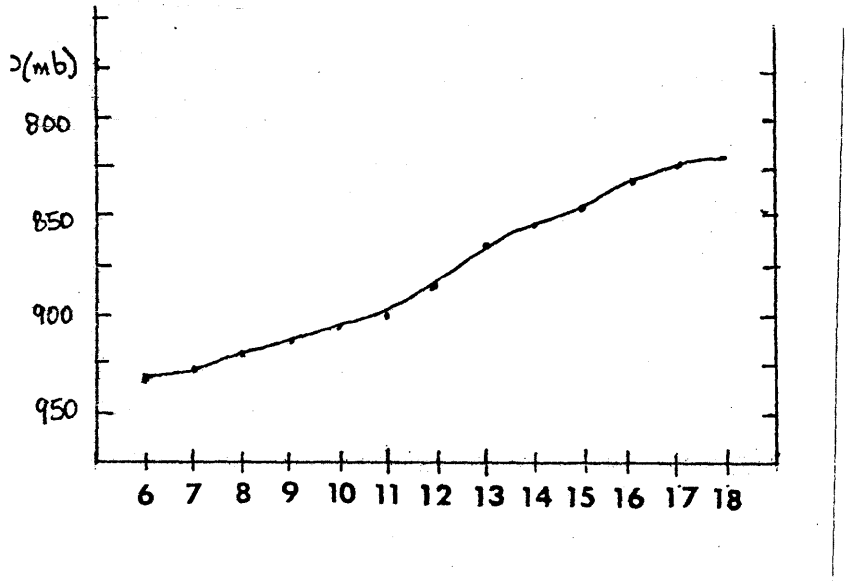


Fig. 2.9 Time variation of pressure level of PBL top (PH) for standard model run.

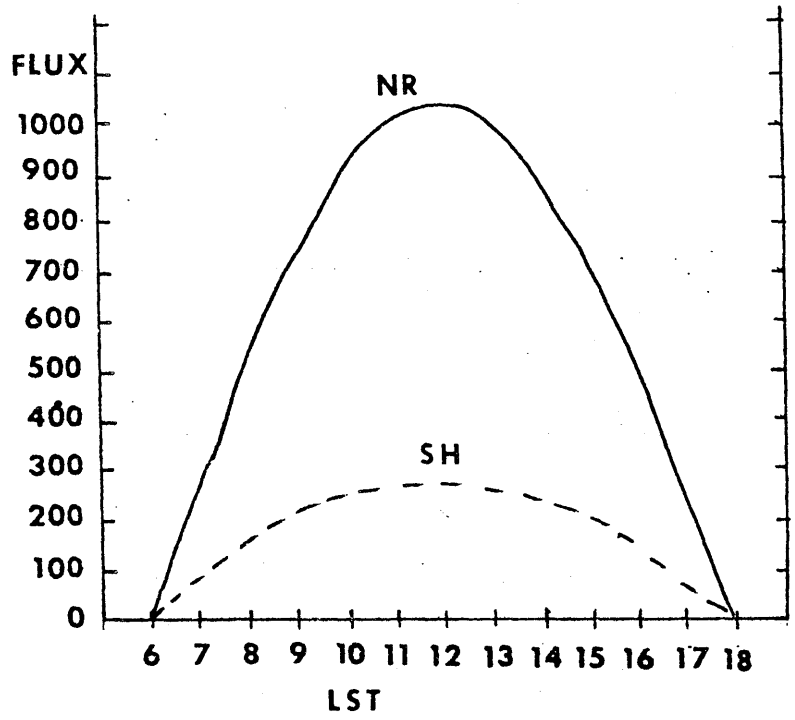


Fig. 2.10 Net radiation (NR) and sensible heat (SH) fluxes (mcal/sq cm min ) for standard model run.

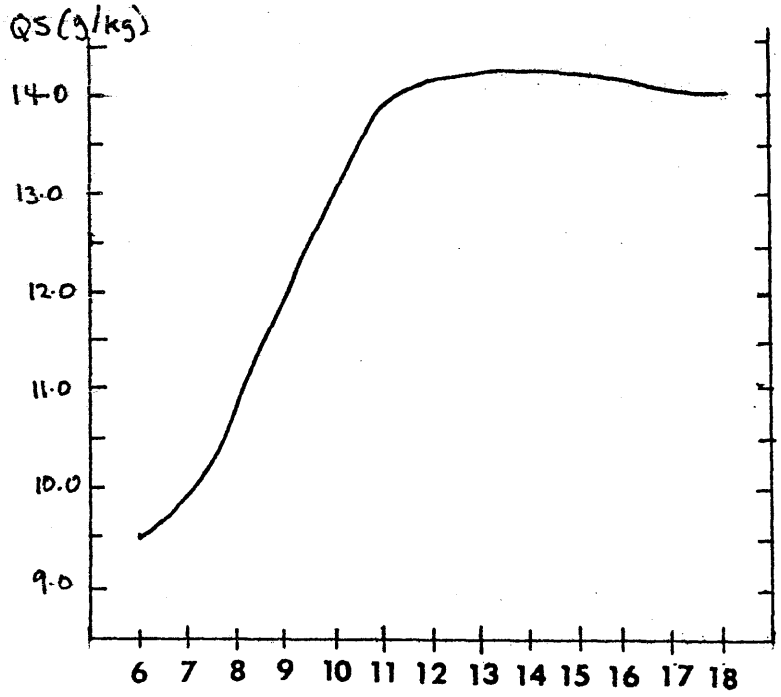


Fig. 2.11 Time variation of PBL mixing ratio (QS) for standard model run.

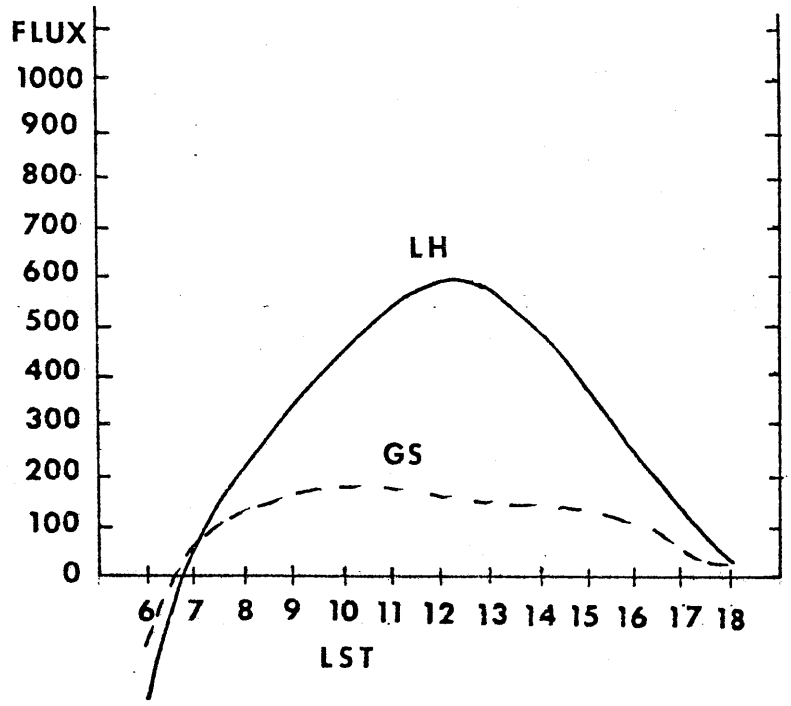


Fig. 2. 12 Same as Fig. 2. 10 for latent heat (LH) and soil heat (GS) fluxes.

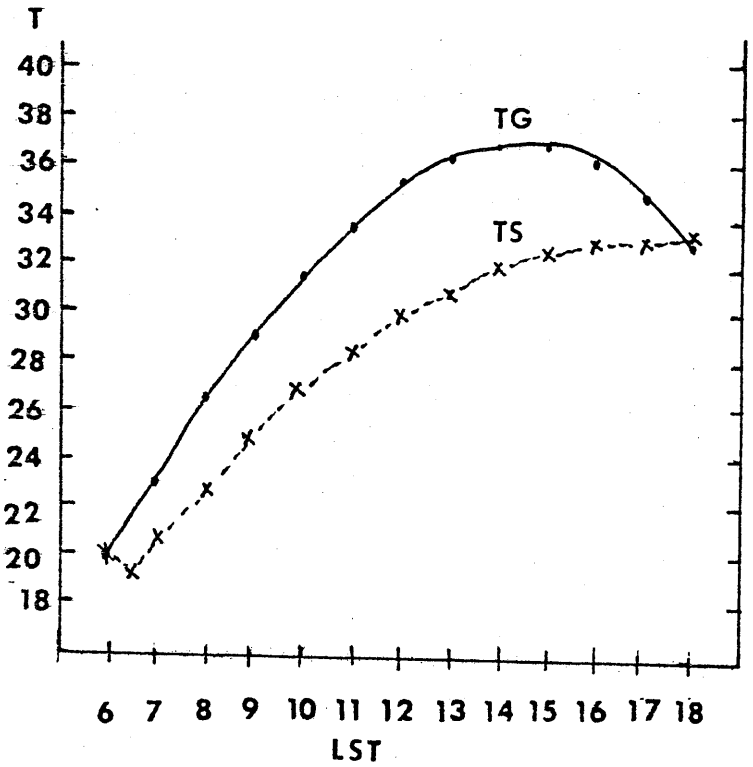


Fig. 2. 13 Time variation of ground temperature (TG) and surface layer temperature (TS) for standard model run.

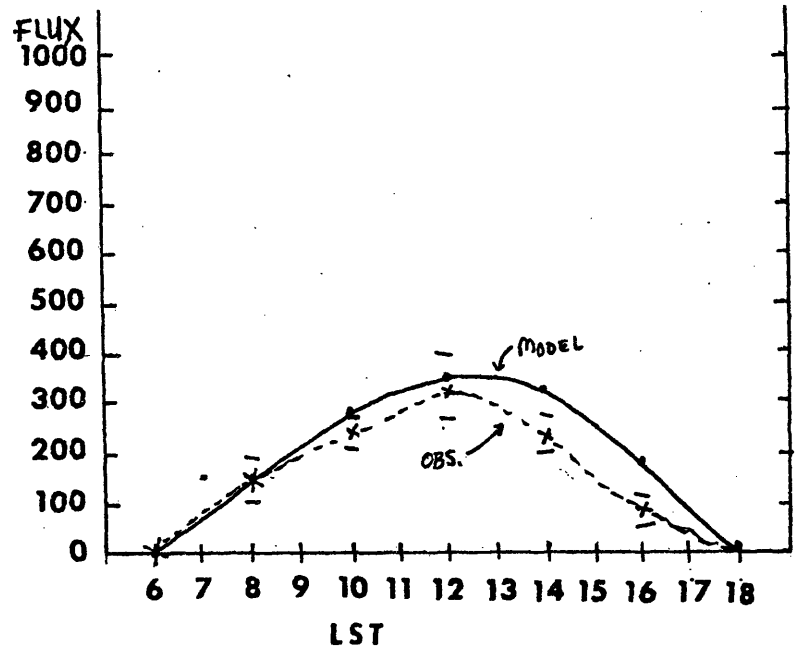


Fig. 2.14 Same as Fig. 2.2 for sensible heat flux (SH).

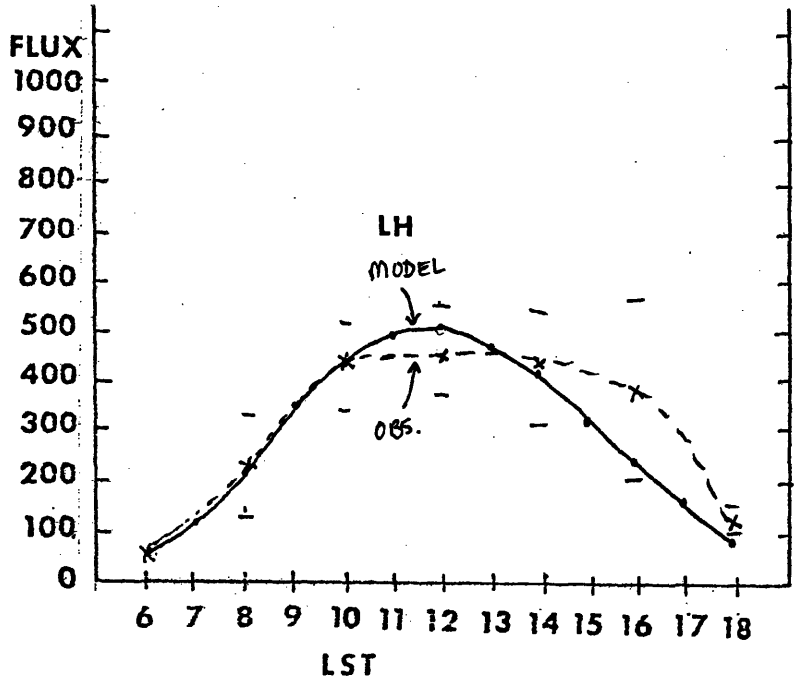


Fig. 2.15 Same as Fig. 2.2 for latent heat flux (LH).

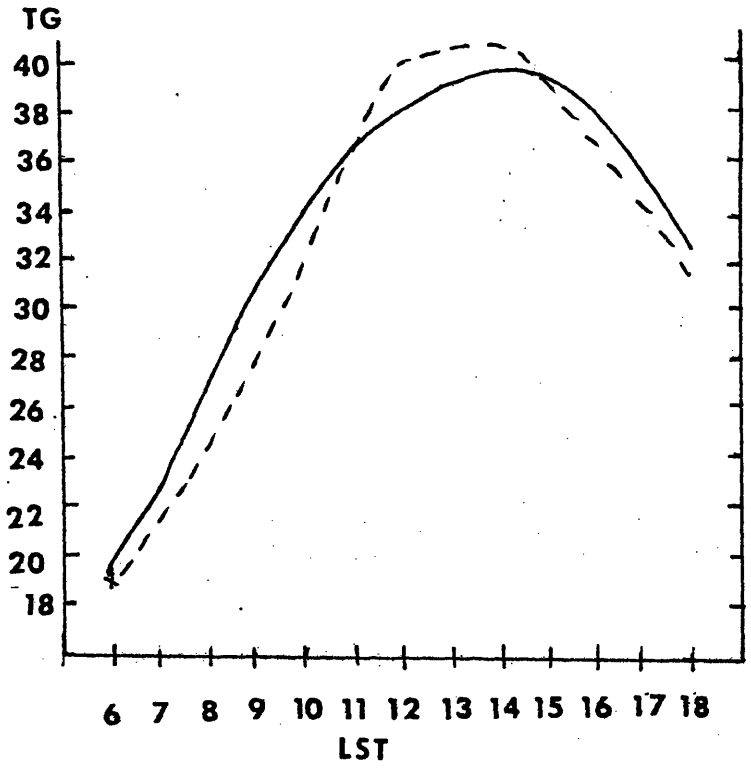


Fig. 2. 16 Comparison of model output (solid line) and observed (dashed line) ground temperature (TG) for O'Neill sounding.

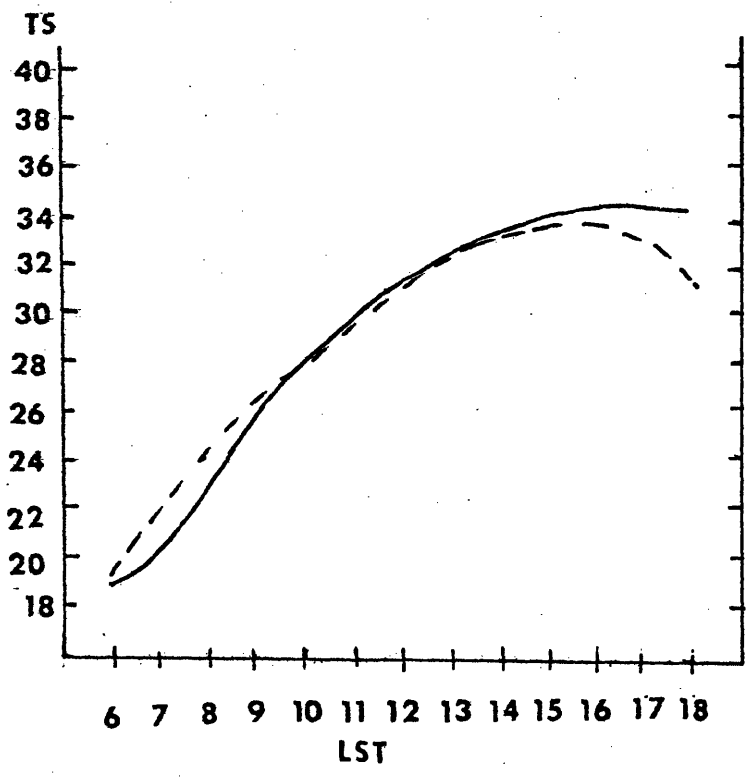


Fig. 2. 17 Same as Fig. 2. 16 for surface layer temperature (TS).

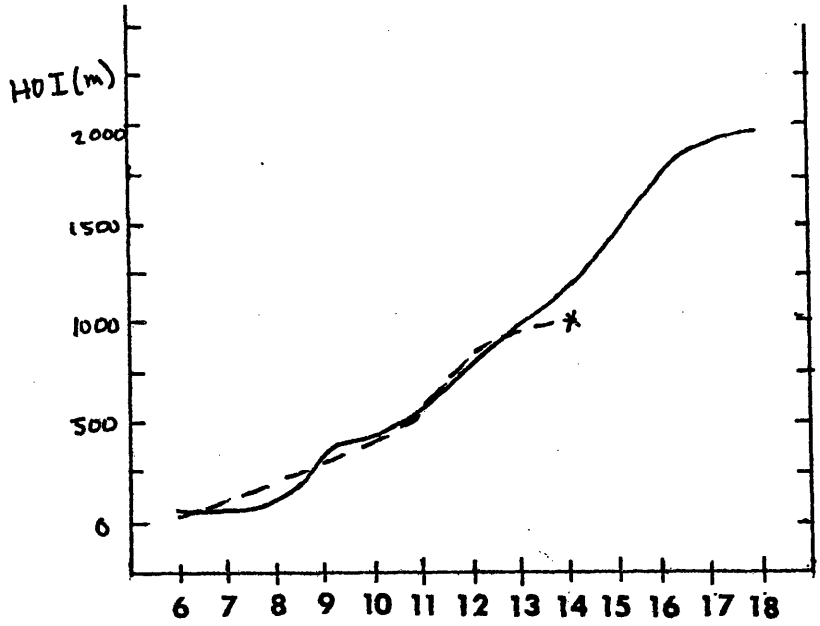


Fig. 2.18 Same as Fig. 2.16 for growth of PBL (HOI in meters).

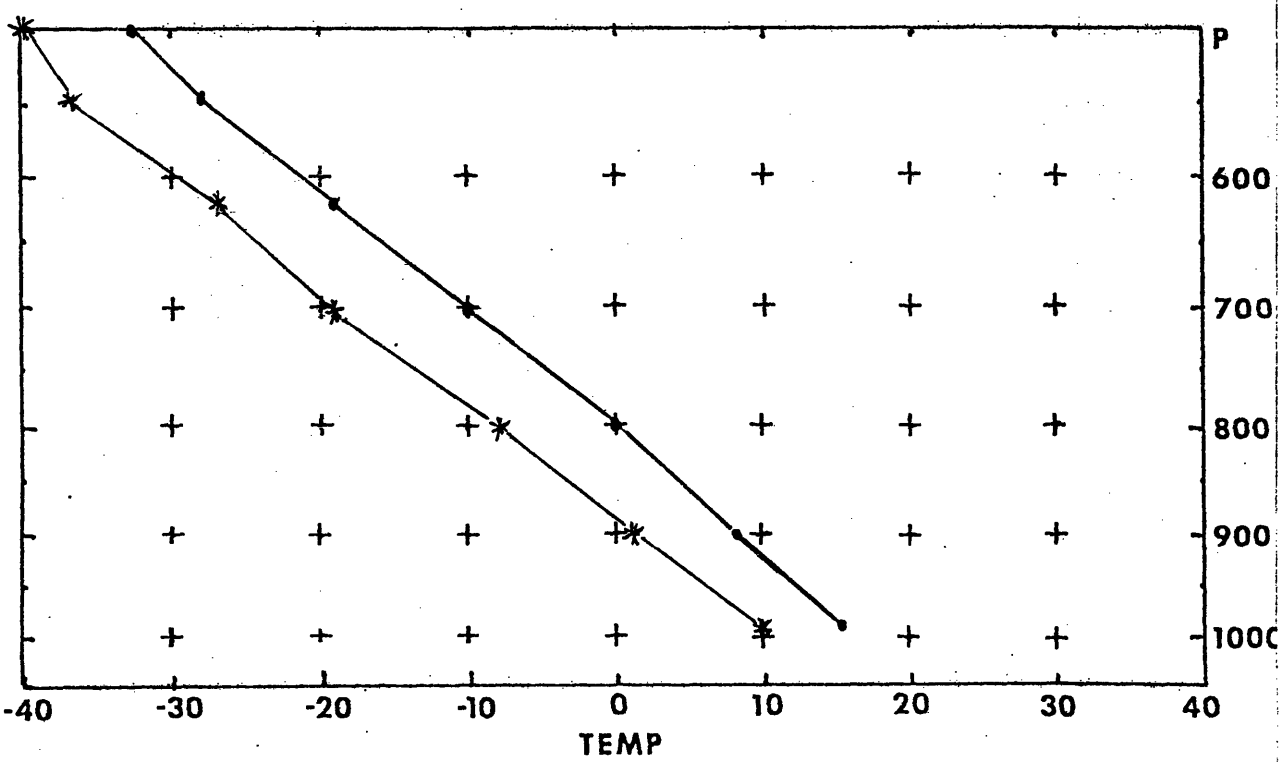


Fig. 2.19 Same as Fig. 2.8 for initial sounding from Barnard (1977).

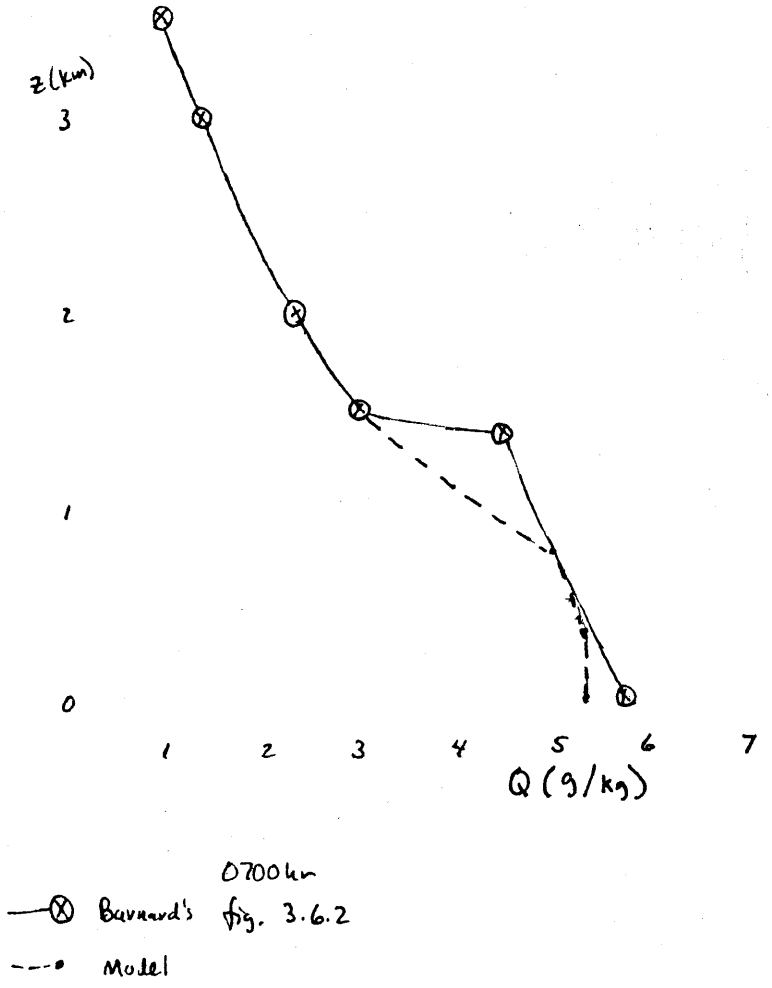


Fig. 2.20

Comparison of Barnard's (1977) model output (dashed line) with present model (solid line) for PBL moisture at 0700 LST.

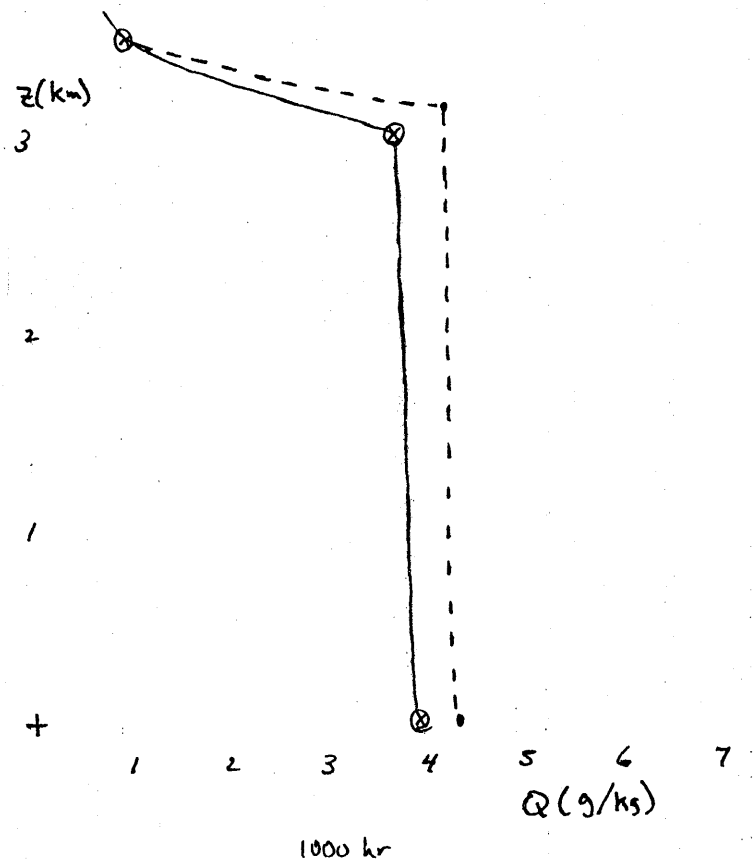


Fig. 2.21 Same as Fig. 2.21 for 1000 LST.

# CASE STUDY I: 19 APRIL

## 3.1: Introduction

The period 12 GMT April 19 to 00 GMT April 20 was characterized by weak synoptic scale activity throughout much of the SESAME region. The SESAME region is defined on Fig. 3.1. Most of the large-scale features were nearly stationary, and were nearly constant in intensity. During this period convection occurred in many different areas at different times. Some of the convection was ongoing at 12 GMT, while one outbreak occurred in western Kansas very late in the day on 19 April. After a brief review of the synoptic conditions, this last outbreak is studied in detail.

## 3.2: Synoptic Analysis

The series of 500 mb analyses (Figs. 3.2 and 3.3) shows that the cyclonic vorticity advection (CVA) from a short wave in Idaho west of the region at 12 GMT moved into western Kansas and Nebraska by 00 GMT 20 April. Fig. 3.4 shows the associated surface trough which stretched north/south across the country just east of the Rocky Mountains at 12 GMT. Even though the forcing aloft had moved over western Kansas and Nebraska, the surface trough barely moved or deepened by 00 GMT, 20 April (Fig. 3.5). The SESAME region experienced

undisturbed southerly flow at the surface most of the 12 hours during this period.

## 3.3: Mesoscale Analysis

The convection broke out almost instantaneously in a line between 21 and 22 GMT in western Kansas. Figs. 3.6 through 3.9 show the radar film taken at Garden City, Kansas (GCK) at four times during this outbreak. Notice that the large echo to the south was a hailstorm which was associated with convection which began earlier near Amarillo, Texas (AMA). The squall line is located to the northeast along the 20-25 degree azimuth. It is clear from these films that the convection to the north in Kansas was not forced by outflow from the southern storm. Fig. 3.7 was only 20 minutes after Fig. 3.6 , and convection was beginning as far away as 100 km north of the southern storm. Also, if this had been redevelopment, the outbreak would have been sequential not simultaneous. This squall line clearly originated by an independent mechanism.

On the surface analyses, a warm tongue was evident at 12 GMT (Fig. 3.10) as a large area of 298-300 K potential temperature in western Kansas and the Texas Panhandle. This tongue of warm air became warmer and better defined with time. By 16 GMT (Fig. 3.11), the cool outflow from the active convection in the Panhandle had distorted the shape of the

tongue. However, to the north in western Kansas, skies were mostly clear (Fig. 3.12) and the BLH continued. By 21 GMT (Fig. 3.13) a strong temperature gradient existed on the eastern edge of the intense warm tongue. Notice that convergence was evident in the surface winds across this gradient.

By 22 GMT (Fig. 3.14) the convection had erupted, but notice that the outbreak was apparently on the warm side of the gradient, near the axis of the warm tongue, just as Darkow et al. (1958) found in their study. This was a region of weak convergence in the surface wind field. The thermodynamic changes were clearly large and are examined here.

## 3.4: Soundings

At 11 GMT the Dodge City, Kansas (DDC) sounding (Fig. 3.15) showed a wet layer near the surface topped by an inversion which gave way to a large, dry adiabatic layer. By 14 GMT (Fig. 3.16), the bottom of the layer near the surface was beginning to heat and the inversion was lower and sharper. An isentropic trajectory at 309 K showed 30 mb of subsidence for the inversion air during this period. By 17 GMT (Fig. 3.17), very little had changed except that the strong BLH had produced a deep, well-mixed boundary layer, still capped by the inversion. This trend continued through the next three

hours. By 20 GMT the earlier hailstorm was just to the south, and likely contributed to the structure shown in Fig. 3.18. The PBL no longer was well-mixed in q, although it still was dry adiabatic.

Another example of the BLH changes was seen in the Goodland, Kansas (GLD) soundings. The 11 GMT GLD sounding (Fig. 3.19) showed a shallow moist layer near the ground capped by a strong inversion, with a large dry adiabatic layer aloft. During the next three hours strong subsidence, as shown by trajectory analysis, sharpened the inversion and lowered it, while the layer near the ground began to heat. By 20 GMT (Fig. 3.20), the GLD sounding had a huge, dry adiabatic boundary layer without an inversion, due mostly to BLH. Surface advection was calculated by computing $\vec{V} \cdot \nabla \theta$ and $\vec{V} \cdot \nabla q$ at each hour. There was very little temperature advection, but the moisture drop at GLD had an advective contribution. On Fig. 3.11, there was dry advection at GLD.

Modelling was used to confirm this explanation of PBL development. The 20 GMT model result is shown on Fig. 3.21. The initial sounding was the 11 GMT GLD sounding, and the soil parameters were 20% and 50% surface soil moisture and bulk soil moisture respectively. The model did not reproduce all of the drying actually observed although it did duplicate the very large PBL growth. The model showed a dewpoint of about 7

deg C , while the 20 GMT observation was about 3 deg C. Dry advection must have been responsible for the rest of the drying.

Notice that this sounding was too dry to support any moist convection. The sounding at Concordia, Kansas (CNK) was on the cool side of the gradient. At 11 GMT (Fig. 3.22) it showed a deep moist layer above the surface and a dry adiabatic layer aloft, with no inversion in between. By 14 GMT (not shown) CNK had a subsidence induced inversion below the dry adiabatic layer. During the next six hours, some upward and some downward vertical motion could be seen on trajectories but all of modest amounts (less than 10 mb in three hours).

The 20 GMT sounding (Fig. 3.23) showed a very small well-mixed boundary layer emerging under the still nearly saturated layer above. This sounding never got enough incident radiation through the clouds to sufficiently heat the boundary layer. Modeling of this sounding confirmed the cloud hypothesis. The soil parameters used were 50% and 50%, reasonable numbers considering that the rainfall of the previous day was only between .02 inches and a trace near CNK. The model run produced saturation at the top of the PBL (it was cloudy all day) and the PBL moisture stayed very high, with a surface dewpoint of 16-17 deg C. The end result for

CNK was a cool, strongly capped PBL, and no convection (see Fig. 3.24).

None of the soundings were in the region where the convection actually broke out. The squall line developed between GLD and CNK, and north of DDC. The field of change of surface potential temperature and dewpoint is shown on Fig. 3.25 for the period 12 to 22 GMT. The area of outbreak was in the region of strong heating (not the strongest) but was also in the area of moderate drop in dewpoint. The convective region experienced very little advection. Calculations were made from hourly analyses at each end of the outbreak area: Hill City, Kansas (HLC) and DDC. The results appear on Table 3.1. The advection contributed between 0 and 2 K to the change in potential temperature of 11 K.

Many possible triggers could be eliminated from consideration in this case. As shown, synoptic-scale frontal activity was weak, and remained to the north. The station reports of altimeter setting were examined for gravity wave activity, but none of any consequence was found. Wind shear was weak in the region, so that symmetric instability was unlikely. The most likely trigger was an inland sea breeze, across the remarkable temperature gradient which formed during the day. As already noted, some convergence was seen on the surface analyses (see Fig. 3.13), although it was weak and did

not seem to change very much with time. An inland sea breeze (or any sea breeze) circulation should increase in intensity as the temperature gradient sharpens. There was no other clear source for the convergence. The creation of the temperature gradient would, through thermal wind arguments, require an increase in the vertical shear. An inland sea breeze circulation would have satisfied this requirement.

## 3.5: Hybrid Modelling

To test the importance of various factors affecting the creation of convective instability and convective inhibition, a hybrid sounding representing the outbreak area was constructed from nearby data. This construction was made for 11 GMT. Surface analysis was used for the surface conditions, and both isentropic and isobaric analyses for the upper air data. Isobaric analyses were done at 500 mb and 700 mb. Most soundings from the eastern side of the network showed a nearly dry adiabatic layer between 311 and 313 K. So analyses for 313 and 311 yielded the top and bottom of this layer. Analyses were also done at theta = 309, 305 and 301 K. Data above 500 mb were interpolated from the three nearest soundings: CNK, DDC, and GLD. This 11 GMT hybrid sounding (APRHYB) is shown in Fig. 3.26. It was used to investigate the significance of various factors, as discussed below. The most important aspect of the hybrid sounding was the prominent

inversion at 750 mb, which represented the bottom of the thick, almost dry adiabatic layer. This inversion proved to be a barrier to growth of the PBL, and the adiabatic layer above was responsible for the large potential for convective instability. The other interesting aspect of this sounding was that the lower part of the sounding was very wet, filled with cloud. This cloud layer was significant in the time evolution of the PBL.

The bulk soil moisture was fixed for the model by trial and error to some extent, as well as by considering rainfall over the past month. This rainfall was not unusually large or small, hence the expected bulk soil moisture was expected to be near 50% and no higher than 80% at the most extreme. The integrations were performed with both values, with the expectation that the 50% bulk moisture would give more realistic results unless the soil proved to have very poor drainage.

The initial surface soil moisture was set in a similar way but using the previous day's (April 18) rainfall pattern. The map for Kansas is shown in Fig. 3.27. Notice that the region around GLD was dry. The area stretching north from DDC to HLC was generally much wetter, with amounts over .10 inches to more than .50 inches in some places. Clearly, the initial soil moisture in this second area was higher than that near

GLD. The rainfall also implied that the soil would not be very dry in an absolute sense, but beyond these general statements, it was difficult to be more precise about what numbers to use for the initial soil moisture. A range of values was therefore used in the modelling.

The model was run first without any clouds or changes above the PBL to establish the importance of the various combinations of bulk moisture and initial soil surface moisture. Several aspects of the model behavior, shown on Table 3.2, were interesting. In this series of runs, there was a direct relationship between the final height of the PBL top, surface temperature, and surface moisture. The warmer the PBL was (higher surface temperature), the higher the PBL top grew and the dryer the PBL was. This could be simply understood. The rise of the PBL top depended upon the sensible heat flux from the ground, which was also responsible for heating the air. So warmer surface temperatures were correlated with deeper PBLs other things staying the same. The PBL top rose by entraining air from above the inversion into the PBL. The initial hybrid sounding was dryer with increasing height from the surface to the top of the atmosphere. So as the PBL grew, dryer air was entrained and hence the PBL dried out.

The deepest any of the PBLs grew was 751 mb; none of the

runs could penetrate the inversion at 750 mb. Indeed as Fig. 3.28 shows, the rate of rise tended to drop off by 21 GMT, almost to zero. This was due to both the decrease in sensible heat flux and the entrainment of stable air from the inversion.

The model predicted saturation or oversaturation at the top of the PBL after 16-17 GMT in all but the dryest of the runs, which could have happened for two reasons. First, the model assumes a perfectly well-mixed PBL, with constant mixing ratio all the way to the top. Often, in reality, and especially with deep PBLs, q decreases with height. However, in the model runs, the saturation occurred with shallow PBLs, and was persistent enough to remain an inconsistency in these runs. A second possible reason for the saturation was that the PBL top rose too quickly at relatively cool temperatures, so that the saturation mixing ratio aloft was too low for the available PBL moisture. This would, in reality, lead to cloud formation at the top of the PBL, which was presumed not to happen in these runs. Hence, the inconsistency was important in judging the realism of the results.

The PBL behavior was understandable in relationship to the various ground wetness parameters. The 20-50 run, (20% initial soil surface moisture, 50% bulk soil moisture) with the dryest soil had the warmest, dryest, and deepest PBL. The

wetter soils, 50-50 and 50-80 had successively cooler, wetter, and shallower PBLs.

The instability measured by PLI values behaved in direct relationship to the ground wetness as well. The coolest run, 50-80, had the highest PLI value, while the dryest run, 20-50, had the lowest. Generally, the PLI rose in response to both warmer temperatures and higher moisture values. The drying effect overcame the heating in these runs, and the PLI was essentially controlled by the soil moisture. For these runs, the negative area calculation followed the same pattern as the PLI values. The most stable run also had the most negative area, by more than 20%. Since no changes were allowed to occur above the PBL during these three runs, the only ways the negative area could increase were for the PBL parcel to follow a "colder" pseudo-adiabat, or for the PBL to be shallower, leaving more of the stable air above the PBL for the parcel to travel through. (The parcels, when lifted for the PLI calculation, follow a line of constant equivalent potential temperature. So by "colder" pseudo-adiabat we mean a smaller equivalent potential temperature.) In these runs, the "warmer" pseudo-adiabats for the wetter soil runs more than offset the shallower PBLs, compared to the 20-50 run. The 50-80 run had slightly more instability than the 50-50 run, but was shallower, giving a slightly larger negative area.

When clouds (as shown on Table 3.3) were added to the model, without any other changes, the results changed in particulars, but not in qualitative terms. That is, the PBL still heated in relation to the soil moisture, just as when no clouds were present. The PBL grew as before and reached nearly as high by 21 GMT as in the cloudless runs. Quantitatively, the runs with clouds behaved similarly to cloudless runs with wetter soil. The results for cloud runs are shown in Table 3.2. For the same soil moisture, adding clouds cut the PBL growth by 6%, and the surface temperature rise by 10%. Notice that the 50-50 run without clouds had almost exactly the same surface temperature and PBL depth as the 20-50 run with clouds. The difference was only 0.1 deg C at the surface and 1 mb in depth.

The PBL moistures for the runs with clouds were, however, only marginally bigger than for the same runs without clouds. The drop in QS was reduced by 7% for the cloudy runs. For instance, the 20-50 cloudy run had a PBL moisture of 10.1 g/kg while the cloudless 20-50 run showed 10.0 g/kg. One explanation for this behavior is that the entrainment for the cloudless runs was only a little greater than the cloud runs (PBL depth 7-13 mb greater). But the same argument could be used when comparing the 20-50 and 50-50 cloudless runs in which the moisture difference was much more than 0.1 g/kg. This suggests that the ground wetness which is the most

important factor in determining the latent heat flux, was the major controlling influence on the PBL moisture.

The initial behavior of the runs with clouds determined the subsequent moisture behavior by raising the surface soil moisture. When the clouds were present, the latent heat flux was low, and the surface soil moisture rose due to flux from lower layers. (In the case of the 50-50 runs, the cloudy 50-50 run's surface soil moisture dropped less quickly.) During this cloudy period, the PBL was growing slowly so the surface moisture changed little. When the clouds broke up, the cycle began as with the cloudless case, but with an increased soil moisture available. Hence the cloudy cases were slightly wetter than the cloudless ones for the same soil moisture.

The PLI behaved in a similar way as for the plain runs. The dryer run was the least unstable, while the wettest run showed the greatest instability. Notice, however, that the runs all showed less instability than their cloudless counterparts. The increase in instability was reduced by 10% when the clouds were added. Although the cloudy runs were wetter and had shallower PBLs, the additional heating in the cloudless runs was enough to give bigger values of convective instability.

The inhibition change between the cloudless and cloudy runs was variable, depending on soil moisture. For the dryest soil, adding clouds more than doubled the negative area. The wettest soil was only greater by 11%. The cloudy 50-50 run showed more than a 25% increase in inhibition. There were two reasons for the increased inhibition. The cloudy 50-50 run had a smaller PLI and therefore followed a "colder" pseudo-adiabat. Also, the cloudy PBL had a shallower PBL, a difference of nine mb between the two runs. Both of these effects increased the negative area. Between the cloudy runs themselves, the behavior was the same as for the cloudless runs. The most stable run had the most negative area, and the most unstable run had the smallest inhibition.

The last point concerning these runs is that all of them showed saturation by about the same time as in the plain runs. Although the clouds reduced the growth of the PBL, the PBL still grew too quickly for the amount of heating, and the top became saturated or oversaturated at the time when the clouds were expected to dissipate.

It was somewhat surprising that the cloudy runs were similar in some respects to the cloudless runs. The clouds which were added were meant to simulate the actual behavior of the outbreak region during the day. As noted already, the low clouds broke up completely by 16-18 GMT, and this behavior was

incorporated in the modeling with clouds. The actual cloud amounts were set by referring to the soundings and relating them to the surface observations of clouds when available. The clouds were thick in the initial sounding (see Table 3.3) and thinner at 14 GMT. As the PBL heated, the cloud layers which were entrained into the PBL were assumed to dissipate, although the PBL top itself could remain cloudy.

This time variation of cloudiness was a crucial part of the model behavior. The initial clouds affected the energy budget of the PBL for the whole day only slightly, since the major portion of the heating took place during the middle of the day. Additionally, the clouds did not shut off all heating, only halved it, so the PBL did heat even with the clouds present. Fig. 3.29 shows the time variation of relevant parameters for the 50-50 run with clouds.

A related model run was made to document the effect clouds could have when present for the whole day. The data used was for CNK, which was cloudy for the whole day. The results for cloudy and cloudless runs are shown in Figs. 3.30 and 3.31. Notice that the net radiation for the cloudy run was less than half that for the cloudless run, and that the height of the PBL top was cut by almost 50%. Similarly, the rise in surface temperature was only 5.2 deg C for the cloudy case compared with 8.2 deg C for the cloudless case.

The next physical factor included in the model was changes imposed at the inversion. In the initial hybrid sounding, the major inversion was most prominent at 750mb. In the SESAME soundings, specifically DDC, GLD, CNK and North Platte, Nebraska (LBF), significant changes occurred at and just below the inversion. The most significant changes occurred between 11 and 14 GMT, and appeared to be the result of subsidence at the bottom (and perhaps throughout all) of the large dry-adiabatic layer in the middle of the atmosphere. A portion of the DDC soundings at 11 and 14 GMT are plotted together on Fig. 3.32 to illustrate the change. The subsidence was between 20 and 50 mb at both the 310 and 307 K isentropes, and also occurred at CNK and GLD between these two times. A similar change occurred at LBF between 14 and 17 GMT.

This effect was included in a series of integrations using the same soil parameters as before. The results appear in Table 3.2. The actual changes incorporated in the hybrid sounding were +3 deg C at 775 mb and +2 deg C at 800 mb along with appropriate drying of the moisture profile. By 21 GMT, the PBL top was 10-20 mb lower with the changes, compared with the runs made without the inversion changes. The time evolution is shown on Fig. 3.33. Notice that for the early part of the run until about 1530 GMT, the run with inversion changes was identical to the plain run in Fig. 3.28. The surface temperatures grew a little faster, by about 4%. The

height of the PBL top began to be different by about 1630 GMT, and the difference was significant by 21 GMT, almost 20 mb. The biggest change appeared in the PBL moisture, starting at 1530 GMT. By the end of the integration the surface moisture for the run with changes had dropped 33% more than the plain run. The drying imposed above the PBL contributed to a dryer PBL through entrainment, since the other parameters were unchanged.

The PLIs varied with moisture and ground wetness as before. The differences in PBL moisture had a big effect on the PLI as expected. The 20-50 run with inversion changes was much more stable than its plain counterpart, a reduction in growth of almost 30%. The difference was less for the 50-80 run, but was still more than 10%.

The negative area changed more than any other aspect of the runs with inversion changes. The values had increased between 80% and 180% over the plain runs. This large change showed the effects of both the increase in the stability above the PBL and the "cooler" pseudo-adiabat which went with the lessened convective instability. Notice that the 50-50 run had less negative area than either the 20-50 run or the 50-80 run. The 20-50 run had a 15 mb higher inversion which could not overcome the effect of a much "colder" pseudo-adiabat. The difference between the 50-50 and 50-80 runs was only 6 mb,

but the "warmer" pseudo-adiabat for the 50-80 run could not overcome the effect of a shallower PBL.

The other change which was apparent in these runs was that the saturation was much reduced. In the 20-50 run with inversion changes, none occurred. In the other two, it only happened for two hours midway through the integration (see Fig. 3.33 for the 50-50 run). The change in PBL moisture due to the enhanced entrainment was enough to almost balance these runs with respect to this saturation condition.

In addition to the changes at the inversion, changes occurred above the inversion level between 14 and 17 GMT. Observations at DDC and GLD were used to determine appropriate changes to use for the model sounding. These changes were similar at DDC and GLD, but had differences in details. At GLD, the middle atmosphere cooled both during 11 to 14 GMT and from 14 to 17 GMT. At DDC, cooling only occurred from 14 to 17 GMT, and was not as pronounced as at GLD. LBF also showed the GLD pattern. The two sets of changes are shown in Tables 3.4 and 3.5, and were applied in separate runs to the hybrid sounding.

The results of the runs with the DDC changes added on are shown in Table 3.6. The most important part of the DDC changes were those which occurred between 14 and 17 GMT near

775 mb and 800 mb. When DDC showed cooling there, it was accompanied by moistening as well. So the effect of entrainment in the PBL was lessened, and the PBL moistures in the DDC runs were much higher than those with only inversion changes. the amount of drying was reduced by 10% to 30% from the plain runs. Surface temperatures were about the same, 5% more rise than the plain runs and the PBL growth was reduced by 1% to 10%, similar to the inversion change only runs.

The PLI responded strongly to this change in moisture with the DDC PLIs ending up 10% to 15% higher than those with inversion changes only. Curiously, the PLI for the 50-80 run with DDC changes was now lower than that for the 50-50 run. The difference in moisture no longer overcame the heating difference. The convective inhibition was less than half that for the run with inversion changes, and near the values computed for the plain model without clouds. This change in the negative area was due to both the cooling above the inversion and the "warmer" pseudo-adiabat of the DDC run. For this series of runs, the 20-50 run was the most stable and had the least negative area, due entirely to the higher PBL tops. The 50-50 and 50-80 runs exhibited the same behavior as most of the previous runs, following the trend in the PLI values. However, with this series the 50-50 run had a higher PLI than the 50-80 run. The extra moisture also gave a longer period of saturation at the top of the PBL in the 50-50 and 50-80

runs. With DDC changes, this condition was present for three hours instead of two (see Fig. 3.34).

The model was next run with the GLD changes in addition to the inversion changes. The sense of the GLD changes was the same as the DDC ones, except the GLD changes began with cooling aloft at 11 GMT and continued till 17 GMT. The results for the GLD runs are shown in Table 3.6. The most striking development was that the 20-50 run showed so much growth. In fact, the PBL heated enough in this run to bypass the inversion at 775 mb, and reached up into the dry adiabatic layer aloft. The surface temperature was very high, and moisture low, due to the entrainment of very dry air aloft. The wetter runs did not heat up as much and could not fill the 775 mb inversion. As a result, the 50-50 and 50-80 runs were almost duplicates of the 50-50 and 50-80 runs with inversion changes only.

This duplication was seen in the PLI values too. The 50-50 runs were identical, even in time sequence (see Figs. 3.33 and 3.35). The 20-50 run had much less instability than the wetter soil runs. The 20-50 run's PBL top was just saturated at 21 GMT, and there was no negative area left. Both the 50-50 and 50-80 runs were oversaturated for two hours just as their counterparts with inversion changes only. The negative area for the 50-50 run was 20% lower than the plain

50-50 without clouds. This low value reflected the low stability above the inversion. Both the PBL depth and the PLI value were identical for the 50-50 GLD run and the 50-50 run with inversion changes.

On Fig. 3.36 the sounding for the hybrid 50-50 run with GLD changes at 21 GMT is plotted. Notice that the layer from 775 mb to 750 mb was superadiabatic. This resulted from having imposed changes at 750 mb and not having any corresponding changes at 775 mb. In reality, the whole adiabatic layer cooled, so that it made sense to include a change at 775 mb. Additionally, the GLD PBL grew past its inversion between 14 and 17 GMT. The PBL temperature at 17 GMT at GLD was not high enough to have enabled this to occur without cooling of the inversion itself. Hence, there was much indirect evidence to support cooling at 775 mb from 14 to 17 GMT. This was incorporated in a later run.

The next series of runs added clouds to the DDC and GLD changes, to combine these effects. For the DDC runs, shown on Table 3.6, the addition of clouds made a small but important difference in the development of the PBL. The PBLs were slightly cooler and wetter, and slightly shallower. The PBLs grew 6% to 16% less than the plain runs, but the surface temperatures were nearly the same. The PBL moisture dropped less, by 10% to 30% depending on soil moisture. The 50-50 and

50-80 runs developed more slowly with time, and were only saturated for two hours instead of three. This effect was due to the reduced heating. At 1600 GMT, the PBL top for the cloudy 50-50 run was 20 mb lower than for the cloudless 50-50 run, and the surface temperature more than 0.5 C cooler (see Figs. 3.34 and 3.37).

Just as for the plain runs, the cloudy runs all showed less instability than the cloudless runs, although the differences were small. Notice by comparison of Figs. 3.34 and 3.37 that the time evolution of the PLI for the cloudy case fell behind the cloudless DDC 50-50 run at about 16 GMT and never quite caught up. The negative area was about 40% higher than the comparable plain runs.

The GLD run with clouds was more different from its cloudless counterparts than the DDC runs. The 20-50 run was totally different, but this run was an anomally in this series. Close examination of the output showed that the two runs (cloudless and cloudy 20-50 with GLD changes) were actually similar, but separated by time. The values of temperature, moisture and PBL depth at 21 GMT with clouds were virtually identical to those of the cloudless run at 20 GMT. Even the PLIs were almost the same, 4.0 and 4.1. The cloudiness delayed the heating cycle by enough to set the PBL dvelopment back one hour.

The 50-50 and 50-80 cloudy GLD runs were less different at 21 GMT than the 20-50 run. The cloudy PBL's moisture dropped 20% more than the plain runs'moisture, compared with the 25% to 110% increase for the cloudless runs with imposed changes. The surface temperatures grew less, by 5%, so that the cloudless runs with imposed changes were warmer than the plain runs. The heights of the PBL tops were lower for the cloudy cases by almost 10 mb. However, the instability development was almost the same, and the final values only 0.1 C different. The cooler PBLs were just wet enough to have similar PLI values. The cloudy PBLs reached saturation for about 2 hours, just as the cloudless runs did, but delayed by one hour. The saturation was, however, nearly consistent with the presence of clouds in the model, so this was not an inconsistency. The negative area for the 50-50 cloudy GLD run was higher than the GLD clear runs, but much smaller than that for the 50-50 plain run. The 50-50 GLD cloudy run and 50-50 GLD clear runs had similar PLI values, so the shallower PBL was responsible for the larger inhibition (compare Figs. 3.35 and 3.38).

The final series of runs used the hybrid sounding with clouds and inversion changes, plus GLD changes modified to remove the superadiabatic layer above the inversion. The modification used was a cooling of 1.5 C at 775 mb, in addition to the GLD changes shown in Table 3.5. The results

of the runs are shown in Table 3.6. The effects were small, especially with the 50-80 run. The height of the PBL top for the 50-80 run was only three mb higher than for the comparable run without modification. The surface temperature was the same and the PBL moisture only slightly reduced. The differences were greater for the dryer runs, but even the 20-50 run was not greatly different. The 20-50 modified run's PBL was 19 mb deeper, 0.1 C warmer, and 0.4 g/kg dryer.

The PLI values for the modified runs were all smaller than those of the unmodified runs, though only slightly so for the 50-80 run. The modification had only a slight effect on these parameters due to the presence of less stable air in the layer between 775 mb and 800 mb. This difference was only realized by the model when the PBL top reached high enough to entrain this air. So, the change was only noticeable late in the runs, and especially late in the 50-80 run.

The negative area responded strongly to the change. The negative area for the 50-50 run was the lowest of any run and lower by 41% from the plain run. The reason for this was clear, since the inversion strength was much reduced in the modified run, and the instability was only slightly lower. Figs. 3.39 and 3.40 show the 21 GMT soundings for the modified and unmodified runs, with the negative area indicated on them.

## 3.6: Summary

The final series was the most realistic set of runs, since it included clouds, initial inversion changes, and the changes above the PBL including the reduction of the superadiabatic layer. Since the winds above the PBL were from the southwest throughout the period, any advective changes at DDC would have been too far south to reach the outbreak area. The pattern of subsidence affected the CNK, GLD, and DDC soundings at the same time, and subsequently moved to LBF, implying movement from the southwest as well. Hence the GLD changes were more representative of the hybrid area than the DDC changes. The surface temperature and moisture from the GLD modified runs were comparable to the observations from the analyses as well. The model surface temperature was not a 10 meter observation temperature, since the 5 mb deep surface layer was superadiabatic. The model output did include an observation temperature calculation which gave, for the GLD 50-50 modified run, a surface potential temperature of 307 K. The dewpoint in the model run was 13.5 deg C. The actual observations for the region of the outbreak were 309 K and 14 C. The dewpoints were very close. The temperature was a little cold in the model, but as the advection calculation in the analysis showed, 0-2 K of the observed rise in the outbreak region could be attributed to horizontal temperature advection. This would raise the model temperature to 309 K,

the observed value.

Some statements can be made concerning the various factors involved in the development of convective instability and negative area in this case. Clearly, most of the observed temperature rise in the PBL was due to BLH. The observations implied this, and the model results confirmed it. On Table 3.7 the sensitivity values for the various parameters are shown. As the modeling showed, the ground wetness played an important role in determining the PBL moisture, which strongly affected the PLI values. The wetter runs, although cooler, were often more unstable. However, the wetter runs had larger negative areas, since the heights of the PBL tops were lower.

The PBL depth was lower when clouds were present and for the inversion only changes. The changes aloft also contributed to shallower PBLs except in the case when the inversion was filled (20-50 run with GLD changes). Aside from that one run, the changes in growth were not large either, at most 17% for the modified GLD runs. Soil surface moisture and bulk moisture variations were similarly ineffective in having much input on PBL growth.

Surface layer temperature was even less sensitive. The presence of clouds reduced the rise by 10%, and the increased surface soil moisture reduced the rise by 11%, but the rest of

the variables had less influence. The PBL moisture values were much more sensitive to all of the factors except the bulk soil moisture and clouds. The imposed changes above the PBL (both at and above the inversion) contributed to increased drying while the increased soil surface moisture reduced the drying significantly.

The convective instability varied with the soil moisture in most of the runs. When drying increased, growth of PLI values was reduced, often by a significant amount (e.g. the inversion changes series). Similarly, increased soil surface moisture had a large positive effect on the growth of convective instability. The biggest part of the convective instability was already present in the 12 GMT sounding, with a PLI of 3.0.

The inhibition to convection was the most variable parameter, and sensitive to all of the factors, even the bulk soil moisture. In some cases, the negative area responded in different ways to the changes depending on individual characteristics. For instance, the soil surface moisture increase generally gave an increase in negative area. For the cloudy runs, however, the dryest soil run had the largest negative area. In general, the presence of clouds increased inhibition, as did the imposed changes at the inversion. The changes aloft (DDC or GLD runs) tended to strongly decrease

convective inhibition, with some exceptions.

We can realistically compare the effects of each physical factor best by considering the change in that factor in the run which includes all of the factors. This allows the non-linear combinations of factors to be present in the comparison. To allow comparison between the three case studies, only the runs with imposed changes and clouds are examined in this manner. (The other factors in each case study are not included in the other case studies.)

Schematically, the results for the 50-50 model run with clouds and GLD imposed changes can be summarized as follows in decreasing order of importance.

PLI = initial conditions + BLH + soil surface moisture - imposed changes + clouds + bulk soil moisture

NA = initial conditions - BLH + soil surface moisture - imposed changes + clouds + bulk soil moisture The effects of clouds are reversed when considered in this manner. The presence of clouds had led to lower PLI, while the addition of clouds to the run with imposed changes gave more instability. The presence of morning cloudiness exerted a strongly non-linear effect on the growth of convective instability.

It was curious and intriguing that the run which gave the most realistic results also had the smallest negative area, (for the 50-50 soil moisture) although it was not the most unstable. This was not conclusive, but it was suggestive that the convection broke out where there was substantial convective instability and where the inhibition was the weakest.

The convective instability and inhibition were calculated and analyzed at 18 and 21 GMT. These are shown on Figs. 3.41 and 3.42. Only the new echoes from the next map time are plotted on each figure. On Fig. 3.41, we see that the convection broke out in an area where NA was a minimum and convective instability a relative maximum. This outbreak was not analyzed in detail but the correlation in this instance is illustrative of the relation between convective outbreaks, NA and PLI.

Fig. 3.42 shows the outbreak which has been analyzed in detail. The convection clearly erupted in a region of moderate instability, but also a minimum of NA. Unfortunately, in both of these figures, the available data are too sparse to allow precision in these conclusions. However, coupled with the model results for the "simulation" run (50-50 run with modified GLD changes and morning clouds) the pattern of outbreak is well established in this case. The

convection began where and when moderate levels of convective instability coincided with low enough values of inhibition to allow the available forcing (surface convergence on Fig. 3.13) to start the convection.

Table 3.1: ADVECTION CALCULATION FOR APRIL CASE

| | DDC | | HLC | |
|---|---|---|---|---|
| Time | Adv. | Obs. | Adv. | Obs. |
| 12-13 | 0 | 0 | <0.2 | unknown |
| 13-14 | 0 | 0.5 | 0 | 1.0 |
| 14-15 | <0 | 2.4 | 0 | 2.4 |
| 15-16 | <0 | 2.2 | 0.1 | 1.7 |
| 16-17 | <0 | 2.9 | 0.4 | 2.4 |
| 17-18 | <0 | 1.2 | 0.7 | 1.1 |
| 18-19 | <0 | 1.2 | 0.5 | 1.2 |
| 19-20 | <0 | -0.6 | 0.4 | 1.7 |
| 20-21 | | | 0.2 | 0 |
| Total | 0 | 9.8 | 2.3 | 11.5 |

Advection calculated at Dodge City, Kansas (DDC) and Hill City, Kansas (HLC) from surface analyses. Changes are for surface potential temperature in degrees K. Time is GMT.

Table 3.2: MODEL RESULTS AT 21 GMT, 19 APRIL

| RUN | PH | TS | QS | PLI | NA | Cond |
|---|---|---|---|---|---|---|
| Plain | | | | | | |
| 20-50 run | 751 | 26.0 | 10.0 | 5.3 | 20.56 | |
| 50-50 run | 759 | 25.0 | 10.9 | 6.0 | 27.39 | S+ |
| 50-80 run | 764 | 24.5 | 11.1 | 6.1 | 28.94 | S+ |
| Morning Clouds | | | | | | |
| 20-50 run | 758 | 25.1 | 10.1 | 5.0 | 42.79 | S |
| 50-50 run | 768 | 24.1 | 11.0 | 5.7 | 34.66 | S+ |
| 50-80 run | 777 | 23.5 | 11.3 | 5.8 | 32.16 | S+ |
| Inversion Changes Only | | | | | | |
| 20-50 run | 762 | 26.5 | 9.1 | 4.4 | 57.67 | |
| 50-50 run | 777 | 25.4 | 10.2 | 5.3 | 50.08 | |
| 50-80 run | 783 | 24.8 | 10.7 | 5.7 | 60.82 | |

21 GMT values of : pressure level of inversion (PH), surface temperature (TS), surface moisture (QS), PBL lifted index (PLI), negative area calculation (NA), and condition at PBL top: blank = unsaturated, ~S = nearly saturated, S = saturated, S+ = oversaturated.

Table 3.3: CLOUDS IMPOSED IN MODEL RUNS FOR APRIL CASE

| P(mb) | 11-14 GMT | 14-17 GMT |
|---|---|---|
| 800 | 80 % | 0 % |
| 825 | 90 % | 80 % |
| 850 | 90 % | 80 % |
| 875 | 80 % | 80 % |
| 900 | 80 % | 80 % |

Cloud amounts are expressed as percentages of complete cloudcover.

Table 3.4: IMPOSED CHANGES FROM DODGE CITY, KANSAS (DDC) (INCLUDES INVERSION CHANGES) FOR 19 APRIL

| | 11-14 GMT | | 14-17 GMT | |
|---|---|---|---|---|
| P(mb) | T(deg C) | Q(g/kg) | T(deg C) | Q(g/kg) |
| 500 | 0 | 0 | 0 | 0 |
| 525 | 0 | 0 | 0 | 0 |
| 550 | 0 | 0 | 0 | 0 |
| 575 | 0 | 0 | 0 | 0 |
| 600 | 0 | 0 | 0 | +0.6 |
| 625 | 0 | 0 | +0.6 | +1.2 |
| 650 | 0 | +0.4 | 0 | +1.2 |
| 675 | 0 | +0.6 | 0 | +0.9 |
| 700 | 0 | +0.6 | -0.9 | +0.9 |
| 725 | +0.6 | +0.6 | -0.9 | +1.2 |
| 750 | 0 | +0.4 | -0.6 | +1.5 |
| 775 | +3.0 | -3.6 | -0.6 | +1.8 |
| 800 | +2.0 | -8.0 | -0.3 | +2.1 |
| 825 | 0 | 0 | 0 | 0 |

Changes taken from Dodge City, Kansas (DDC) soundings used in some model runs. Levels not mentioned or times not covered had zero changes.

Table 3.5: IMPOSED CHANGES FROM GOODLAND, KANSAS (INCLUDES INVERSION CHANGES) FOR 19 APRIL

| | 11-14 GMT | | 14-17 GMT | |
|---|---|---|---|---|
| P(mb) | T(deg C) | Q(g/kg) | T(deg C) | Q(g/kg) |
| 500 | -1.0 | 0 | 0 | 0 |
| 525 | -0.6 | 0 | 0 | 0 |
| 550 | -1.0 | 0 | 0 | 0 |
| 575 | 0 | 0 | 0 | 0 |
| 600 | -0.6 | -0.4 | 0 | 0 |
| 625 | -1.0 | +0.4 | 0 | 0 |
| 650 | -1.2 | +0.4 | -0.9 | 0 |
| 675 | -1.2 | 0 | -1.0 | 0 |
| 700 | -1.2 | 0 | -1.0 | 0 |
| 725 | -0.8 | 0 | -1.2 | 0 |
| 750 | -0.6 | -0.4 | -1.0 | 0 |
| 775 | +3.0 | -3.6 | 0 | 0 |
| 800 | +2.0 | -8.0 | 0 | 0 |
| 825 | 0 | 0 | 0 | 0 |

Changes taken from Goodland, Kansas (GLD) soundings imposed on some model runs. Levels not mentioned or times not covered had zero changes.

Table 3.6: MODEL RESULTS AT 21 GMT, 19 APRIL

| RUN | PH | TS | QS | PLI | NA | Cond |
|---|---|---|---|---|---|---|
| Inversion Changes + DDC Changes | | | | | | |
| 20-50 run | 752 | 26.7 | 9.4 | 4.9 | 16.15 | |
| 50-50 run | 773 | 25.4 | 10.7 | 6.0 | 19.42 | |
| 50-80 run | 780 | 24.8 | 10.9 | 5.9 | 31.83 | |
| Inversion Changes + GLD Changes | | | | | | |
| 20-50 run | 694 | 27.0 | 7.8 | 2.9 | 0 | S |
| 50-50 run | 778 | 25.3 | 10.2 | 5.3 | 22.12 | |
| 50-80 run | 783 | 24.7 | 10.6 | 5.5 | 24.63 | |
| Inversion Changes + DDC Changes + Morning Clouds | | | | | | |
| 20-50 run | 760 | 26.3 | 9.5 | 4.8 | 29.38 | |
| 50-50 run | 777 | 25.1 | 10.8 | 5.9 | 31.16 | |
| 50-80 run | 789 | 24.1 | 11.0 | 5.7 | 39.59 | |
| Inversion Changes + GLD Changes + Morning Clouds | | | | | | |
| 20-50 run | 776 | 25.6 | 9.4 | 4.4 | 10.84 | |
| 50-50 run | 786 | 24.5 | 10.6 | 5.4 | 24.60 | |
| 50-80 run | 792 | 24.0 | 10.8 | 5.4 | 27.33 | |
| Inversion Changes + Modified GLD Changes + Morning Clouds | | | | | | |
| 20-50 run | 757 | 25.7 | 9.0 | 3.9 | 10.02 | |
| 50-50 run | 780 | 24.6 | 10.4 | 5.2 | 16.09 | |
| 50-80 run | 789 | 24.0 | 10.7 | 5.3 | 18.67 | |

This table is in the same format as Table 3.2.

Table 3.7: SENSITIVITY VALUES FOR 21 GMT, 19 APRIL MODEL RUNS

| Physical Factor | PH | TS | QS | PLI | NA |
|---|---|---|---|---|---|
| Morning Clouds | -6 | -10 | -7 | -10 | +11 to +108 |
| Inversion Changes | -10 | +4 | +33 | -22 | +83 to +180 |
| Inversion Changes + DDC Changes | -1 to -10 | +5 | +10 to +30 | -6 | +10 to -21 |
| Inversion Changes + GLD Changes | -12 to +36 | +3 to +11 | +25 to +110 | -19 to -77 | -15 to -100 |
| Inversion Changes + DDC Changes + Morning Clouds | -6 to -16 | +3 to -4 | +5 to +25 | -11 | +40 |
| Inversion Changes + GLD Changes + Morning Clouds | -17 | -5 | +20 | -24 | -6 to -42 |
| Inversion Changes + Modified GLD Changes + Morning Clouds | -4 to -16 | -4 | +32 | -32 | -35 to -51 |
| Soil surface moisture | -7 | -11 | -31 | +23 to +77 | -22 to +61 |
| Bulk soil moisture | -4 | -6 | -15 | +3 to -3 | -8 to +21 |

Sensitivity measured as percentage change of a given variable compared with maximum amount of change in that variable after application of physical parameter. Variables as defined on TABLE 3.2. Application of soil surface moisture defined as increase from 20% to 50% of saturation. Bulk soil moisture application defined as increase from 50% to 80%.

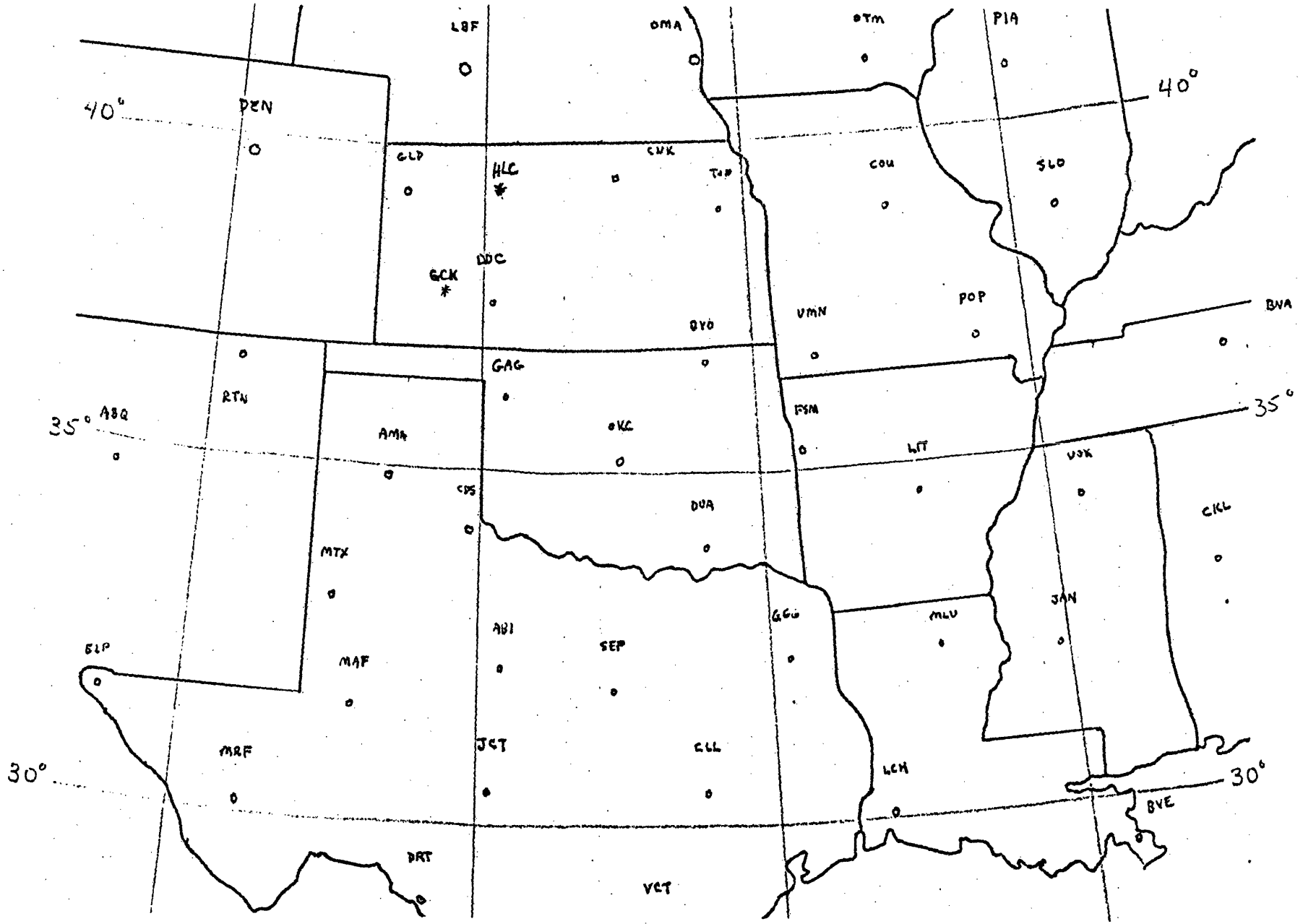


Fig. 3.1 Map of SESAME region showing sounding stations in April, and two surface observation stations mentioned later in the text.

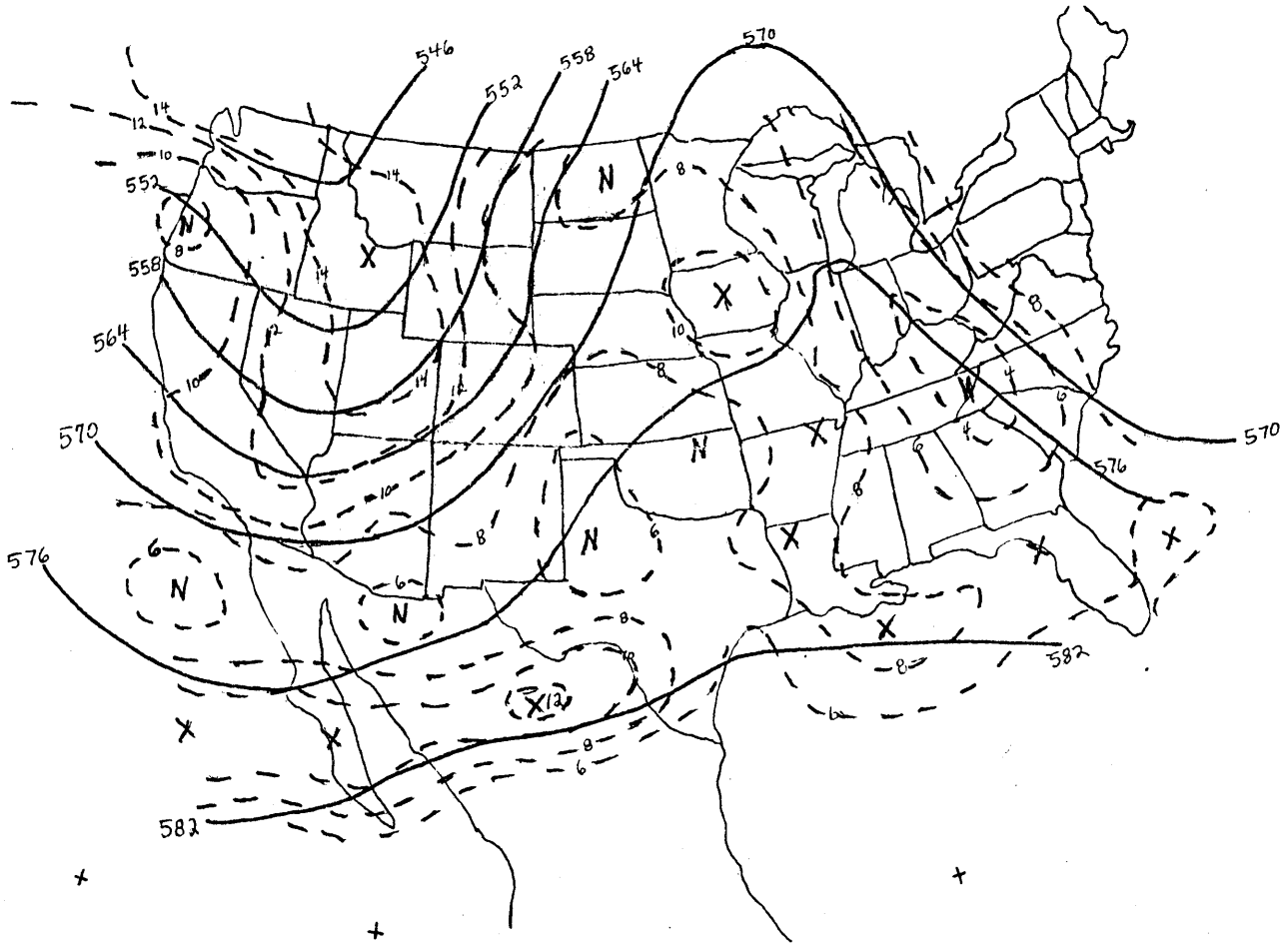


Fig. 3.2 Synoptic-scale 500 mb analysis for 12 GMT, 19 April. Heights in solid lines (dm) and vorticity in dashed lines (x 10**-5 sec*-1).

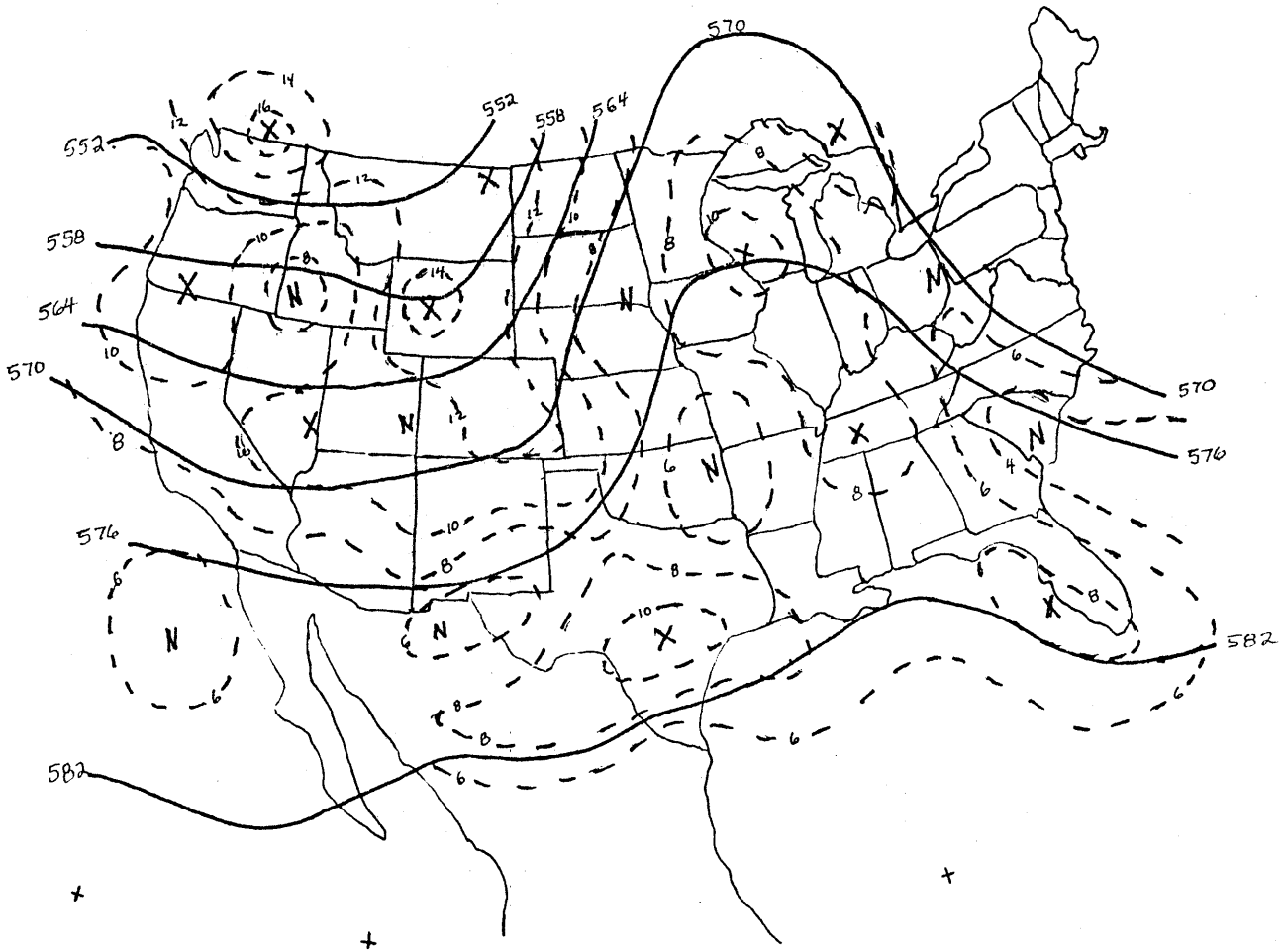


Fig. 3.3 Same as Fig. 3.2 for 00 GMT, 20 April.

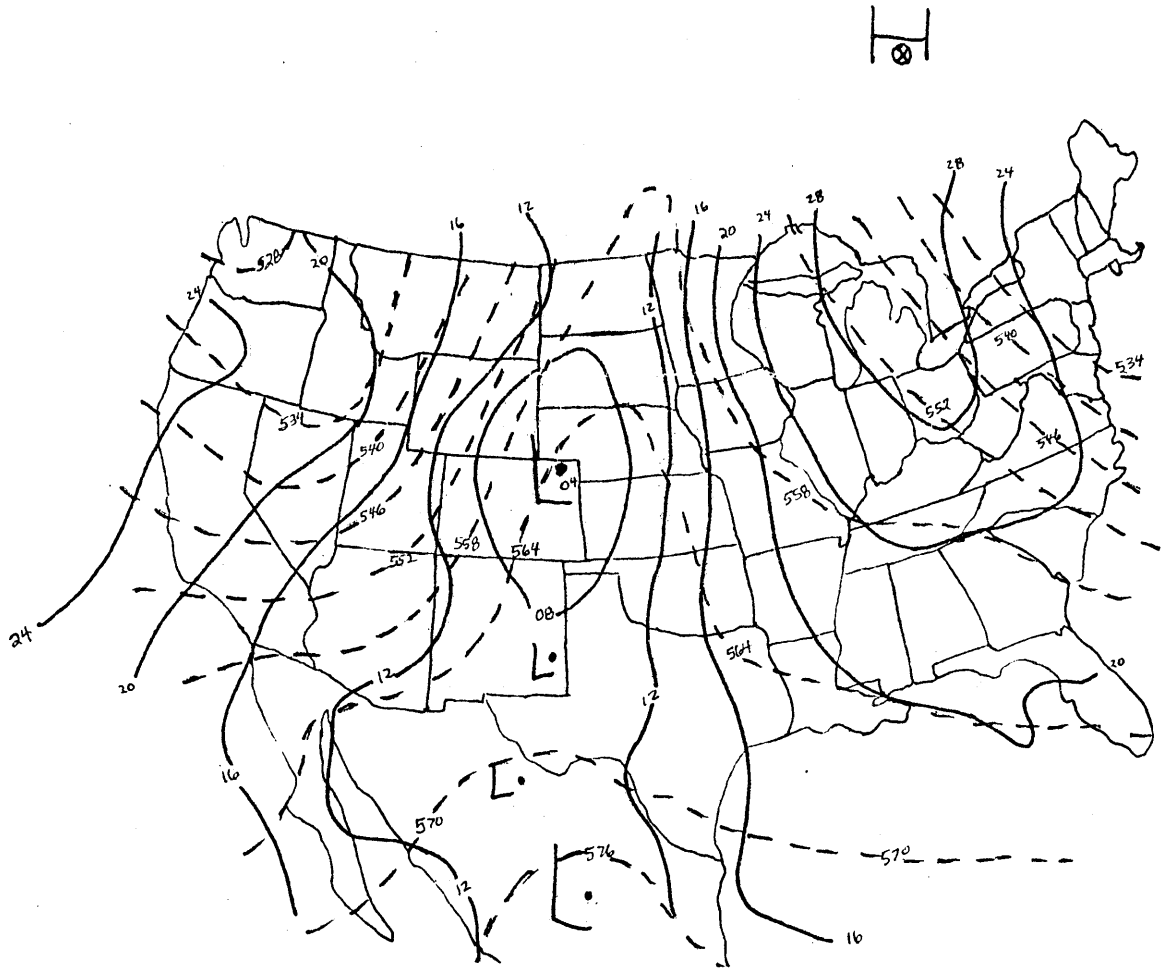


Fig. 3.4 Synoptic-scale surface analysis for 12 GMT, 19 April. Sea level pressure in solid lines (mb) with leading 9 or 10 dropped and 1000 to 500 mb thickness in dashed lines (dm).

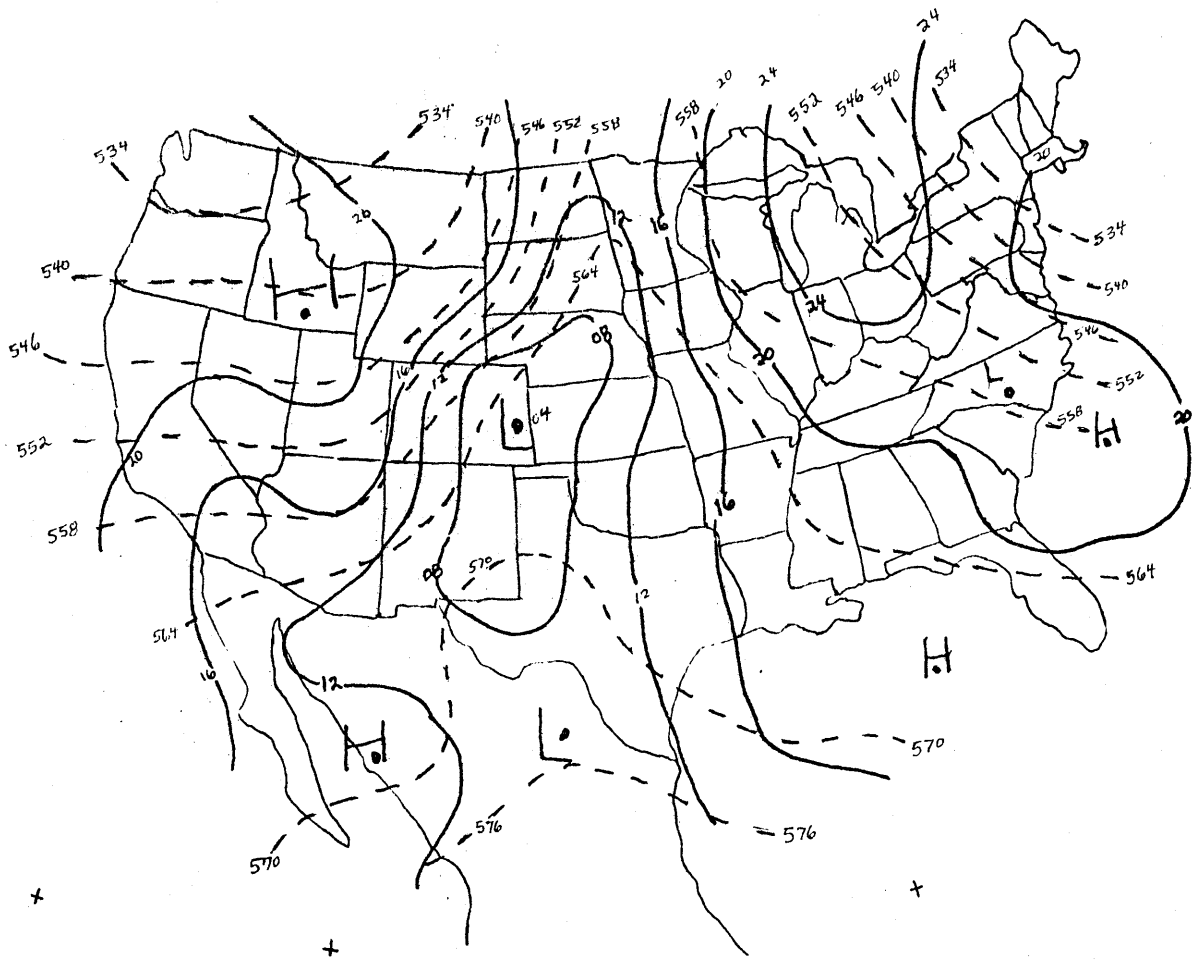


Fig. 3.5 Same as Fig. 3.4 for 00 GMT, 20 April.

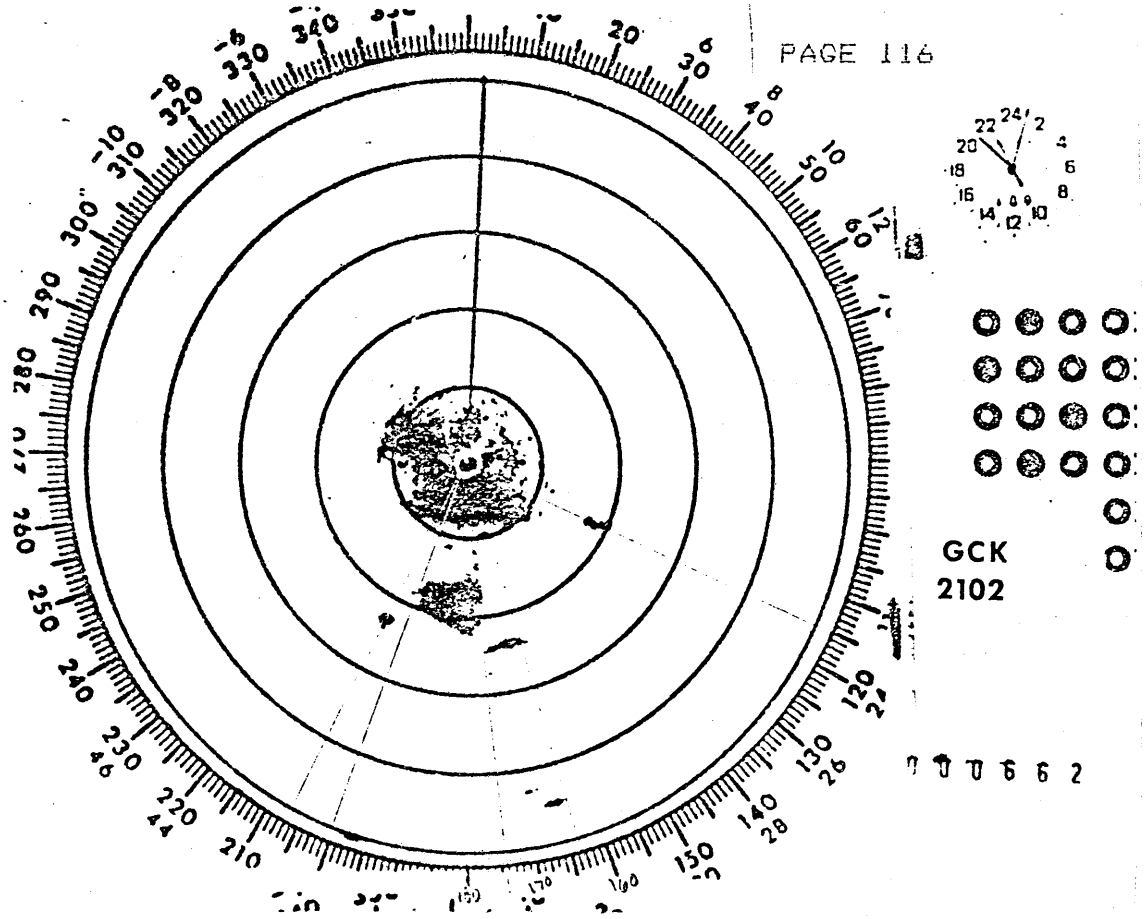


Fig. 3.6 Photograph of low-elevation angle display from radar screen at Garden City, Kansas, 2102 GMT, 19 April. Range rings are 20 nm apart.

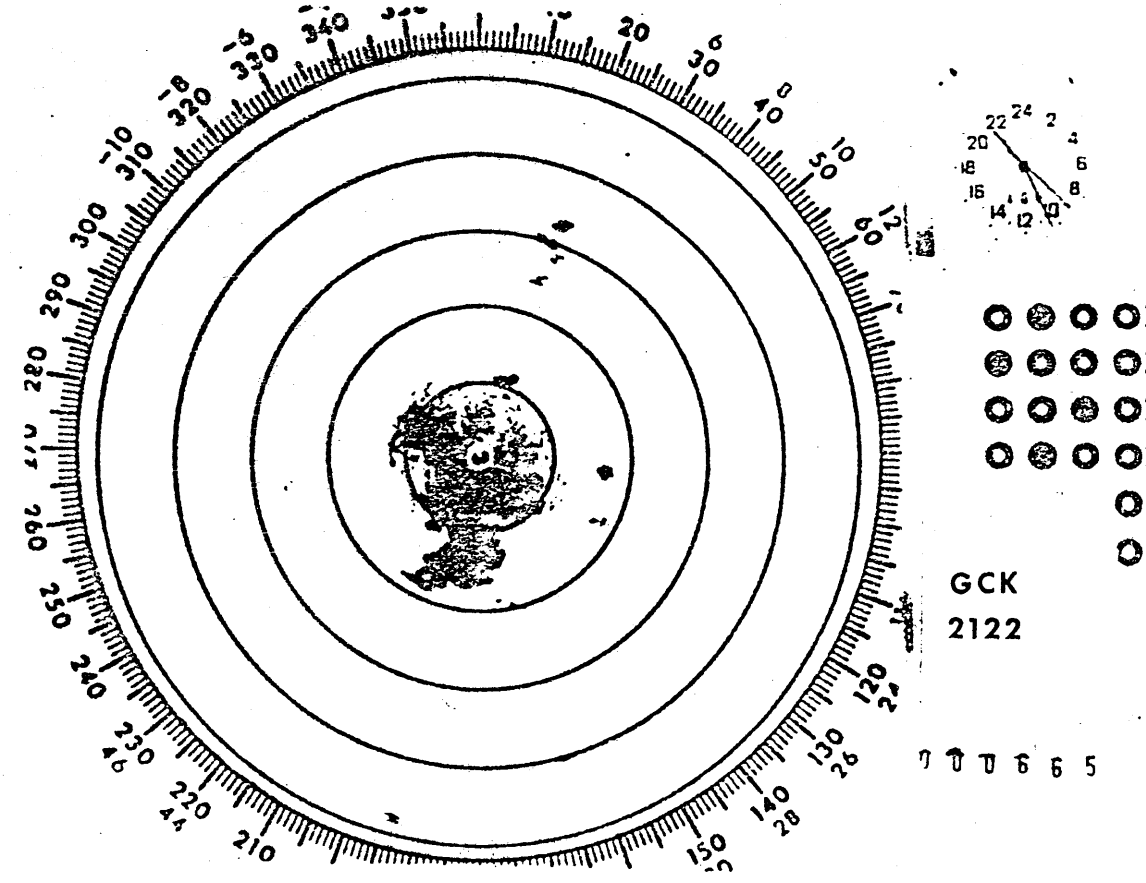


Fig. 3.7 Same as Fig. 3.6 for 2122 GMT.

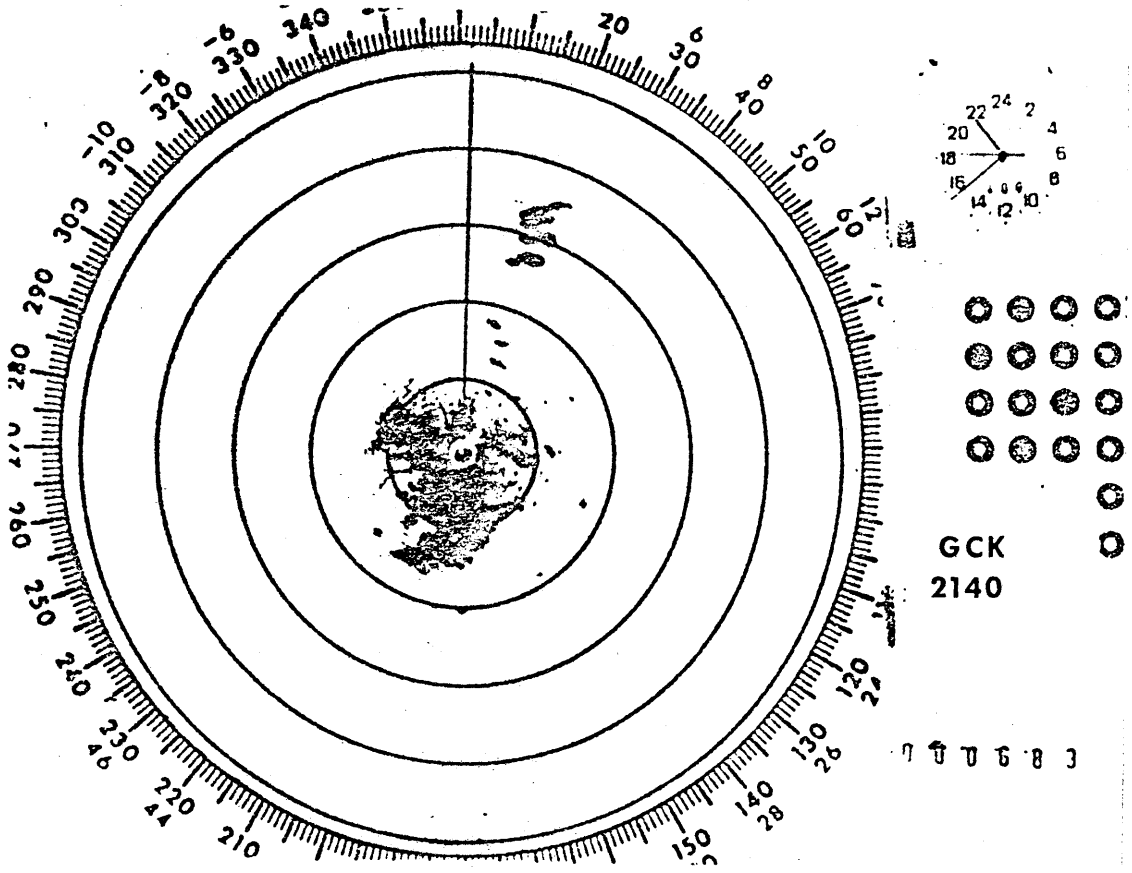


Fig. 3.8 Same as Fig. 3.6 for 2140 GMT.

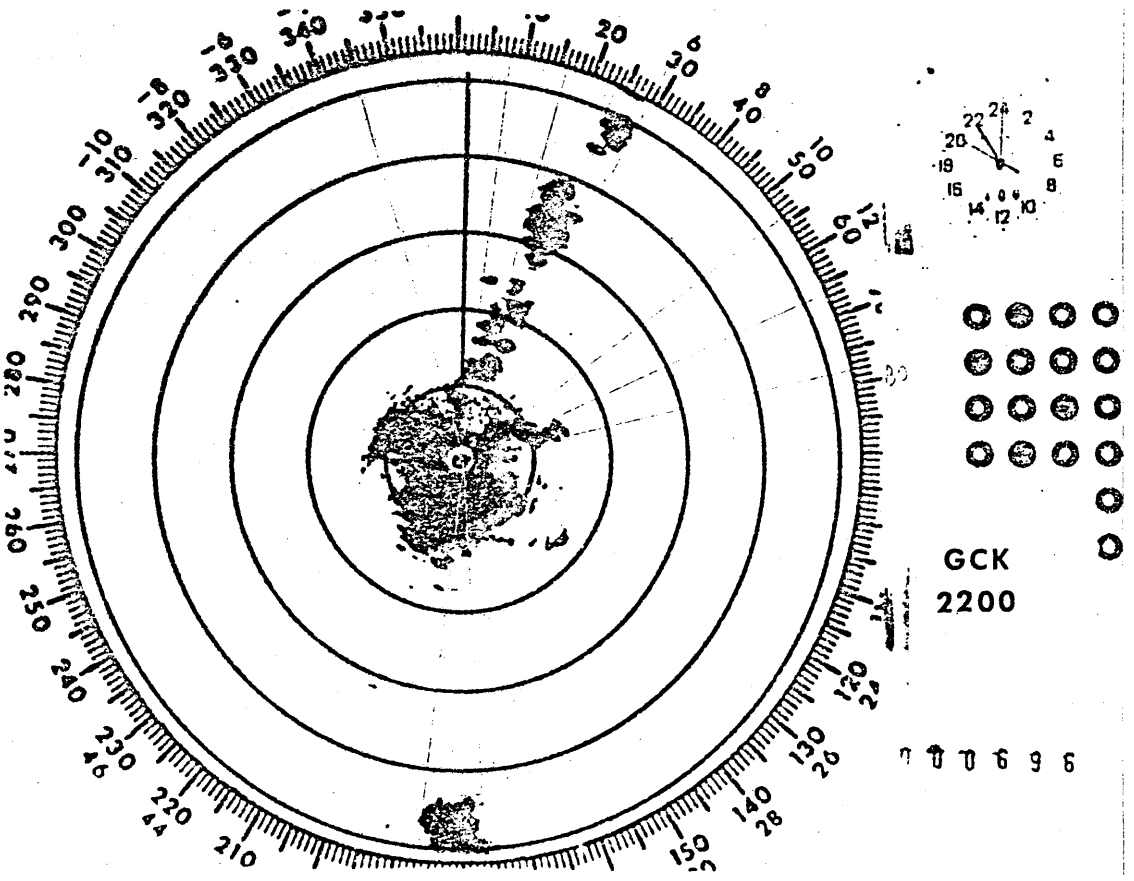


Fig. 3.9 Same as Fig. 3.6 for 2200 GMT.

Fig. 3.10 Mesoscale surface analysis for 12 GMT, 19 April. Solid lines are surface potential temperatures (K) and dashed lines are dewpoints (deg C). Winds are plotted in the convential manner (knots). Sky condition is clear (open circle), scattered (single bar), broken (double bar), overcast (filled circle), and obscured (x in circle). Cloud type is plotted (if available) as is current weather according to conventional synoptic code. Radar echoes are cross-hatched irregularly shaped areas.

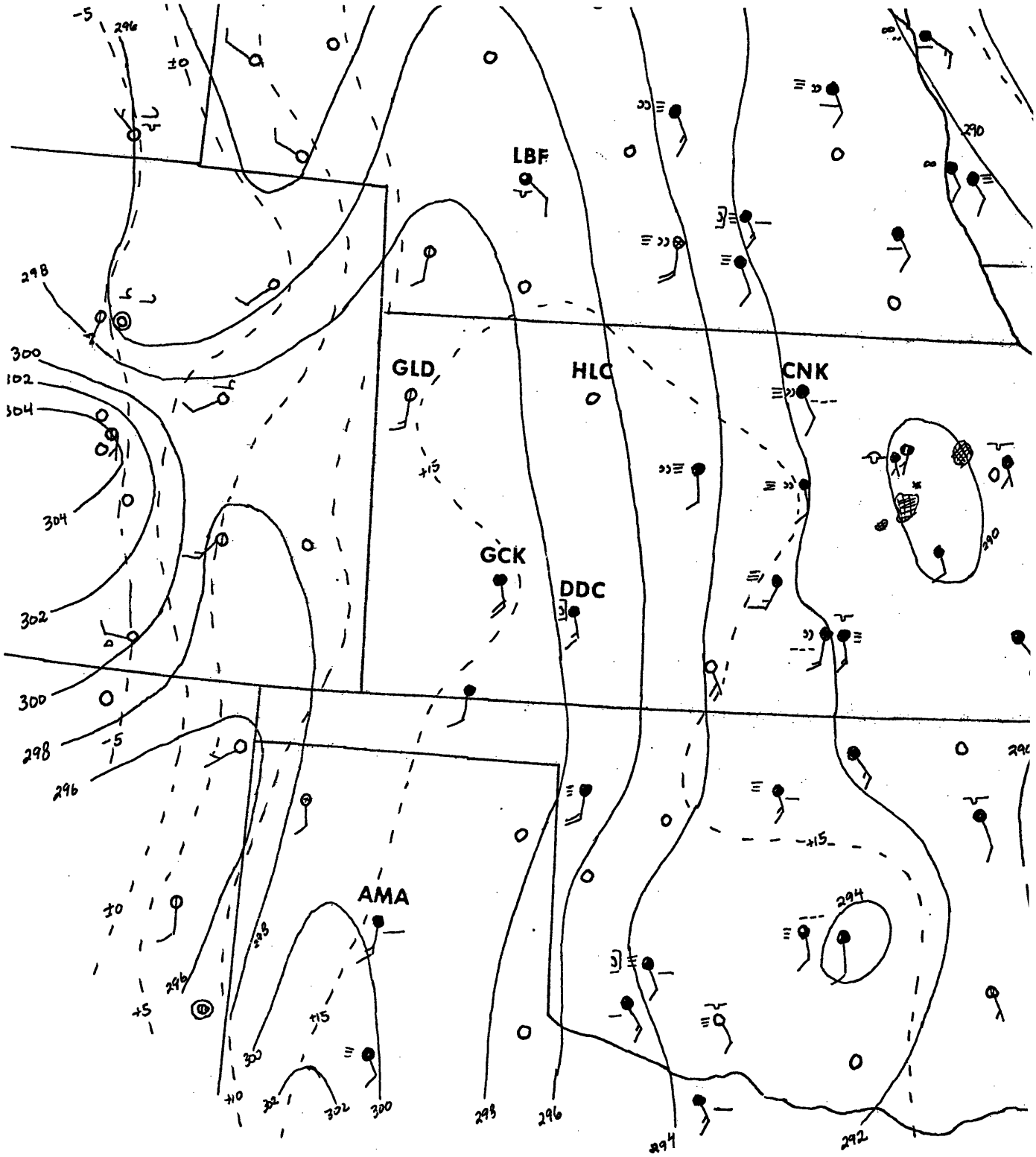

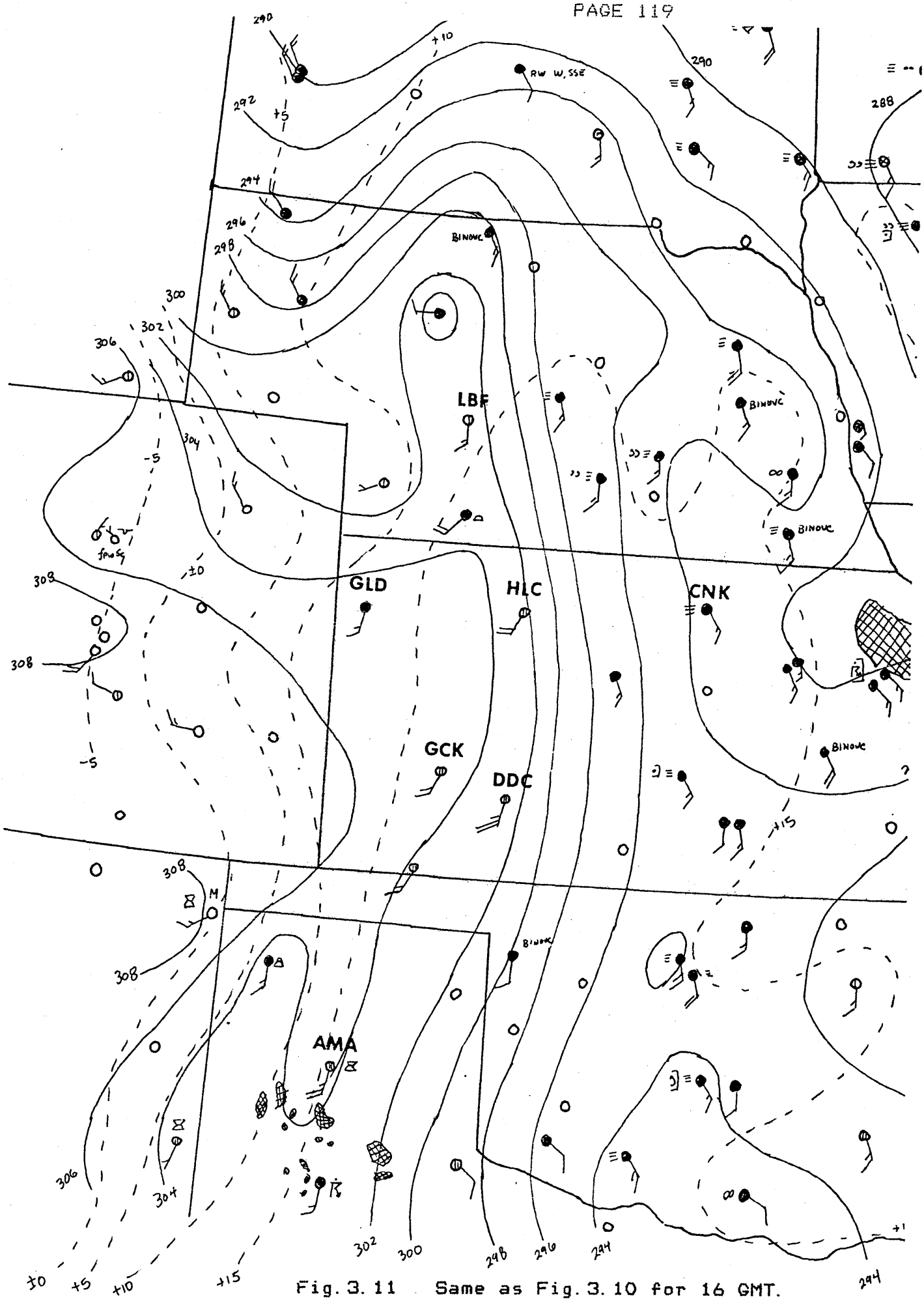


Fig. 3.11 Same as Fig. 3.10 for 16 GMT.

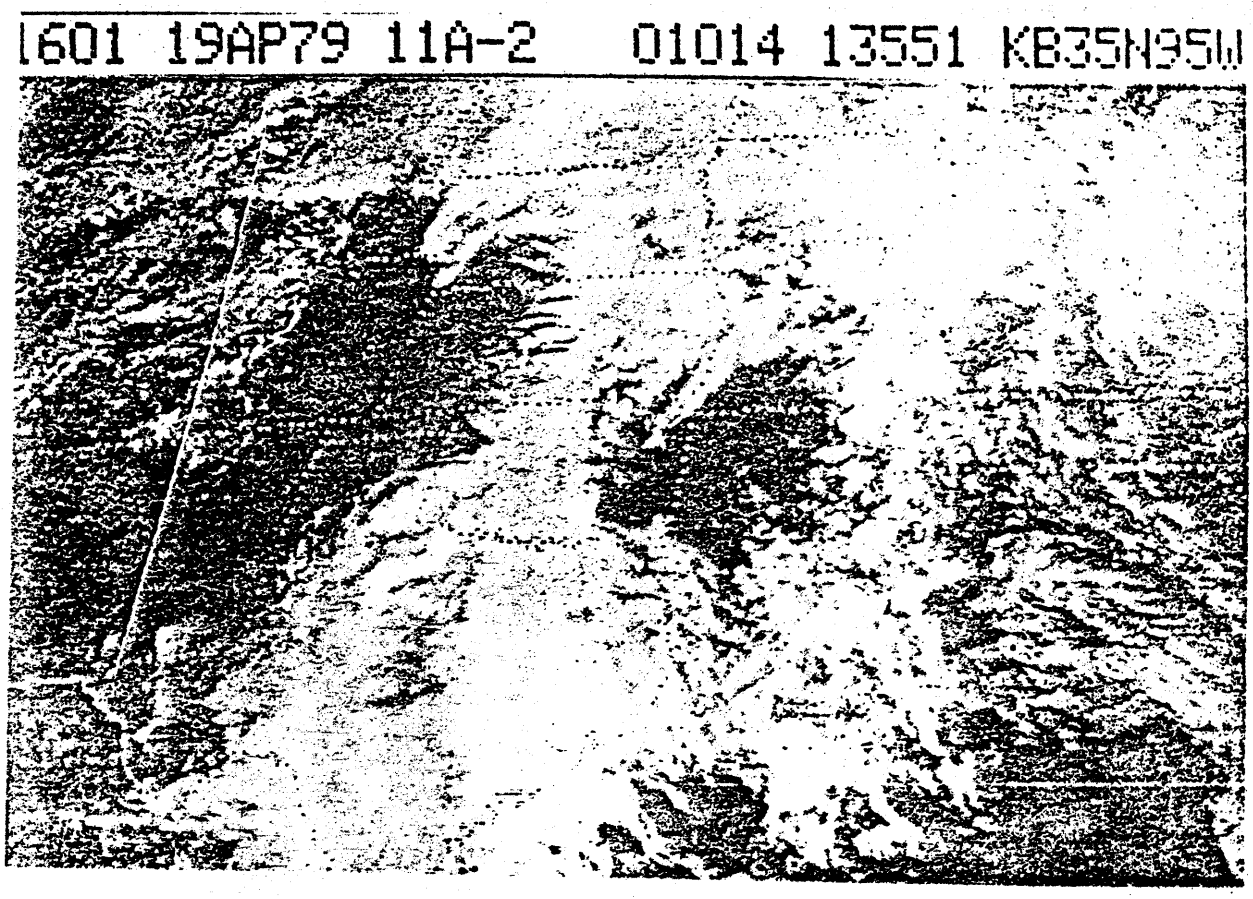


Fig. 3.12 Visible satellite photograph for 1601 GMT, 19 April.

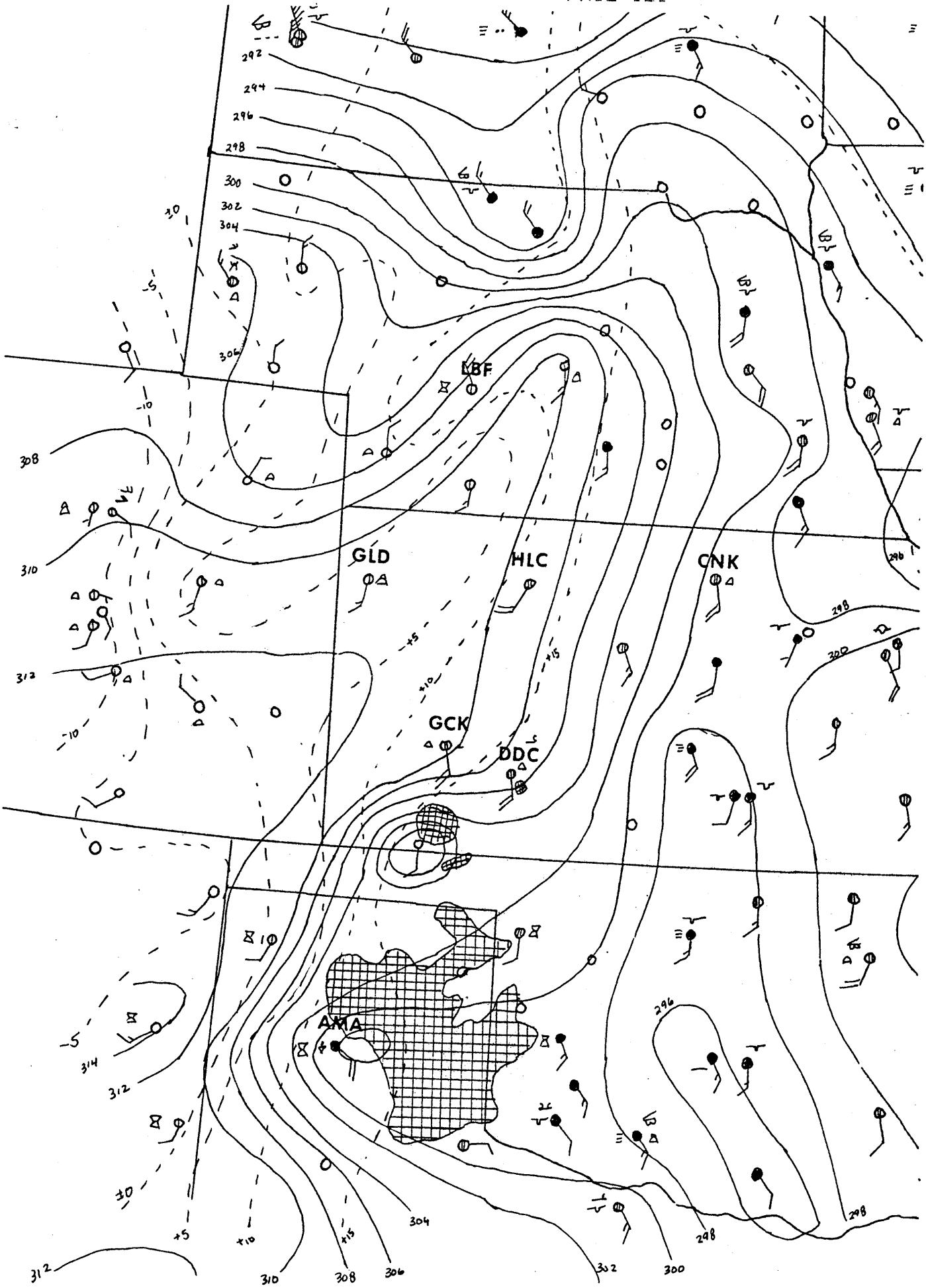


Fig. 3.13 Same as Fig. 3.10 for 21 GMT.

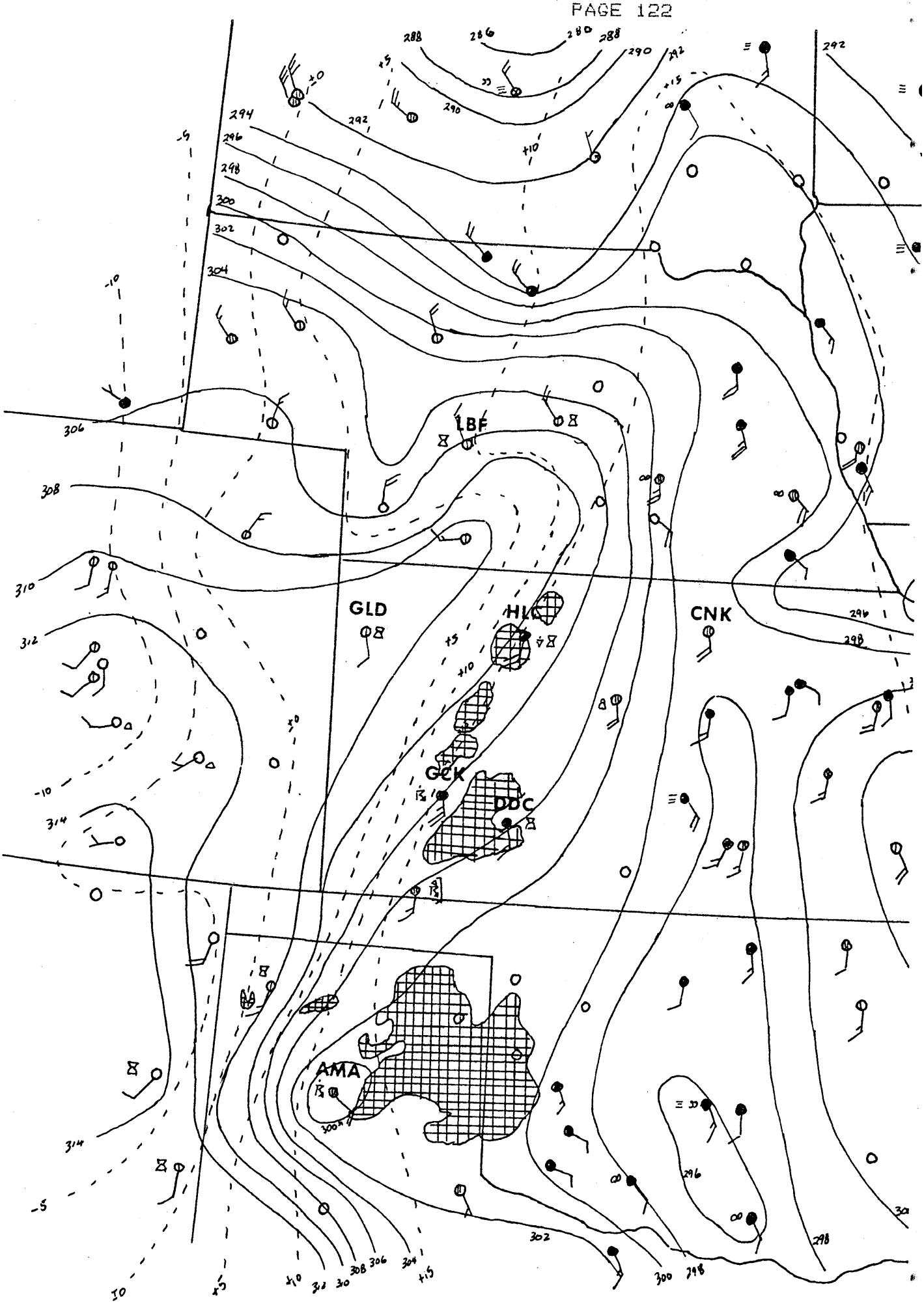


Fig. 3.14 Same as Fig. 3.10 for 22 GMT.

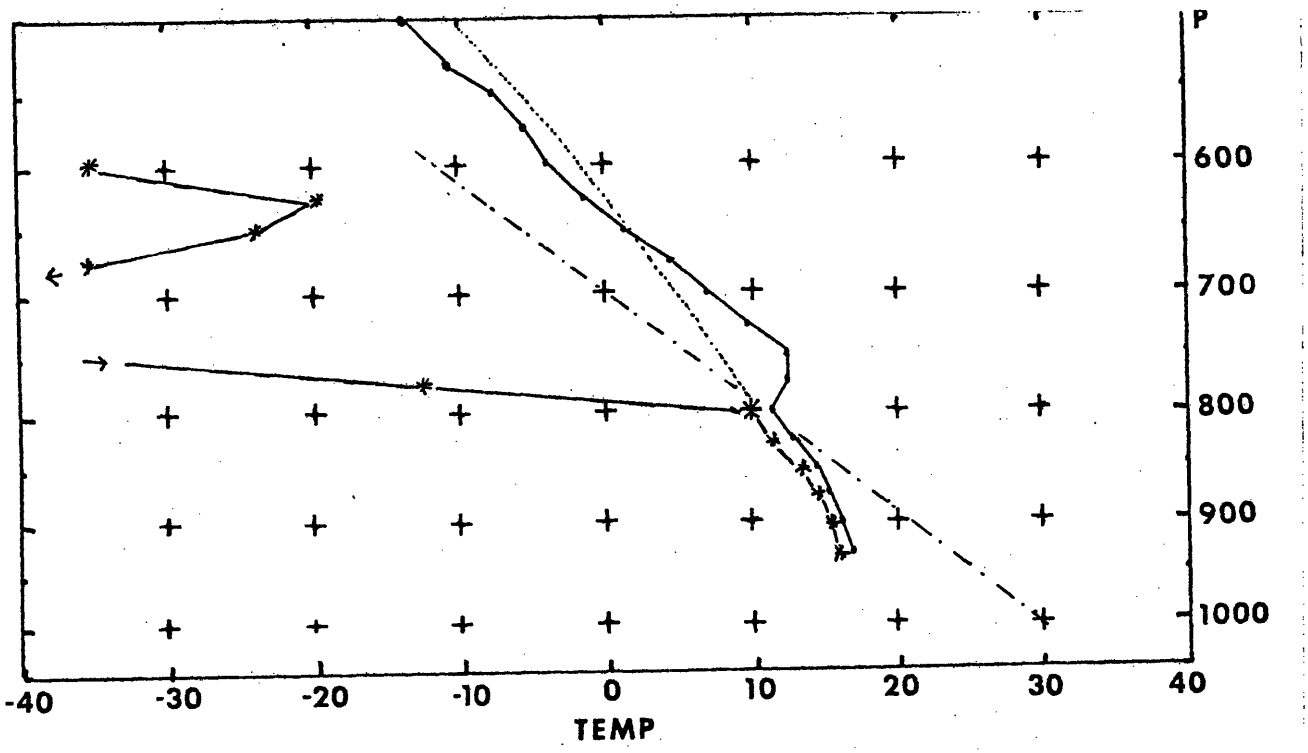


Fig. 3.15 Sounding plotted on a pseudoadiabatic diagram from Dodge City, Kansas for 1115 GMT, 19 April. Solid line connecting dots for temperature (deg C), solid line connecting * for dewpoint (deg C), dash-dotted line for 303 K isentrope and dotted line showing moist adiabat for mean PBL parcel (or selected parcel if PBL is not well-defined). Dewpoints colder than -40 C are plotted at -40 C.

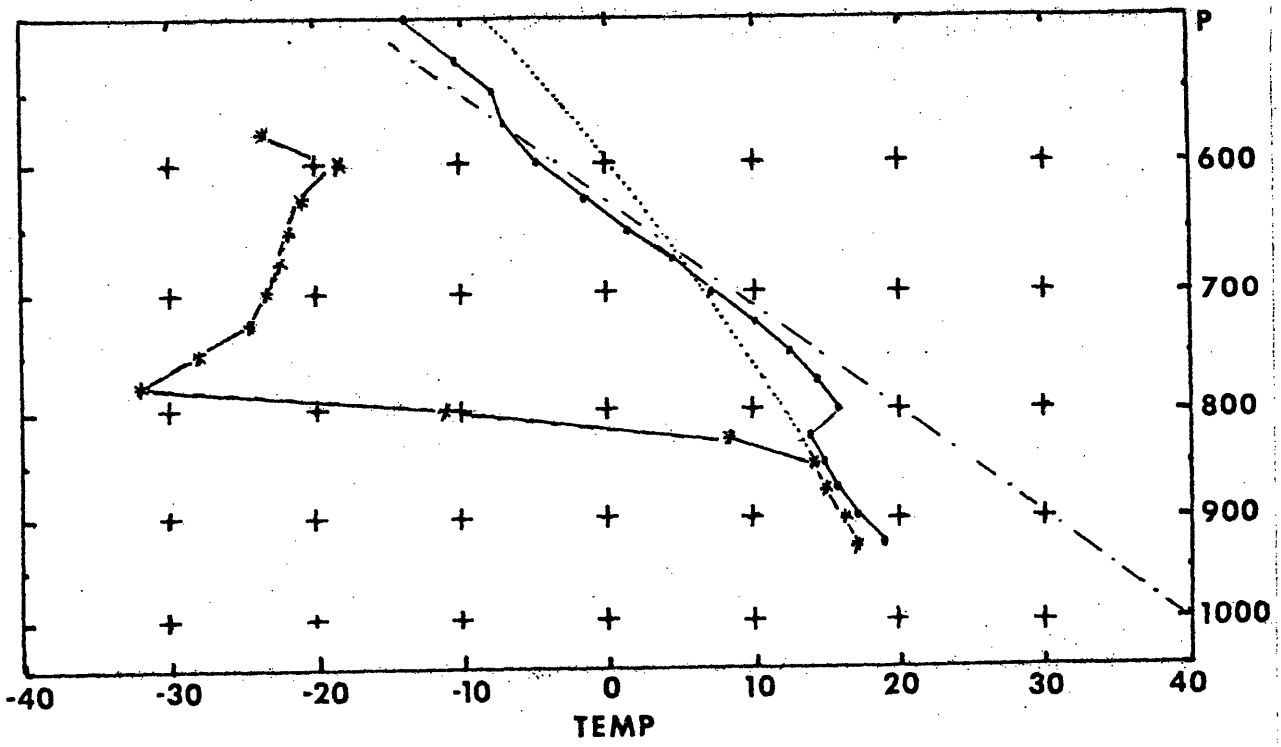


Fig. 3.16 Same as Fig. 3.15 for 1415 GMT. Isentrope is for 313 K.

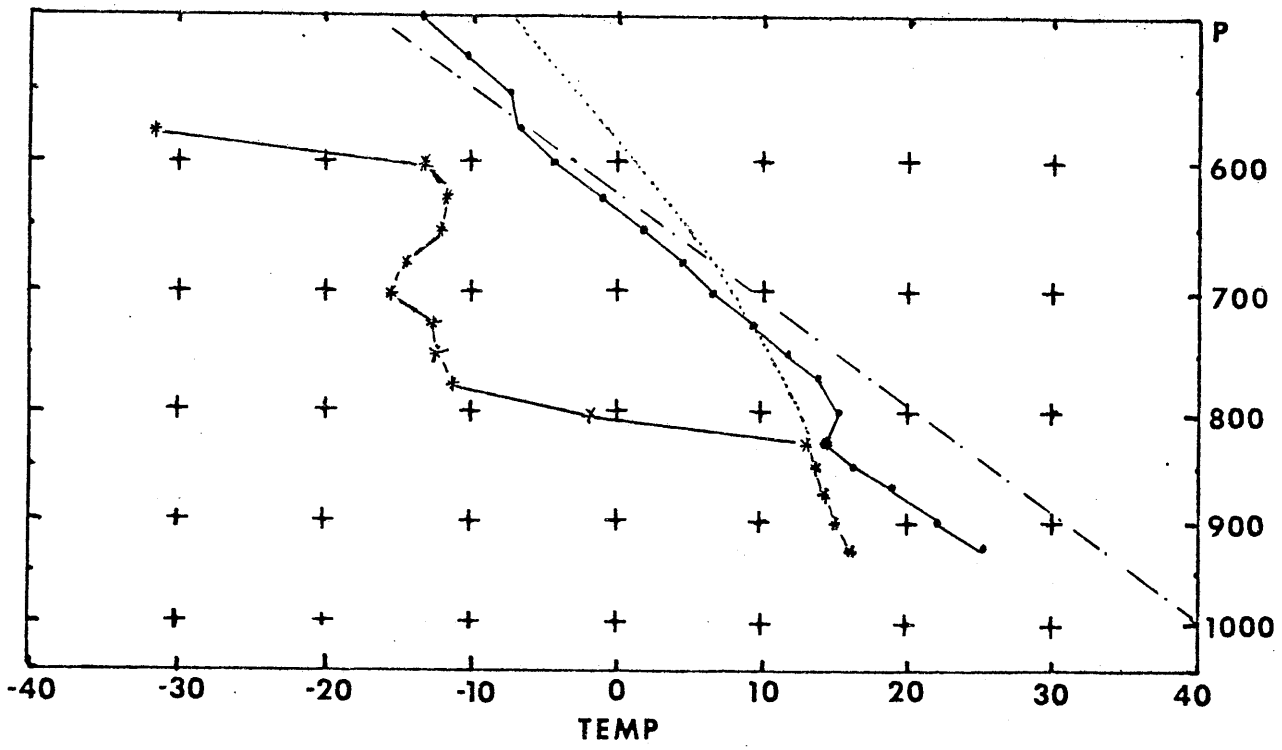


Fig. 3. 17 Same as Fig. 3. 16 for 1715 GMT.

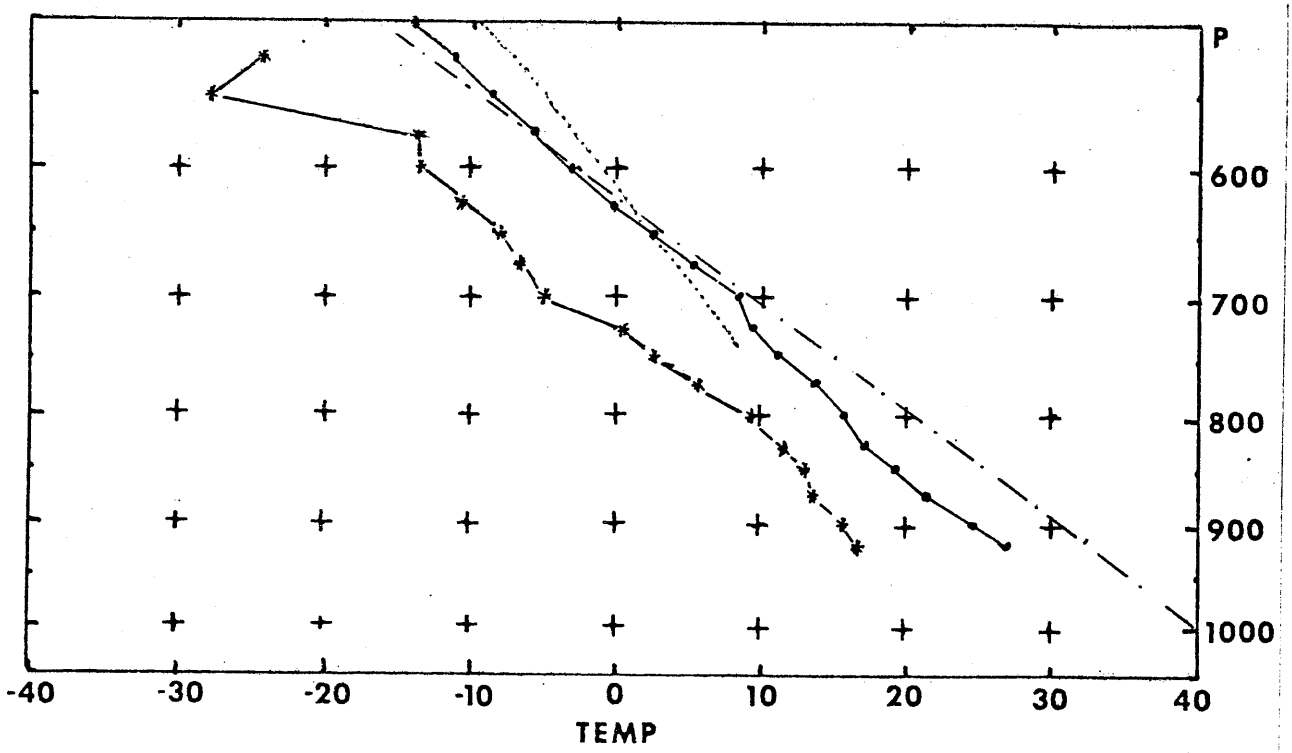


Fig. 3. 18 Same as Fig. 3. 16 for 2015 GMT.

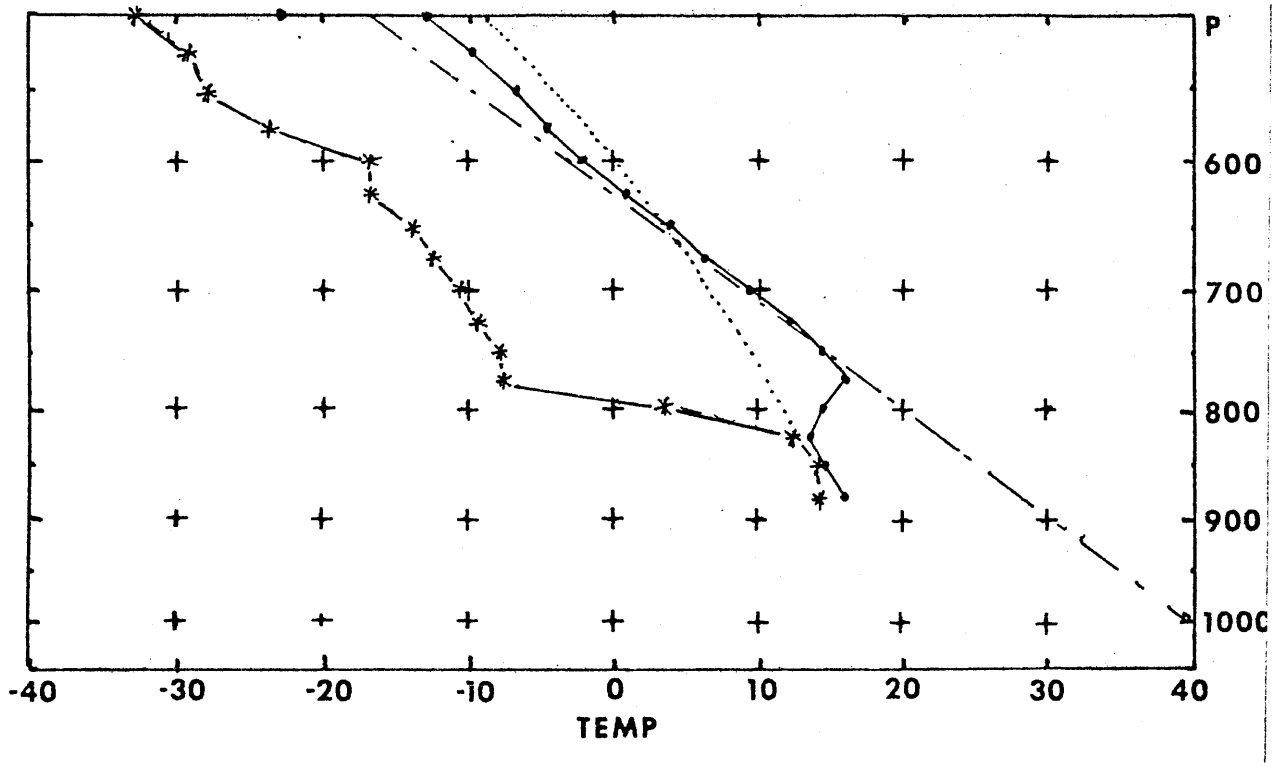


Fig. 3.19 Same as Fig. 3.16 for Goodland, Kansas at 1124 GMT.

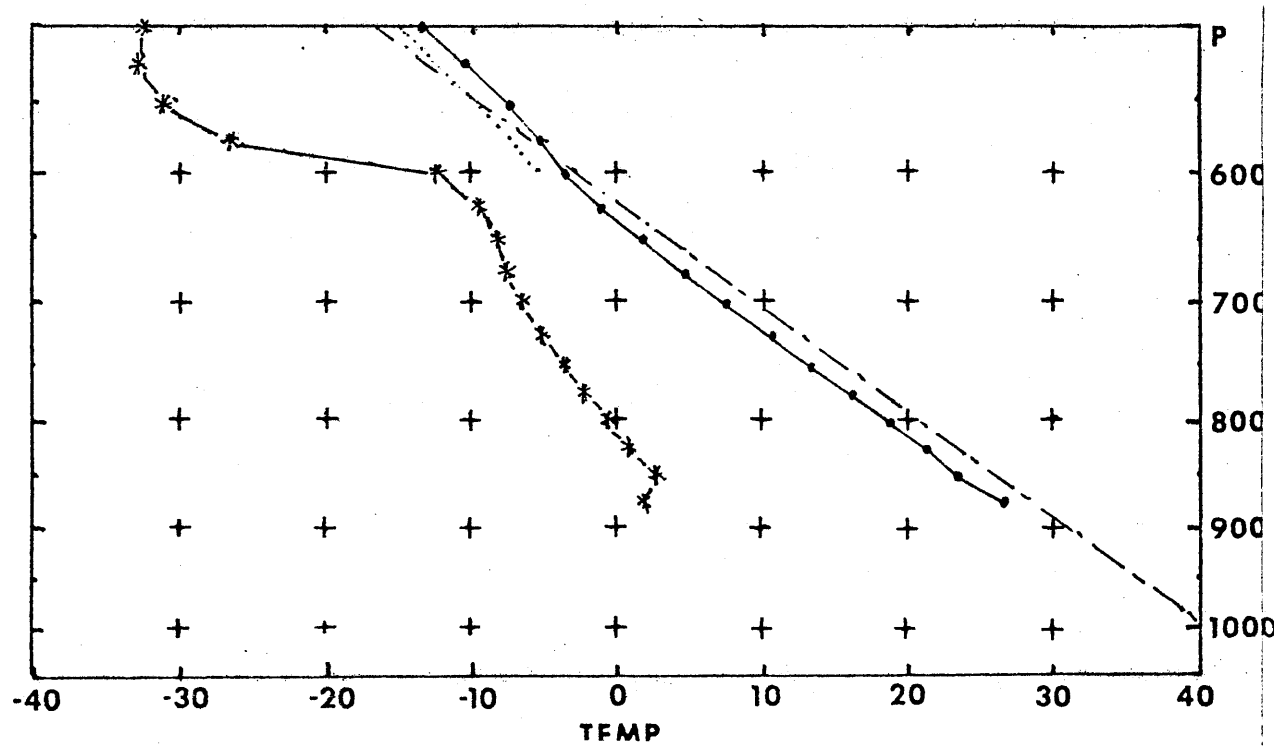


Fig. 3.20 Same as Fig. 3.19 for 2007 GMT.

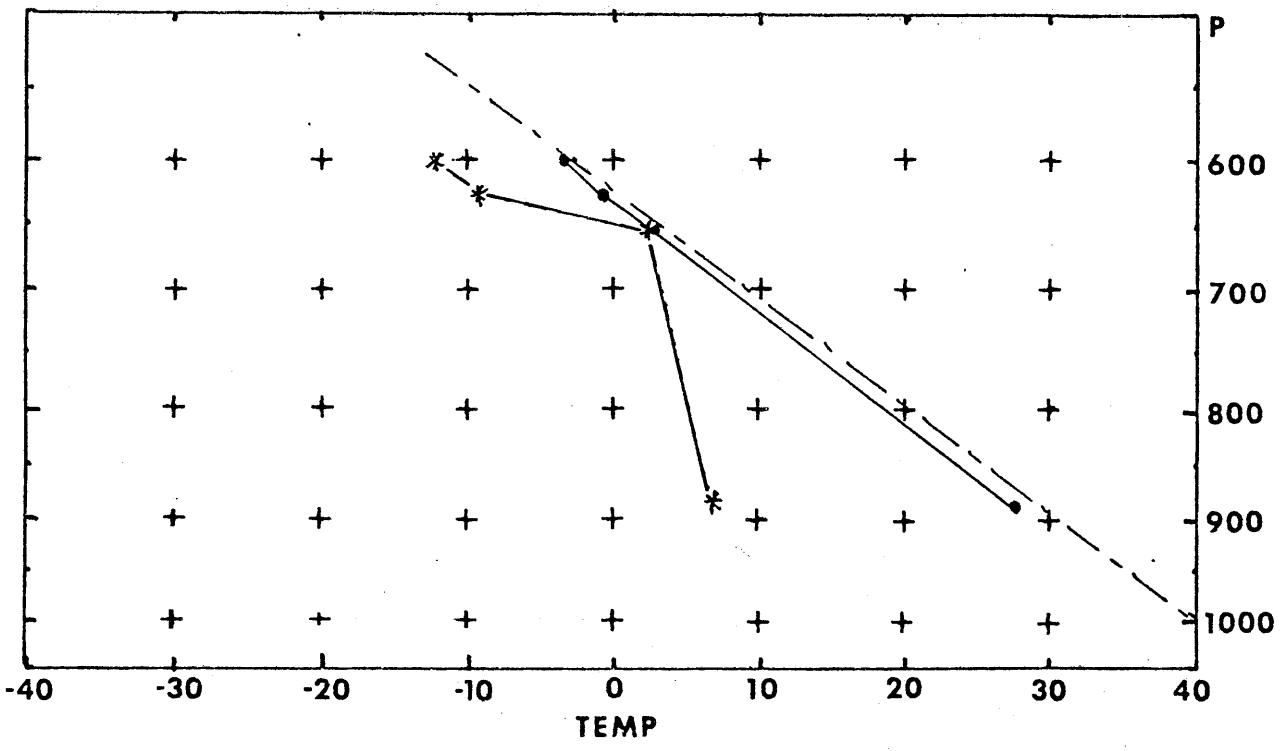


Fig. 3.21 Same as Fig. 3.16 for model output at 20 GMT from GLD initial sounding. No moist adiabat is plotted, and data above 600 mb is not shown.

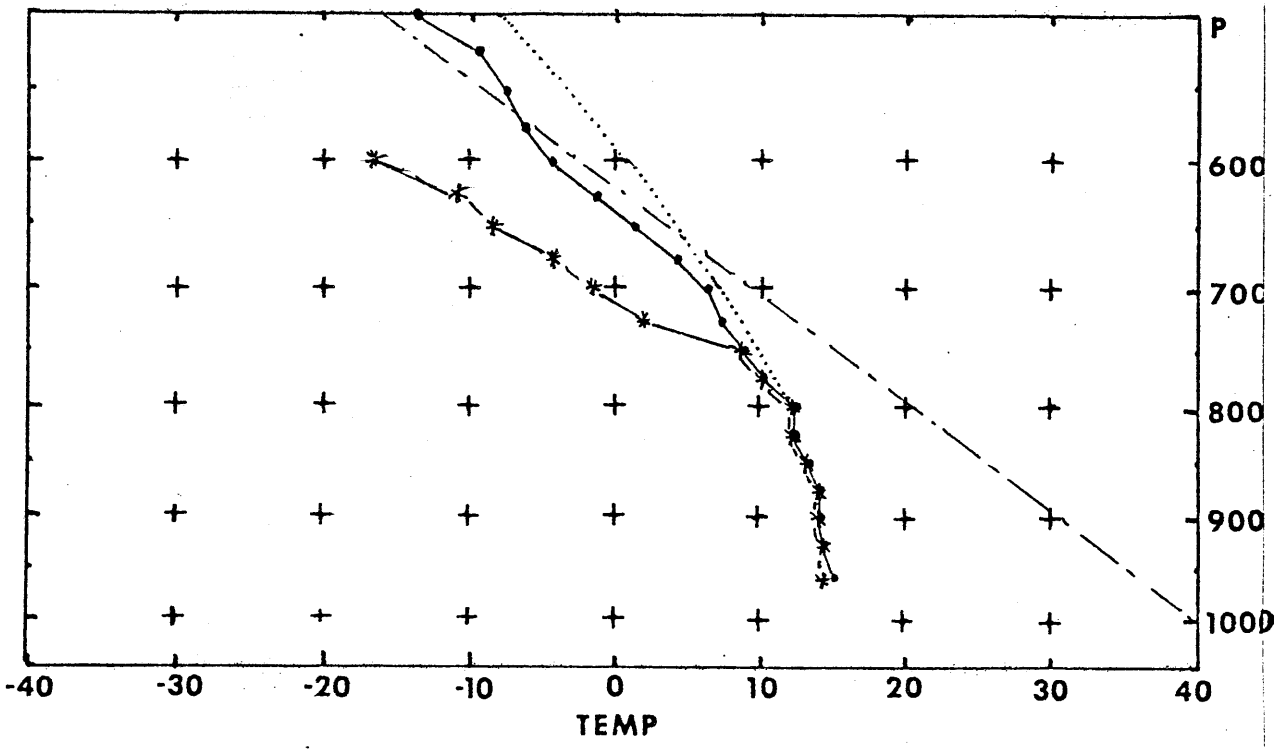


Fig. 3.22 Same as Fig. 3.16 for Concordia, Kansas at 1108 GMT.

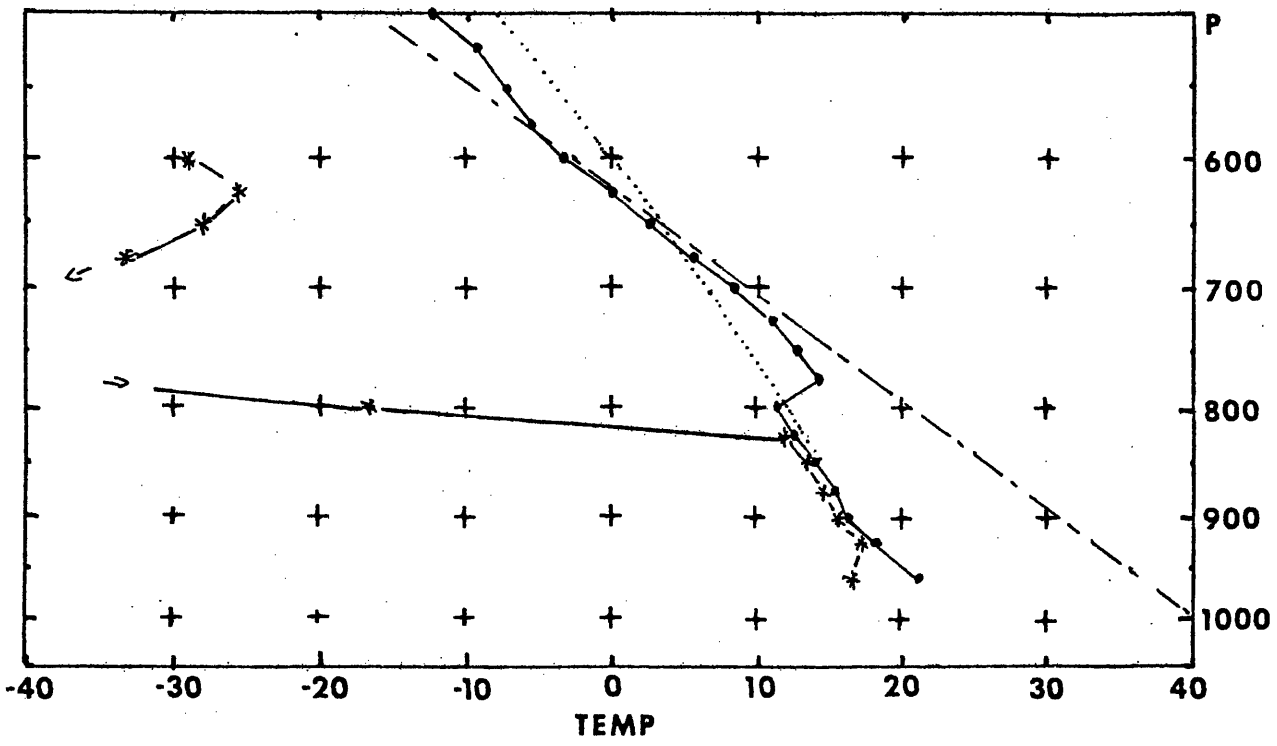


Fig. 3.23 Same as Fig. 3.22 for 2008 GMT.

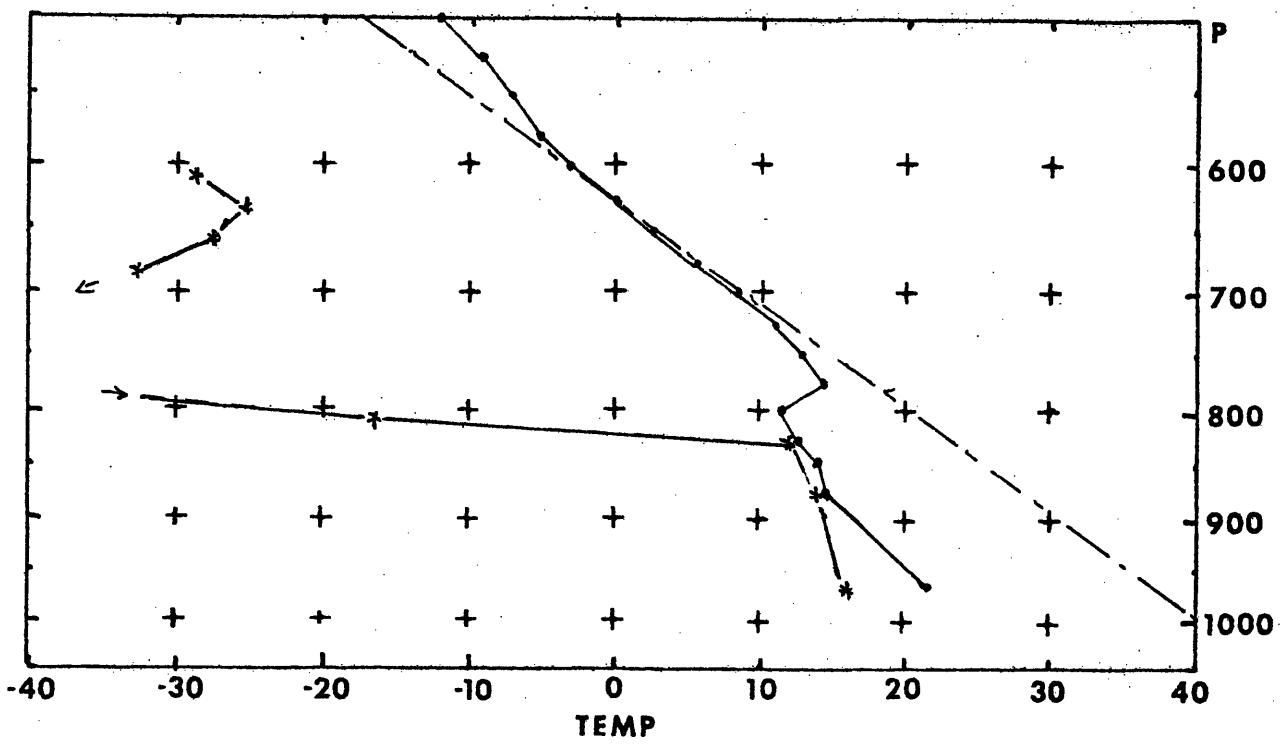


Fig. 3.24 Same as Fig. 3.16 for model output at 20 GMT from CNK initial sounding. No moist adiabat is plotted.

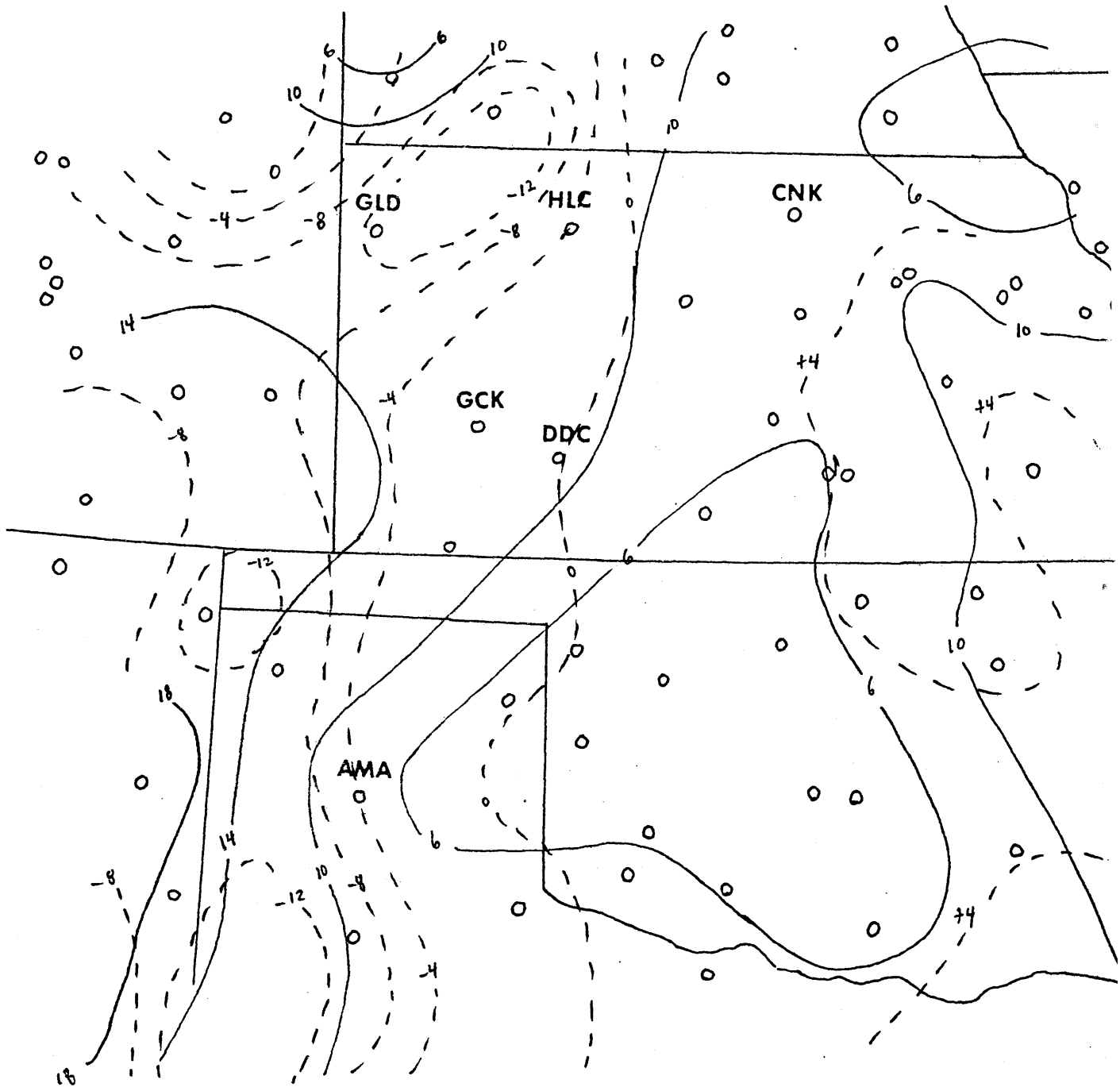


Fig. 3.25 Change in surface potential temperature and dewpoint between 12 and 22 GMT, 19 April. Solid lines for potential temperature (K) and dashed lines for dewpoint (deg C).

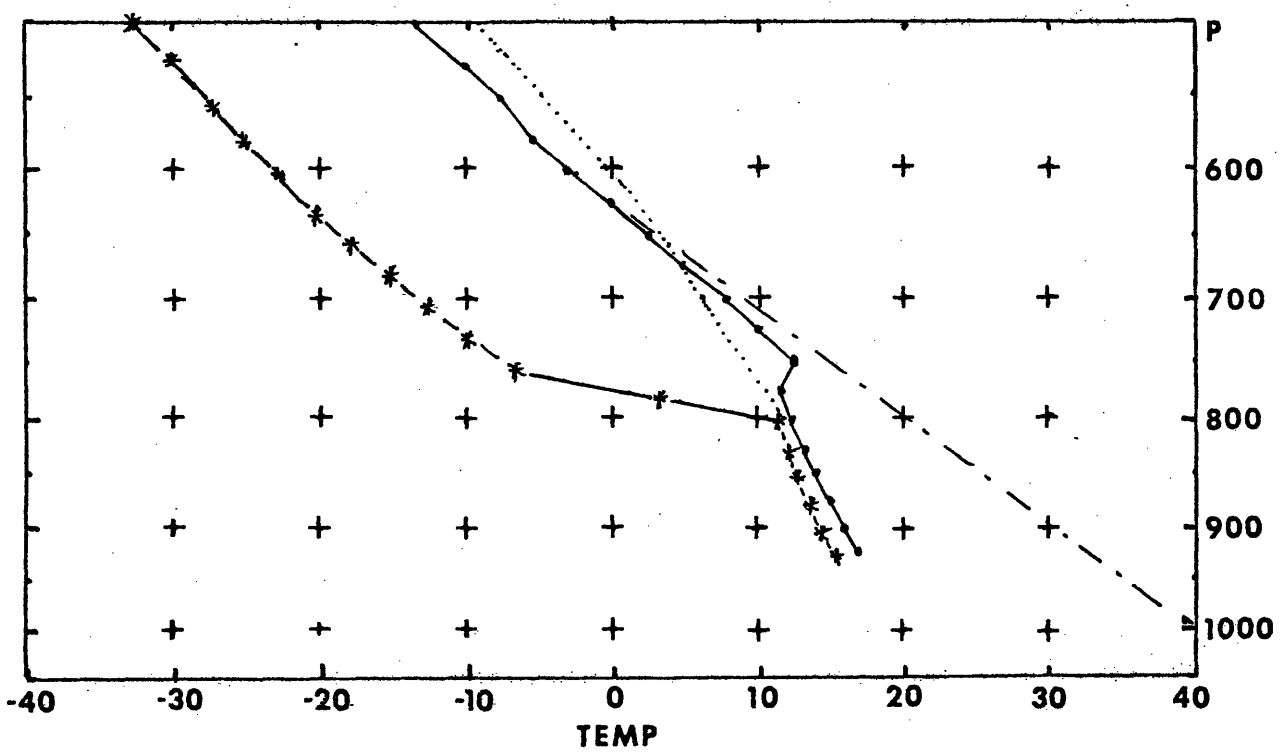


Fig. 3.26 Same as Fig. 3.16 for initial hybrid sounding, 11 GMT.

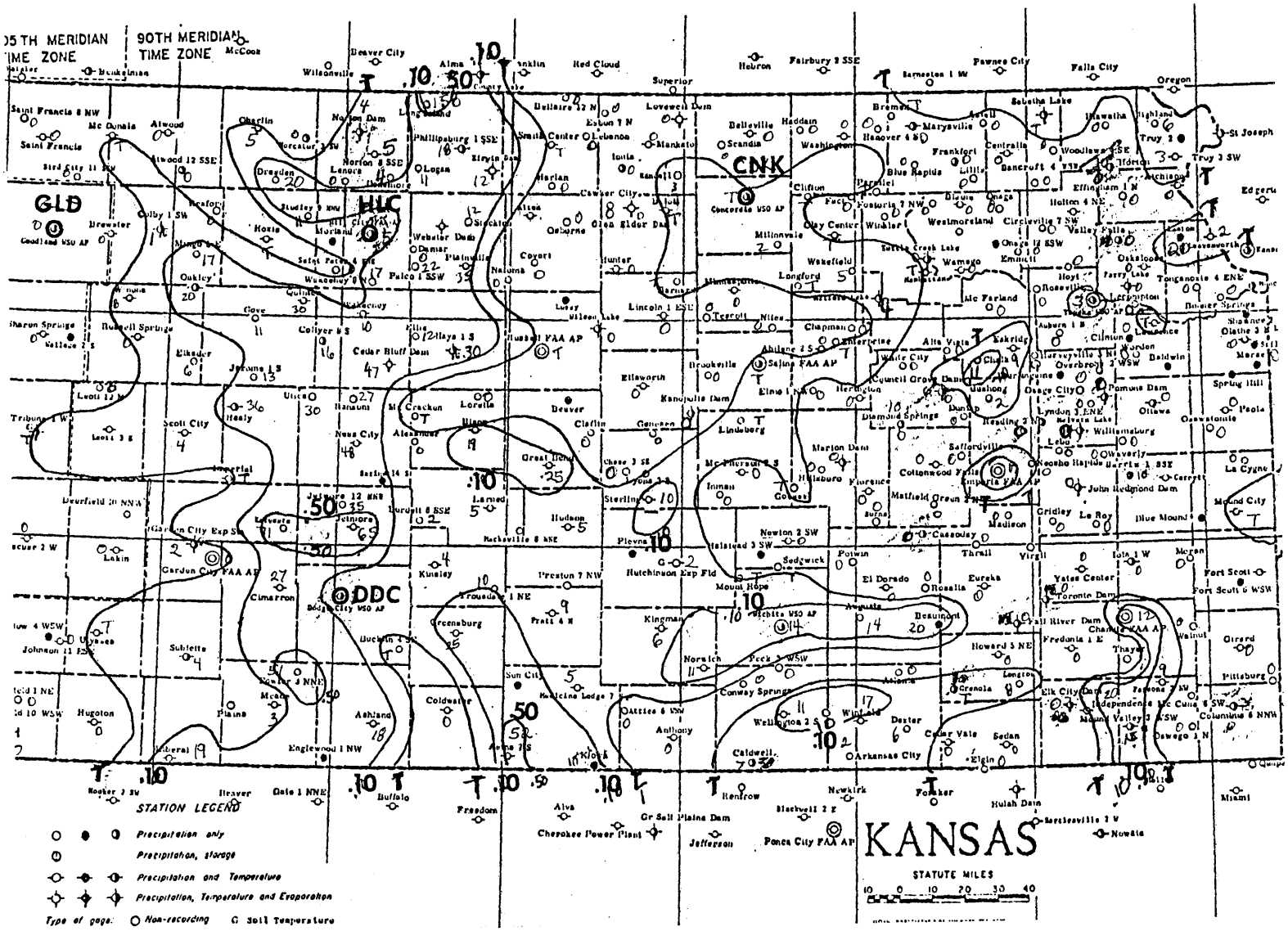


Fig. 3.27 Map of rainfall in Kansas on 18 April. Contours are drawn for amounts as follows: trace (T), .10 and .50 inches

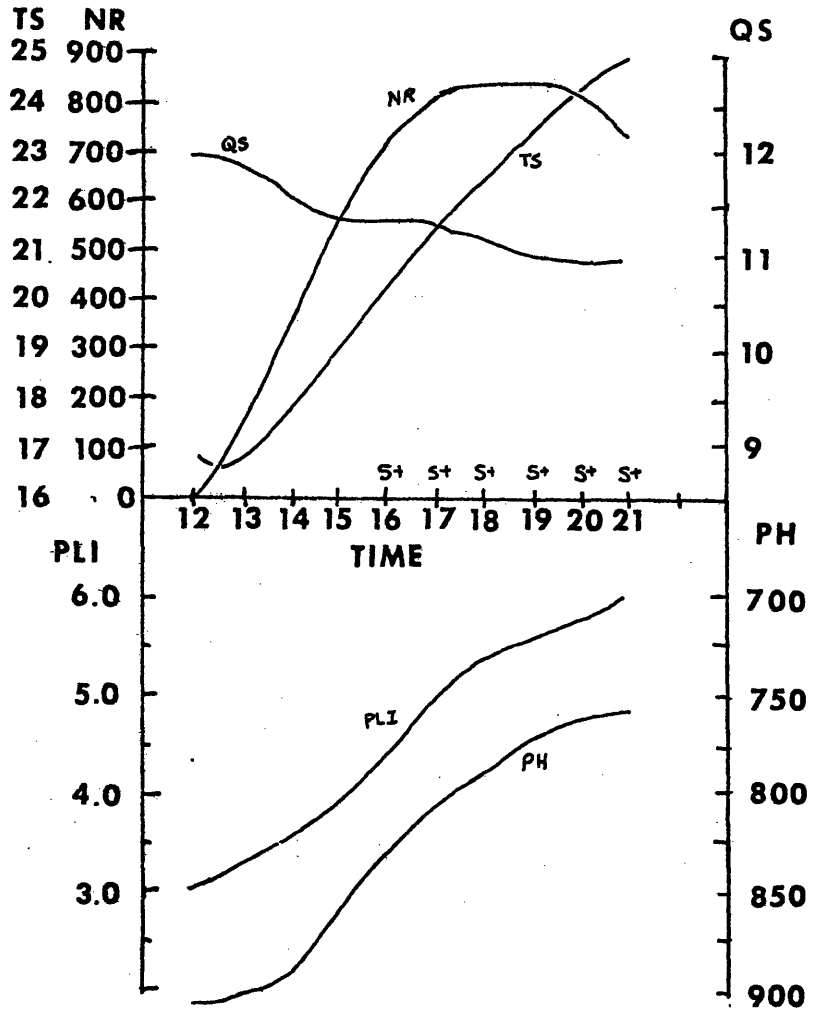


Fig. 3.28 Time variation of model output for APRHYB sounding 19 April, 50-50 soil parameters, with no extra factors modelled (Plain). NR is net radiation into the surface (mcal/sq cm min), TS is temperature at top of surface layer (deg C), QS is PBL mixing ratio (g/kg), PLI is convective instability (deg C), PH is pressure at top of PBL (mb). Condition at top of PBL is indicated above time axis: blank = unsaturated, ~S = nearly saturated, S = saturated, S+ = oversaturated.

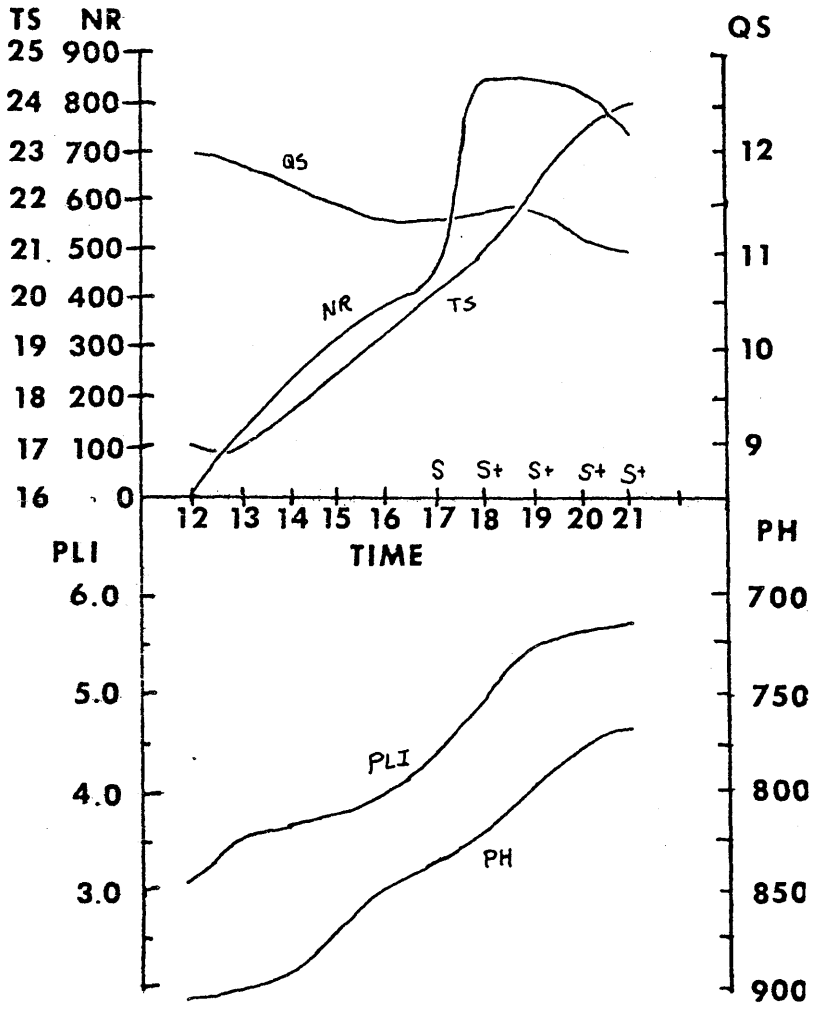


Fig. 3.29 Same as Fig. 3.28 for run with morning clouds imposed.

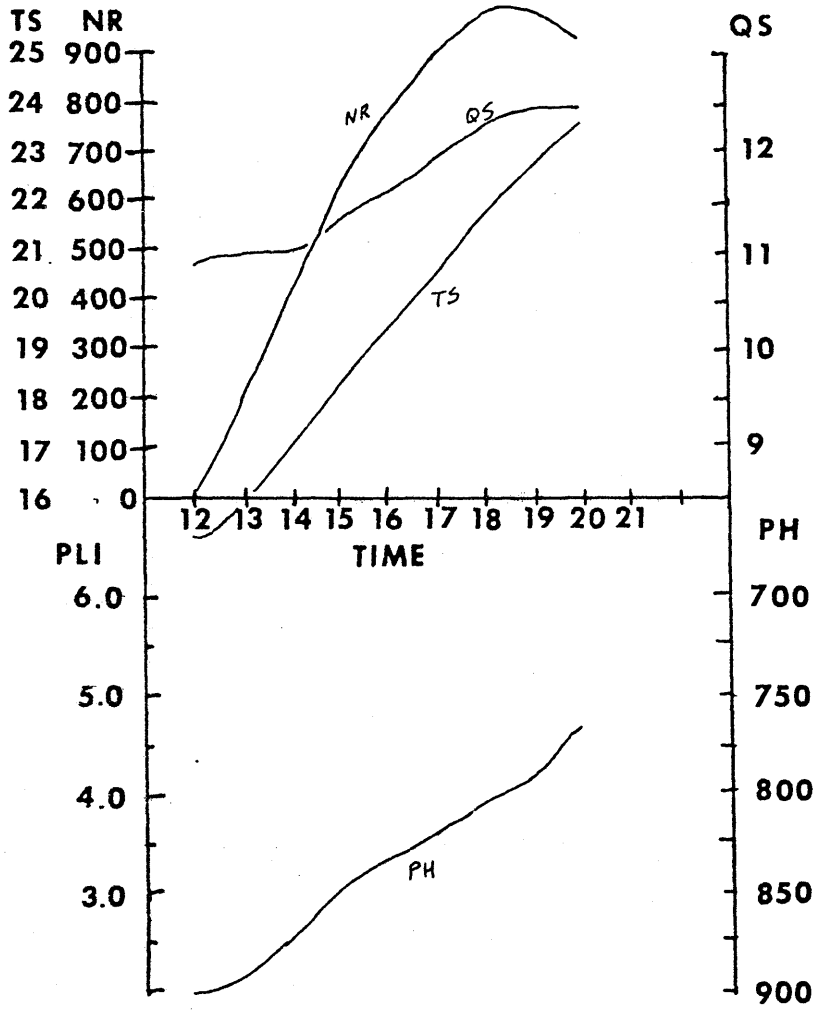


Fig. 3.30 Same as Fig. 3.28 for CNK sounding, 70-80 soil parameters.

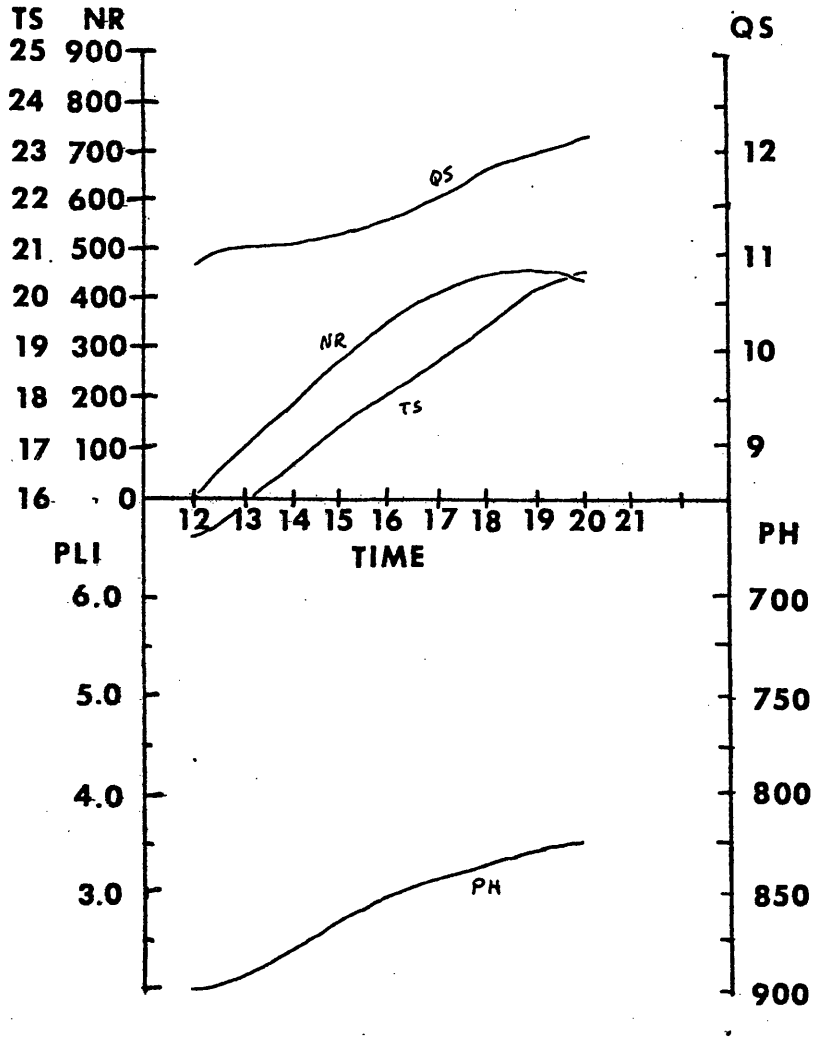


Fig. 3.31 Same as Fig. 3.30 for run with all day cloudiness imposed.

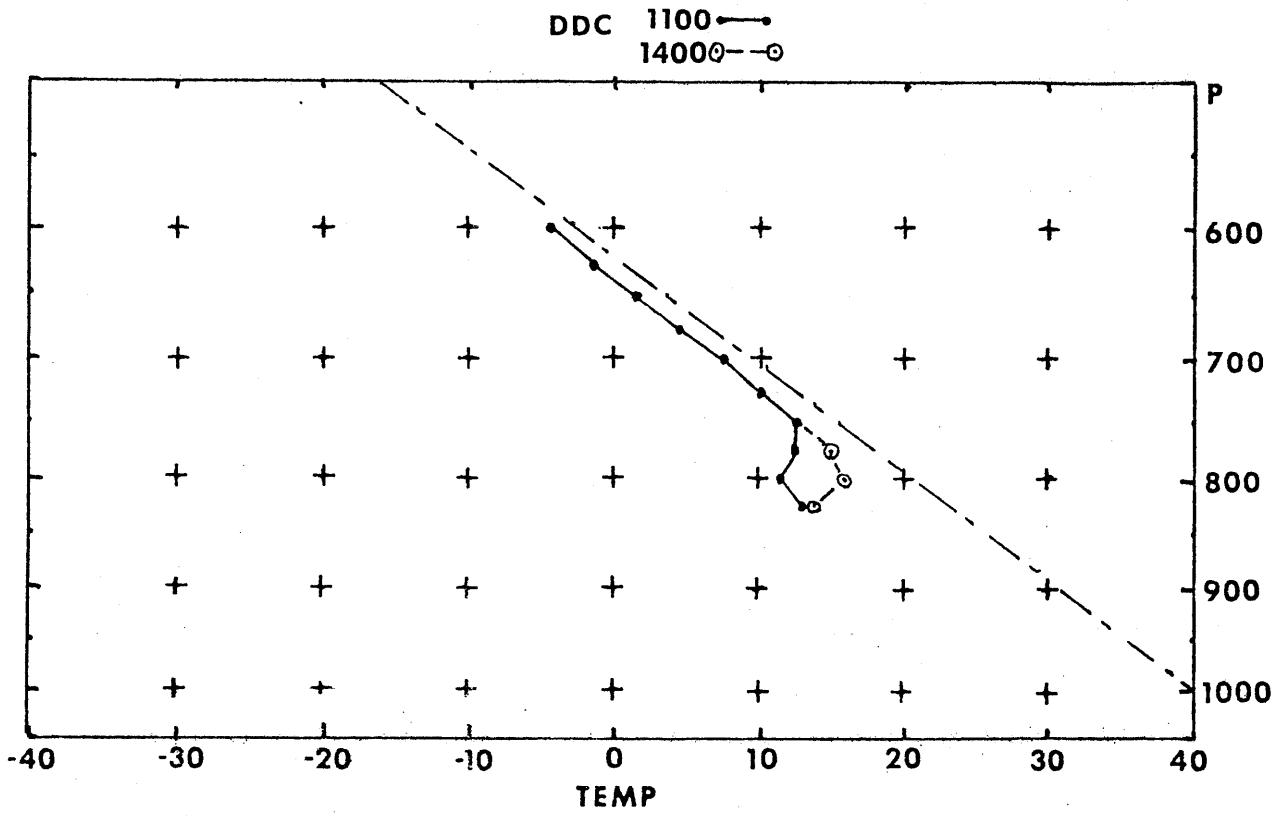


Fig. 3.32 Portion of sounding data from Dodge City, Kansas plotted on a pseudoadiabatic diagram, 11 and 14 GMT, 19 April. Solid line connecting dots is 11 GMT temperatures, and dashed line connecting circled dots is 14 GMT temperatures, where they are different from the 11 GMT data. Dash-dotted line is 313 K isentrope.

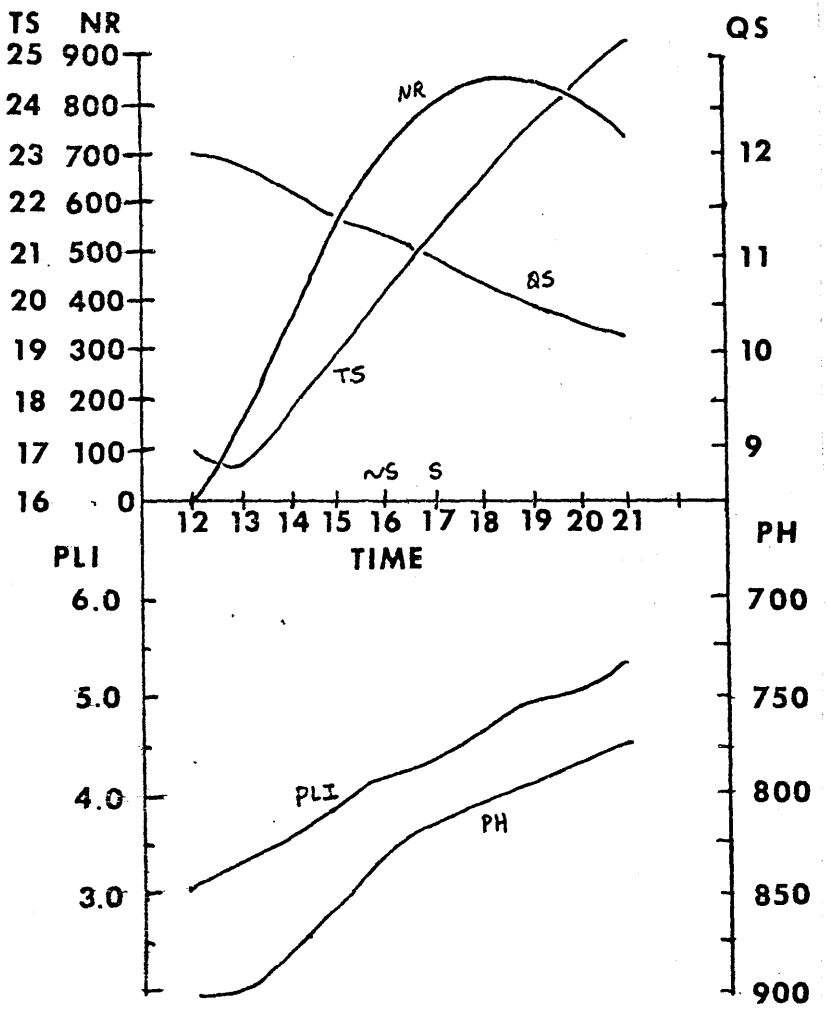


Fig. 3.33 Same as Fig. 3.28 for model run with inversion changes imposed.

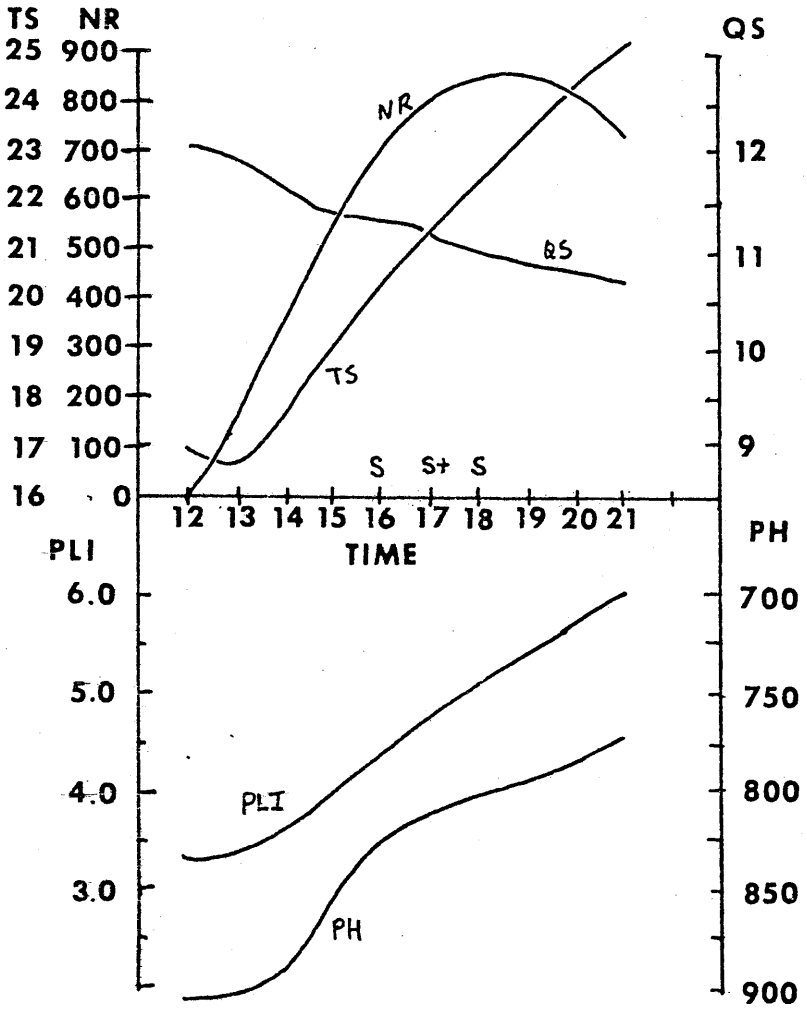


Fig. 3.34 Same as Fig. 3.28 for model run with DDC and inversion changes imposed.

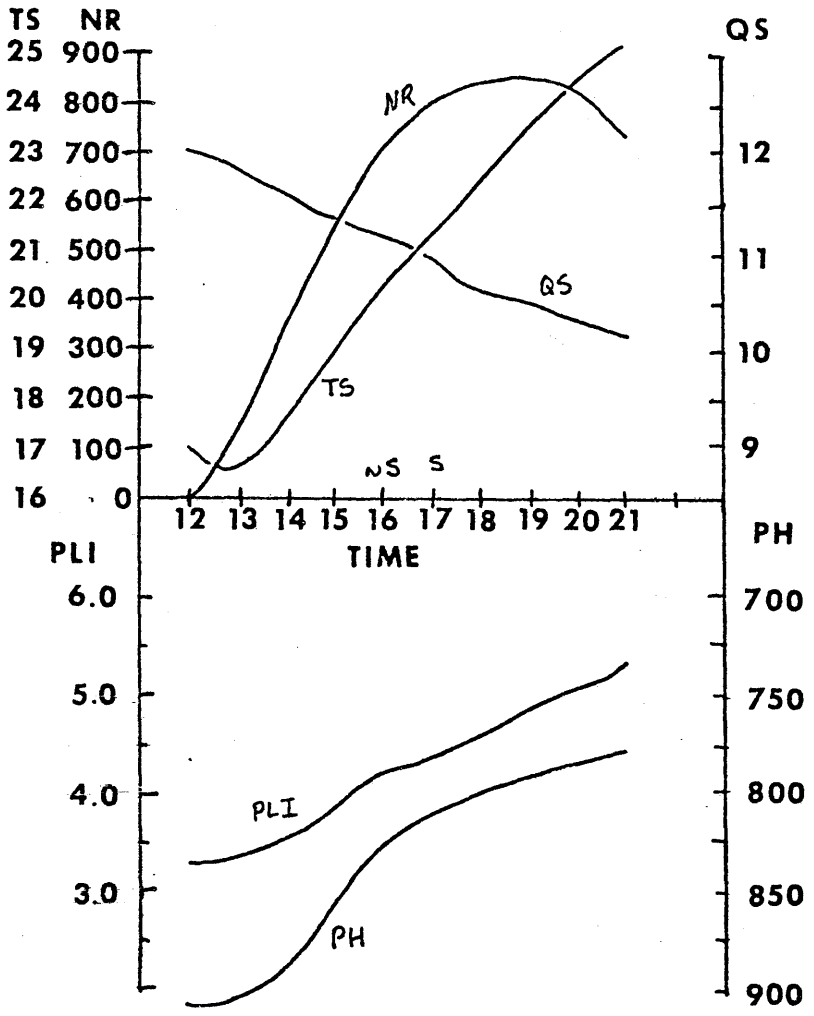


Fig. 3.35 Same as Fig. 3.28 for model run with GLD and inversion changes imposed.

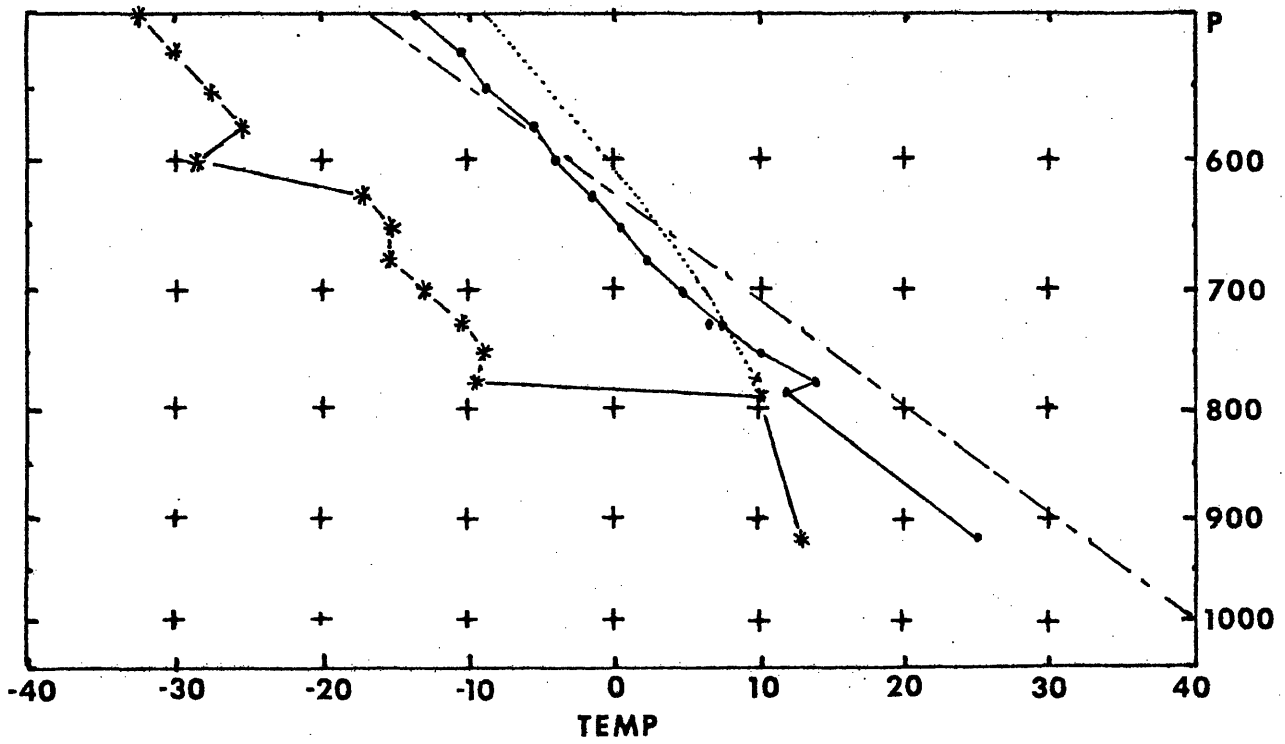


Fig. 3.36 Same as Fig. 3.16 for model output from APRHYB initial sounding at 21 GMT with GLD and inversion changes imposed.

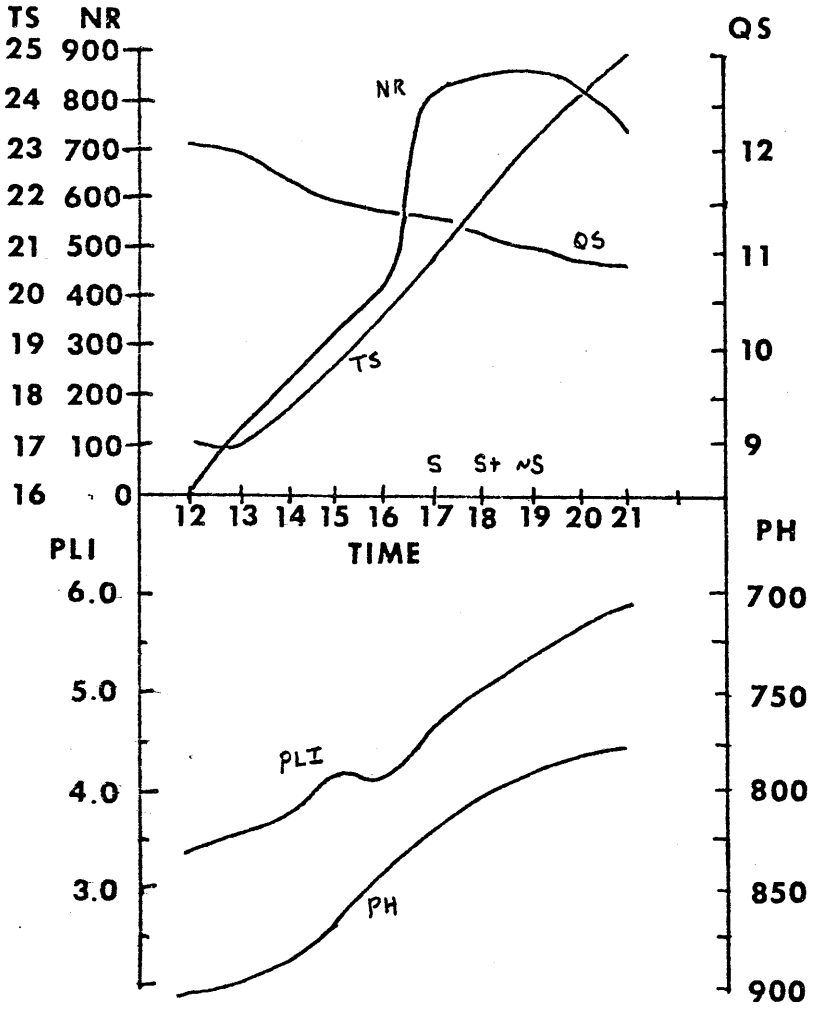


Fig. 3.37 Same as Fig. 3.28 for model run with DDC and inversion changes and clouds imposed.

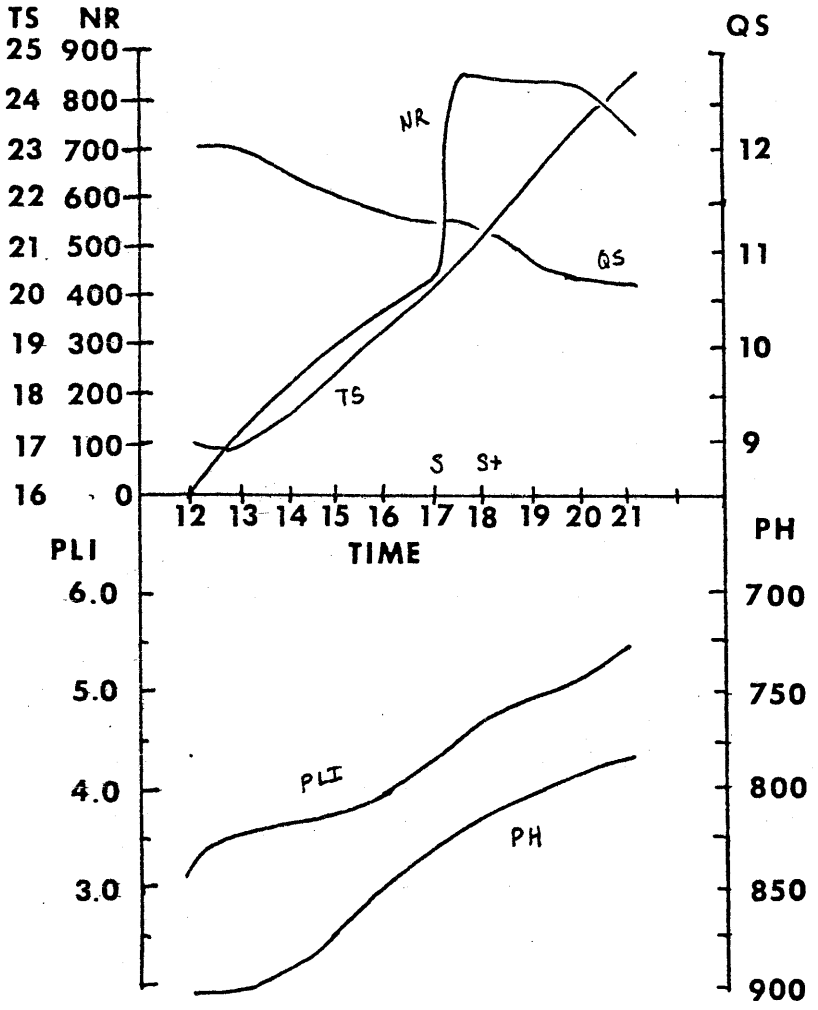


Fig. 3.38 Same as Fig. 3.28 for model run with GLD and inversion changes and clouds imposed

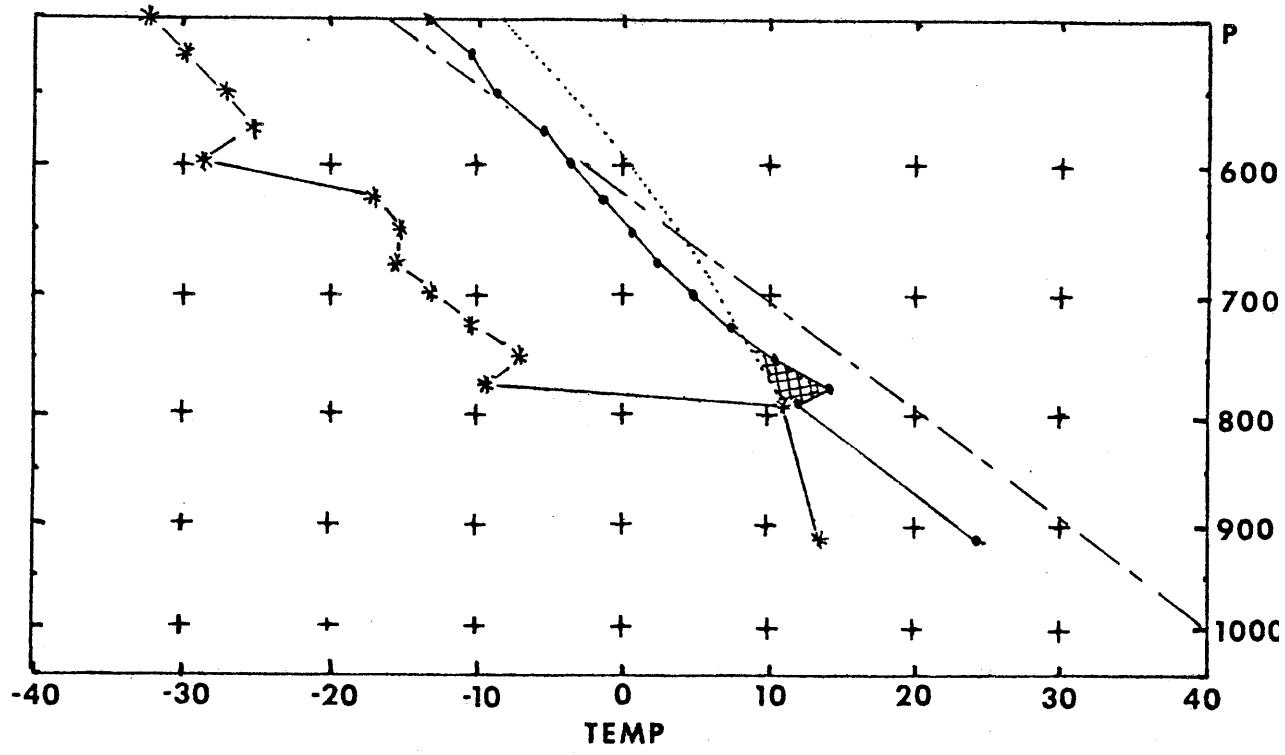


Fig. 3.39 Same as Fig. 3.36 for run with GLD and inversion changes and clouds imposed. Negative area is cross-hatched.

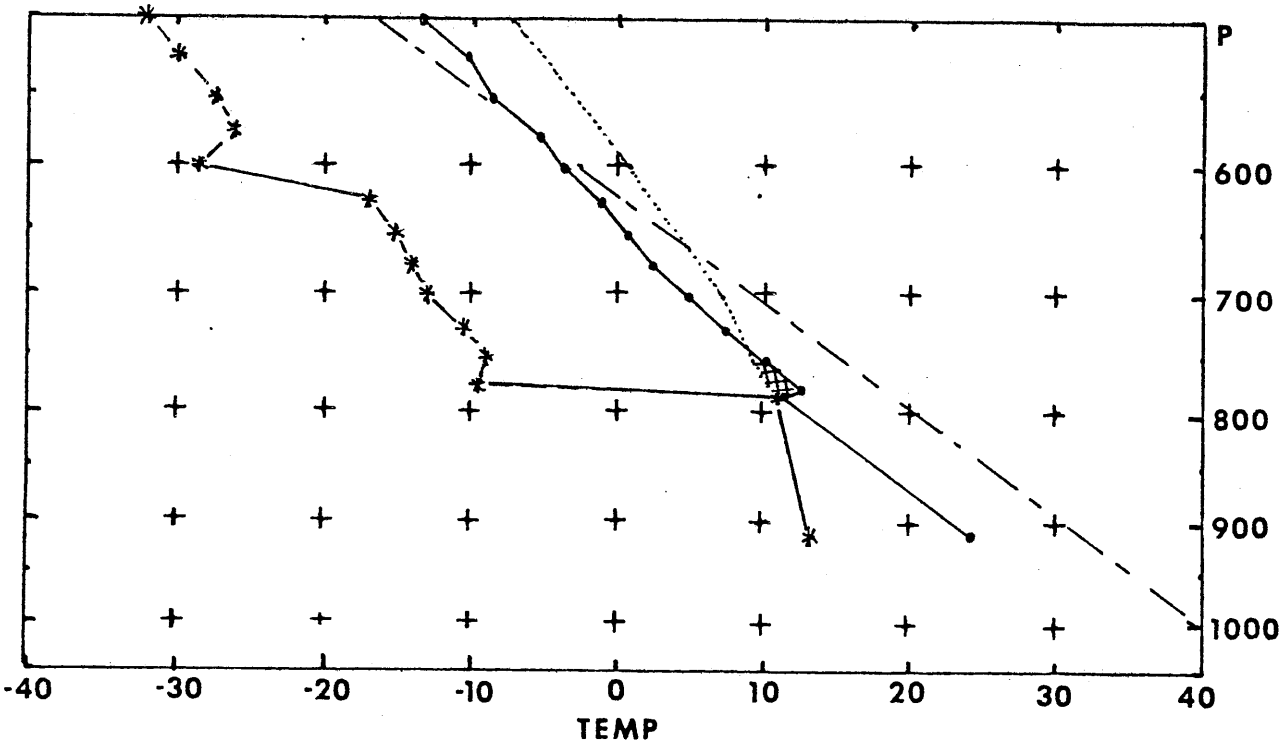


Fig. 3.40 Same as Fig. 3.39 for run with modified GLD and inversion changes and clouds imposed.

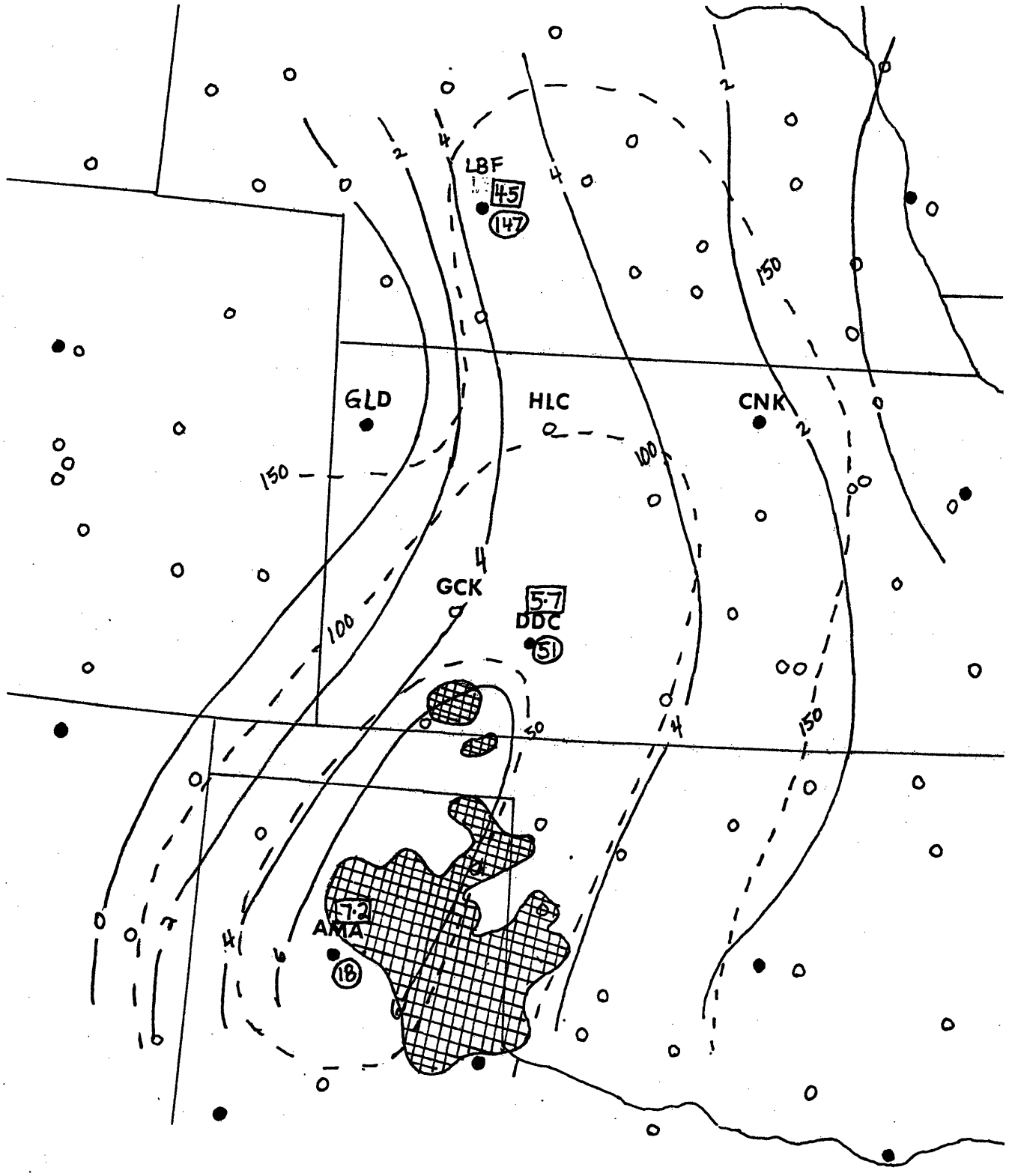


Fig. 3.41 Mesoscale analysis of convective instability (PLI) and convective inhibition (NA) for 17 GMT, 19 April. Solid lines are PLI (deg C) and dashed lines are NA (m**2/s**2). Cross hatching is for new radar echoes appearing between 18 and 21 GMT. Numbers in boxes are point values of PLI, circled numbers for NA. Filled circles denote data points.

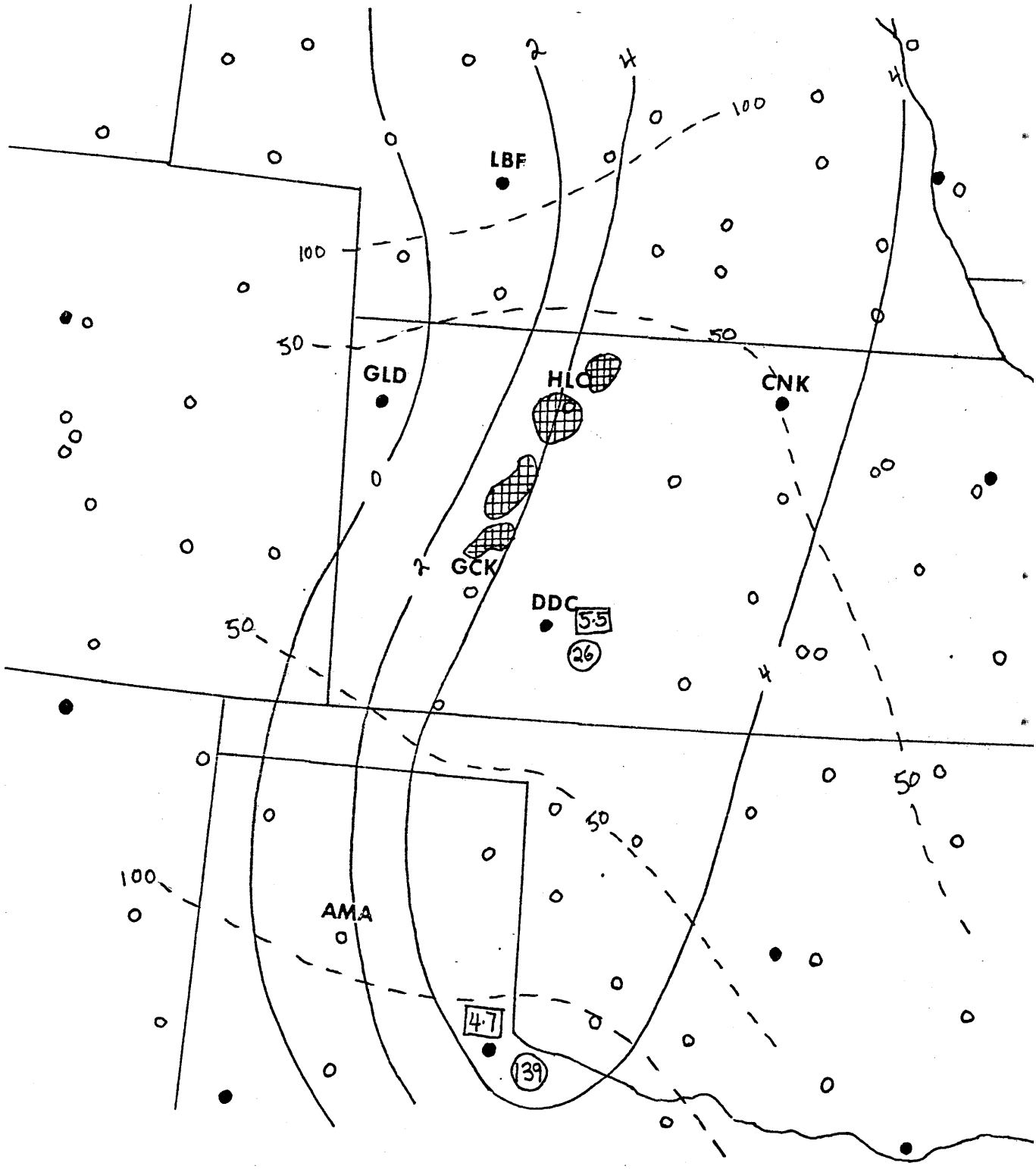


Fig. 3.42 Same as Fig. 3.41 for 20 GMT, and new radar echoes from 21 to 23 GMT.

# CASE STUDY .II: 9 MAY

## 4.1: Introduction

On this day, two convective outbreaks formed in the afternoon in the Texas panhandle region near the Oklahoma border. The convective activity became severe and caused hail and tornadoes as illustrated on Fig. 4.1 which is taken from July and Turner (1980). A brief discussion of the synoptic organization on this day follows, after which the mesoscale details of the case are described. The character of the soundings pertinent to this case are included in the mesoscale discussion. Finally, the modelling results for these two outbreaks are presented.

## 4.2: Synoptic Analysis

The synoptic organization in this case proved to be of importance to the convection. On Fig. 4.2, a strong vorticity maximum could be seen near the base of the long wave trough at 500 mb at 12 GMT, 9 May. Notice the region of cyclonic vorticity advection (CVA) which stretched from Mexico northeast into New Mexico. By 00 GMT on 10 May, (Fig. 4.3 ) this area of CVA moved north to the New Mexico/Texas border near the Texas Panhandle, suggesting upper-level support for cyclogenesis in that region. At the surface, at 12 GMT, 9 May

(Fig. 4.4) a v-shaped region of low pressure stretched northeast across the Texas panhandle, and reached southeast into Mexico. Geostrophic winds were south-southwesterly over most of Texas and Oklahoma. By 00 GMT May 10 (Fig. 4.5) this trough had moved slightly east. Also, a cold front located northwest of Texas had sharpened and had moved to the northwest corner of the Texas panhandle by this time. The presence of these synoptic-scale features implied that synoptic-scale forcing could have been important in the Texas Panhandle during the later hours of 9 May. Notice that the geostrophic wind was southerly or southeasterly across most of Texas and Oklahoma even at 00 GMT, 10 May (Fig. 4.5).

## 4.3: Mesoscale Analysis

Using the data available from the special radiosonde network, shown in Fig. 4.6, analyses were made at 500 mb and 700 mb for each of the four nominal times 11 GMT, 14 GMT, 17 GMT, and 20 GMT. The 500mb analyses for 11 GMT and 20 GMT are shown on Figs. 4.7 and 4.8. A band of 50-70 knot winds curved from El Paso, Texas (ELP) to Omaha, Nebraska (OMA). These winds changed little in direction or location, and increased slightly in speed between the two times. Winds in the network were southwesterly from the mountains in the west to the Mississippi river.

At 500mb, the expected cooling associated with the approaching trough occurred primarily after 20 GMT. Figs. 4.9 and 4.10 show the fields of change in temperature and mixing ratio from 12 to 20 GMT and from 20 to 23 GMT. The magnitudes of moisture change were small during both periods, but the temperatures fell sharply in a band from North Platte, Nebraska (LBF), to Dodge City, Kansas (DDC) to Albequerque, New Mexico (ABQ) after 20 GMT. We can conclude that the thermodynamic changes at 500mb were small prior to the outbreak of convection.

At 700mb (Figs. 4.11 and 4.12), the winds were essentially from the same direction although lower in speed. There was a dramatic change in moisture gradient from the Texas Panhandle to western Illinois, so that by 20 GMT the moisture difference from Amarillo, Texas (AMA) to Oklahoma City, Oklahoma (OKC) grew from 2.7 g/kg to 6.1 g/kg. The panhandle region experienced a strong increase in moisture through this period. The fields of change of temperature and mixing ratio at 700mb are shown on Figs. 4.13 and 4.14. Notice that cooling of one to two degrees C occurred in a band along with the large moisture increases which were responsible for the increase in gradient noted above by 20 GMT. These changes were likely the result of vertical motion associated with a frontal circulation at low levels. Ogura et al. (1982) calculated kinematic vertical motion for this case, and their results

show upward motion along this band region.

At the surface, the situation also showed change during this period. The 12 GMT conditions are shown on Fig. 4.15. There was southerly to southeasterly flow over Texas and Oklahoma becoming southwesterly in western Texas and the Mid-Panhandle region. There was a cold front stretching from the Panhandle northeast through Kansas, associated with a wind shift and a sharp drop in dewpoint and temperature. A warm pool lay ahead of the front centered near Lubbock, Texas (LBB). The warm side of the front was very moist, with dewpoints of 17-18 deg C, and low cloud or fog reported at many stations such as AMA, LBB, or Childress, Texas (CDS).

By 15 GMT (not shown), the warm pool showed evidence of warming (up almost 2 K at LBB) and to the north (+ 3 K at Dalhart, Texas [DHT]). The slopes of the Rocky Mountains showed very strong rises in temperature, as much as 7 K at Clovis, New Mexico (CVS), and 4 K at Tucumcari, New Mexico (TCC). Consequently, the temperature gradient in the panhandle lost some of its strength.

By 18 GMT (Fig. 4.16), the warm pool had become a warm tongue, with central warming of about 6 K from 15 GMT. This warming covered a large region from the mountains all the way to Oklahoma, and north to Kansas. The front retreated to the

Oklahoma panhandle, while the winds on the slopes region of the Texas panhandle became easterly. A wind shift line was located near the Oklahoms/Texas Panhandle border (northerly winds at Gage, Oklahoma [GAG] and Canadian, Texas [CAN]), but the temperature gradient was farther north. The moisture gradient was not sharp, at least within the resolution of the available data, with a gradual drying east to west from CDS to the mountains (CVS). Moisture at CDS was still near its 12 GMT value. Cloud cover was now mostly cirrus with only some Oklahoma stations still reporting stratocumulus.

At 21 GMT (Fig. 4.17) convection began at the wind shift line near CAN and GAG. To the southwest heating continued, with changes of 4 K/3 hours in the center of the tongue. The temperature gradient was still intense to the north along the Oklahoma/Kansas border, curving northeast through central Kansas. The source air for the convection must have had characteristics of the upwind (southerly) side of the wind shift: potential temperature of 306 to 310 K, mixing ratio of 13.0 to 9.5 g/kg respectively, resulting in equivalent potential temperatures ranging from 338 to 342 K. The pattern of warming and drying can be seen on Fig. 4.18 for the entire period of 12 GMT to 21 GMT. Notice that the major centers of warming and drying were in the western side of the region, and the convection broke out in a region of relatively moderate warming and little drying.

By 23 GMT, Fig. 4.19, the second convective outbreak began southwest of the first. The radar film from AMA shows that the second outbreak was separate from the first just as in the April 19 case in chapter 3. Notice in this sequence of pictures (Fig. 4.20) that the line of echoes between points A and B appeared simultaneously, not sequentially the way a gust front triggered outbreak would begin. The inflow air for this second convective outbreak likely had potential temperatures of 316 to 313 K and mixing ratios of 8.5 to 11.5 g/kg. This gave equivalent potential temperatures of 341 to 346 K. The moisture was lower for a combination of reasons: dry advection, vertical mixing of available moisture into the growing PBL, and dry entrainment from above the PBL. From the observations, particularly at LBB, the values for moisture and temperature advection were estimated. The quantities $\vec{V}\cdot\nabla\theta$ and $\vec{V}\cdot\nabla q$ were estimated on each analysis. The moisture advection was on the order of -1.5 g/kg between 12 and 23 GMT at LBB. The temperature advection was zero for the inflow to the first outbreak, and at least +2 K for the inflow to the second outbreak, occurring between 21 and 23 GMT.

Unlike the first outbreak, the second outbreak was not located at a clear wind shift line. There was some indication of a region of weak convergence on either side of the convection, but the data does not indicate strong dynamical forcing.

## 4.4: Soundings

For the 21 GMT outbreak, GAG and CAN at 20 GMT were the closest sounding locations to the actual outbreak area. However both stations had been experiencing northerly surface flow, so these soundings were not representative of the inflow air. Shamrock, Texas (SHM) was apparently in the inflow air, although parcels would have required about 3 hours to reach the wind shift line from SHM. At SHM at 11 GMT, the sounding showed a moist layer near the ground extending upwards about 100 mb (Fig. 4.21). This was capped by a dry stable layer which became almost dry adiabatic above 700 mb. The PLI for SHM at 11 GMT was 4.5.

By 17 GMT (Fig. 4.22), an approximately well-mixed PBL had developed in the lowest 60 mb. Parcels lifted from the top of this PBL 25 mb higher, became saturated and positively buoyant from 800 to 700 mb. After a brief region of small negative buoyancy, the parcels were buoyant past 500 mb, with an equivalent potential temperature of about 346 K. This was a higher equivalent potential temperature than inferred from the surface observations at 21 GMT, but this air had to travel over 100 km before being lifted at 21 GMT, during which time warming and drying took place, lowering the equivalent potential temperature. Soundings closer to the center of the warm tongue showed less moisture and deeper PBL development.

CDS at 17 GMT (not shown) had a well-mixed PBL of over 100 mb depth, with slightly lower values of mixing ratio in the PBL.

At 23 GMT, the nearest soundings to the second convective outbreak were AMA and CDS, neither of which were actually upwind. The AMA sounding was downwind of the convection. The warming and drying were pronounced at AMA during the day, both the result of BLH and mixing. There was a very deep dry mixed layer up to almost 600 mb at AMA by 23 GMT (Fig. 4.23).

The CDS sounding at 23 GMT was noisy, with superadiabatic layers aloft. A comparison of the CDS 20 GMT sounding (Fig. 4.24) with the 23 GMT sounding (not shown) suggested that dynamical forcing had modified the vertical structure. The structure at 20 GMT showed an almost perfectly dry adiabatic PBL from the surface to 725mb. This PBL was shallower by 50 mb on the 23 GMT sounding. So, the 23 GMT CDS sounding was not useful for the analysis. The 20 GMT sounding was characterized by a surface equivalent potential temperature of about 342 K, although the value was uncertain due to missing moisture data (see Fig. 4.24).

This variability in structure accounted for the difficulty in analyzing this case. Ogura et al. (1982), after studying this case to determine what trigger mechanisms were present, could make only conjectural conclusions. There was a

noticeable lack of specificity in their analysis. "The lack of sufficient rawinsonde data over the critical area where the storms developed..." is the reason that their "...conclusions are admittedly speculative".

One aspect of the upper air data emerged from isentropic analyses, and subsequent examination of the soundings. The soundings could generally be characterized by the heights of 4 isentropes: 307, 313, 317, and 319 K. The layer between 307 and 313 K usually contained a strong inversion, while the layer from 317 to 319 K represented a nearly dry adiabatic layer of sometimes considerable depth. The size of the latter layer was plotted on Fig. 4.25 at 11 GMT and on Fig. 4.26 at 20 GMT. The overall pattern was one of large depth through a north/south strip and very small depth to each side. This pattern seemed quasi-steady throughout the period, and moved slowly eastward with time at an average speed of about 10 knots. Ogura et al. (1982) determined that this layer of air had been advected over the region from the Mexican Plateau region. The pattern on Figs. 4.25 and 4.26 suggests that this air was in the form of a finite pool rather than a continuous layer. The depth of the pool varied mostly by the variation of the height of the bottom of the pool (i.e. at potential temperature of 317 K). Where the pool was deep (and therefore low) strong inhibition of convection existed. This point was well illustrated by the Oklahoma City, Oklahoma (OKC) 20 GMT

sounding shown on Fig. 4.27. At this time the deepest part of the pool was over OKC. Notice that PBL parcels following even the 342 K pseudoadiabat on Fig. 4.27 were negatively buoyant for more than 100 mb, as a result of the low level of the bottom of the nearly dry adiabatic layer from 317 to 319 K. The low level of the bottom of the pool and the coincident large depth could have been the result of subsidence. Since the movement of the pool was independent of the winds in the pool (500 to 700 mb), this pattern of movement and depth could have been the result of a wave passing through the middle troposphere.

During the time period 11 to 20 GMT, the eastward shift of this feature left the Texas and Oklahoma Panhandle regions with 317 to 319 K layers less than half of their initial depth. This change was important to the outbreak of convection, since the thinner layers were associated with higher bottoms of the layers.

The convection, at least by data analysis, seemed to have been the result of PBL heating, frontal surface convergence with its associated vertical motion, and movement aloft of the 317 to 319 K lid. Ogura et al. (1982) also found evidence for the possibility of symmetric instability and perhaps the inland sea-breeze effect. The modelling results for this case are examined below to quantify the thermodynamic factors

including BLH, clouds and changes above the PBL.

## 4.5: 21 GMT Modelling

The modelling was analyzed at two times, 21 GMT and 23 GMT, corresponding to the two convective outbreaks. Since the convective regions were not well represented by any of the soundings, a hybrid sounding (MAYHYB) was created using isentropic analysis and interpolation. The AMA and CDS 11 GMT soundings were averaged, and these data were plotted. Then the 4 isentropic surfaces, theta = 307, 313, 317, 319 K were analyzed, and were used to interpolate the pressure levels for those 4 points for comparison with the averaged data. The profile below the 307 K isentropic level was adjusted to give a moist adiabatic lapse rate, since the corresponding layers at CDS and AMA as well as other nearby soundings were also moist adiabatic. The profiles in the rest of the layers in the hybrid sounding needed no such adjustment. The result of this process was the hybrid sounding used for the modelling shown in Fig. 4.28.

The area was without rainfall during the previous two days, so low soil surface moistures (GWD) were expected to give the most realistic results. The few pan evaporation measurements (not shown) available from the National Climatic Center suggested lower moisture to the west, but we can infer

that the soil surface was fairly dry over the entire region west of Arkansas and Missouri. The previous month's rainfall (not shown) was near normal, suggesting moderate values of bulk soil moisture (GWB). With these aids, the values for soil surface moisture were varied between 5% and 30% of saturation and the bulk moisture was varied between 30% and 70%. One additional value for GWD was tried for the 70% GWB value, namely a 50% value (GWD = 50%, GWB = 70%), to test the effect of a more moist soil, even though this was unrealistic in this case.

The model was first run plain (P), without clouds or changes above the PBL to determine sensitivity to soil moisture parameters alone. All PBL characteristics behaved in an easily understood way. The wetter soil runs had shallower, cooler, and wetter PBLs as evidenced by the pressure level of the PBL top (PH), the surface layer temperature (TS), and the PBL moisture (QS) behavior (see Table 4.1). The instability was higher for the wetter soils, indicating greater sensitivity to the moisture than to the heating. The negative area (NA) varied with moisture, but in a complicated manner. The higher soil surface moisture runs had lower NA, while the higher bulk moisture runs had higher NA.

The sensitivity parameters explained what was happening. For GWD from 5 to 30%, the sensitivity in QS was 20%.

However, for the GWB range, QS sensitivity was only 11%. The TS and PH sensitivity for both GWO and GWB were similar and fairly small (5-6%), so the sensitivity of NA must have depended only on the QS values. High QS sensitivity (as in GWO) allowed the additional moisture to overcome the small drop in PBL height and temperature. But for the GWB, the moisture increase was not sufficient to overcome the other effects for the NA, and the result was an increase in NA for wetter bulk soil values. Notice that the increase in moisture for the GWB values was sufficient to increase the PLI, although only slightly. The sensitivity of PLI to GWB was only 8%, while for GWO it was 28%.

The time variation of various parameters for one plain run, 5-70 P, is shown on Fig. 4.29. Notice that the PBL top remained unsaturated through 21 GMT. As Table 4.1 shows, this was not true for all runs, only those with low soil surface moisture. The temperature rose continuously during the day, while the moisture dropped. The PLI dropped briefly then quickly rose until 15 GMT. After this time, little change in instability occurred.

The first modification made to the plain runs was the addition of clouds. The surface observations showed evidence of fog and stratus cloud in the vicinity of CDS, AMA, and Clinton Sherman AFB , Oklahoma (CSM) through 15 GMT. The

cloud amounts used in these runs are shown in Table 4.2. The amounts were based subjectively on the surface observations, and the relative humidity in the soundings. The importance of these clouds was tested in this series (C) of runs.

As Table 4.1 shows, the clouds contributed to lower PBLs with lower temperature and higher moisture values. The change in growth of PBL tops averaged about 9% for all soil conditions. Similarly the temperatures rose 11% less, and the moisture losses were 9% smaller. These sensitivities were greater than the soil moisture sensitivities discussed above for PH and TS, but the PBL moisture was less sensitive to cloud cover than to soil moisture.

The resultant PBLs were slightly less unstable, with PLI growth 6% lower. The change in NA was significant however. The NA for the cloudy cases were roughly 35% higher than for the clear runs. The lower PBL tops and lower surface temperatures were sufficient to overcome the slightly higher QS values to give "cooler" pseudoadiabats for parcels in the cloudy runs. The cooler pseudoadiabats combined with the greater depth in the atmosphere for parcels to travel, gave significantly higher NA.

The time variation of the cloudy 5-70 run is shown in Fig. 4.30. Notice the response of the net radiation to the

removal of clouds at 17 GMT. The temperature began to rise more quickly afterwards, although it remained lower than in the plain run. The moisture began to drop faster at 17 GMT, but was still higher at 23 GMT than in the plain run. Notice that the diminution of PLI mirrored the moisture drop at 17 GMT. The height of the PBL rose more slowly under cloud and ended up leveling off at a slightly lower level than in the plain run.

As already noted, during this period many changes occurred above the PBL. These changes were incorporated into a series of model runs to test their effect on mixed layer development. The changes used in the model runs (H) were derived in the following manner. The changes between each sounding at CDS and AMA were determined in terms of vertical motion of theta surfaces at each 2 deg K. These changes were averaged at each time to give a profile of changes at each 2 deg K for the hybrid sounding. These were then plotted for the hybrid sounding and the changes in temperature measured. The changes in moisture were taken directly from the average of moisture changes for the AMA and CDS soundings between each time. Clearly, this method was an approximation to the actual, but unknown changes which did occur. Since there was variability in the changes over the SESAME region, assuming a linear variation between AMA and CDS was crude on a small scale. However, the important mesoscale changes related to

the movement of the pool of Mexican air were similar at both stations. The resulting profiles of change in temperature and moisture are shown in Table 4.3. They show that the atmosphere generally cooled aloft with time, and warmed at lower levels. The moisture varied by a large amount and oscillated with time. Notice that a moistening over drying pattern during the first period gave way to opposite tendencies of nearly the same magnitude during the next period. This wave-like behavior is more indirect evidence for a wave disturbance above the PBL which could have been responsible for the Mexican pool movement.

The results from these runs (H series) are shown in Table 4.1. The PBLs were all deeper, with about 10% larger growth for all soil runs. The temperatures were lower than the plain runs, but by a small amount (2% less growth) and the moisture values were down by a large amount (almost a 20% larger drop). Comparing the 5-70 runs (P and H) in time sequence (Figs. 4.29 and 4.31), it is clear that the H runs showed a jump in depth during the 14-17 GMT period, when strong cooling took place at relatively low levels. The cooling lessened the stability above the PBL and allowed faster growth. The accelerated drying out took place early since the change imposed on the H run was drying low in the atmosphere in the first period. The moistening in the 775 to 825 mb layers kept the two runs from further diverging until after 16 GMT when the PBL in the H run

grew past the moistening layers and began entraining the dryer air above 750 mb.

The accelerated growth due to smaller stability was responsible for the slightly cooler PBL temperatures. Both the growth of the PBL and the rise in temperature in the PBL use the available sensible heat flux from the ground. With smaller stability, more growth in the PBL will occur at the expense of the heating if the sensible heat flux is the same (i.e. for similar soil moisture contents). So the H runs were cooler than the plain runs for the same soil moisture parameters. Additionally, since the stability was less above the PBL, the temperature of entrained air was less, so that the entrainment added less heat to the growing PBL, which then stayed cooler.

These differences, especially the lower QS values, contributed to a large drop in the development of convective instability. In three of the H runs, the PLI actually dropped from its initial value of 4.0. The sensitivity value was 58%. The difference between the plain run and the H run began, as shown on Figs. 4.29 and 4.31 at about 15 GMT. The NA responded positively to the changes, dropping by 52%. The high soil moisture cases contributed strongly to this percentage. The higher PBLs and lessened stability aloft overcame completely the "cooler" pseudoadiabat effect as shown by the PLI changes,

and gave all of the H runs less inhibition to convection. The higher PBLs also contributed to saturating the PBL tops, as all of the runs were oversaturated at 21 GMT.

Finally, a series of runs was performed incorporating both morning clouds and the imposed changes aloft (HC series). Since many of the tendencies had opposite signs for the clouds only (C) runs and the runs with imposed changes (H series), the expected outcome of their combined effects was not predictable. The results appear on Table 4.1. The change in PBL height was generally towards lower values (up to 6% less growth), although the dryest soil run, 5-30 HC showed no net change at all compared with the plain 5-30 run. The temperature rises were all lower for the combined run by 12% from the plain run. The PBL moisture obeyed no clear trend. For the 5-30 run, the net effect was greater drying, by 8%. The 30-30 HC run ended up with the same QS as the 30-30 plain. The other three runs all were wetter than the plain runs, (as much as 6% less drying). The TS changes were the simplest to understand. Both the clouds and the imposed changes separately gave lower PBL temperatures, so it would have been very strange for the combination to show anything else. The height of the PBL was not as simple to understand, since the H runs produced a slightly larger effect on the model, but the combination tendency was in the direction of the C runs, namely towards lower PBL tops. Evidently, the loss of

incident radiation was sufficient to limit the PBL growth more than the reduced stability could make up for. A comparison of the time variation of PH on Fig. 4.32, with that of the 5-70 plain run (Fig. 4.29), shows that while the clouds were present the plain run built up a 40 mb head start over the HC run. After the clouds were removed, the combination run's PBL top rose faster than the plain run, but could not quite make up the deficit by 21 GMT.

The QS variations were related to the PH values. For the 5-30 run, with the same PH values, the H run was dryer due to dryer air entrained during the 17-21 GMT period, the rapid growth period of the HC run. By the time the clouds were removed from the combination run, the QS value was higher than the plain run. But the PBL was now shallower, and actually had less total moisture content. When the PBL grew to the same level as the plain run, the moisture was spread more thinly and the concentration (mixing ratio) was less. For the wetter runs, the PBL never grew quite deep enough for this effect to take place, and the wetter soil runs had slightly higher QS values.

The instability values were all smaller for the HC runs than in the plain runs. The dryer runs showed the biggest differences (PLI dropped from its original value instead of rising for the 5-30 run) while the wetter runs showed only

small differences (10% less increase in PLI for the 50-70 run). This behavior was clearly a result of the higher PBL moisture. As a group, and individually, the addition of clouds to the H runs produced significantly higher instability.

The NA for all of the HC runs was lower than for the plain runs, by an average of more than 60%. The HC runs had less convective instability than the plain runs, and so followed cooler pseudoadiabats, which gives higher NA if all other aspects are unchanged. This obviously did not contribute to lower NA. Similarly, the lower NA could not be due to higher PBLs, since the HC runs were all lower or equal to their plain counterparts. The only reason left for the lower NA was the changes imposed above the PBL. On Figs. 4.33 and 4.34 the soundings for the 5-70 P and 5-70 HC runs are plotted on a pseudoadiabatic diagram. A comparison of these two figures clearly shows that the difference in NA was a result of the different structure above the PBL in the HC run. The time variation shown in Fig. 4.32 showed the very flat behavior of PLI and saturation of the PBL top at and after 21 GMT. The convective instability changed little through the entire heating cycle despite the clouds and changes in TS and QS.

## 4.6: Summary for 21 GMT Modelling

The responses of the various parameters are summarized in Table 4.4 for the 21 GMT runs. The PH values were relatively insensitive to all of the effects, although the imposed changes (H) made a 10% increase in the growth of the PBL. The surface temperatures responded to the presence of cloud and this effect was enhanced slightly when coupled to the imposed changes aloft (HC). Surface soil moisture and imposed changes both had a profound effect on the PBL moisture, QS. The presence of clouds made a noticeable difference too, but the sensitivity was only one half that of GWO and imposed changes.

The convective instability responded most to the imposed changes above the PBL, and also to soil surface moisture. The negative area proved to be sensitive to nearly all of the factors, particularly the imposed changes aloft. In fact, the imposed changes seemed to be dominant in both the PLI values and the NA calculation, reducing both instability and NA. The soil moisture parameters were the only positive contributors to convective instability besides the basic heating itself. The other factors, clouds and changes aloft, tended to reduce the PLI. The NA tended to drop, on the other hand, for both increased soil surface moisture and imposed changes. Both the addition of clouds and an increase in bulk soil moisture gave increased inhibition.

The non-linearity of the problem becomes acute in this case. As in the April case, the presence of clouds had opposite effects when considered alone and when examined in connection with the other factors. When the 5-70 run with clouds and imposed changes aloft is compared with the same run without clouds, the results are as follows: the addition of clouds yields higher instability and lower inhibition. For the 5-70 run, in decreasing order of importance, the relation is:

PLI = initial conditions + BLH + soil surface moisture + clouds + bulk soil moisture - imposed changes

NA = initial conditions - BLH - imposed changes - clouds - soil surface moisture - bulk soil moisture

The net effect for the sum of the factors (HC runs) was a lower convective instability exchanged for a drastically reduced NA.

The comparison with observations was reasonably close when using the 5-70 HC run. This comparison of TS and QS is shown in Fig. 4.35. The model was slightly too hot and dry after 15 GMT. This suggests that the PBL depth was likely too high. At Cheyenne, Oklahoma (CHE) and SHM at 20 GMT, the PBL top was near 800 mb, compared with 725 mb for the model at 20

GMT. However, the hybrid sounding was designed originally to represent the region farther southwest, and in particular, the clouds used in the model were not as thick or long lasting as in the CHE and SHM soundings. The 17 GMT SHM sounding (Fig. 4.22) showed relative humidity >75% over a 100 mb depth above the PBL implying some cloudiness. AMA at 17 GMT (Fig. 4.36) showed RH < 75% everywhere. These observations implied gradients of cloudiness and hence PBL heating across the data void region where the convection broke out. With the passage of time, this translated into gradients of PBL depth as well as surface temperature differences. The model PBL depth at 21 GMT was therefore closer to the actual PBL depth in the outbreak area. Notice finally that the convection began at the wind shift line, even though the CHE sounding at 20 GMT showed very low NA (2.86), and high convective instability (6.0).

These results suggested that the critical factor determining the first convective outbreak's timing and location was the existence of the wind shift line. This vertical motion was sufficient to remove the inhibition present and release the convective instability. Of course, the factors modeled were important in determining what inhibition was present for the vertical motion to remove, but the model results implied that the NA was greater at the outbreak area than to the east near CHE. Similarly, the CHE

region showed higher instability than the region of outbreak.

Fig. 4.37 shows the analyzed fields of convective instability and inhibition at 18 GMT, with the echoes at 21 GMT superimposed. Notice that the outbreak of convection occurred west of the region of lowest NA and in an area of low PLI. This figure agrees well with the conclusions made on the basis of the model results. The model showed lower NA than might be interpolated from the analysis, but there clearly was inhibition still in the outbreak region. The surface wind convergence was necessary to overcome this inhibition in order to release the instability.

## 4.7: 23 GMT Modelling

The modelling performed for the 23 GMT outbreak was largely an extension of the 21 GMT runs. The initial sounding was the same and the imposed changes aloft and clouds amounts were also the same. One additional effect was added, that of simulating dry advection in the PBL. As noted in the observations, 1.5 g/kg of the drop in mixing ratio at LBB was due to advection. The temperature advection was not simulated. This omission was made since the temperature is much more intimately involved in the model parameterizations for the PBL characteristics than the moisture. To include temperature advection would have required significant model

changes, and this was deemed beyond the present scope of work. The expected effects were estimated, however, and are discussed below. Many of the model responses were similar to the 21 GMT runs, so only those which were different will be discussed in detail here.

The plain runs were used to determine the sensitivity to soil moisture. The results for PH, TS, QS, and PLI were essentially the same as for the 21 GMT runs, and are shown on Table 4.5. The NA reaction was quite different. The response of the NA to the different soil moistures was variable. The 5-30 run had less NA than the 30-30 run, implying that additional GWD increased the NA. However, the 5-70 run had more NA than the 30-70 run, suggesting the opposite tendency. Similarly, the bulk moisture showed conflicting results. The 21 GMT HC runs previously discussed also showed this ambiguity for NA, implying that the inhibition to convection can be very sensitive to particular combinations of parameters. It will be seen that this trend continued throughout the 23 GMT runs.

Clouds were added as in the 21 GMT runs (Table 4.2) and the results were similar in all categories (see Table 4.5). The PBL growth was 8% less, surface temperature rise 8% less and PBL moisture drop 10% less. The PLI values behaved exactly as for the 21 GMT runs, resulting in 6% less growth. Again, the lower and cooler PBLs were less unstable even

though surface moisture increased. The NA was higher in these runs by more than 40% over the plain runs. This was expected, since all of the inputs, (cooler pseudoadiabat, lower PBL top) were in the direction of increasing NA. One other change was that 3 of the runs were saturated at the PBL top by 23 GMT, whereas only 2 were saturated by 21 GMT.

When changes above the PBL were imposed (Table 4.3), the results were again similar in most respects to the 21 GMT runs (see Table 4.5). The instability growth was reduced less for the 2 extra hours of integration, down only 47% from the plain run compared with 58% for the 21 GMT runs. The NA change was the most variable, ranging from an increase of 18% for dry soil to a decrease of 100% for wet soil. In these runs, the NA was very sensitive to the exact pseudoadiabat which characterized the instability. The wettest soil run was just unstable enough for PBL parcels to be able to miss the inversion at 650 mb when lifted moist adiabatically, yeilding zero NA. Notice on Table 4.5, however, that all of the runs were saturated at the PBL top, suggesting that the PBL rose too quickly for the available PBL moisture, and that this 23 GMT structure could not be realized in the real atmosphere.

The HC runs had both clouds and imposed changes. All PBL characteristics except the surface layer temperature were dependent on soil moisture. The range of variation for PBL

growth was 4% more growth to 3% less growth, a small effect. The surface temperature was held back by both clouds and imposed changes, resulting in a 10% smaller temperature rise. The moisture change, varied +/- 5% depending on soil moisture. The instability was generally lower, although the amount of change also depended on the soil moisture. Higher soil moisture runs were closer to their plain counterparts in PLI values than the dry soil runs. The NA variation essentially duplicated its behavior in the H runs. The dry soil HC runs had marginally higher inhibition, and the wet soil runs had almost no NA. However, just as with the H runs, all of the PBLs in the HC series were oversaturated at their tops, a physically unrealistic structure.

The simulation of the dry advection produced greater drying by a factor of 30% (see Table 4.6). This did not affect either the PBL depth or the surface temperatures. The change in QS was not significant in affecting the surface energy balance, hence the flux distribution was the same, giving the same PBL depth and temperature. The lower PBL moisture reduced the growth in PLI by almost 60%, yielding less instability than the initial values for the dryer soil runs. The effect on NA was also important, adding on the order of 65% to the NA of the plain runs. The reduction in QS also kept all of the runs from saturating at the PBL top.

When dry advection was added to clouds and imposed changes (QCH) the results were not surprising (see Table 4.6). The temperature and PBL depth were unchanged from the QH runs, and the PLI values were consistently lower, by 75% over the plain runs. The behavior of the NA calculations was soil moisture dependent. The 5-30 run had a NA 67% higher than the plain run, while the 50-70 run had no NA at all. All of the runs were saturated or oversaturated at the PBL top. However, as the time variation of the 5-70 run shows (Fig. 4.38), the run remained subsaturated until just prior to 23 GMT. This pattern characterized the 30-30 and 30-70 runs as well. The 50-70 run reached saturation much earlier, so it was the only run in this series which was physically unrealistic.

## 4.8: Summary for 23 GMT Modelling

Table 4.7 summarizes the modelling results for 23 GMT. The most important differences from the 21 GMT results were the variability in the NA calculations for most of the runs, and the PLI variation in the HC run. The growth of the PBL and the surface layer temperatures were relatively unaffected by all of the physical factors included. Surface moisture depended mostly on the imposed changes aloft, dry advection at the surface, and soil surface moisture. The convective instability was affected significantly by all of the factors except the presence of clouds, with only soil surface moisture

contributing positively to the amount. The NA seemed to depend in a very complicated way on soil moisture and the imposed changes. It responded more consistently to the presence of clouds (adding to NA) and dry advection (also adding inhibition).

When the effects of the various factors are examined, not in isolation, but in connection with each other, the results discussed above change, just as in the previous cases. In particular, the role of clouds reverses, and their presence contributed to less inhibition and more instability. Symbolically, in order of decreasing importance for the 30-70 run with clouds and imposed changes:

PLI = initial conditions + BLH + soil surface moisture + clouds - imposed changes + bulk soil moisture

NA = initial conditions - BLH - imposed changes - soil surface moisture - clouds - bulk soil moisture

Determining which run was closest to a simulation of the inflow air was somewhat difficult. None of the runs with all of the effects (QCH) heated enough to reach potential temperatures as high as 313 K, the low end of the implied observations. This was actually fortunate and physically reasonable since the inflow air reached 313-316 K only with

the help of warm advection which was not simulated in the model. An estimate of the effect of 2 K of warm advection between 21 and 23 GMT was made by considering the mechanisms in the model.

The sensible heat flux from the ground depends on the vertical gradient of potential temperature between the atmosphere and the ground. If warmer air is advected over a location, the immediate result would be a drop in sensible heat flux. However, this would change the surface energy balance, letting some of the available net solar radiation heat the soil. This would lead to a higher soil surface temperature, and an increase in the sensible heat flux. Thus, the first order effect would be no change in the sensible heat flux.

The growth of the PBL depends on the sensible heat flux and the stability above the PBL. If the PBL is warmer, then the effective stability of an inversion or stable layer above the PBL would be reduced. The PBL would then grow faster, since the sensible heat flux would still be the same and the stability reduced. However, the faster growth of the PBL would lead to an increase in the stability, because the available sensible heat flux must bring the low turbulence of the entrained air up to the level of the PBL turbulence. This feedback effect would tend to limit the increased growth rate.

To include the advection of temperature in a crude way, the opposing tendencies were assumed to balance, and the PBL temperature was simply raised 2 K without any change in PBL height. The soundings for the QCH 5-70 run and the modified QCH 5-70 run (with the temperature advection effect) are shown on Figs. 4.39 and 4.40. The PLI was increased from 3.1 to 3.9, and the NA reduced by 50%. The effect also removed the overrsaturation at the PBL top in all of the runs (see Table 4.6). It is safe to conclude that the QCH integrations were reasonable simulations when suitably modified for the surface temperature advection. Due to the imprecision in the available surface data, it was difficult to pick a particular run from the QCH group as being especially close to being a simulation. However, since there was no indication of a strong convergence line at the surface, it was expected that the integration which most likely simulated reality would yield a nearly saturated PBL top, with low NA and relatively high convective instability. The 50-70 run was best in this sense, except that it became supersaturated at 19 GMT, long before the surface advection acted. Both the 30-30 run and the 30-70 run gave reasonable results (nearly saturated PBL tops) with an equivalent potential temperature in the range discussed in the observations and very low NA. This result may well explain the small radar echo at 23 GMT between the major second outbreak and CDS (see Fig. 4.19). More than one set of PBL characteristics had become unstable and needed only

a small amount of forcing to become convective storms. In this case, the location and timing of the outbreak were directly related to the modeled parameters. There was little or no dynamic forcing available to remove inhibition and release the instability. The convection occurred when and where the convective inhibition was reduced to near zero.

This conclusion is reinforced by the analysis of convective instability and inhibition shown on Fig. 4.41. The values were obtained from 21 GMT soundings and the echoes (one large, one small) are new echoes at the next map time (23 GMT). Notice that the convection broke out in a region of moderate instability (~4.0) and was contained within the area of minimum inhibition. Just as in the April case, the observations show the pattern which the modelling results predicted.

Table 4.1: MODEL RESULTS AT 21 GMT, 9 MAY

| Run Type | PH | TS | QS | PLI | NA | COND |
|---|---|---|---|---|---|---|
| Plain | | | | | | |
| 5-30 | 693 | 30.5 | 10.2 | 4.7 | 31.17 | |
| 30-30 | 702 | 30.0 | 10.8 | 5.2 | 20.23 | ~SAT |
| 5-70 | 705 | 29.8 | 10.5 | 4.8 | 42.38 | |
| 30-70 | 716 | 29.2 | 11.2 | 5.4 | 29.57 | ~SAT |
| 50-70 | 728 | 28.3 | 12.1 | 6.0 | 22.71 | +SAT |
| Early Clouds | | | | | | |
| 5-30 | 710 | 29.5 | 10.5 | 4.7 | 47.29 | |
| 30-30 | 721 | 28.8 | 11.0 | 5.0 | 41.67 | |
| 5-70 | 723 | 28.7 | 10.8 | 4.7 | 53.22 | |
| 30-70 | 734 | 27.9 | 11.5 | 5.2 | 49.14 | ~SAT |
| 50-70 | 750 | 26.8 | 12.5 | 5.9 | 37.55 | +SAT |
| Imposed Changes | | | | | | |
| 5-30 | 667 | 30.2 | 9.3 | 3.5 | 23.45 | +SAT |
| 30-30 | 674 | 29.7 | 10.3 | 3.8 | 6.08 | +SAT |
| 5-70 | 676 | 29.6 | 9.5 | 3.5 | 28.42 | +SAT |
| 30-70 | 694 | 29.0 | 10.3 | 4.2 | 14.41 | +SAT |
| 50-70 | 716 | 28.2 | 11.5 | 5.3 | 4.60 | +SAT |
| Clouds and Imposed Changes | | | | | | |
| 5-30 | 693 | 29.2 | 9.9 | 3.8 | 20.40 | +SAT |
| 30-30 | 712 | 28.5 | 10.8 | 4.6 | 6.53 | +SAT |
| 5-70 | 714 | 28.4 | 10.6 | 4.3 | 12.83 | ~SAT |
| 30-70 | 728 | 27.8 | 11.4 | 5.0 | 8.46 | +SAT |
| 50-70 | 737 | 27.1 | 12.3 | 5.8 | 7.44 | +SAT |

Run Type is soil surface moisture-bulk soil moisture. PH is pressure level in mb of top of PBL. TS,QS are temperature(deg C) and moisture (g/kg) at top of surface layer. PLI is instability index (deg C). NA is negative area above PBL which a parcel must overcome to reach the level of free convection (m**2/gs**2).

Table 4.2: CLOUDS IMPOSED IN MODEL RUNS FOR MAY CASE

| Pressure | 11 GMT | 14 GMT | 17,20 GMT |
|---|---|---|---|
| 800 mb | 80 % | 50 % | 0 % |
| 825 mb | 70 % | 60 % | 0 % |
| 850 mb | 70 % | 0 % | 0 % |
| 875 mb | 70 % | 0 % | 0 % |

Percentage cloudiness used in the early cloud runs. Pressure levels not listed had 0 %.

Table 4.3: IMPOSED CHANGES ON MODEL RUNS FOR MAY CASE

| | 12-14 GMT | | 14-17 GMT | | 17-20 GMT | |
|---|---|---|---|---|---|---|
| Pressure | T | Q | T | Q | T | Q |
| 600 | 0.0 | 0.0 | 0.0 | 0.0 | 0.0 | 0.0 |
| 625 | -0.4 | 0.2 | 0.0 | 0.0 | 0.0 | 0.0 |
| 650 | -0.6 | 0.4 | 0.0 | 0.0 | -0.3 | 2.1 |
| 675 | -0.8 | 0.6 | -0.6 | -0.9 | -1.2 | 2.1 |
| 700 | -1.0 | 0.4 | -0.9 | -1.2 | 0.0 | 3.0 |
| 725 | -0.6 | 0.4 | -1.2 | -1.5 | 0.9 | 3.0 |
| 750 | 0.0 | 0.0 | -1.2 | -1.2 | 1.2 | 0.9 |
| 775 | 0.0 | -1.0 | -0.6 | 3.0 | 0.0 | 0.0 |
| 800 | 0.4 | -3.4 | -0.6 | 4.5 | 0.0 | 0.0 |
| 825 | 0.0 | -1.4 | 0.0 | 1.5 | 0.0 | 0.0 |
| 850 | 0.0 | -1.6 | 0.0 | 0.0 | 0.0 | 0.0 |

Imposed changes in temperature (deg C) and moisture (g/kg) between sounding times. Imposed linearly in the model with time. Pressure levels not listed have zero changes at all times. Times not covered also have zero changes.

Table 4.4. SENSITIVITY VALUES FOR 21 GMT, 9 MAY MODEL RUNS

| Changes in: Factor | PH | TS | QS | PLI | NA |
|---|---|---|---|---|---|
| Early clouds | - 9 | -11 | - 9 | - 6 | +37 |
| Imposed changes | +10 | - 2 | +19 | -58 | -52 |
| Both clouds and imposed changes | 0 to - 6 | -12 | + 8 to - 6 | -28 | -62 |
| Soil surface moisture | - 6 | - 6 | -21 | +29 | -39 |
| Bulk soil moisture | - 7 | - 7 | -11 | +11 | +22 |

Sensitivity measured as percentage change of a given variable compared with maximum amount of change in that variable after application of physical parameter. Variables as defined on Table 4.1. Application of soil surface moisture defined as increase from 5% to 30% of saturation. Bulk soil moisture application defined as increase from 30% to 70% of saturation.

Table 4.5: MODEL RESULTS AT 23 GMT, 9 MAY

| Run Type | PH | TS | QS | PLI | NA | CONDITION |
|---|---|---|---|---|---|---|
| **Plain** | | | | | | |
| 5-30 | 671 | 31.6 | 9.8 | 4.7 | 12.47 | ~SAT |
| 30-30 | 681 | 31.1 | 10.4 | 5.2 | 17.28 | +SAT |
| 5-70 | 685 | 30.9 | 10.2 | 4.9 | 23.95 | ~SAT |
| 30-70 | 696 | 30.2 | 10.9 | 5.4 | 15.38 | +SAT |
| 50-70 | 711 | 29.4 | 11.9 | 6.2 | 10.21 | +SAT |
| **Early Clouds** | | | | | | |
| 5-30 | 687 | 30.7 | 10.0 | 4.6 | 30.63 | |
| 30-30 | 697 | 30.1 | 10.6 | 5.0 | 23.24 | ~SAT |
| 5-70 | 701 | 29.9 | 10.4 | 4.7 | 32.41 | |
| 30-70 | 716 | 29.1 | 11.2 | 5.3 | 30.47 | ~SAT |
| 50-70 | 733 | 28.0 | 12.3 | 6.1 | 20.30 | +SAT |
| **Imposed Changes** | | | | | | |
| 5-30 | 655 | 31.1 | 9.1 | 3.7 | 15.12 | +SAT |
| 30-30 | 661 | 30.6 | 9.6 | 4.1 | 10.29 | +SAT |
| 5-70 | 663 | 30.4 | 9.4 | 3.7 | 15.17 | +SAT |
| 30-70 | 670 | 29.9 | 10.1 | 4.4 | 5.72 | +SAT |
| 50-70 | 686 | 29.3 | 11.1 | 5.3 | <0.0 | +SAT |
| **Clouds and Imposed Changes** | | | | | | |
| 5-30 | 665 | 30.3 | 9.6 | 3.9 | 12.67 | +SAT |
| 30-30 | 672 | 29.8 | 10.2 | 4.4 | 4.48 | +SAT |
| 5-70 | 676 | 29.6 | 10.1 | 4.2 | 7.27 | +SAT |
| 30-70 | 697 | 29.1 | 10.9 | 5.0 | 0.30 | +SAT |
| 50-70 | 717 | 28.3 | 12.1 | 6.0 | <0.0 | +SAT |

See Table 4.1 for legend.

Table 4.6: MODEL RESULTS AT 23 GMT, 9 MAY CONTINUED

| Run Type | PH | TS | QS | PLI | NA | CONDITION |
|---|---|---|---|---|---|---|
| **Surface Moisture Advection** | | | | | | |
| 5-30 | 671 | 31.6 | 8.7 | 3.4 | 39.08 | |
| 30-30 | 681 | 31.1 | 9.3 | 3.9 | 43.85 | |
| 5-70 | 685 | 30.9 | 9.1 | 3.6 | 55.62 | |
| 30-70 | 697 | 30.2 | 9.8 | 4.1 | 46.42 | |
| 50-70 | 711 | 29.4 | 10.8 | 5.0 | 38.48 | |
| **Surface Moisture Advection, Clouds, and Imposed Changes (QCH)** | | | | | | |
| 5-30 | 664 | 30.3 | 8.6 | 2.7 | 37.93 | ~SAT |
| 30-30 | 672 | 29.8 | 9.3 | 3.4 | 27.93 | +SAT |
| 5-70 | 674 | 29.7 | 9.1 | 3.1 | 30.86 | +SAT |
| 30-70 | 695 | 29.1 | 10.0 | 3.9 | 14.01 | +SAT |
| 50-70 | 718 | 28.2 | 11.2 | 5.0 | 0.50 | +SAT |
| **QCH Modified for Surface Temperature Advection** | | | | | | |
| 5-30 | 664 | 32.3 | 8.6 | 3.6 | 18.45 | |
| 30-30 | 672 | 31.8 | 9.3 | 4.2 | 7.62 | |
| 5-70 | 674 | 31.7 | 9.1 | 3.9 | 15.43 | |
| 30-70 | 695 | 31.1 | 10.0 | 4.7 | 1.31 | |
| 50-70 | 718 | 30.2 | 11.2 | 5.8 | 0.21 | |

See Table 4.1 for legend.

Table 4.7: SENSITIVITY VALUES FOR 23 GMT, 9 MAY MODEL RUNS

| Changes in: Factor | PH | TS | QS | PLI | NA |
|---|---|---|---|---|---|
| Early Clouds | - 8 | - 8 | -10 | - 6 | +42 |
| Imposed Changes | +10 | - 4 | +21 | -47 | +18 to -100 |
| Clouds and Imposed Changes | + 4 to - 3 | -10 | + 5 to - 5 | -26 | + 2 to -100 |
| Surface Moisture Advection | 0 | 0 | +30 | -59 | +65 |
| Clouds, Imposed Changes, and Surface Moisture Advection | + 4 to - 3 | -10 | +27 | -75 | +67 to -95 |
| Surface Soil Moisture | - 5 | - 5 | -16 | +30 | + 3 to -59 |
| Bulk Soil Moisture | - 6 | - 7 | -10 | +14 | +26 to -44 |

See Table 4.4 for legend.

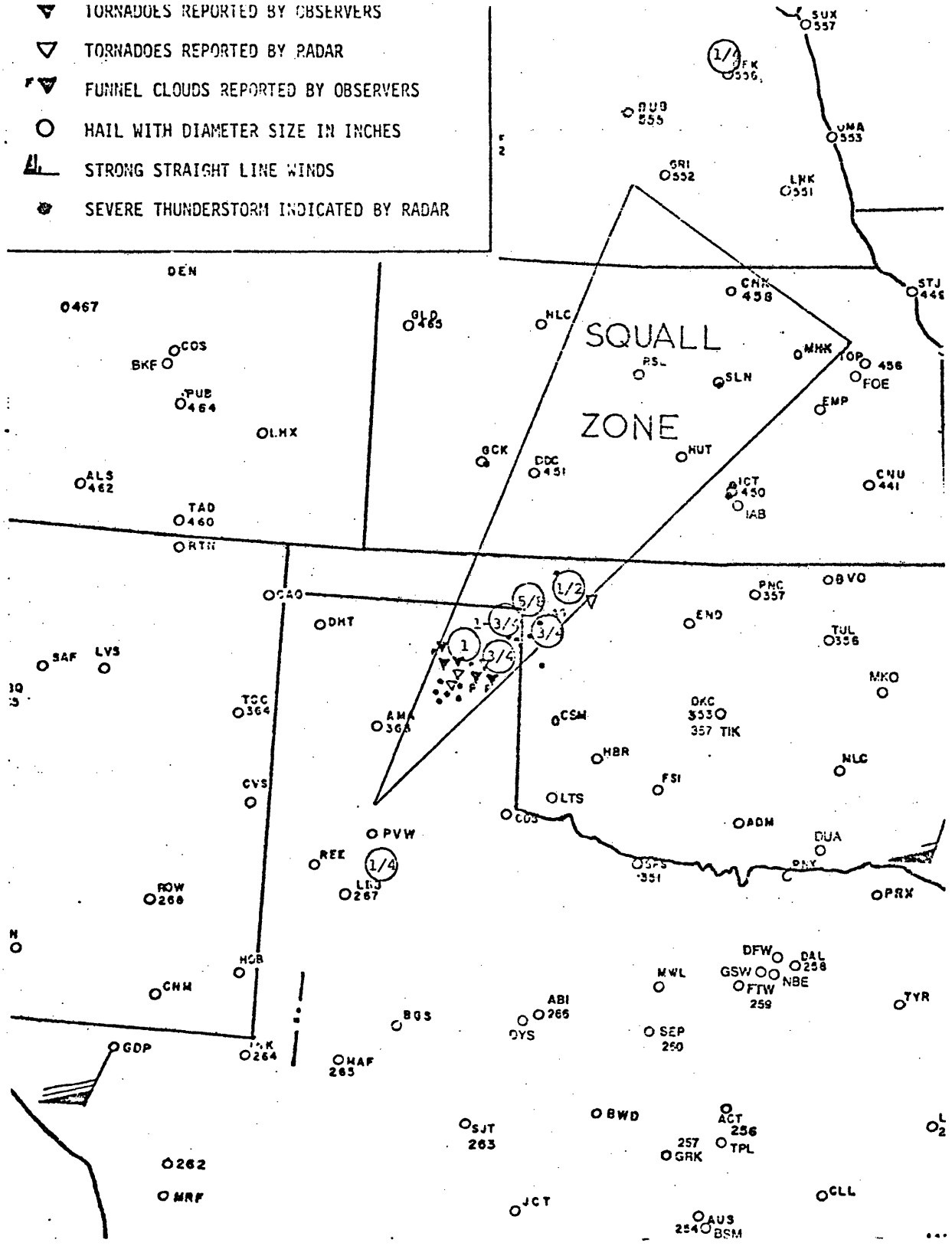


Fig. 4.1 Severe weather events during period 12 GMT, 9 May to 12 GMT, 10 May 1979. Squall zone refers to area of convective outbreaks during 24 hour period.

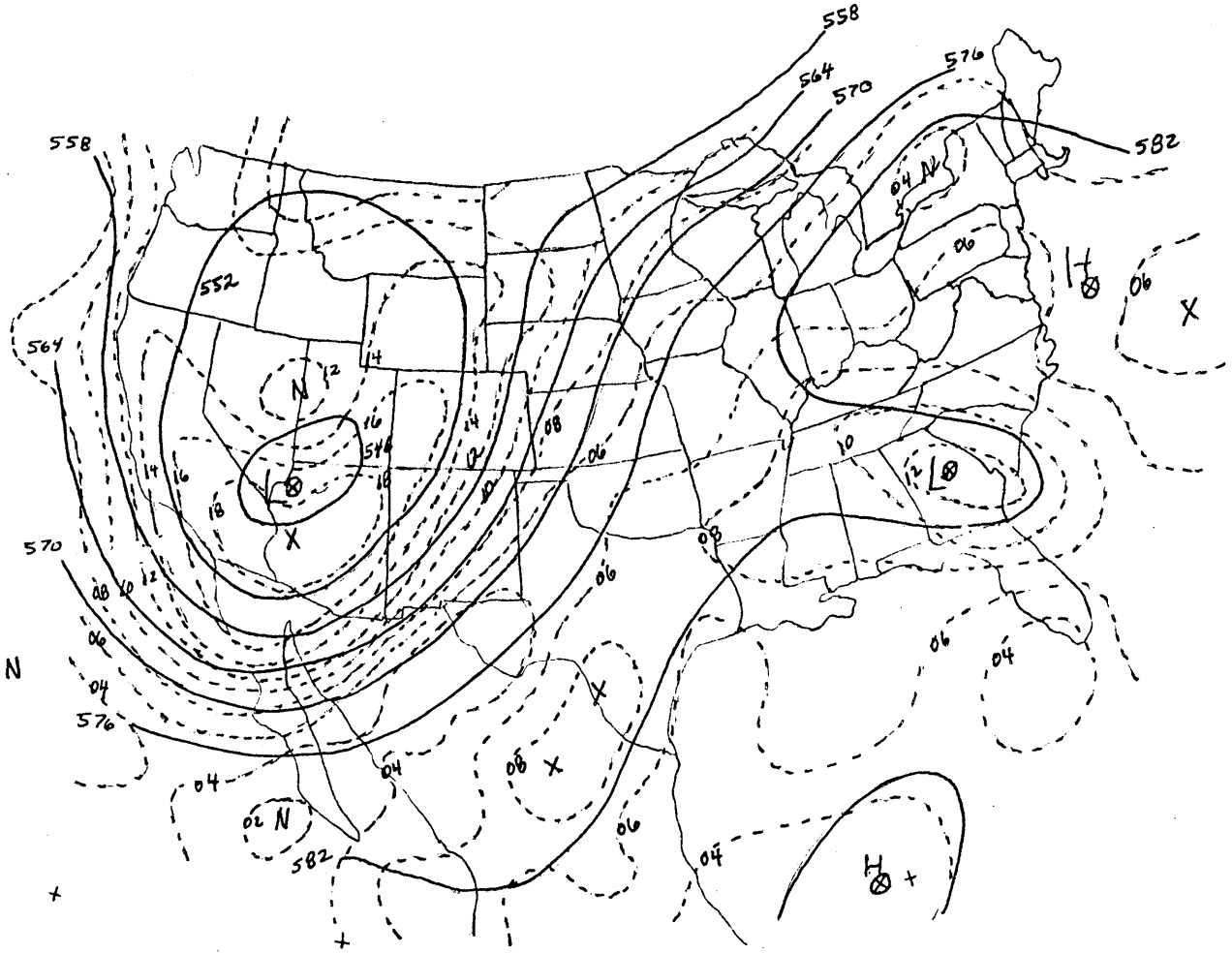


Fig. 4.2 Synoptic-scale 500 mb analysis for 12 GMT, 9 May. Solid lines are heights (dm), and dashed lines are vorticity (10**-5 1/s).

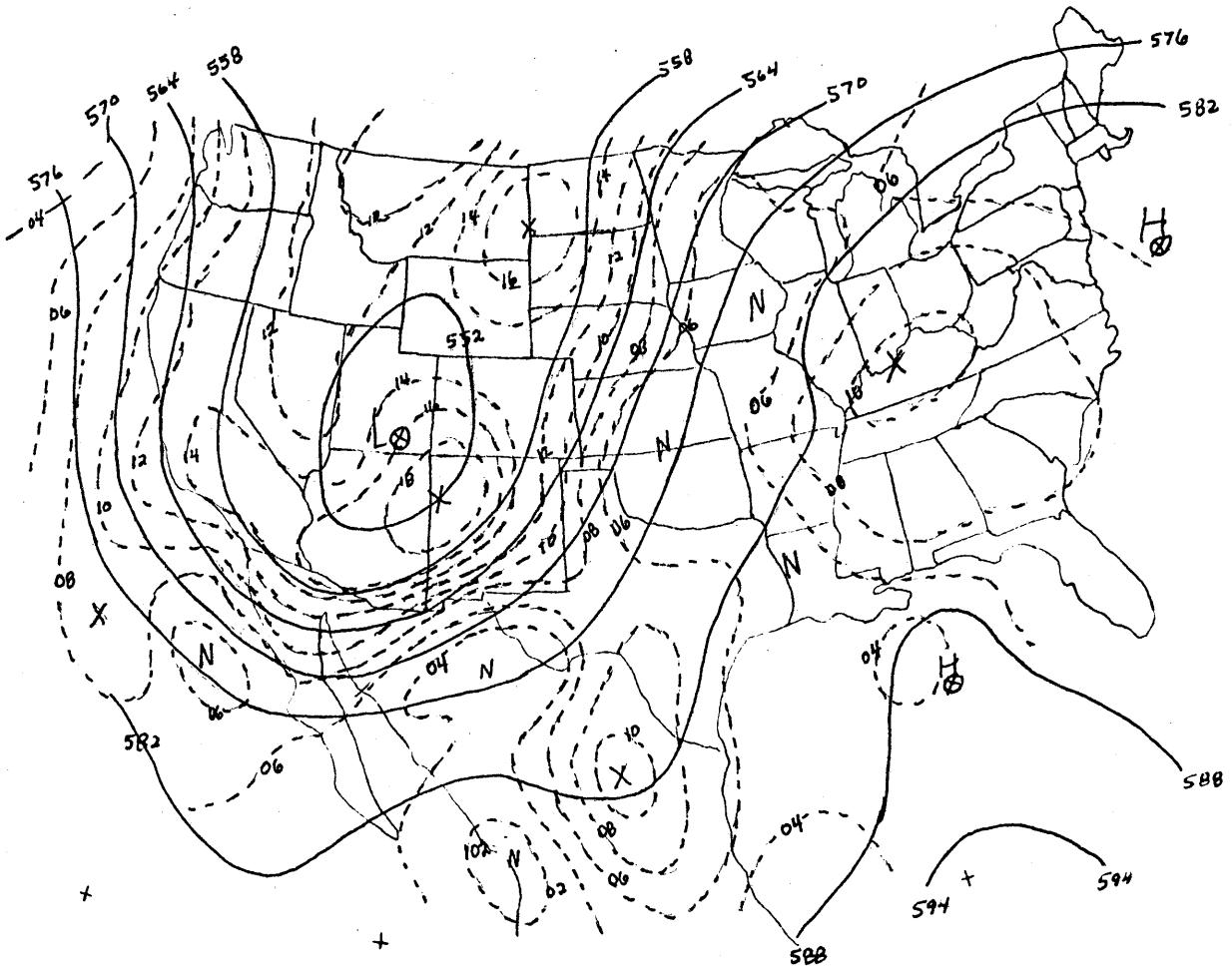


Fig. 4.3 Same as Fig. 4.2 for 00 GMT, 10 May.

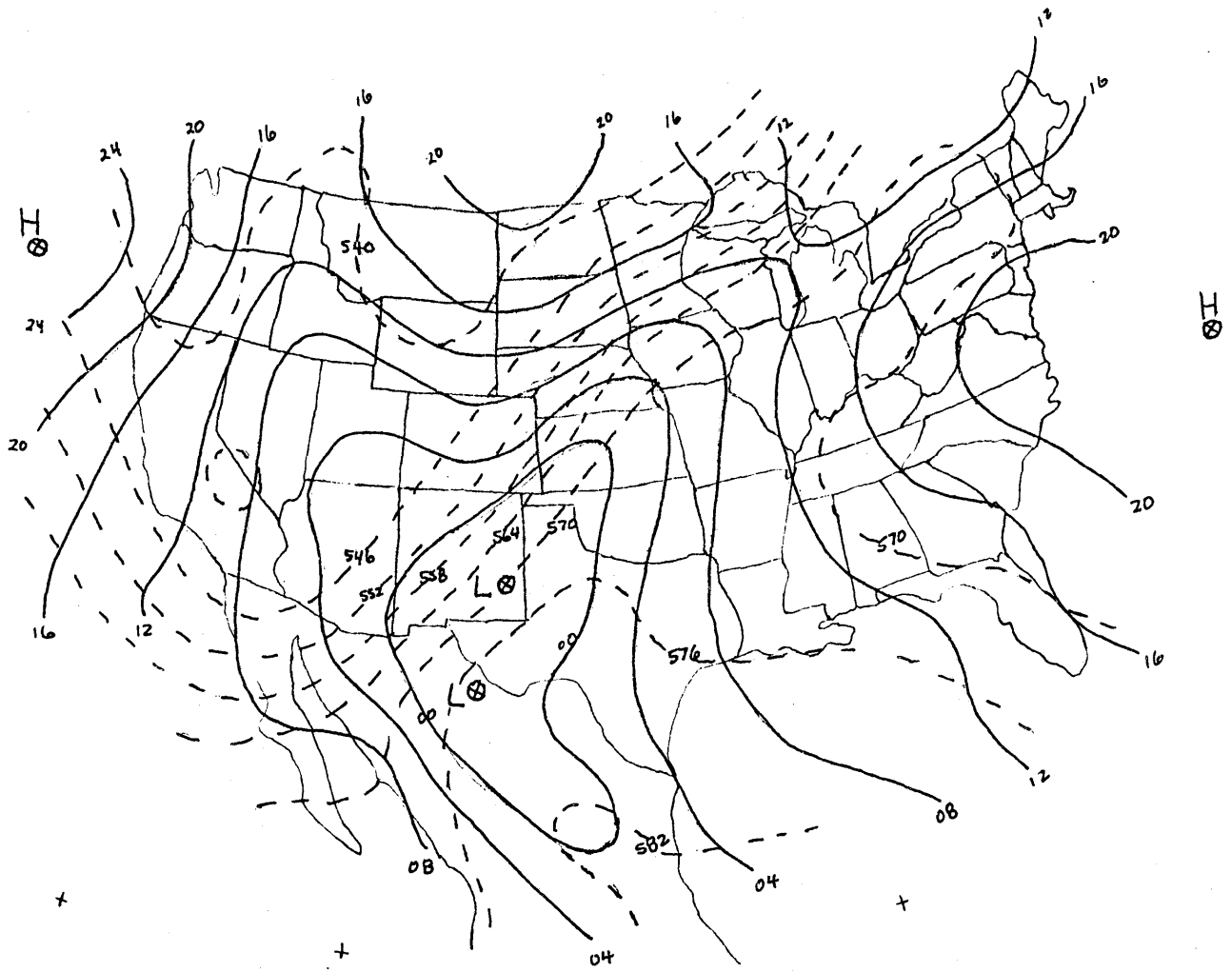


Fig. 4. 4 Synoptic scale surface analysis for 12 GMT, 9 May. Solid lines are sea level pressure (mb), leading 9 or 10 digit(s) dropped and dashed lines for 1000 mb to 500 mb thickness (dm).

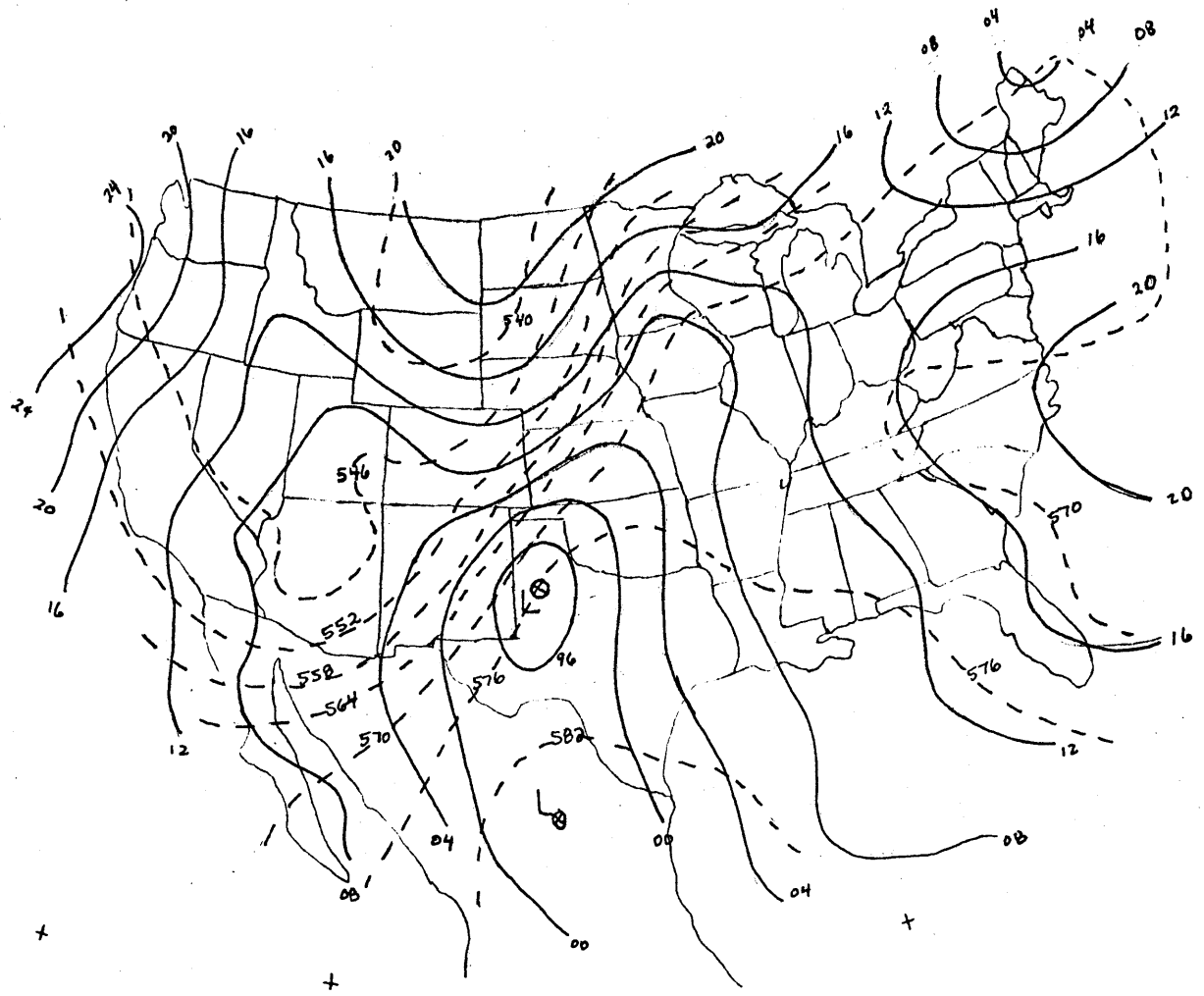


Fig. 4.5 Same as Fig. 4.4 for 00 GMT, 10 May.

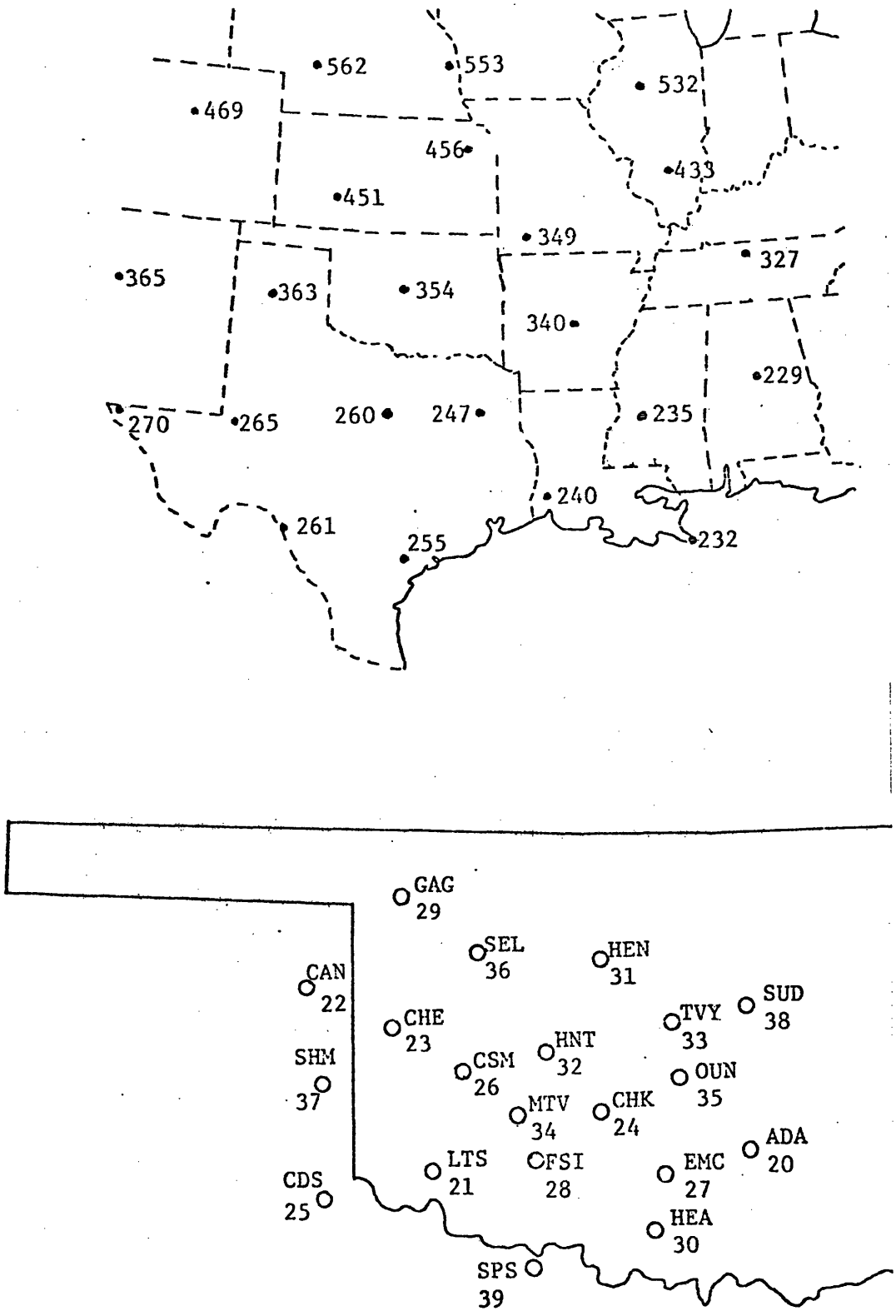


Fig. 4.6 Locations of radiosonde launch sites for this case.

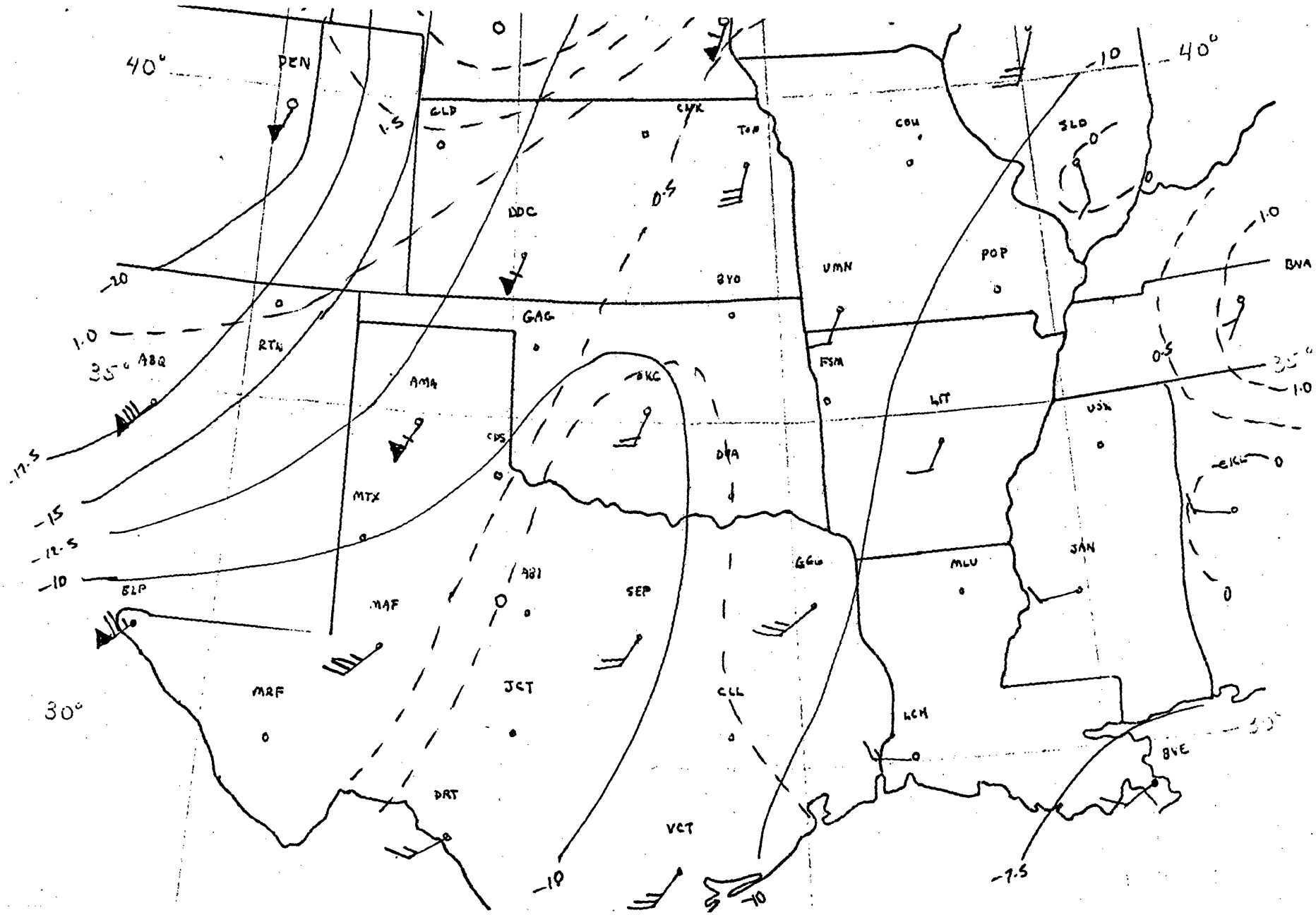


Fig. 4.7 500 mb analysis using special network of Fig. 4.6 for 11 GMT, 9 May. Solid lines for temperatures (deg C), and dashed lines for mixing ratio (g/kg). Winds plotted conventionally (knots).

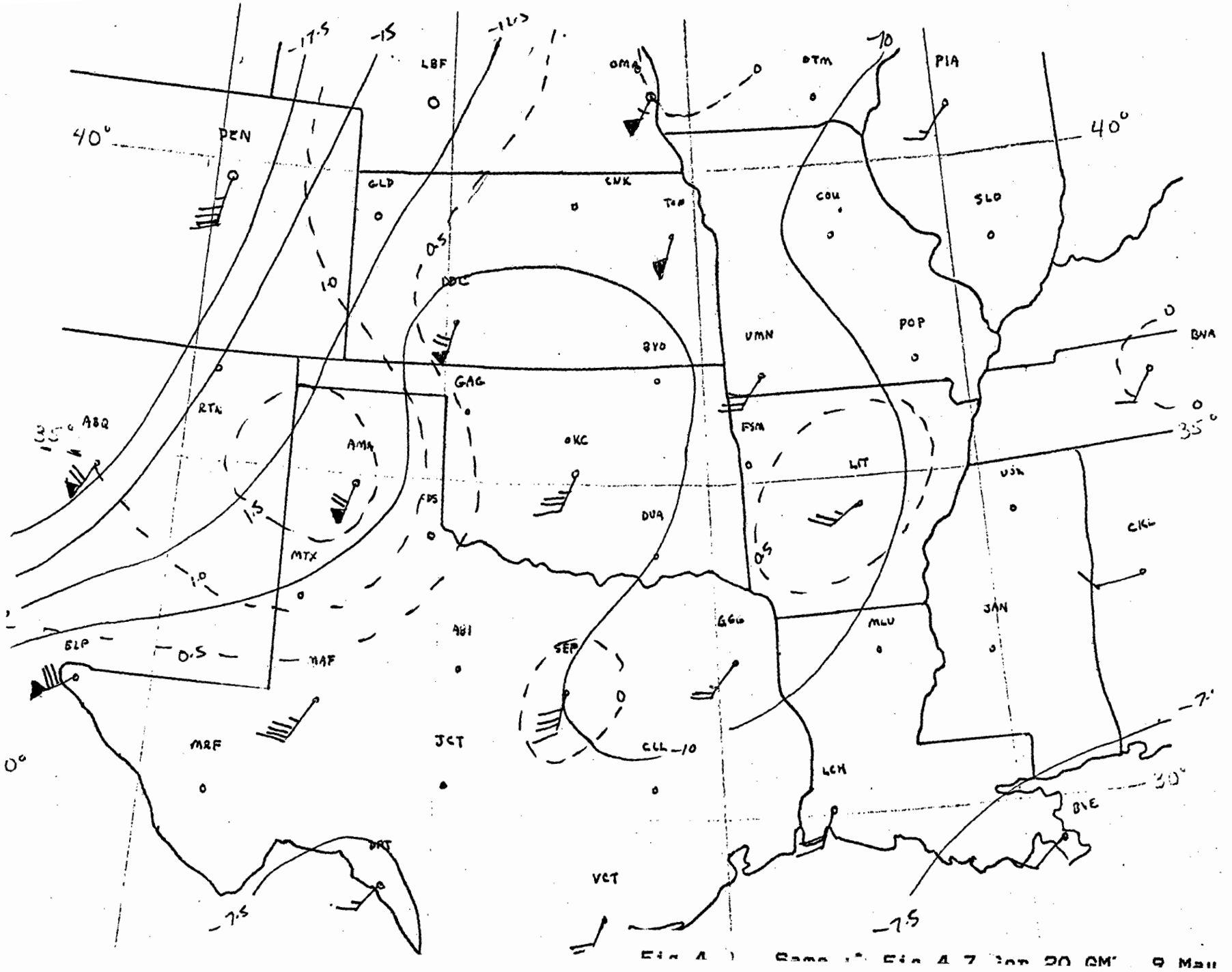
-17.5
-15
-12.5
LBF
OMA
STM
PIA
40°
DEN
GLD
CNK
TOP
COU
SLD
0.5
1.0
DDC
BYO
UMN
POP
BNA
GAG
RTN
ABQ
35°
AMA
OKC
FSM
LIT
USH
CKL
FDS
DUA
MTX
1.5
1.0
ELP
0.5
ABI
SEP
GGG
MLU
JAN
MAF
MRF
JCT
CLL
-10
LCH
BLE
30°
DRT
VCT
-7.5
-7.5
-7.
0°

PAGE 190

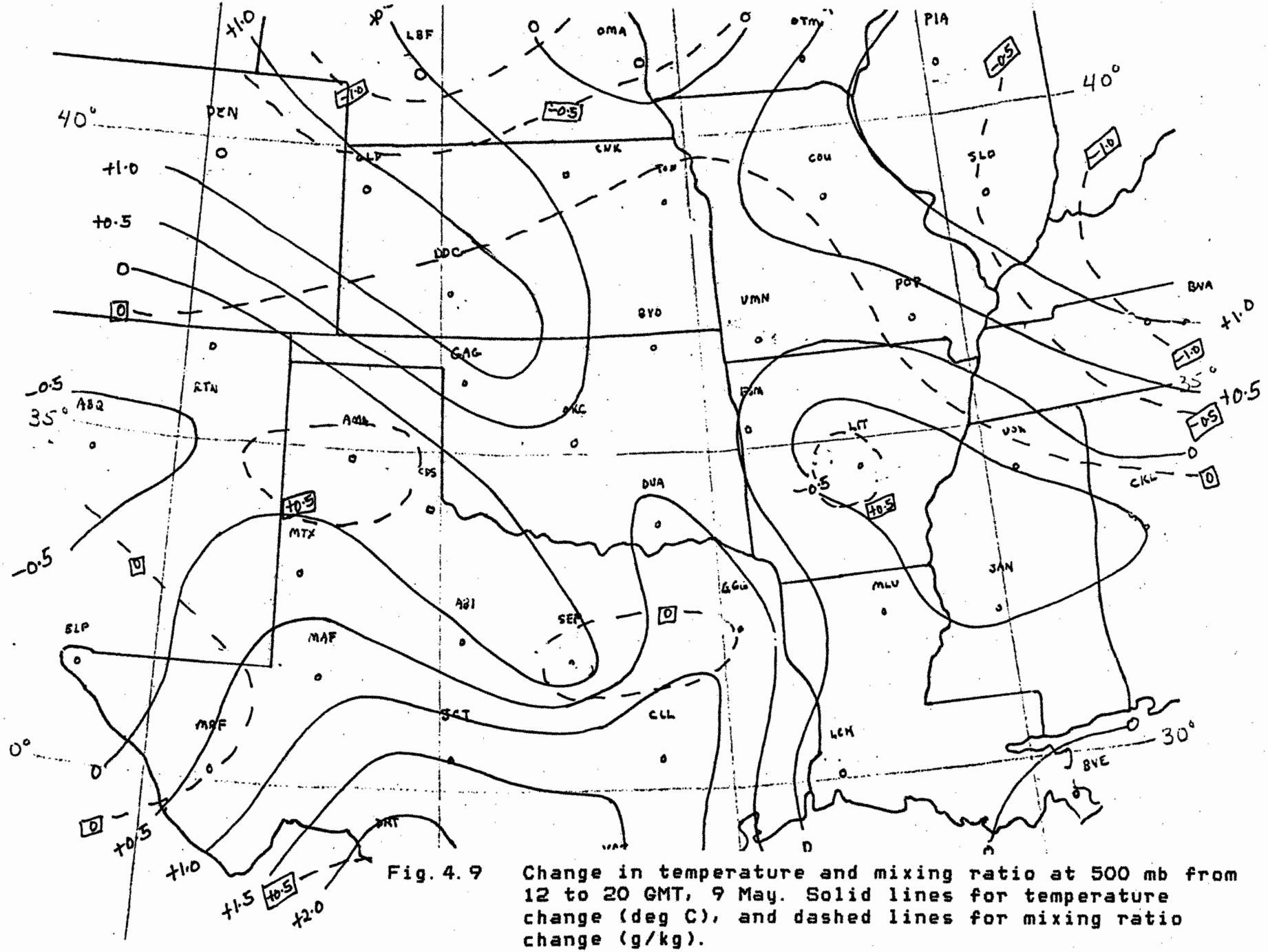


Fig. 4.9 Change in temperature and mixing ratio at 500 mb from 12 to 20 GMT, 9 May. Solid lines for temperature change (deg C), and dashed lines for mixing ratio change (g/kg).

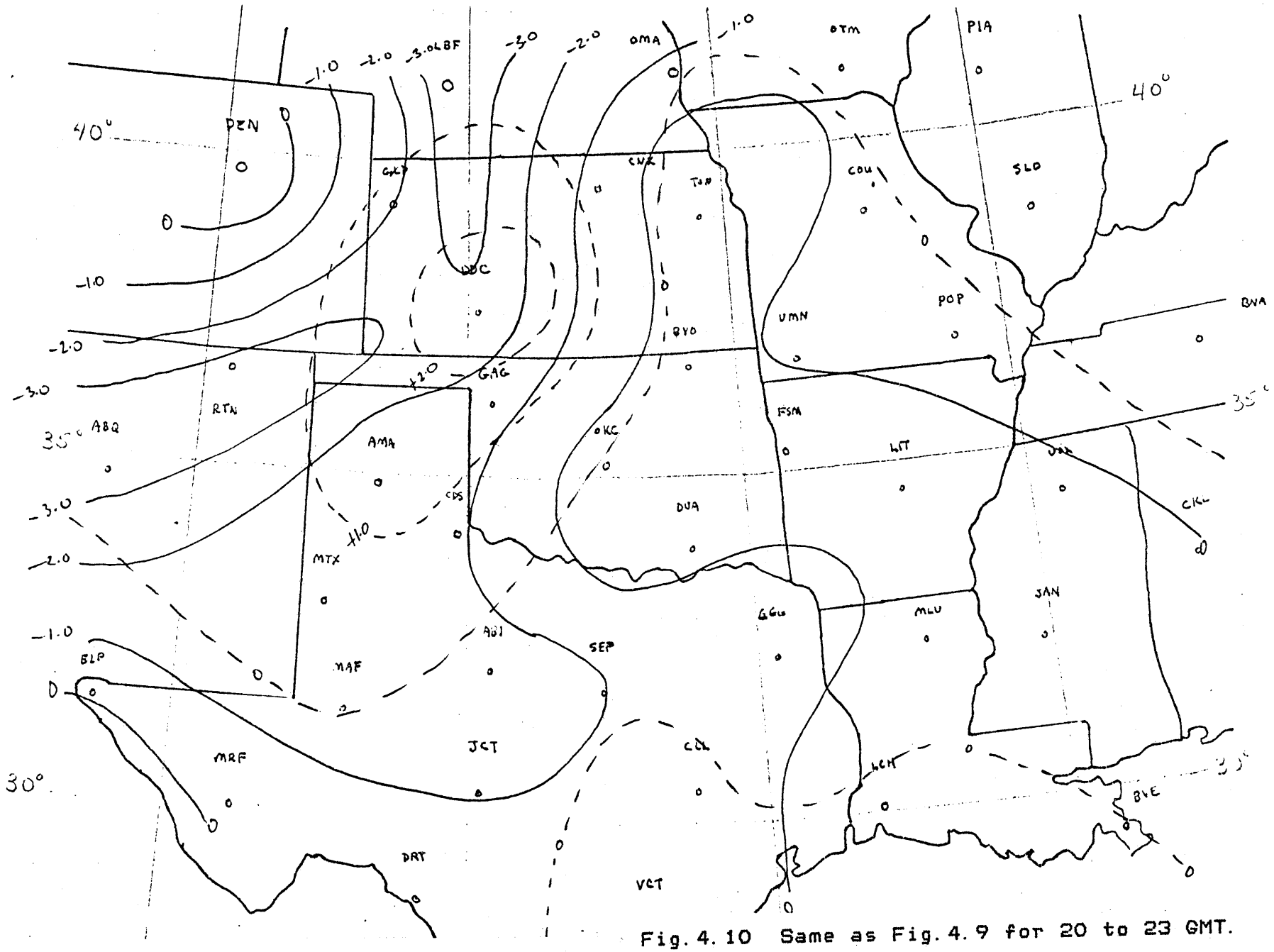


Fig. 4.10 Same as Fig. 4.9 for 20 to 23 GMT.

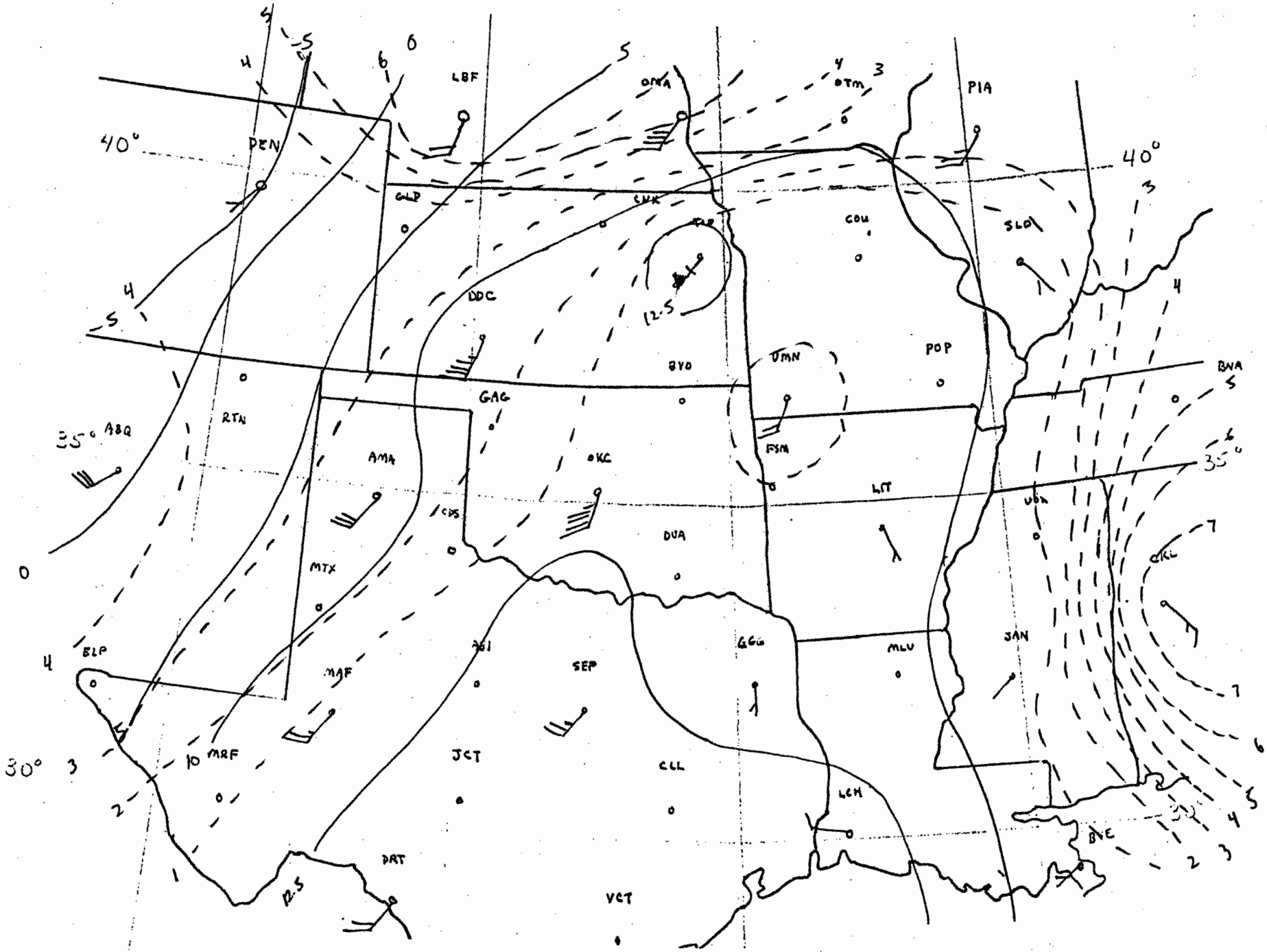


Fig. 4.11 Same as Fig. 4.7 for 700 mb.

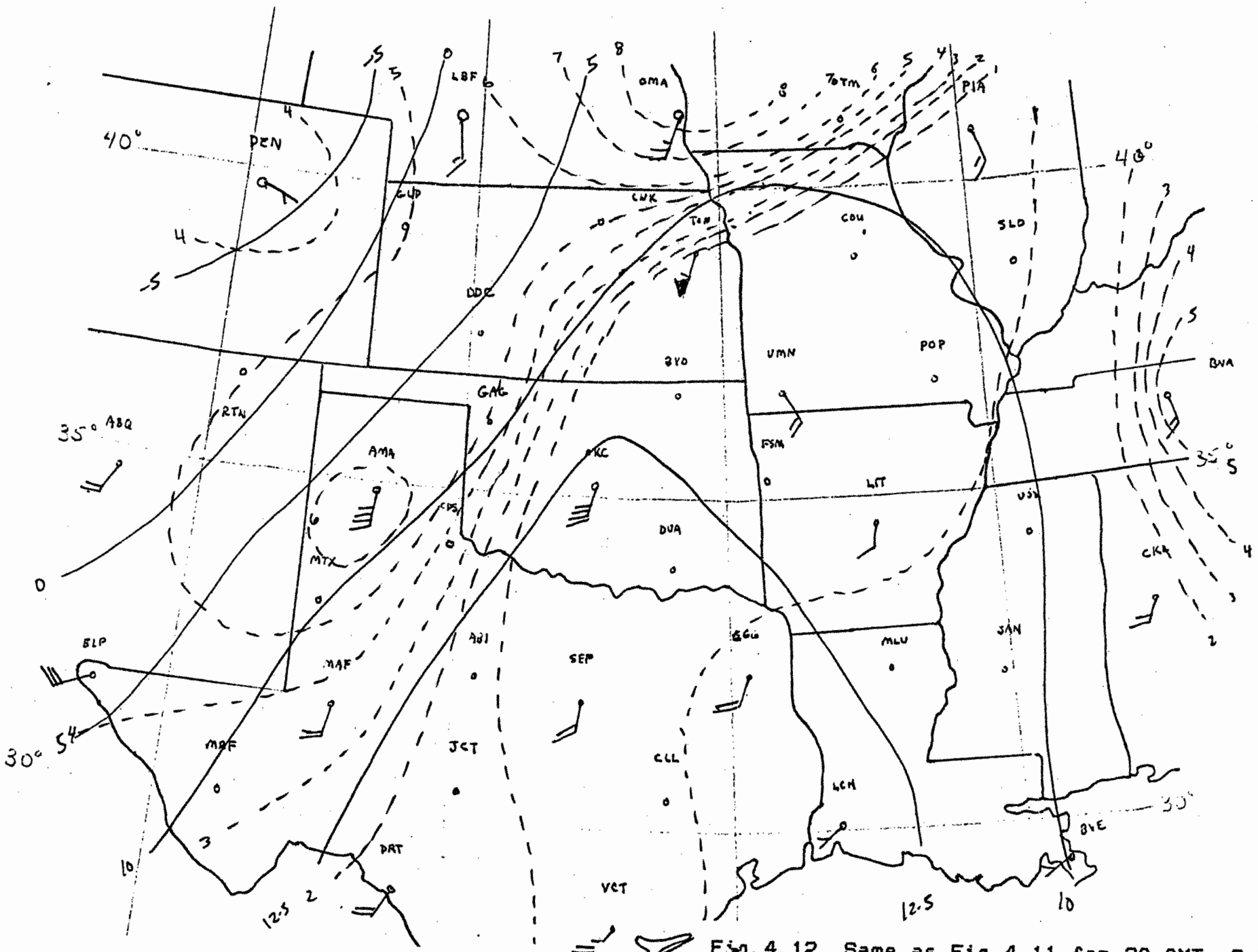


Fig. 4.12 Same as Fig. 4.11 for 20 GMT, 9 May.

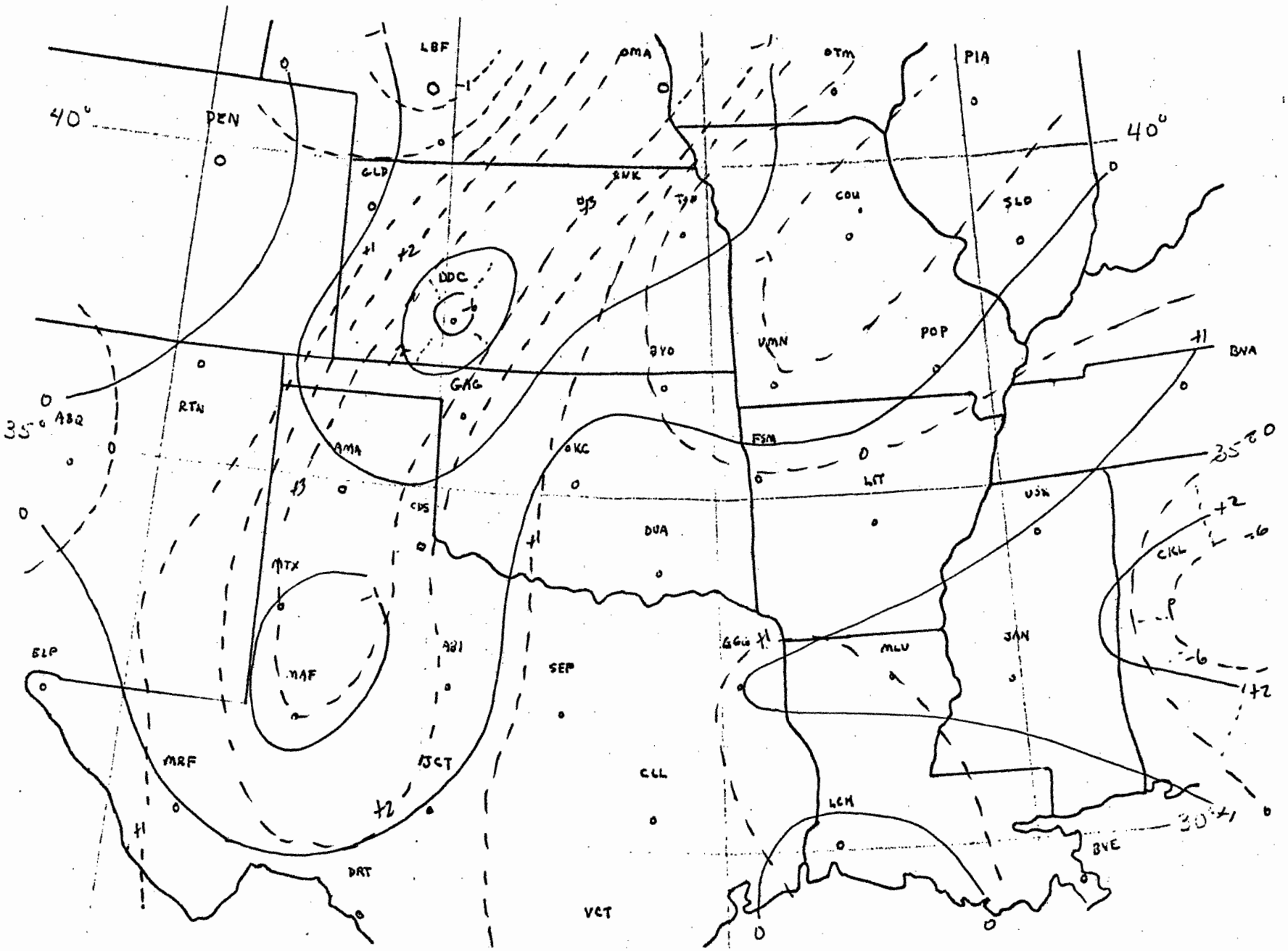


Fig. 4.13 Same as Fig. 4.9 for 700 mb.

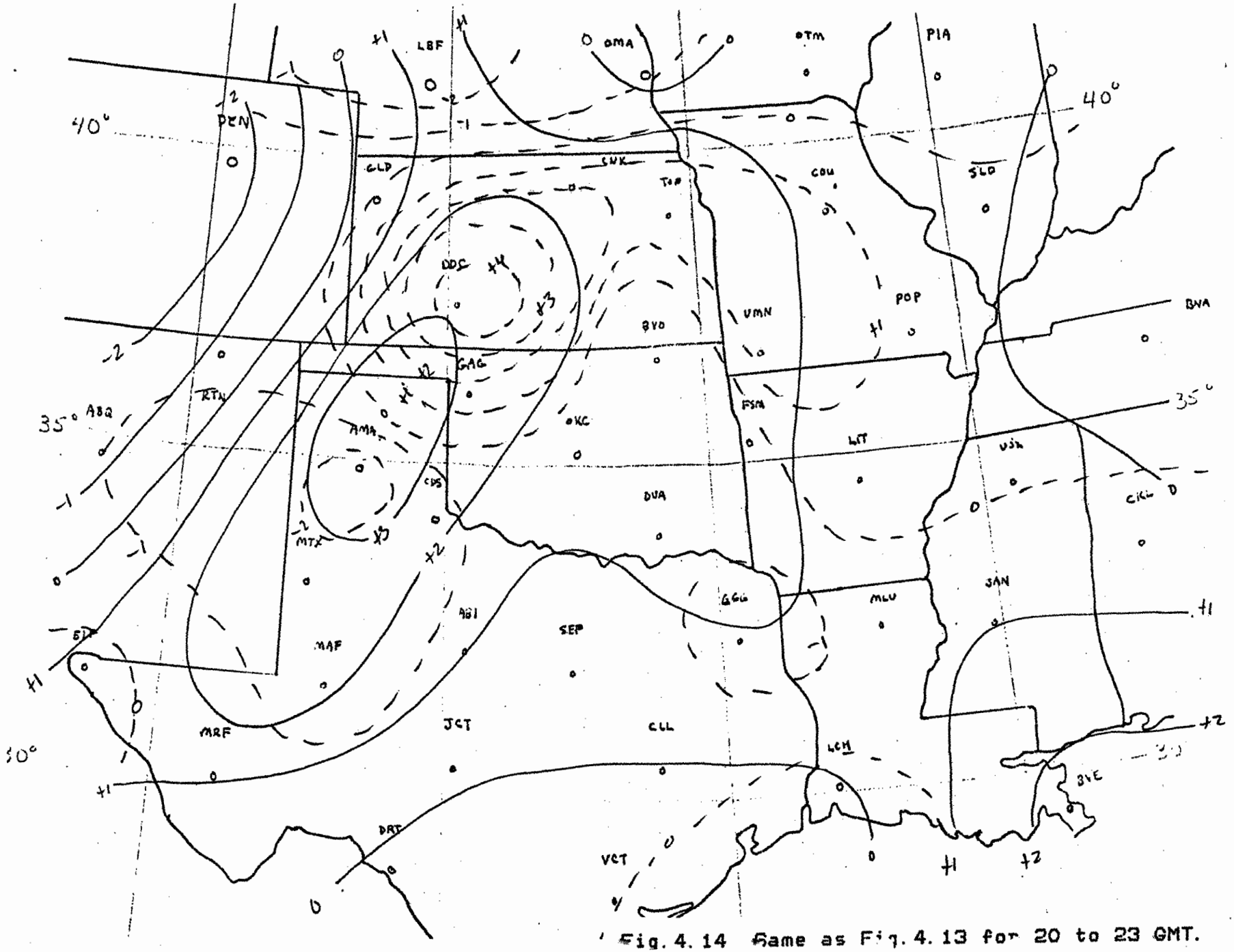


Fig. 4.14 Same as Fig. 4.13 for 20 to 23 GMT.

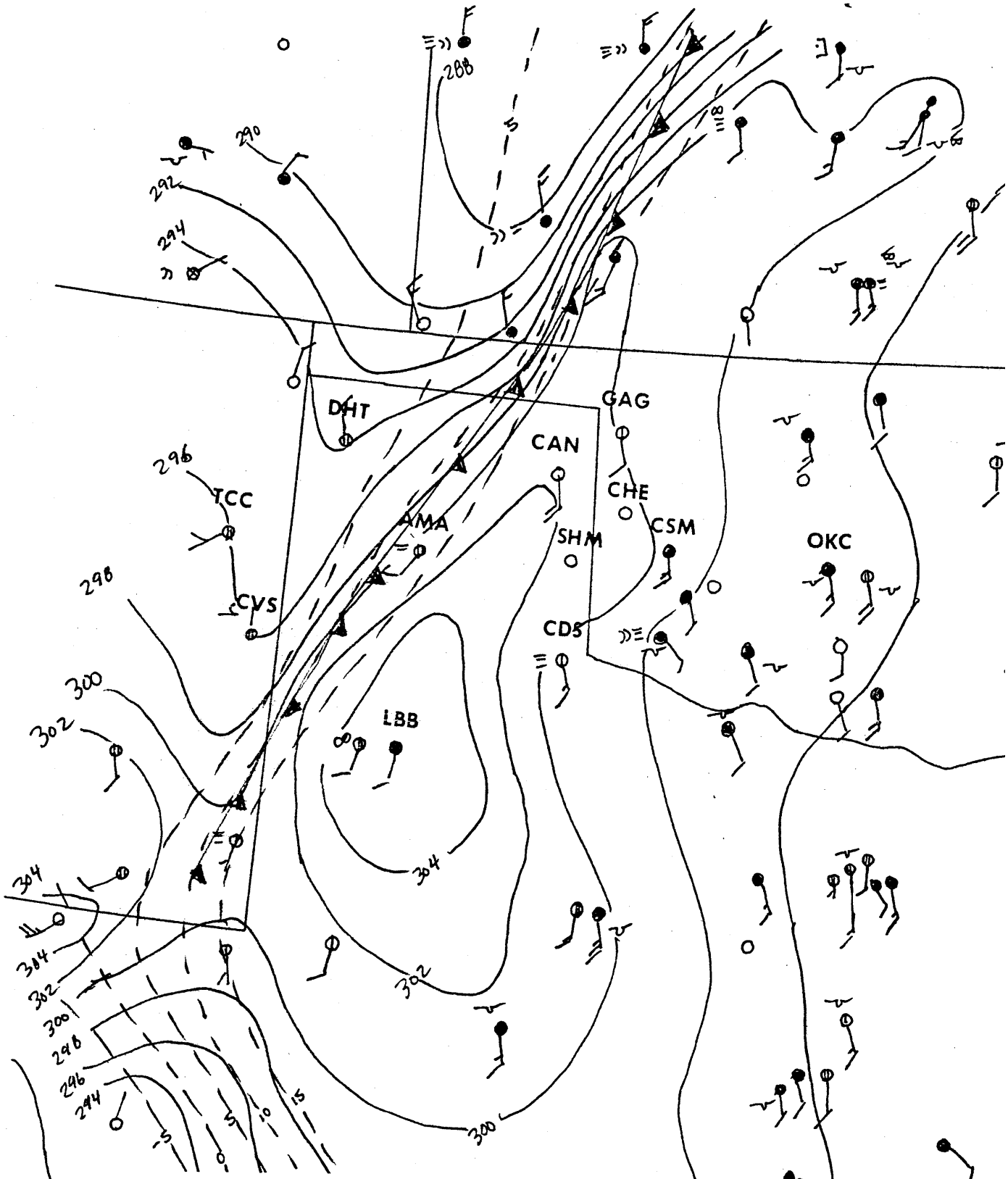


Fig. 4.15 Mesoscale surface analysis for 12 GMT, 9 May. Solid lines are surface potential temperatures (K) and dashed lines are dewpoints (deg C). Winds are plotte conventionally (knots). Sky condition is clear (open circle), scattered (single bar), broken (double bar) overcast (filled circle), and obscurred (x in circle). Cloud type is plotted (if available) as is current weather according to conventional synoptic code. Radar echoes are cross-hatched irregularly shaped areas. Surface cold front is depicted by a line with triangles along it.

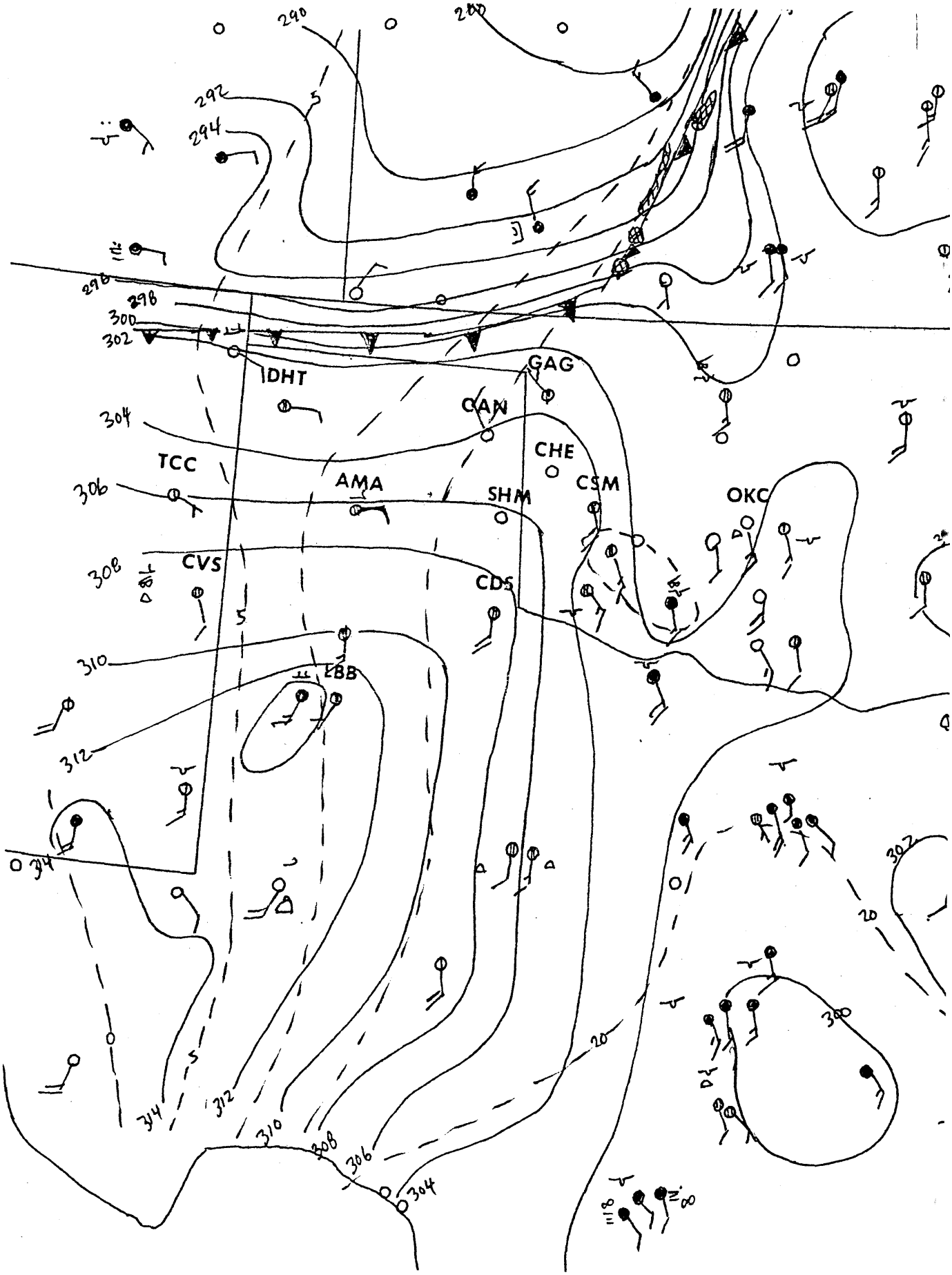


Fig. 4.16 Same as Fig. 4.15 for 18 GMT, 9 May.

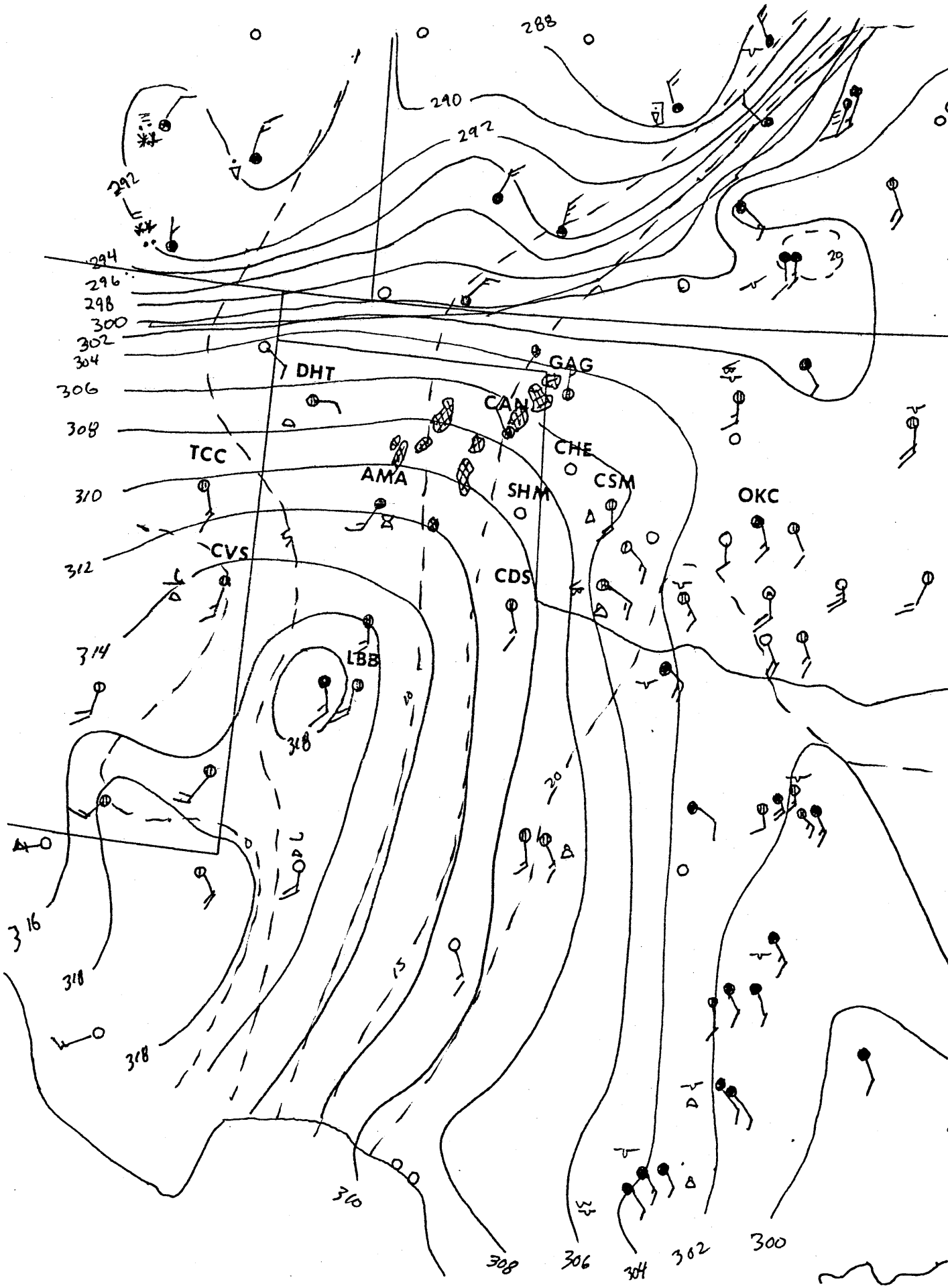


Fig. 4.17 Same as Fig. 4.15 for 21 GMT, 9 May.

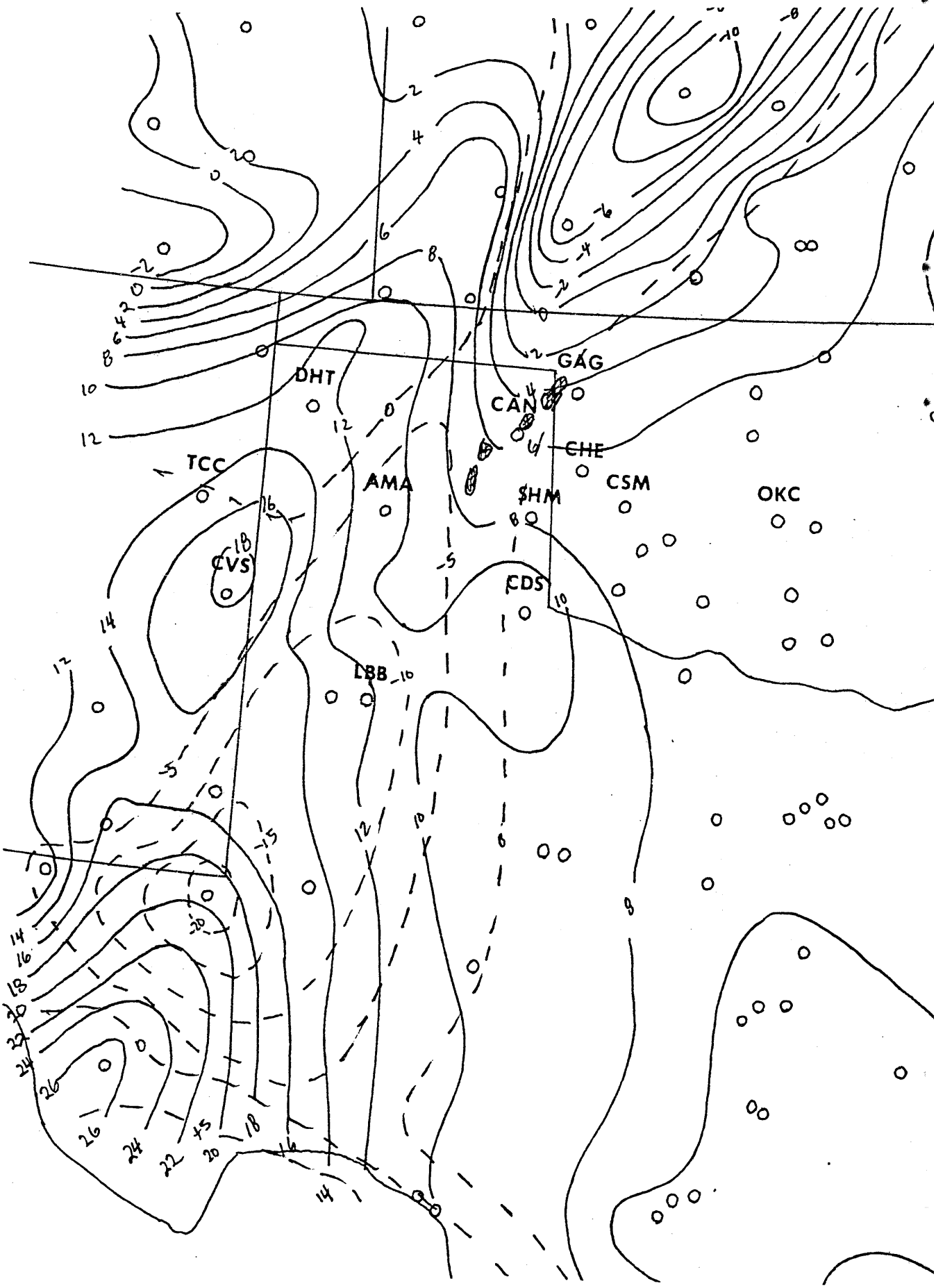


Fig. 4.18 Change in potential temperature and dewpoint from 12 GMT to 21 GMT, 9 May. Solid lines for potential temperature change (K) and dashed lines for change in dewpoint (deg C).

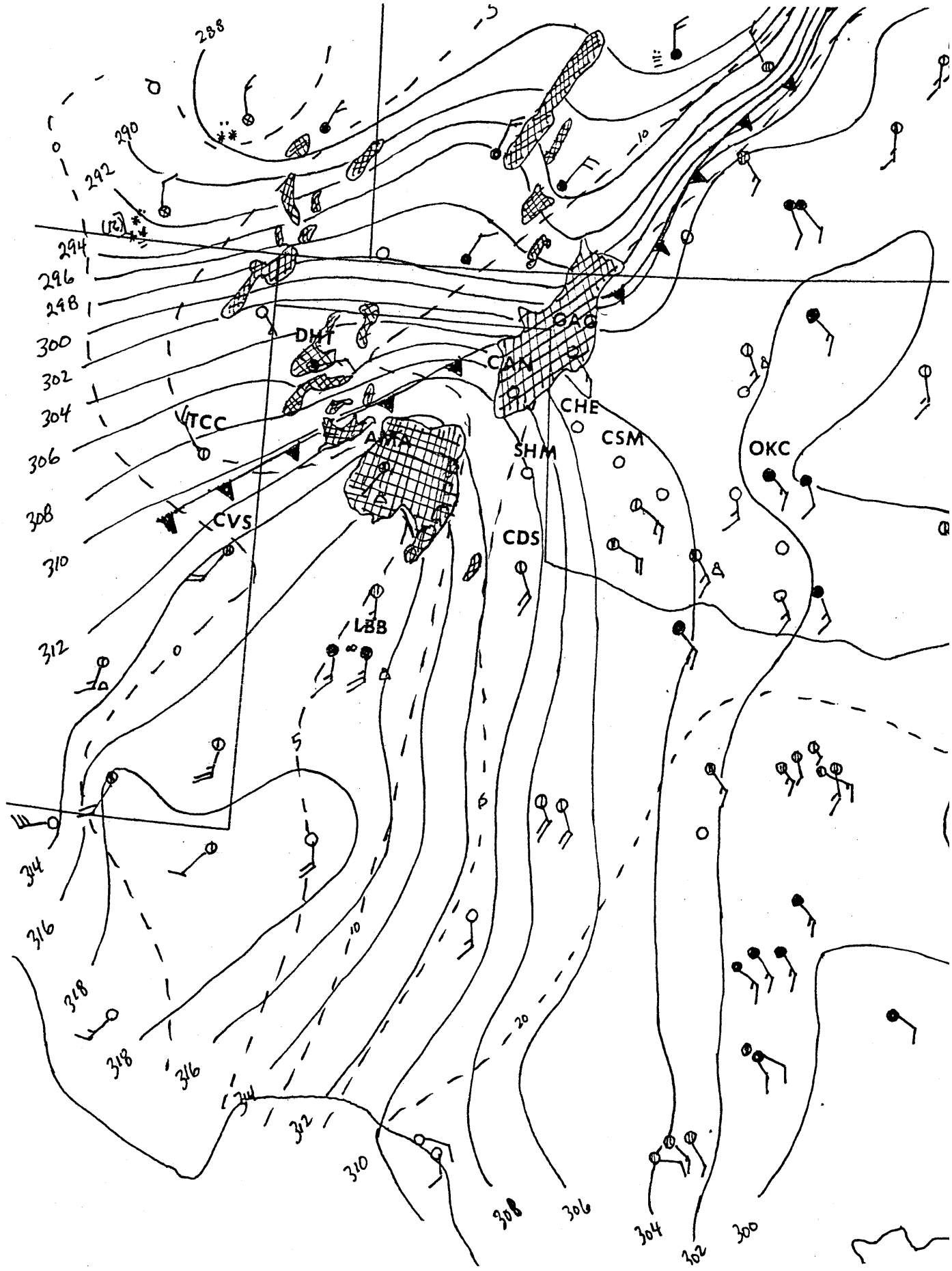


Fig. 4.19 Same as Fig. 4.15 for 23 GMT, 9 May.

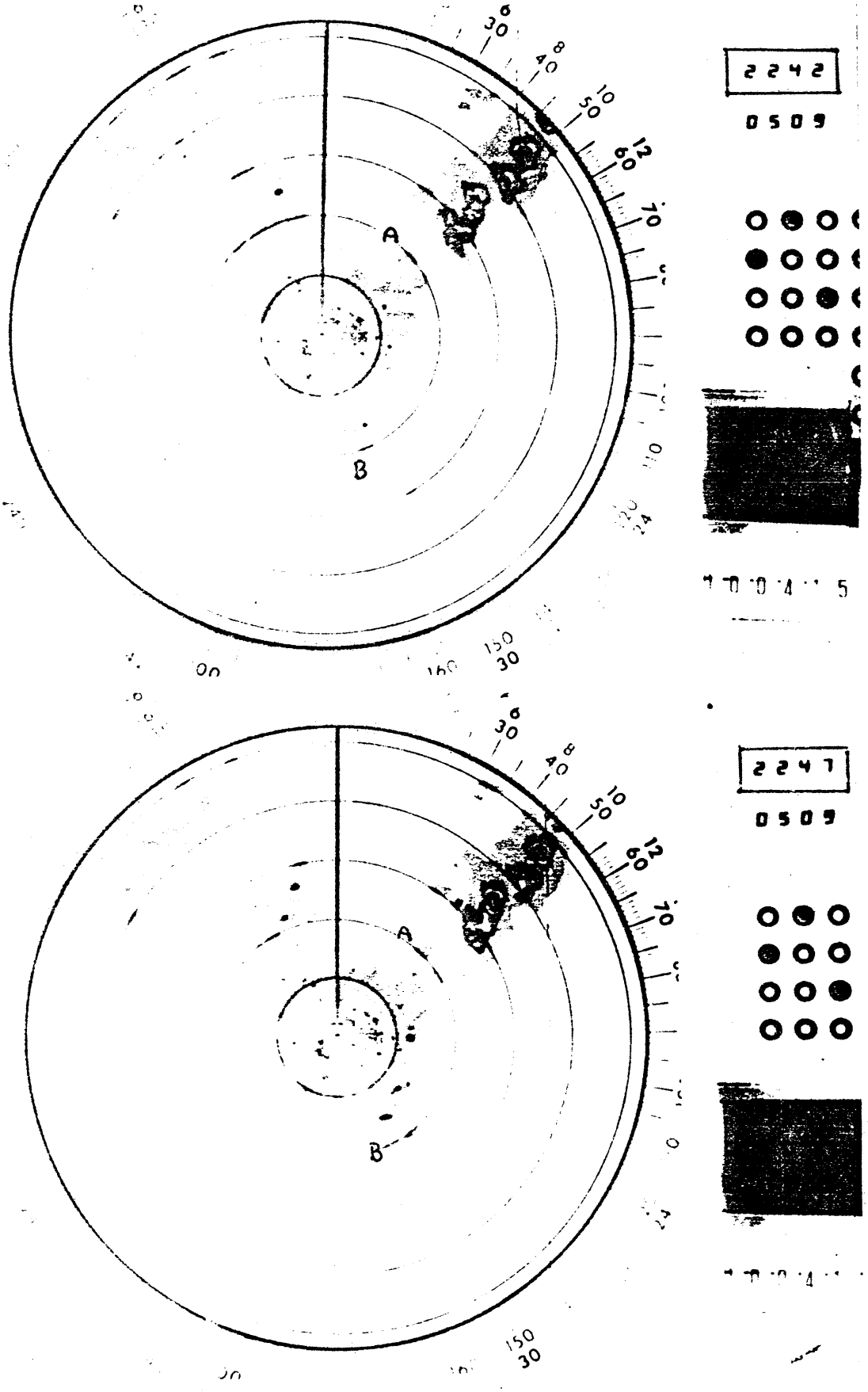


Fig. 4.20 Photograph of low-elevation angle display from radar screen at Amarillo, Texas at 2242, 2247, and 2254 GMT, 9 May. Range rings are 20 nm apart.

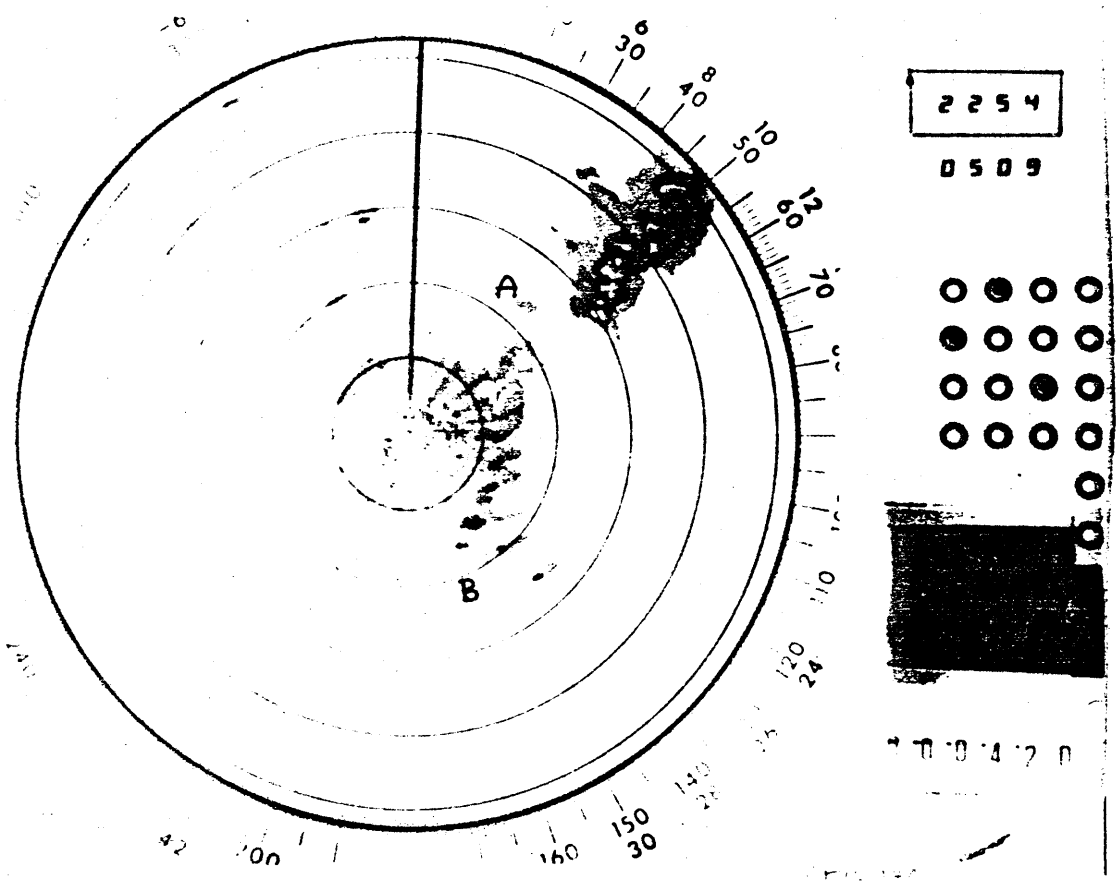


Fig. 4.20 Continued

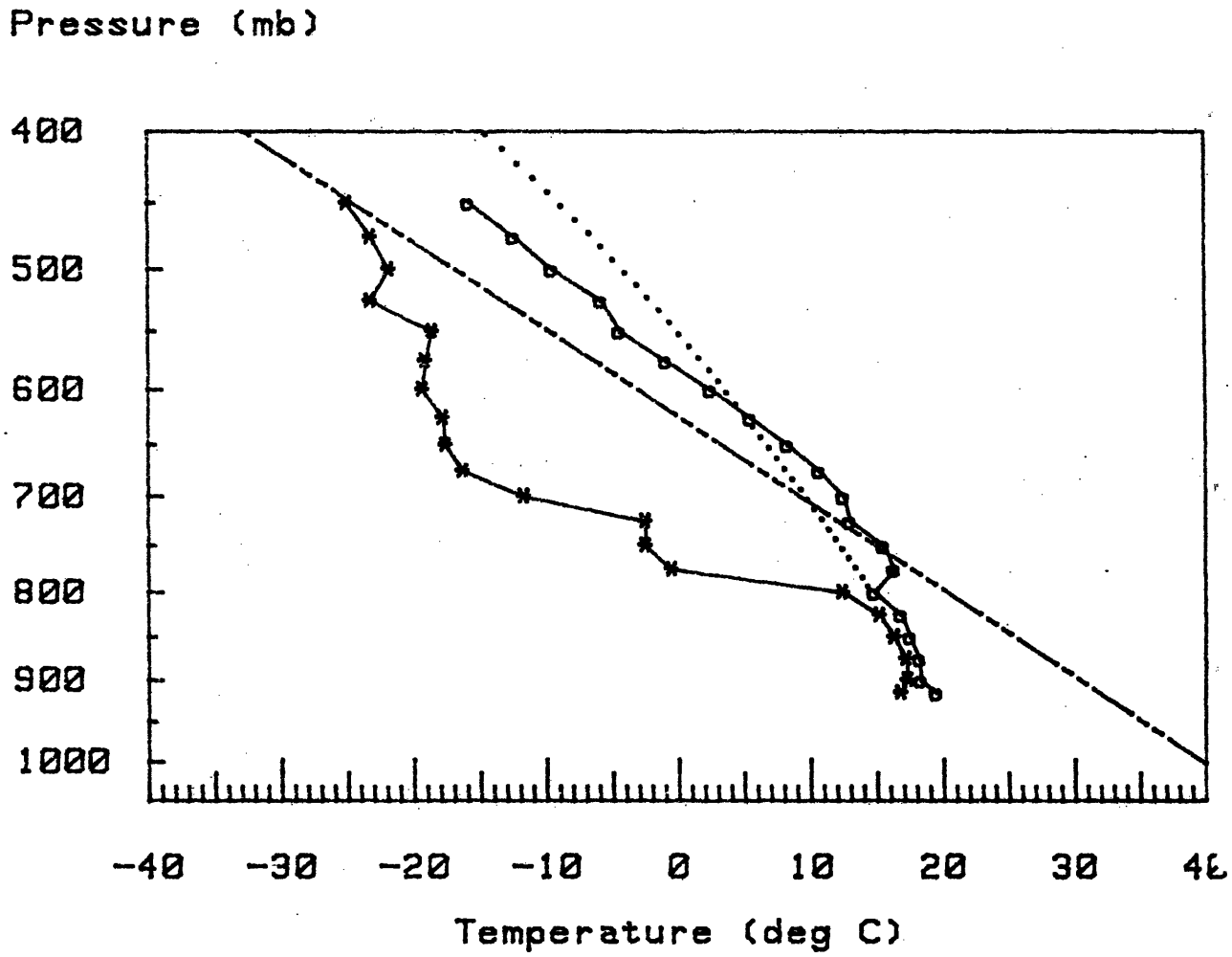


Fig. 4.21 Sounding plotted on a pseudoadiabatic diagram from Shamrock, Texas for 1143 GMT, 9 May. Solid line connecting dots for temperature (deg C), solid line connecting * for dewpoint (deg C), dash-dotted line for 313 K isentrope, and dotted line showing moist adiabat for mean PBL parcel (or selected parcel if PBL is not well-defined.) Dewpoints colder than -40 C are plotted at -40 C.

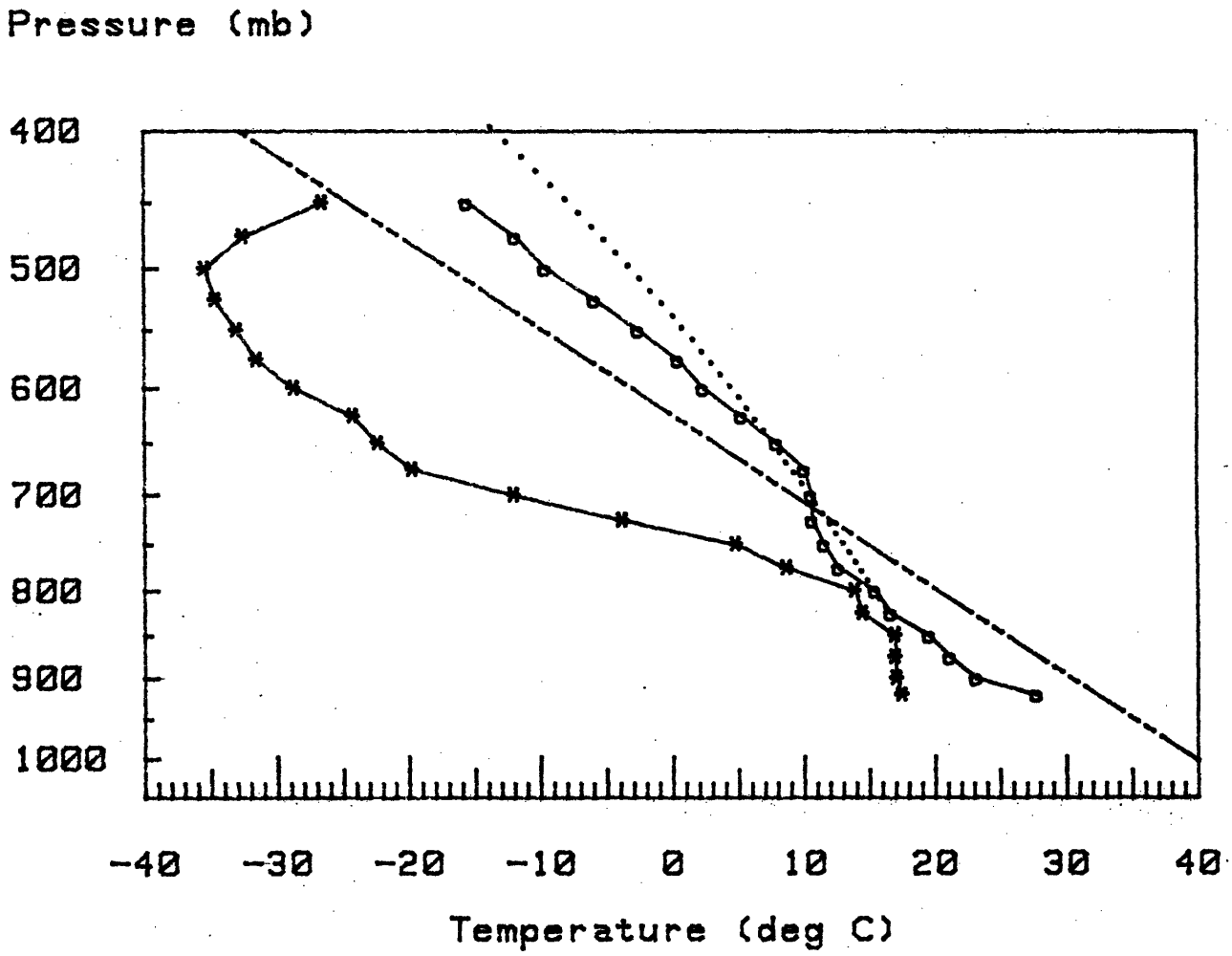


Fig. 4.22 Same as Fig. 4.21 for 1705 GMT, 9 May.

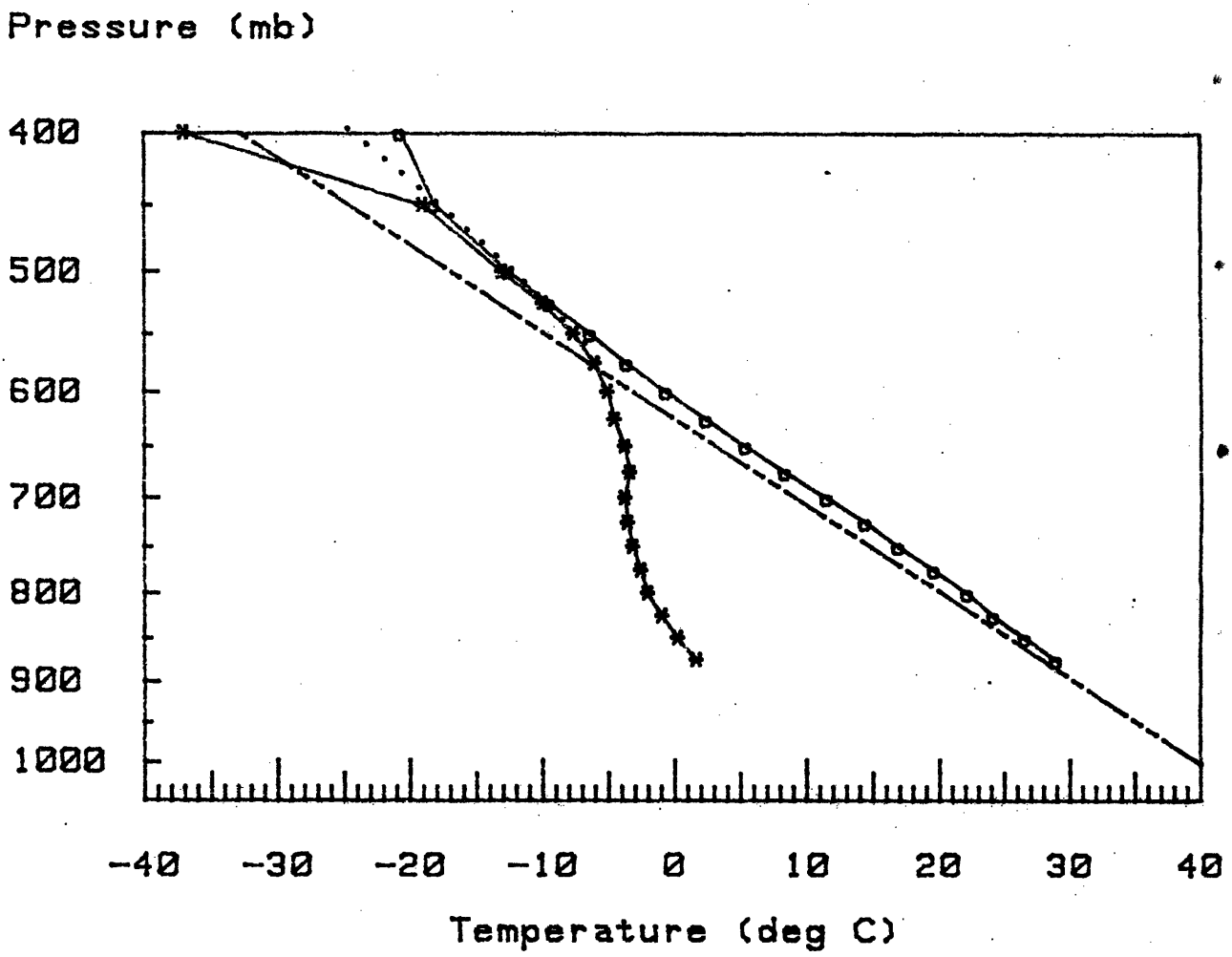


Fig. 4.23 Same as Fig. 4.21 for Amarillo, Texas 23 GMT, 9 May.

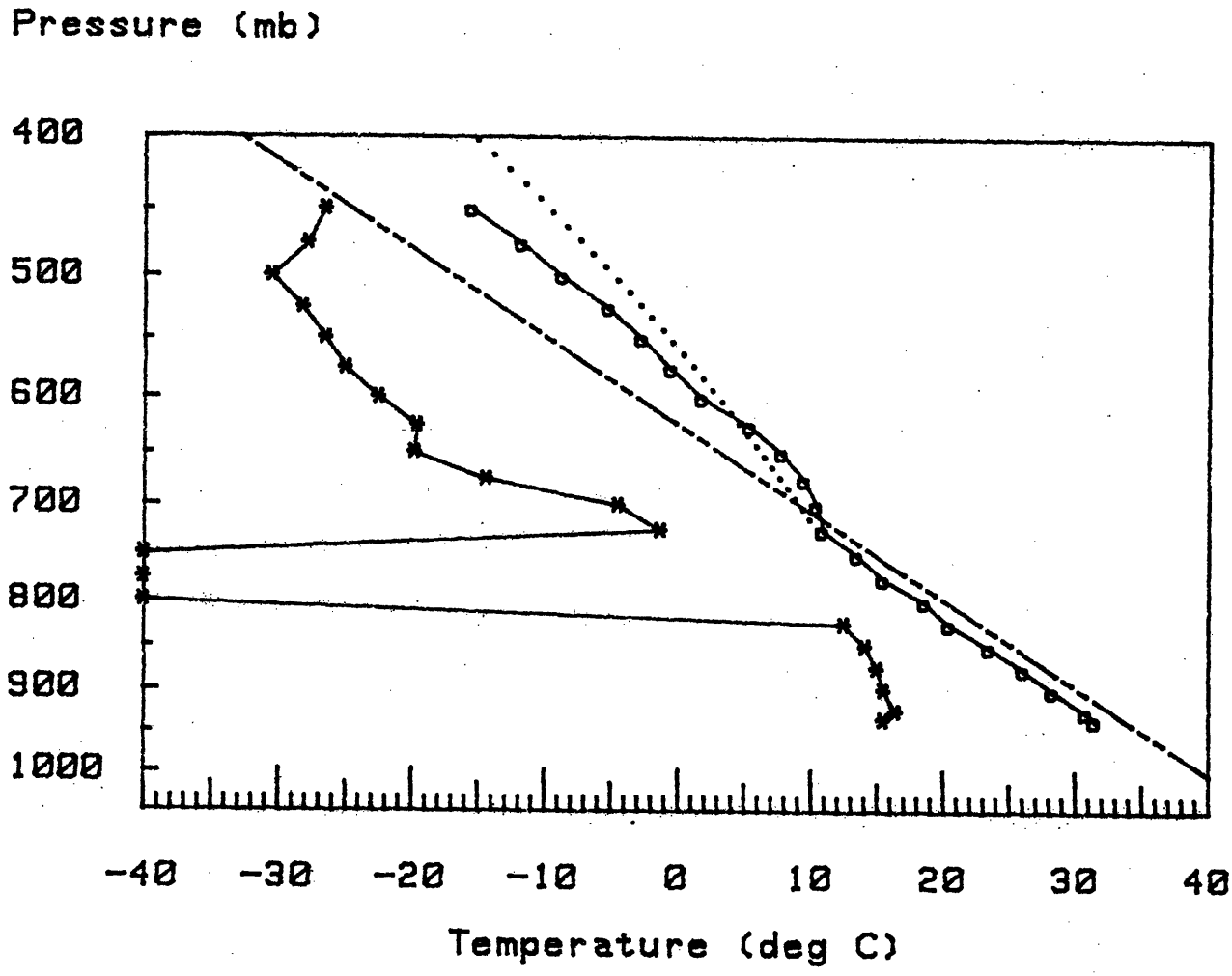


Fig. 4.24 Same as Fig. 4.21 for Childress, Texas 2006 GMT, 9 May. Missing dewpoints between 825 and 725 mb are plotted as -40 C.

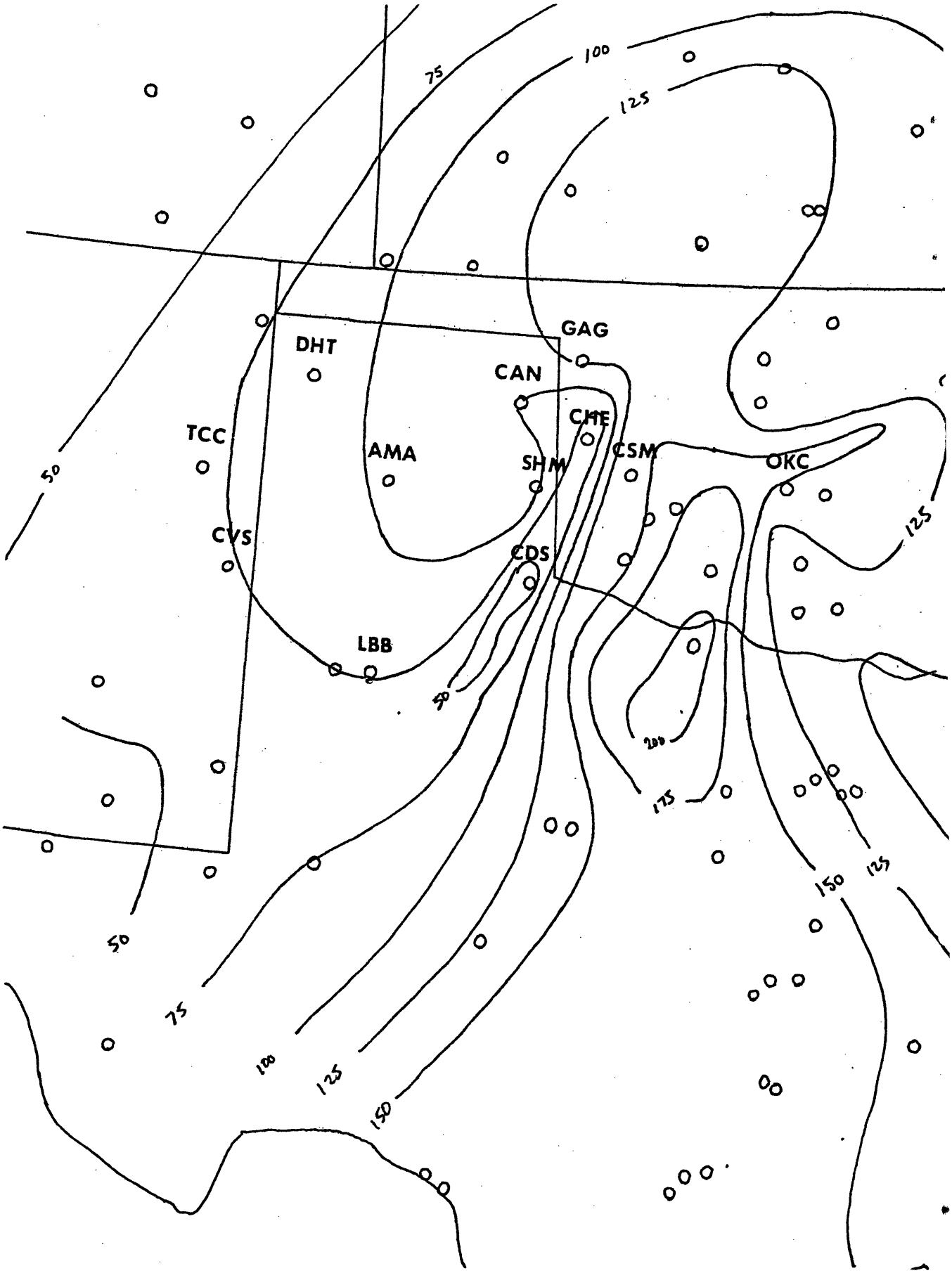


Fig. 4.25 Depth of nearly dry adiabatic layer (mb) between 319 and 317 K isentropes, 11 GMT, 9 May.

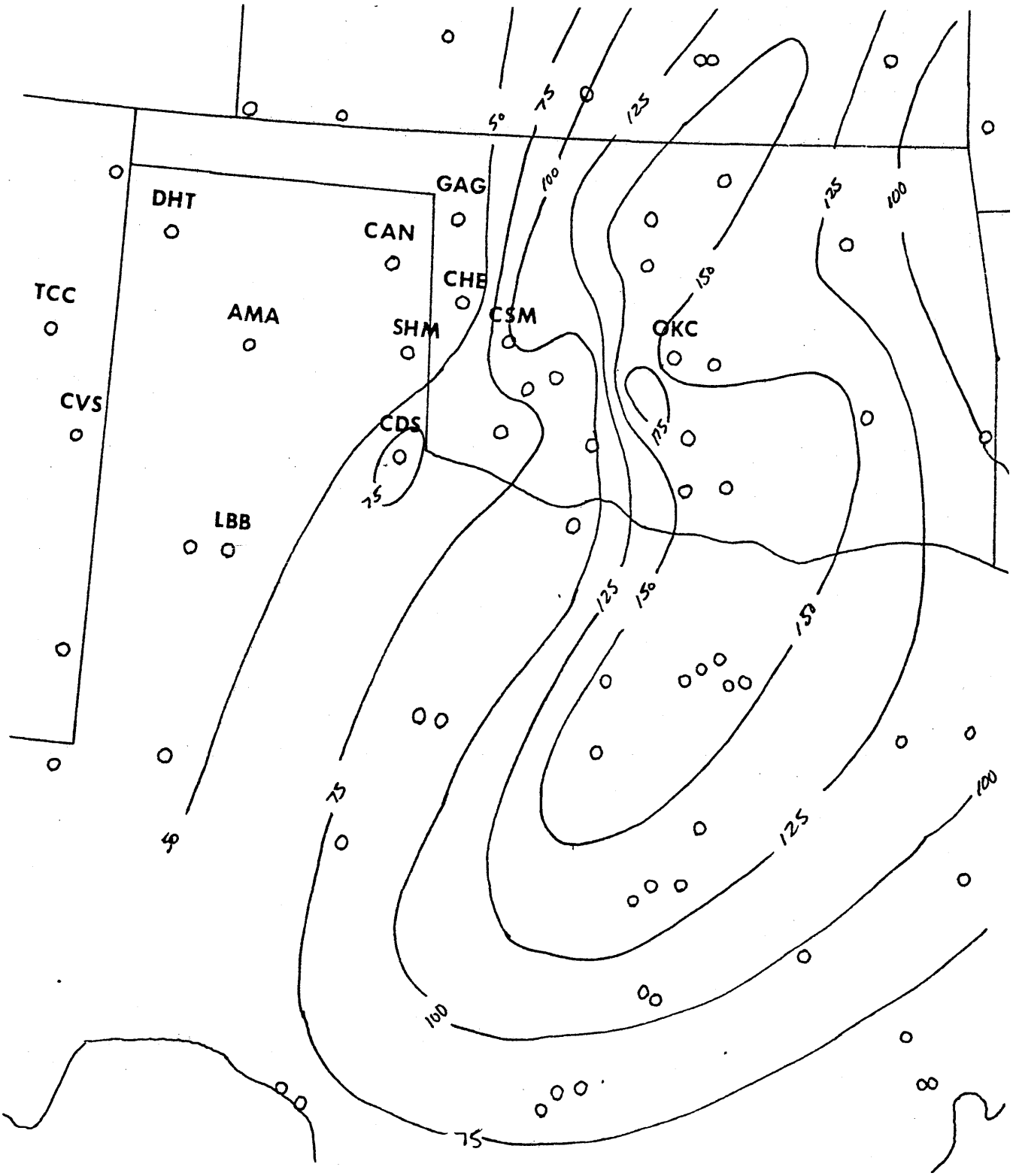


Fig. 4.26 Same as Fig. 4.25 for 20 GMT, 9 May.

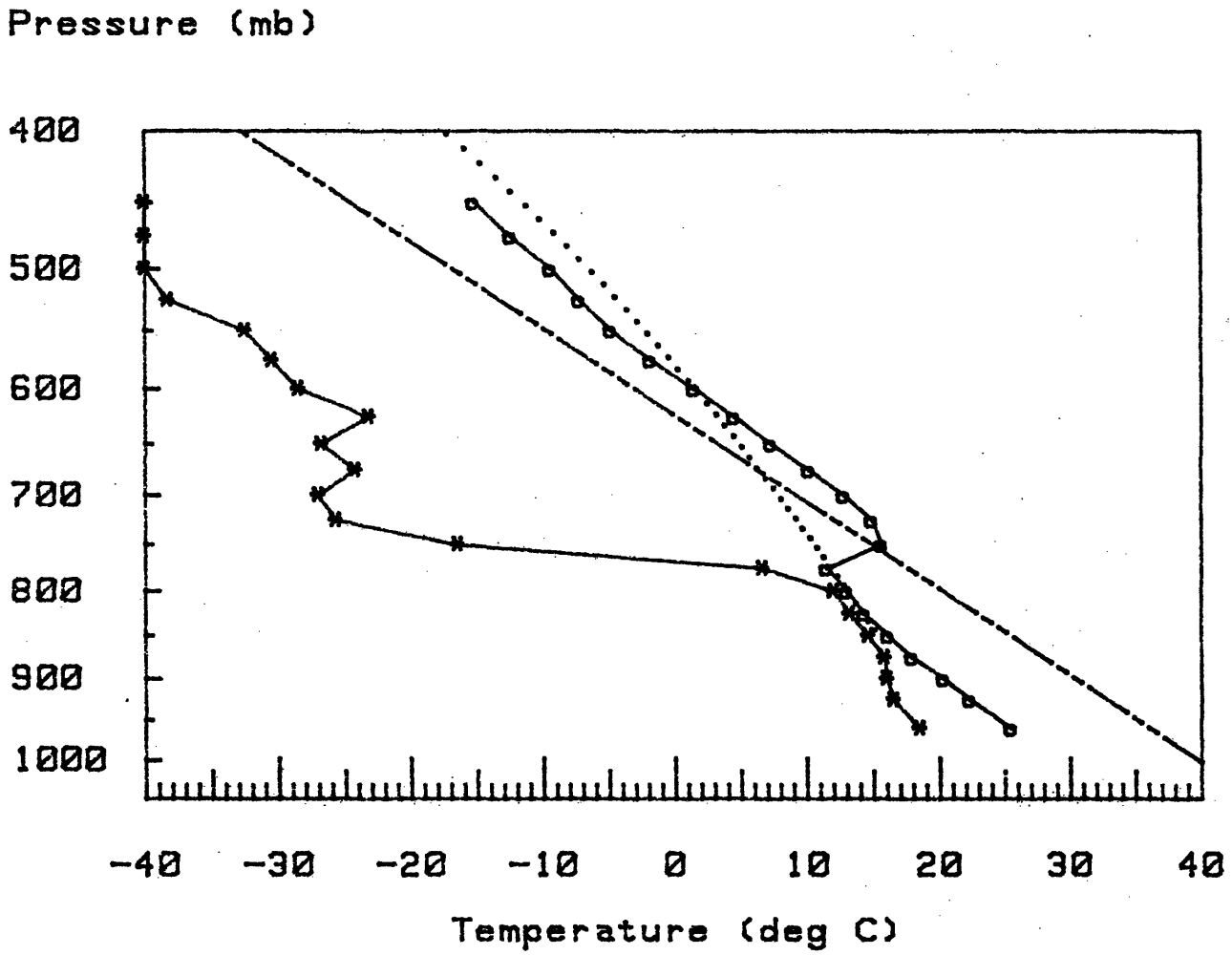


Fig. 4.27 Same as Fig. 4.21 for Oklahoma City, Oklahoma 20 GMT, 9 May.

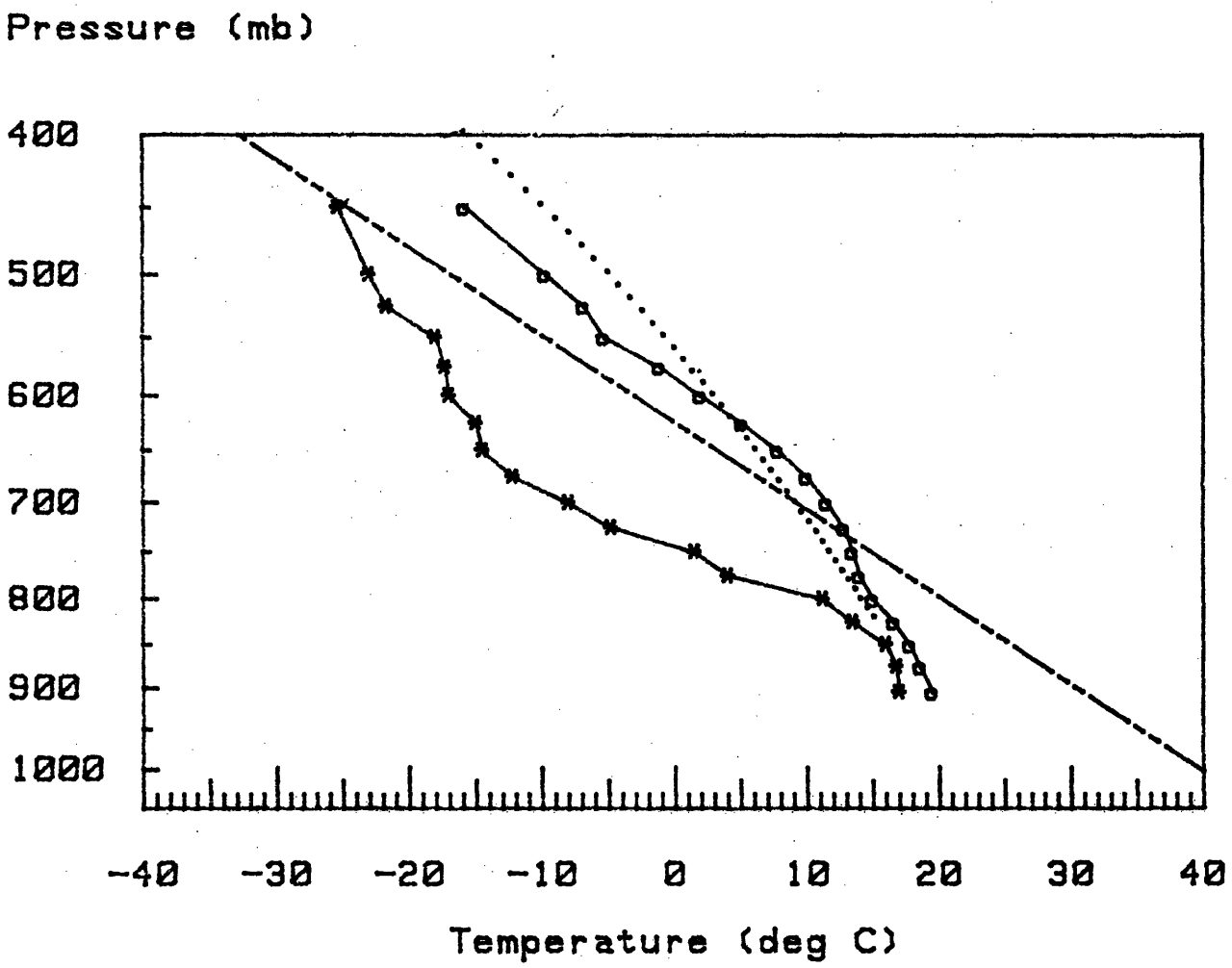


Fig. 4.28 Same as Fig. 4.21 for MAYHYB sounding at 11 GMT, 9 May.

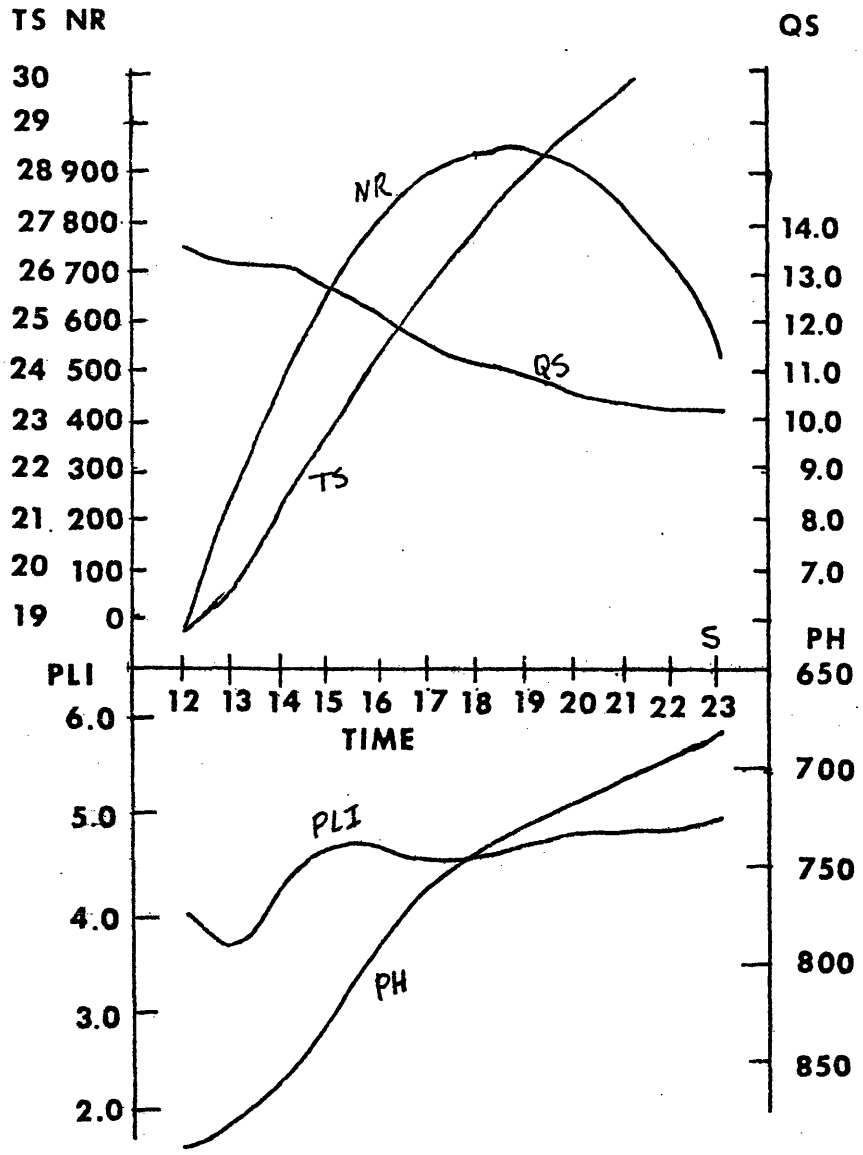


Fig. 4.29 Time variation of model output for MAYHYB sounding, 9 May, 5-70 soil parameters, with no extra factors modelled (Plain). NR is net radiation into surface (mcal/sq cm min ), TS is temperature at top of surface layer (deg C), QS is PBL mixing ratio (g/kg), PLI is convective instability (deg C), PH is pressure at top of PBL (mb). Condition at top of PBL is indicated above time axis: blank = unsaturated, ~S = nearly saturated, S = saturated, S+ = oversaturated (P).

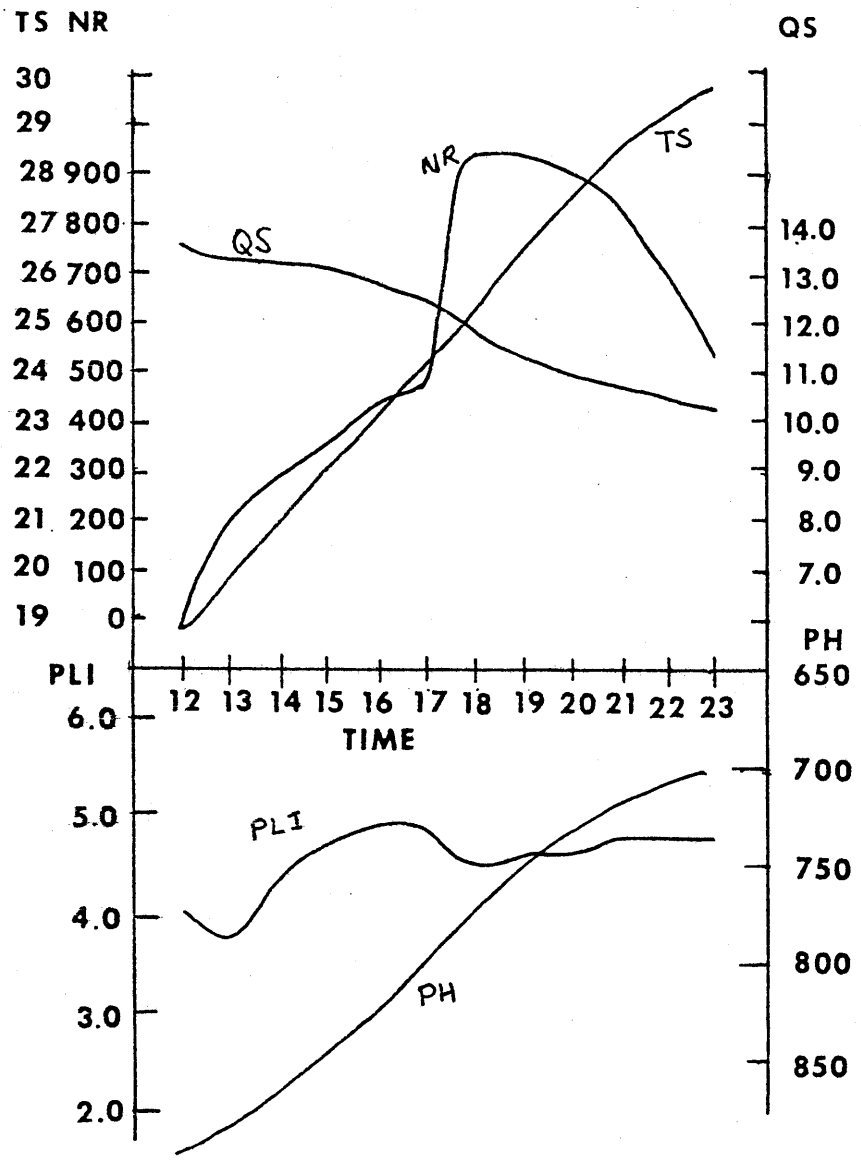


Fig. 4.30 Same as Fig. 4.29 for run with morning clouds imposed (C).

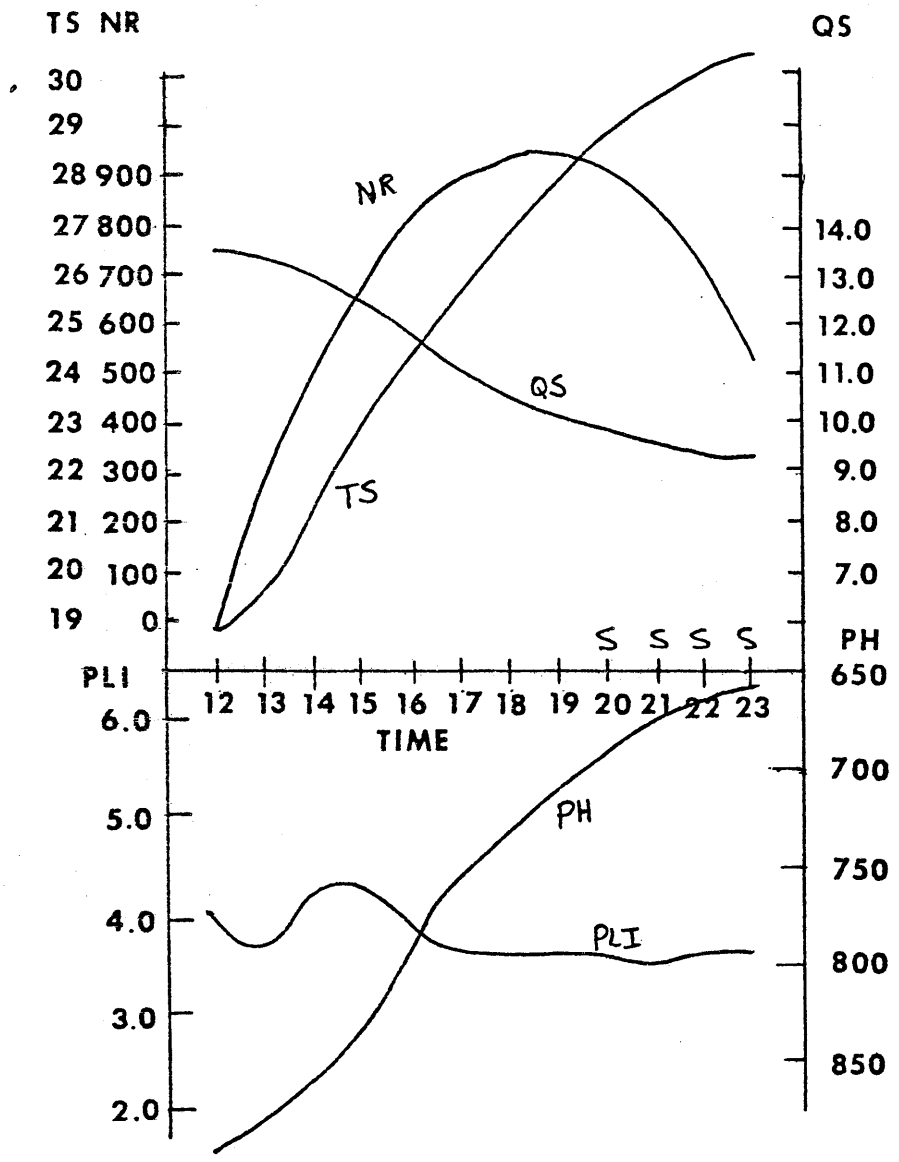


Fig. 4.31 Same as Fig. 4.29 for run with imposed changes above PBL (H).

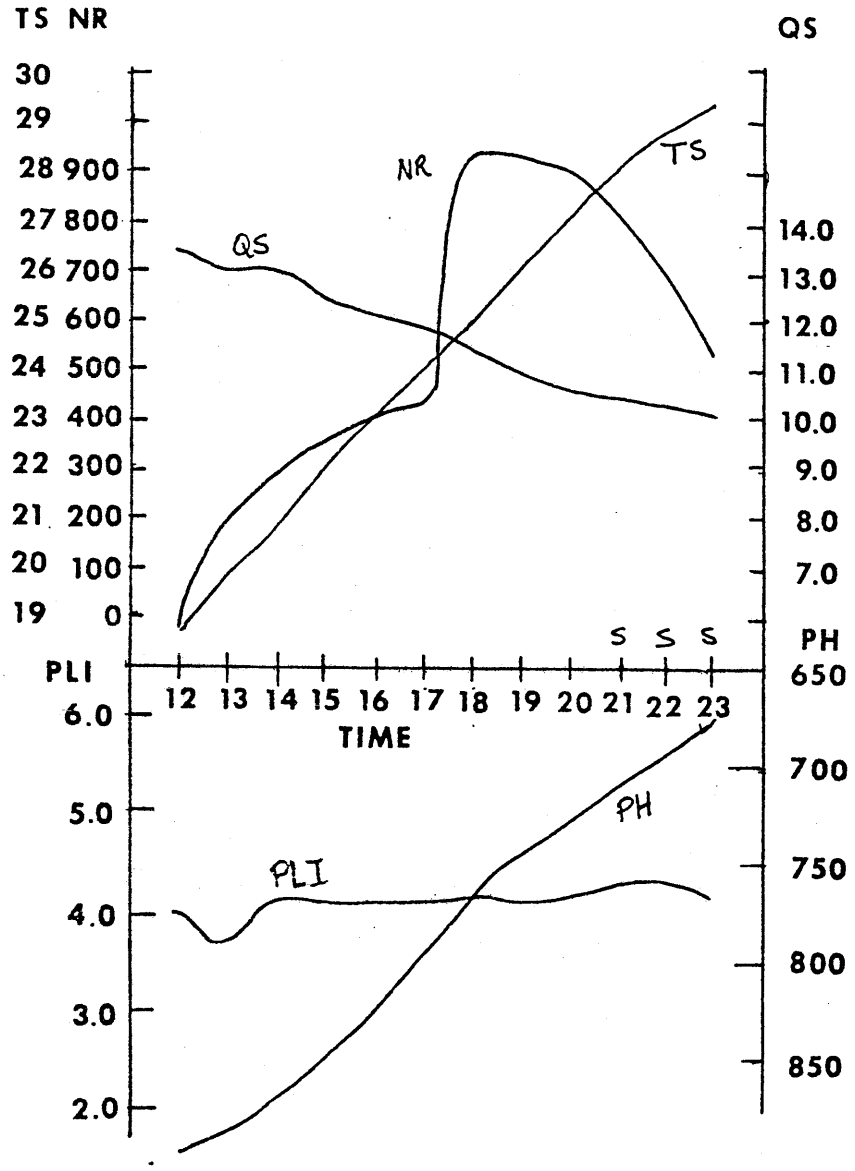


Fig. 4.32 Same as Fig. 4.29 for run with both morning clouds and imposed changes (HC).

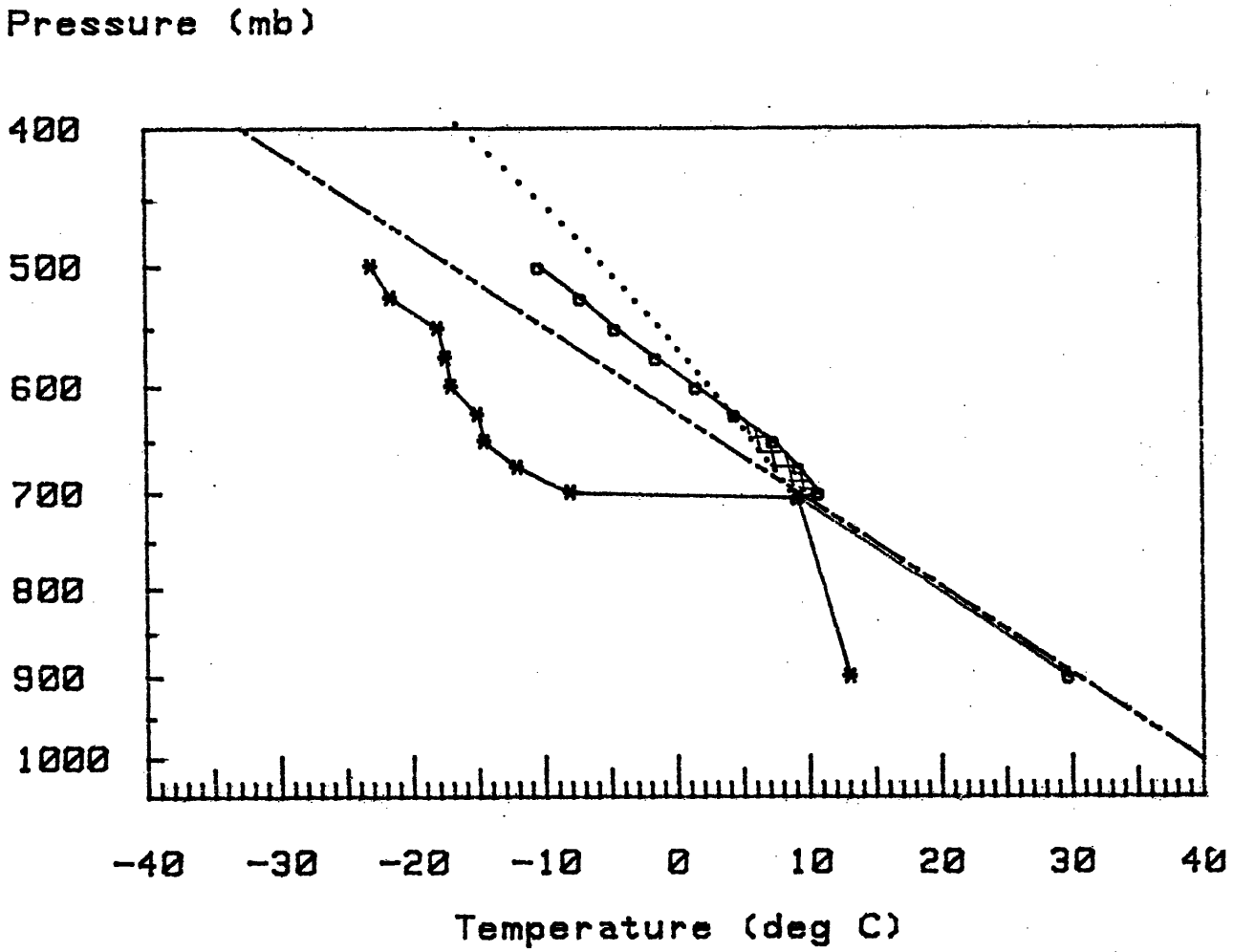


Fig. 4.33 Same as Fig. 4.21 for model output at 21 GMT from MAYHYB initial sounding, 5-70 soil parameters, and no additional factors modelled (Plain). Negative area is cross-hatched (P).

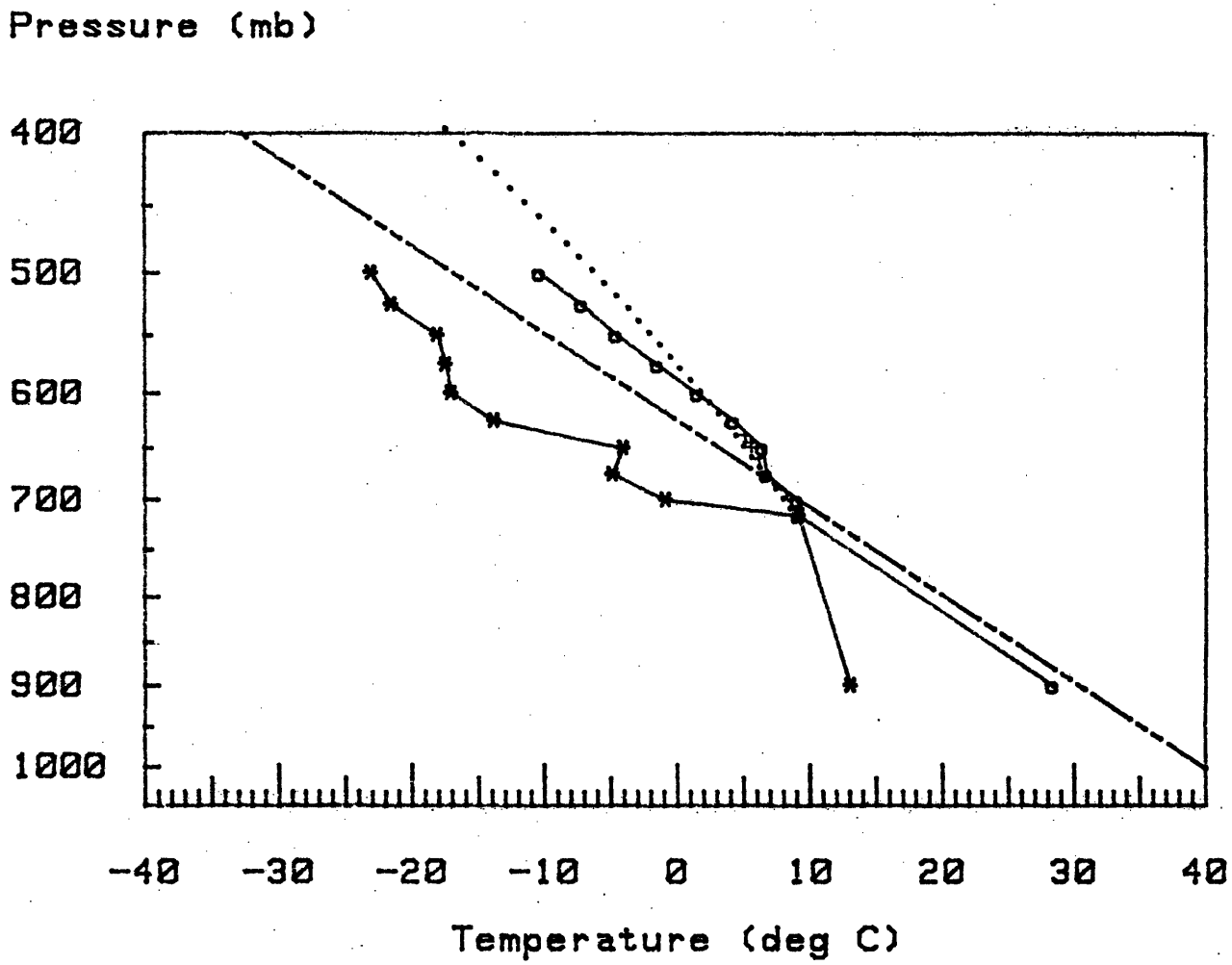


Fig. 4.34 Same as Fig. 4.33 for model with both clouds and imposed changes (HC).

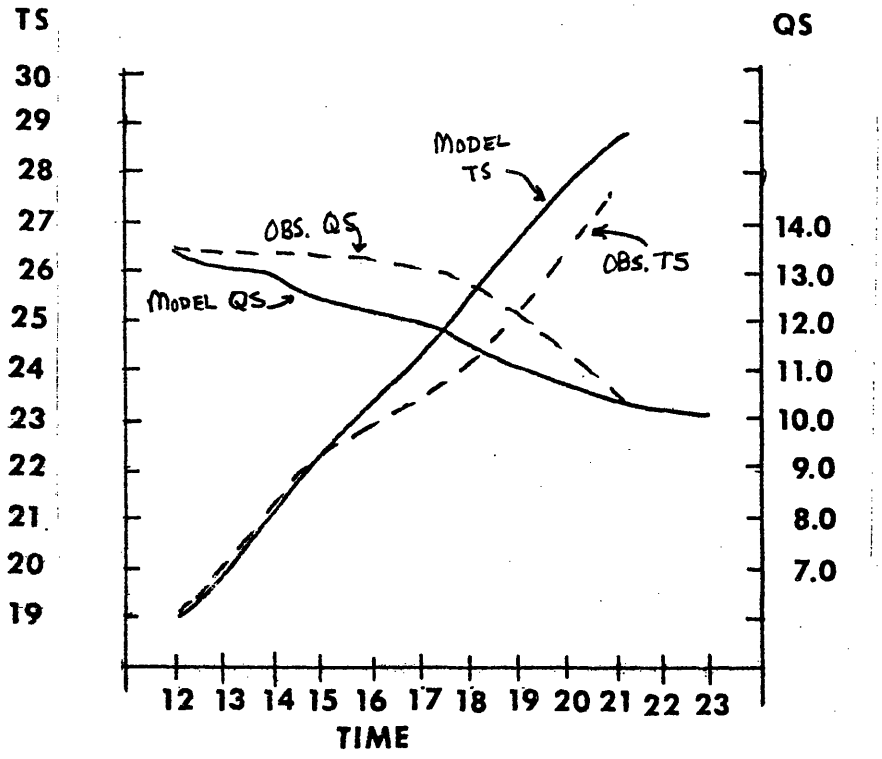


Fig. 4.35 Comparison between 5-70 HC model run and surface observations taken from analyses. TS, QS as in Fig. 4.29.

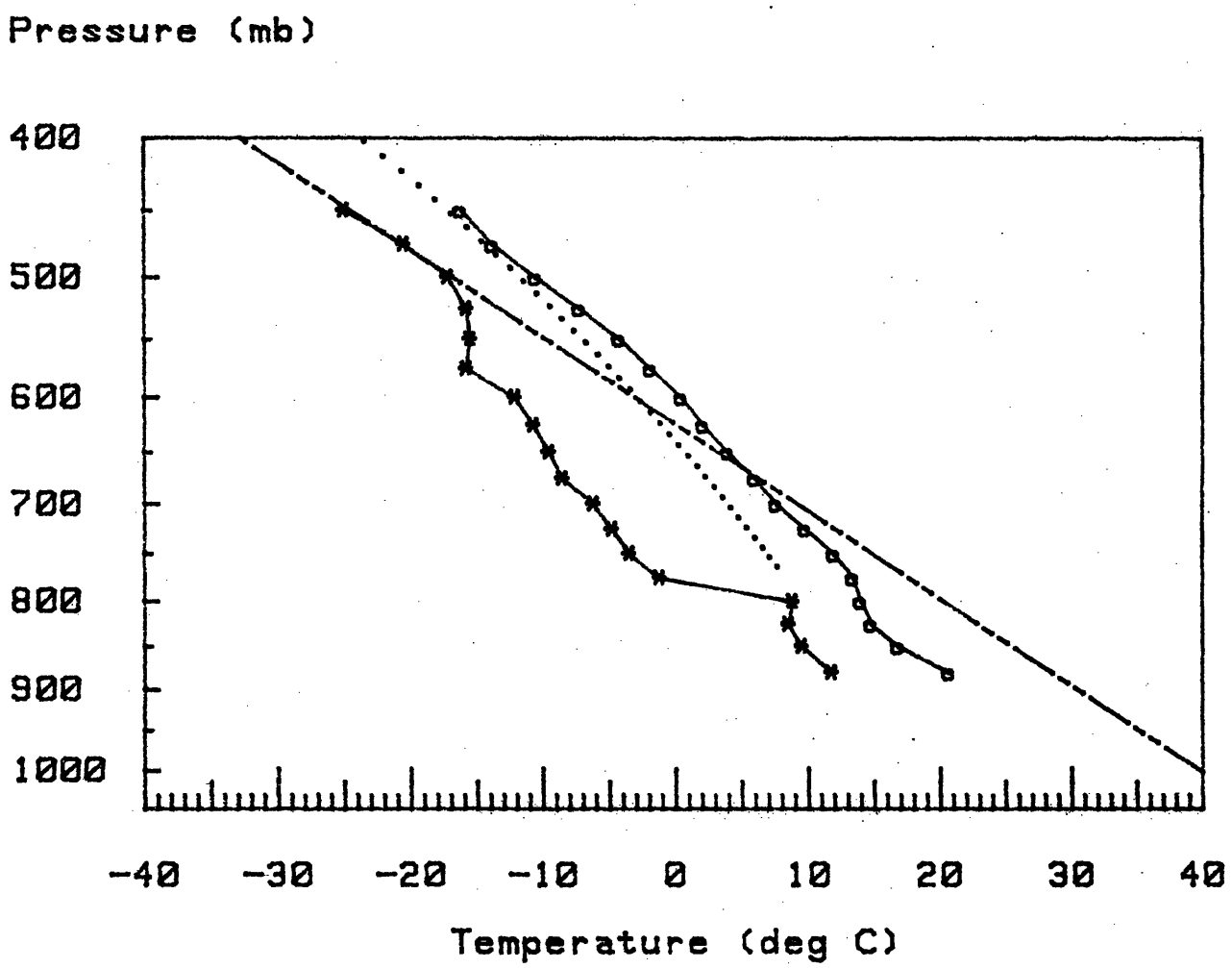


Fig. 4.36 Same as Fig. 4.21 for Amarillo, Texas at 17 GMT, 9 May.

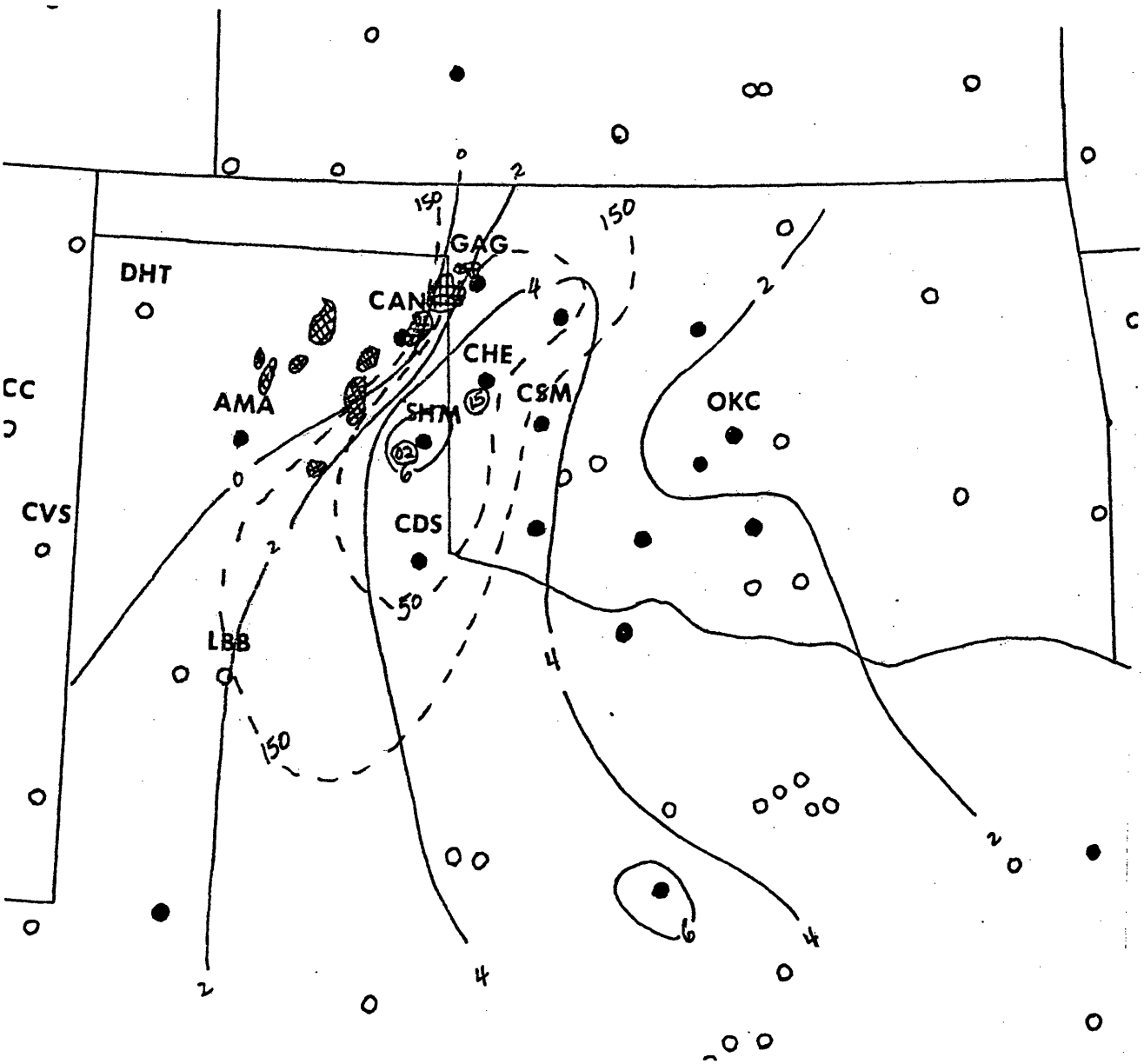


Fig. 4.37 Mesoscale analysis of convective instability (PLI) and convective inhibition (NA) for 17 GMT, 9 May. Solid lines are PLI (deg C) and dashed lines are NA (m**2/s**s). Cross hatching is new radar echoes appearing between 18 and 21 GMT. Numbers in boxes are point values of PLI, circled numbers for NA.

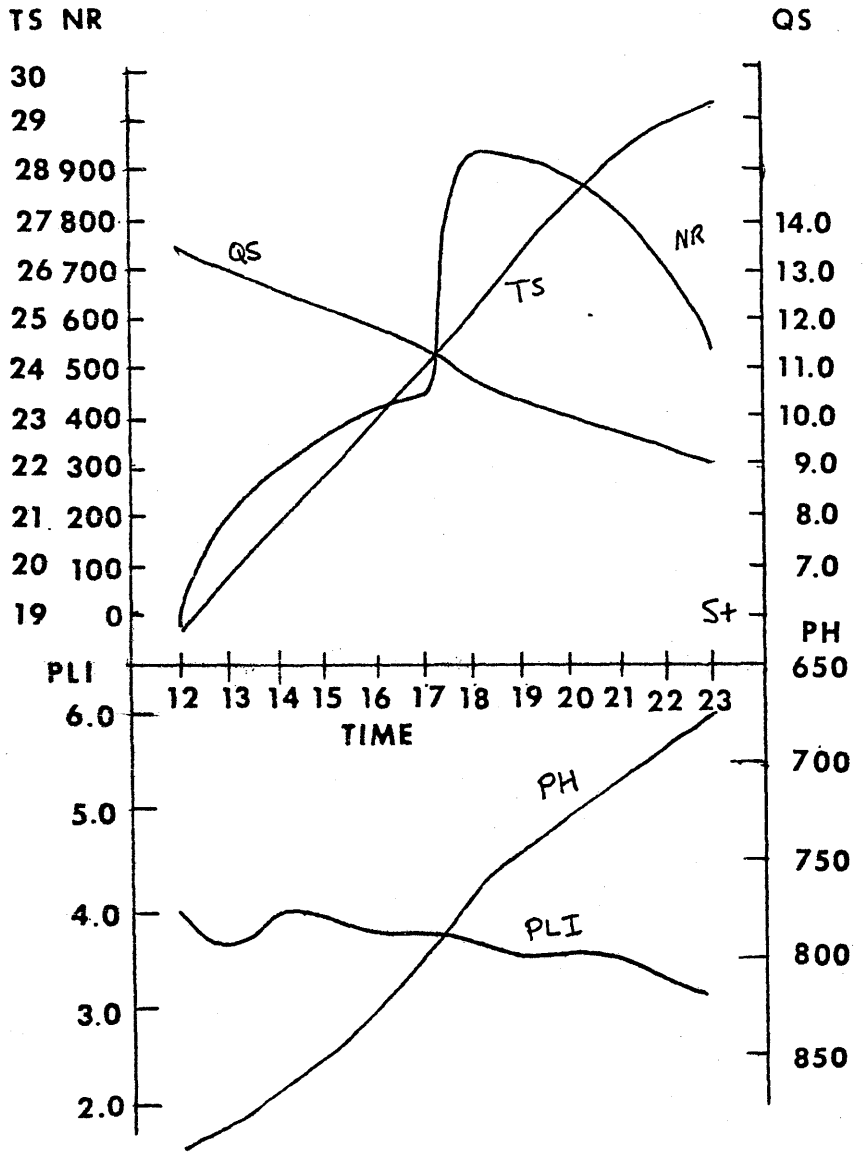


Fig. 4.30 Same as Fig. 4.29 for run with clouds, imposed changes, and surface moisture advection (QCH).

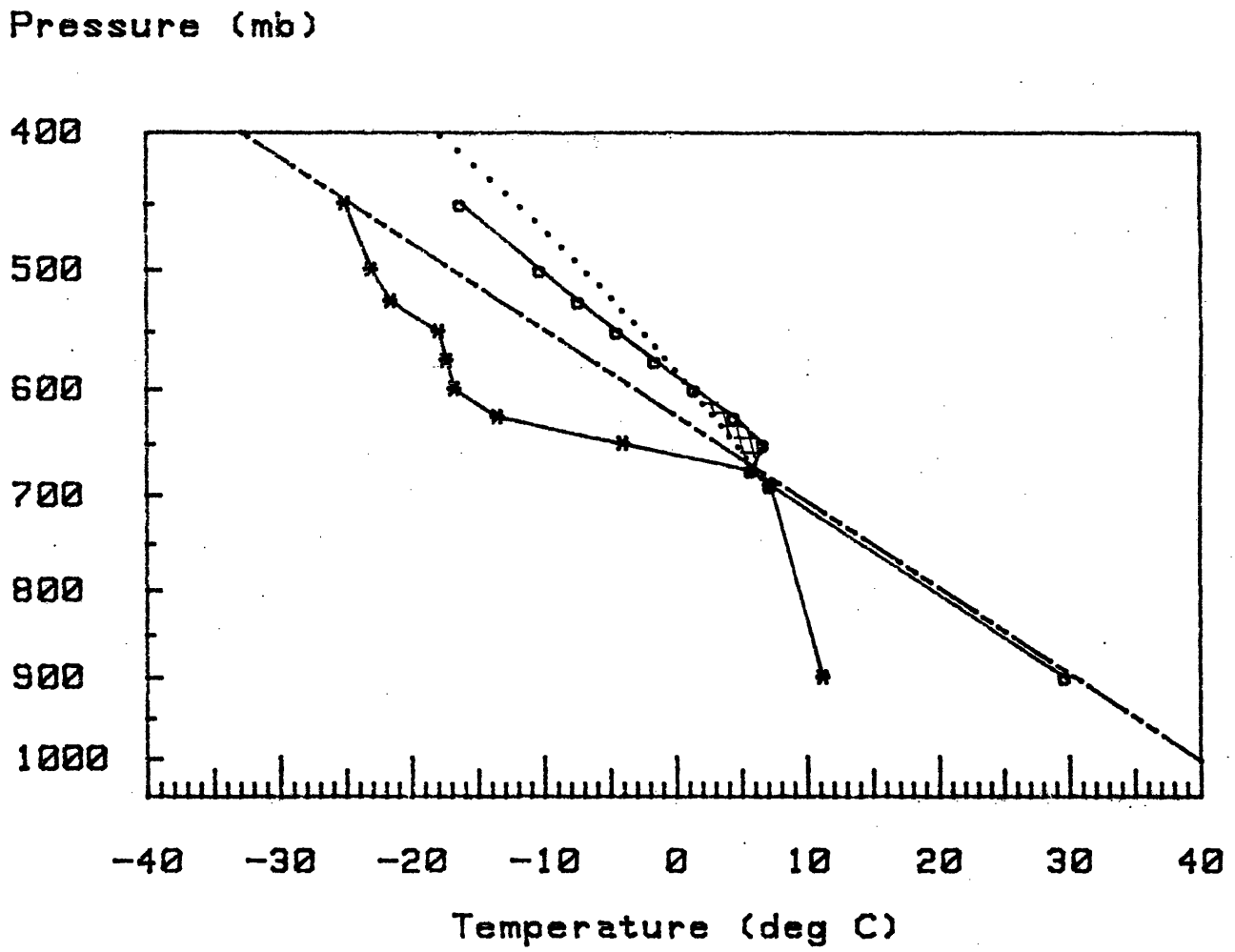


Fig. 4.39 Same as Fig. 4.33 for run at 23 GMT with clouds, imposed changes, and surface moisture advection (QCH).

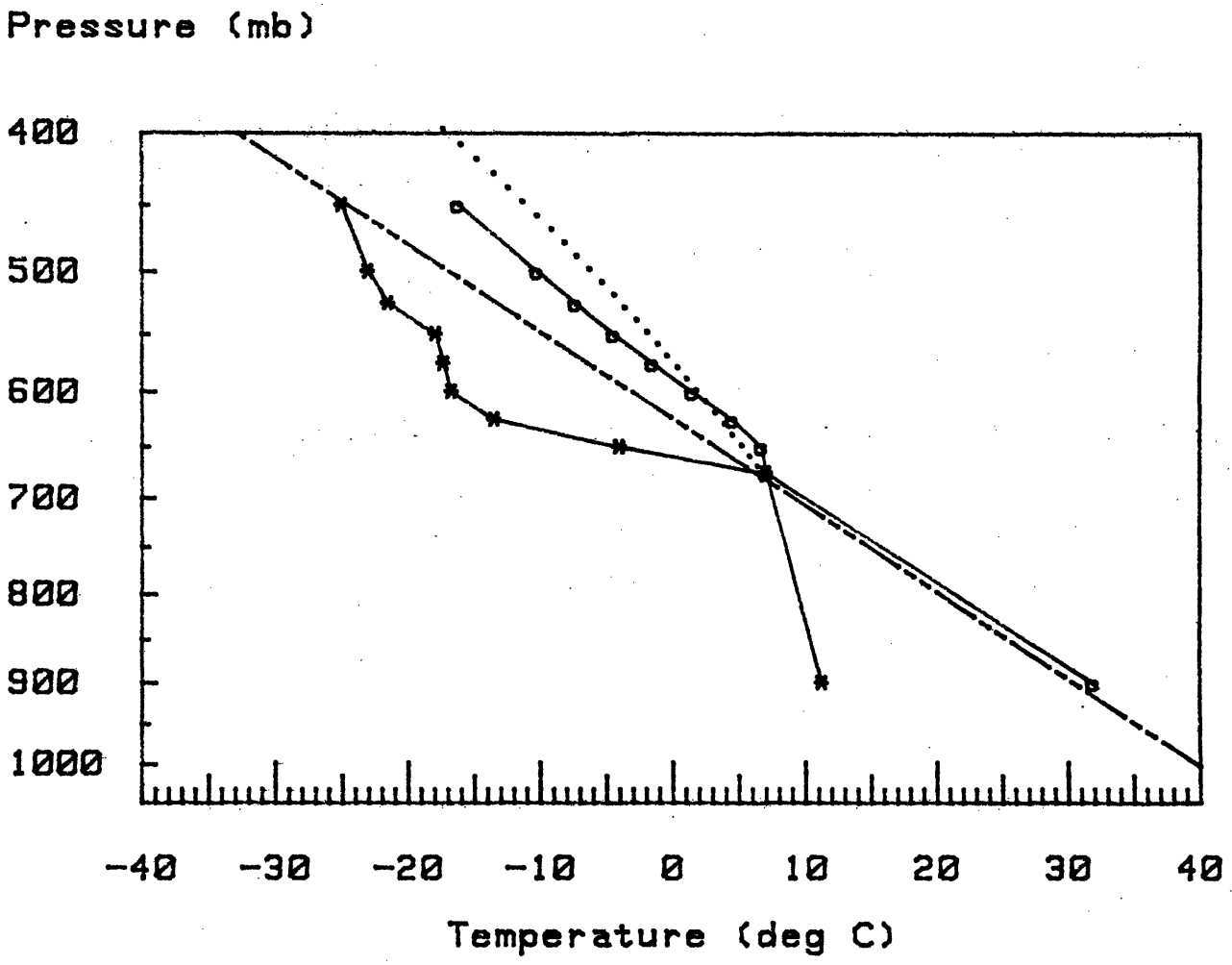


Fig. 4.40 Same as Fig. 4.33 for run at 23 GMT with clouds, imposed changes, surface moisture advection, and modified for surface temperature advection (QCH modified).

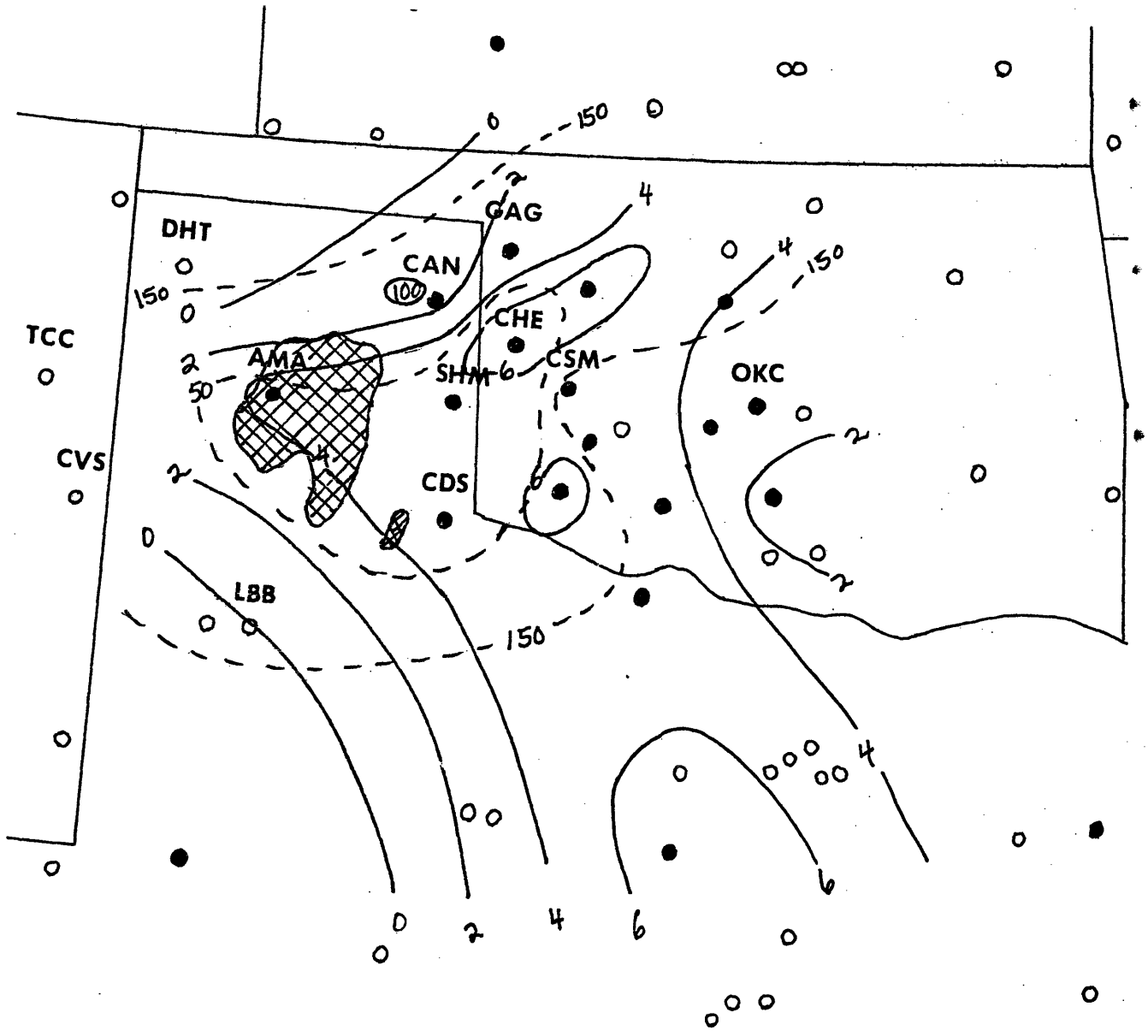


Fig. 4.41 Same as Fig. 4.37 for 20 GMT. New radar echoes are from 21 to 23 GMT.

# CASE STUDY III: 6 June

## 5.1: Introduction

This case, unlike the previous two, was not associated with a large number of tornadoes or severe hail. No funnels or tornado precursors (e.g. wall clouds) were sighted, although a mesocyclone was seen on radar. Maximum hail size was 1.5 cm. The thunderstorms which formed were substantial, but not severe. The interesting aspect of this case was that the convection broke out unexpectedly. Morning analysis did not indicate any convergence in the SESAME region. Nevertheless, isolated cells formed just northeast of Oklahoma City, Oklahoma (OKC) around 18 GMT, and more formed to the southwest by 19 GMT. Eventually a squall line formed from these cells.

The synoptic factors are discussed first, and then the mesoscale analysis is documented. The soundings, available at 15 and 18 GMT before the convection, are discussed and finally modeling results are shown and interpreted.

## 5.2: Synoptic Analysis

At 500 mb, 6 June, 12 GMT (Fig. 5.1) a trough lay in the High Plains area of the United States, with an elongated

vorticity maximum co-located with the trough axis. CVA was weak or zero throughout most of the SESAME region with the largest of the weak CVA in eastern Kansas. There was southwesterly flow over nearly all of Texas and Oklahoma at this time. By 00 GMT, 7 June (Fig. 5.2), a significant change had occurred. The weak, spread-out vorticity had become stronger and more localized with weak CVA extending northeast from central Oklahoma to the Kansas/Missouri border. The flow was still southwesterly over Oklahoma.

At the surface, the map for 12 GMT, 6 June (Fig. 5.3), showed only weak south-southwest geostrophic flow over Oklahoma, with no well-defined thickness gradient within 500 km. At 00 GMT, 7 June (Fig. 5.4) a low developed (west of the CVA at 500 mb) over CO, as an extension of a trough which stretched north to a low center in Canada. There was still no well-defined thickness gradient nearby, and the geostrophic flow was still south-southwest, stronger than before. Increased organization of the synoptic-scale features occurred both at 500 mb and the surface in this case, but there were no discontinuities in the wind field or thermal field in any of the analyses, suggesting that low-level convergence along a well-defined synoptic-scale front was not present.

## 5.3: Mesoscale Analysis

The analyses of the mesoscale fields of upper air data were performed at 500 mb and 700 mb at 15 and 18 GMT. The available data consisted of soundings at the 15 stations mostly in Oklahoma, shown in Fig. 5.5. The data were noisy, and in some cases clearly in error. Fort Sill, Oklahoma (FSI) at 15 GMT reported heights which were about 6 dm lower than any of the surrounding stations. Winds at Chickasha, Oklahoma (CHK) and Altus, Oklahoma (LTS) were much stronger than at the other stations, and were not associated with any discernible height gradients.

Some conclusions could be drawn from these data. Using the curvature of the streamlines as a guide, the vorticity maximum, noted on the synoptic-scale analyses remained west of Oklahoma at 18 GMT. Indeed, at 15 GMT there was more evidence for a mesoscale vorticity maximum as indicated by the curvature of the streamlines on Fig. 5.6 than at 18 GMT on Fig. 5.7. The wind at Gage, Oklahoma (GAG), and Hennessey, Oklahoma (HEN) veered at 500 mb between 15 and 18 GMT, leaving the flow at 18 GMT over most of Oklahoma (including the central part) uniformly from the southwest. The temperatures dropped noticeably at 500 mb as can be seen by comparing Figs. 5.6 and 5.7. This cooling aloft represented a contribution to convective instability over the region. The convection broke out near the edge of the strong cooling aloft rather than in the center of the region of cooling.

The 700 mb field (Figs. 5.8 and 5.9) showed nearly the same tendencies for the wind field, and temperatures increased generally over Oklahoma. Notice the very moist conditions which were in the same region as the coolest 500 mb temperatures at 18 GMT. The convection began at the edge of this moist 700 mb air.

On Fig. 5.10 at 12 GMT, 6 June, the mesoscale surface analysis showed that Oklahoma was mostly cloud covered and foggy. Winds at the surface were weak, mostly from the south or southeast. A cool pool was located in the region from Childress, Texas (CDS) northeast to Hobart, Oklahoma (HBR), and the winds were calm or weak northerly in this air. To the southeast of this slightly cool air, the dewpoints were above 20 C, but in the cooler air they were 3-5 C lower. Weak radar echoes were located northeast of OKC. No stations reported any thunderstorm activity however, or even any visual sightings of cumulus clouds.

At 15 GMT (Fig. 5.11) the cool pool was still in existence, with slightly higher dewpoints of 18-19 C, and winds generally from the south or southeast. Stratus or stratocumulus clouds were still covering most of the state of Oklahoma although just over the border at Wichita Falls, Texas (SPS) skies had cleared and BLH had begun (increase in potential temperature of 5.7 K between 12 and 15 GMT).

At 18 GMT (Fig. 5.12), scattered weak echoes had appeared near OKC, and towering cumulus clouds were observed at FSI and Ardmore, Oklahoma (ADM). The cool pool was still observable, centered on LTS, although it was weaker than at 15 GMT. Heating at the surface was occurring all over Oklahoma, and winds were generally moderate from the south. Notice that no strong convergence line was observed in Oklahoma at this time. the cool pool area was still dryer than the warmer region to the southeast near FSI and especially SPS.

At 19 GMT, shown on Fig. 5.13, the precursors to the heavy squall line formed north of FSI and southwest of CHK. This broken line of radar echoes extended northeast past OKC, and was visible from Tinker AFB, Oklahoma (TIK) which reported seeing a line of cumulonimbus clouds east and southeast. FSI was reporting towering cumulus clouds. The inflow air to the convection had a potential temperature between 305 and 306 K, and a dewpoint at the surface of 21 to 22 C. Notice the uniformity of the observations at FSI, OKC, TIK, and SPS. Warmer temperatures were north of HBR and Clinton Sherman AFB, Oklahoma (CSM), while LTS was still cooler and dryer. Later on, as seen on the radar sequence (not shown), the storms north of FSI and southwest of CHK eventually developed into strong storms, one of which formed a mesocyclone after 21 GMT. The cool pool was reduced to a cool trough by 19 GMT, having lost much of its temperature deficit to BLH.

Fig. 5.14 shows the net changes in potential temperature and dewpoint between 12 and 19 GMT. The largest changes in temperature occurred along the High Plains region of New Mexico, Colorado, and Texas. Most of Oklahoma warmed less than 10 K, and a significant tongue extending northwest from ADM and McAlester (MLC) up to OKC and TIK showed less than 7.5 K rise. LTS, the cool center, had a very large rise in potential temperature, more than 11 K. The dewpoints in Oklahoma rose slightly during this period, about 1 C. This rise, in addition to heating, suggested a large change in instability, at least in terms of surface equivalent potential temperature. This will be addressed in detail in connection with the soundings.

Advection was unimportant north of the Texas border. SPS had an anomalously high potential temperature and dewpoint, so the gradient between SPS and the Oklahoma border was ignored in this analysis. The parcels arriving in the initial convective outbreak region came from east of SPS, where advection was weak. The impact of advection will be considered in connection with the soundings.

## 5.4 Soundings

The special radiosondes were launched from the sites shown on Fig. 5.5 at 15 and 18 GMT prior to convection. No 12

GMT soundings were launched from these sites. Additionally, the regular OKC 12 GMT sounding was available, as well as a 1312 GMT sounding at HEN. Soundings from Stephenville, Texas (SEP), Monett, Missouri (UMN), and Dodge City, Kansas (DDC) were also plotted at 12 GMT. The OKC sounding (Fig. 5.15) showed a very smooth structure, slightly less stable than a moist adiabatic lapse rate, from the surface to 500 mb. At 500 mb there was a small stable layer of 20 mb. The UMN sounding at 12 GMT had a similar structure, but had a dry adiabatic layer from 650 mb to 600 mb, capped by an additional stable layer from 600 to 500 mb. The plot of the SEP sounding showed a variation of this pattern with one inversion from 575 to 565 mb and a stable layer above the inversion up to 535 mb. The DDC sounding was different in other respects. It had a 30 mb dry adiabatic layer above 800 mb, and a second dry adiabatic layer from 540 to 585 mb with a simple, sharp inversion from 490 to 500 mb. All of these soundings had nearly moist adiabatic layers form the surface up to an inversion or stable layer. The height of this stable layer varied from 500 mb to 575 mb. The OKC and SEP soundings had no dry adiabatic layers, but the DDC sounding had two and the UMN sounding had one.

All of these 12 GMT soundings had high relative humidity at or near the surface. Above the surface, only the UMN sounding had saturated layers. Above 500 mb, all of the

soundings were quite dry, except for OKC which had a moist layer just above 500 mb. The plot of the sounding from HEN at 1312 GMT showed features similar to those of the OKC 12 GMT sounding. Aside from a low level inversion at 885 mb, the temperature nearly followed the 334 K moist adiabat all the way to 400 mb. It had an inversion just above 600 mb similar to SEP, with only very small dry adiabatic layers at 860, 800 and 585 mb.

Just as in the upper air analyses, changes occurred in the soundings as well. All of the 15 GMT soundings except GAG had a sharp inversion between 800 and 900 mb, separating an apparently well-mixed PBL from the free atmosphere. Generally speaking, these inversions were sharply reduced or gone by 18 GMT. Using the HEN sequence as a guide, and assuming the initial sounding was as smooth as OKC at 12 GMT (Fig. 5.15), it was clear that the inversion between 870 and 885 mb at HEN (Fig. 5.16) was above the PBL top.

Two soundings, Elmore City, Oklahoma (EMC) and FSI, were located upwind of the convection, and hence were useful in examining the changes which preceded convection. At EMC, 15 GMT (Fig. 5.17), the sounding apparently had a superadiabatic surface layer of very shallow depth and a well-mixed PBL above up to 915 mb. With only the surface values and the values at the top of the PBL, it is entirely possible that the coarse

resolution sounding missed the well-mixed PBL's beginning above the surface layer.

An inversion capped the PBL between 915 and 875 mb. Another inversion was located between 600 and 535 mb. In between, the lapse rate was conditionally unstable, and the relative humidity was over 70% for nearly the whole sounding. Assuming that relative humidity above 75% implies the existence of clouds, there should have been clouds present between 600 and 630 mb, and near 915 mb. Surface reports from Fig. 5.11 suggested that cloud cover was between 5 tenths and overcast, which agreed with the sounding indications. When lifted adiabatically, PBL parcels (potential temperature of 301 K, mixing ratio of 16 g/kg) became saturated at 905 mb, and were negatively buoyant up to 775 mb. The PLI for this sounding was 3.3. By 18 GMT, the well-mixed PBL extended up to 895 mb, and the lower inversion had disappeared (see Fig. 5.18). The upper level inversion was gone as well, and the 500 mb temperature had dropped almost 1.5 C. Clouds were still indicated by the surface observations, and the relative humidities in the sounding indicated the presence of clouds above the PBL top. When lifted adiabatically, PBL parcels were saturated at 870 mb, and were negatively buoyant for only about 20 mb. The PLI was 4.9. By 19 GMT, more heating had taken place, so the convective instability had increased during this 7 hour period. Notice that the mixing ratio in

the PBL decreased slightly between 15 and 18 GMT at EMC.

The convective outbreak region at 19 GMT was just to the northeast of FSI. Later, convection broke out around FSI, suggesting either FSI was slower to destabilize or that a triggering mechanism acted later at FSI than to the east. The 15 GMT FSI sounding (Fig. 5.19) had a poorly defined PBL. The sounding showed a strong inversion at 865 mb, and another at 600 mb. It also was fairly wet, with one cloud layer at 650 mb and another near 885 mb. When PBL parcels (potential temperature of 303.5 K, mixing ratio of 14.5 g/kg) were lifted, they became saturated at 920 mb (probably the PBL top), and were negatively buoyant up to about 800 mb. The PLI for this sounding was 3.6.

By 18 GMT, FSI had a well-mixed PBL extending up to 875 mb, and the lower inversion was gone (see Fig. 5.20). A surface layer was delineated by the sounding, with a superadiabatic lapse rate, and a strong gradient in mixing ratio. Aloft, the sonde apparently traversed a cloud between 565 mb and 600 mb, which over-emphasized the upper level inversion. The temperature at 500 mb dropped only 0.5 C at FSI, unlike the 500 mb temperature at EMC. When lifted adiabatically, PBL parcels (potential temperature of 303.5, mixing ratio of 14.5 g/kg) became saturated at 850 mb, and negatively buoyant for 50 mb. This sounding was clearly more

stable than that at EMC at 18 GMT from the standpoint of convective inhibition. The PLI for this sounding was 3.9, less instability than at EMC. More heating of this air took place until near 20 GMT when convection began to spread to the FSI area.

As happened for the EMC sounding, the PBL mixing ratio decreased during the PBL heating, as it should have in the absence of moist advection. It is difficult to reconcile this decrease with the apparent lack of change in the surface values from the surface analyses. It may well have been that the surface measurements were sampling the lower part of the gradient in moisture that must have existed to give upward latent heat fluxes. The sounding at FSI at 18 GMT was a good example of this (Fig. 5.20). The question of moisture advection will be addressed again when the modelling results are discussed.

For comparison, it is interesting to examine soundings in the regions north and south of the convective area, particularly at 18 GMT. The 18 GMT sounding at CSM is shown in Fig. 5.21. Notice that the PBL apparently extended 100 mb from the surface, up to the base of a small inversion. In this case, the surface values seem too low, since CSM was reporting only scattered sky conditions, and had been warming all morning. It should have had a superadiabatic surface

layer by this time. The PLI for this sounding was 1.7 and much negative area remained above the PBL. Parcels from the boundary layer were negatively buoyant for almost 100 mb. To the south, SPS at 17 GMT (Fig. 5.22) had a PLI of 4.2, and also had a significant amount of negative area to overcome.

The CSM sounding had a deep but dry PBL, and still had an inversion capping the PBL. SPS was characterized by a shallower, more moist PBL, but also had a stable layer aloft. Although SPS had almost as much convective instability as EMC, convection was held back by the inversion. As already noted, there were inversions in almost all of the soundings at 15 GMT (including SPS). These inversions changed little in strength between 15 and 18 GMT. This suggests that a mesoscale inversion moved into Oklahoma by 15 GMT, and was steady for the next three hours. During this time, BLH took place, the strength depending on cloud cover and perhaps soil moisture. Convection broke out at those places where and when the BLH and/or a convective trigger released the convective instability.

The soundings showed that the convective instability of the PBL increased during the period 12 GMT to 19 GMT, but the increase was modest, and due in part to changes at 500 mb. The convective inhibition changed relatively more, from considerable values at 15 GMT to nearly zero by 18 GMT at EMC.

To quantify the factors involved, a hybrid sounding (JUNHYB) was constructed to represent the inflow air between EMC and FSI, and the PBL model was run with this sounding to give the time evolution. These results follow.

## 5.5 Hybrid Modelling

The hybrid sounding for 12 GMT is shown in Fig. 5.23. Notice that it was quite humid at low levels. The cloud amounts used initially were derived from the relative humidity values, and are shown on Table 5.1. The 12 GMT OKC and SEP soundings were averaged to derive the initial profile. The average was weighted 3 to 1 to give primary input to the OKC sounding. The position of the hybrid sounding was chosen to be upwind of the middle of the convective outbreak area. This location was midway between CHK, FSI and EMC. Surface values at 12 GMT were interpolated from the surface analyses. The imposed changes were interpolated from the three soundings (FSI, CHK, EMC) and applied to JUNHYB as shown in Table 5.2.

Rainfall from the previous day (5 June) was plotted on Fig. 5.24 to help set the soil moisture parameters. A tongue of moderate precipitation extended northeast from SPS to MLC, with amounts reaching over one inch along the axis. Rain also fell at OKC on 5 June. The region of the hybrid sounding (shown with an asterisk on Fig. 5.24) was dry the previous day.

On 4 June, one day earlier, rain had only fallen on four stations in Oklahoma, all in the southeast corner. So the soil surface moisture could not have been very high for this region, certainly no higher than 60%. The soil surface moisture for the inflow air had to reflect a contribution from the band of moderate rainfall, since the trajectories from 12 GMT to 19 GMT crossed this band.

The previous month, and indeed, the first 3 days of June were moderately wet in Oklahoma, so the bulk soil moisture was moderate. Likely values should have been in the range of 30% to 60%. So the following values were used for the model runs: (soil surface moisture-bulk soil moisture) 10-30, 30-30, 30-60, 60-60 with the expectation that the middle two runs would be most realistic.

The modeling results for the runs without clouds or imposed changes above the PBL presented no surprises. The figures appear in Table 5.3. The dryest soil run (10-30) had the deepest and dryest PBL, and also the least instability. In fact, the 19 GMT PLI was lower for the 10-30 run than for the initial sounding. The top of the PBL varied roughly 50 mb over the range of soil moistures, and the PBL moisture values showed a wide variation as well, almost 2 g/kg. There was a large difference between the PLI value for the 60-60 run and that for 30-60 run. This difference in convective instability

was due to the much higher PBL moisture content. Notice how both QS and PLI "jumped" from the 30-60 run. This was also true for the surface temperature, going in the other direction, but the moisture increase easily offset the cooler temperature to give higher convective instability.

None of the runs showed any negative area. This was coupled to the observation that all of the runs were oversaturated at the PBL tops. The runs were actually oversaturated by a large amount, and throughout the model runs. The behavior in time of the 30-60 run is shown in Fig. 5.25. Although the QS dropped quickly with time, the PBL top rose fast enough to stay oversaturated the entire time. This implied that the model runs were all unrealistic, an expected result, since they lacked important physical effects.

When clouds were added, large changes occurred in the model behavior. The clouds were present, in some form, throughout the run, although they were thinner at the end of the run (see Table 5.1 for details). The results are shown on Table 5.3. Generally, all of the PBLs were shallower, cooler and more moist. The amount of change in PBL growth was 33%. That is, the PBL growth under cloud was 1/3 less than that of the plain runs. The surface temperatures were very sensitive to the clouds as well, and grew 25% less than without the clouds. The PBL moisture stayed higher, as expected. The

drying in the PBL was reduced more than 25%. Fig. 5.26 shows the time evolution for the 30-60 run. Notice, when compared with the plain run on Fig. 5.25 that the differences were built up throughout the run. The behavior of the PBL was the same qualitatively: rising PBL top, heating of the surface, and drying as the moisture was mixed upwards. However the magnitude of the changes was drastically cut under the clouds.

The growth of convective instability, however, proved relatively insensitive to the clouds. For the wettest run, it even decreased slightly. In all of these runs, the cooling and moistening effects were nearly balanced, yielding almost the same growth in PLI. As before, none of the runs had any negative area by 19 GMT, and all were oversaturated throughout the run. In this case, oversaturation was not obviously unrealistic since clouds were included in the runs. However, the PBL growth predicted by the model was still excessive, yielding PBL tops much higher than the saturation level of the PBL parcels. So these runs were still unrealistic.

The sensitivity of PBL characteristics to the imposed changes (Table 5.2) was nearly the opposite of the sensitivity to clouds. The results are shown in Table 5.3 and Fig. 5.27 shows the 30-60 run. The PBL growth was slower than the plain runs, but only by about 7%. The surface temperatures were higher with the changes, by almost 10%, again not a large

impact. The PBL moisture dropped a little slower, but by only 6%. The PBL responses to the imposed changes were minimal, resulting in PBLs which were shallower, warmer and wetter.

When compared closely, the plain run began to diverge from the run with imposed changes at 15 GMT. The character of the imposed changes explains what happened. Between 12 and 15 GMT, the layers between 750 mb and the PBL top warmed by more than 1 deg C. After 15 GMT no further changes occurred in temperatures above the PBL. This created the inversion seen on the 15 GMT soundings. This inversion slowed the PBL growth, which became noticeable at 15 GMT. Slower growth for the same sensible heat flux gave higher PBL temperatures. Entrainment at the PBL top gave warmer values as well. Both of these effects contributed to higher TS values. The PBL moisture responded similarly, having less room for the spreading out of similar amounts of moisture, giving less PBL drying.

The combination of warmer and wetter PBLs was enough to make a significant difference in the PLI values. The tendencies for temperature and moisture were both in the direction of higher instability. The small PBL changes under the imposed changes aloft resulted in more than a 40% increase in growth of convective instability. The imposed changes had a significant effect only on the PLI values. The negative

area was zero for all the runs again, and the runs were all unrealistically oversaturated just as before.

When both clouds and imposed changes aloft were added to the model, the results were as shown in Table 5.3. The tendencies for smaller PBLs combined to give PBL growth rates more than 40% lower than the plain runs. The dryest soil run only reached above 820 mb, and the wettest only 860 mb. The surface temperatures stayed lower than in the plain runs, growing 20% more slowly. This was clearly due to the effect of the clouds, which had induced such a large change by themselves. The moisture value tendencies combined to give 35% less drying. This resulted in PBLs which were saturated or oversaturated, and had no negative area just as before. The PLIs responded to the higher QS values, generally growing more than the plain runs by 40% .

The time evolution of the 30-60 run appears on Fig. 5.28. The figure looks very much like the run with clouds (Fig. 5.26), except for the behavior of the PLI. The convective instability rose between 16 and 19 GMT when both clouds and imposed changes aloft were added, as opposed to the clouds only run in which the PLI was approximately level during this time. The other noteworthy aspect of Fig. 5.28 was that the run showed oversaturation only during the first three hours, the period of heaviest cloud. After that, the PBL

growth was balanced giving just saturated conditions until the end of the run. This behavior was very realistic for the convective region. This qualitative behavior was also present for the two dryer soil runs, which were oversaturated only for the first three hours and the last 15 minutes of the run Apparently the clouds and imposed changes balanced the PBL growth in these runs. The wettest soil run, however, was oversaturated for several hours, so that clouds and imposed changes were unable to control it.

## 5.6 Summary

The sensitivity values are summarized on Table 5.4. Values are shown for the soil moisture parameters as well. The bulk soil moisture (GWB) was generally not of great importance for any of the parameters. Changing GWB by a factor of 2 (30% to 60%) changed the PBL growth by only 5%, the surface temperature rise by 5%, the PBL moisture drop by 6%, and the PLI growth by 6%.

The surface soil moisture (GWD) was more important, although its effect was less than the clouds or imposed changes for some variables. The GWD varied from 10% to 30% to 60%. The two numbers for each PBL characteristic reflect the difference between the two jumps. Curiously, the tripling of GWD from 10% to 30% was less important than the doubling from

30% to 60%. The PBL growth was cut 5% to 11% by the two increases, and the rise in temperature was affected similarly. The PBL moisture was more sensitive, and dropped 12% to 30% less for the additional moisture. This was understandable, since the surface soil moisture plays a direct role in the PBL moisture budget. The convective instability responded strongly to the soil surface moisture, even for the change from 10% to 30%. The PLI grew 25% to almost 75% more for the increased GWD. As in the other case studies, it is possible to summarize the sensitivity of convective instability to the various factors in a conceptual manner for one of the runs. The following is from the 30-60 run with clouds and imposed changes, in decreasing order of importance:

PLI = initial conditions + soil surface moisture + imposed changes (+ clouds + bulk soil moisture)

The factors in parantheses exerted too weak an influence on this series of runs to show up in the non-linear comparison. PLI for imposed changes only was the same when clouds were added for the 30-60 run. The effects of clouds and bulk soil moisture were inferred from the isolated runs ("plain", clouds only).

In this case it was fairly simple to find a model run which agreed with the surface observations. The only runs

which were not oversaturated for most of the time were the 10-30, 30-30 and 30-60 runs with both clouds and imposed changes aloft. Of these, only the 30-60 run did not predict a clear PBL top for any period during the run. The 30-60 values for TS and QS were compared with comparable values taken from the nearby soundings. The comparison, shown on Fig. 5.29, was excellent. Hence, the 30-60 run with clouds and imposed changes simulated reality quite well.

No dynamic forcing seemed to be involved as a trigger to start the convection. Strong temperature gradients were not observed at the surface, wind shear was weak, and no surface convergence was discovered. However, the 30-60 model run with clouds and imposed changes ("simulation" run) had no convective inhibition at 19 GMT. EMC at 18 GMT was close to this condition, but it was not clear from the coarse resolution of the sounding data, what the PBL structure really was. Using the model output from the "simulation" run, negative areas were calculated hourly starting at 15 GMT. These values are shown on Table 5.5. Notice that the negative area went to zero at 19 GMT, but was positive before that. In fact, the amount of negative area was substantial, so that even by 18 GMT a parcel would have required almost 3 m/s vertical velocity to penetrate to the level of positive buoyancy. The sounding for 15 GMT (Fig. 5.30) shows the considerable negative area at that time. At 18 GMT (Fig. 5.31)

there was still a small region of negative buoyancy for PBL parcels. Fig. 5.32, at 19 GMT, shows that no negative area was left, and PBL parcels were free to rise out of the PBL with any small vertical velocity perturbations as a trigger.

These conclusions are confirmed by observations. Fig. 5.33 shows the analyzed fields of convective instability and inhibition at 18 GMT. Notice that the echoes which appeared at 19 GMT were contained within the region of minimum inhibition, and were not in the areas of greatest convective instability. This pattern is the same as in the May 23 GMT case and the April case.

Table 5.1: CLOUDS IMPOSED IN MODEL RUNS FOR JUNE CASE

| | 12 GMT | | 15 GMT | | 18 GMT | |
|---|---|---|---|---|---|---|
| Pressure | | | | | | |
| 800 | 10 % | | 0 % | | 0 % | |
| 825 | 10 % | | 0 % | | 0 % | |
| 850 | 30 % | PBL top -25mb | 30 % | | 0 % | |
| 875 | 50 % | PBL top | 70 % | | PBL top | 30 % |
| 900 | 70 % | | | | | |
| 925 | 80 % | | | | | |

Cloud amounts expressed as a percentage of complete cloud cover. PBL tops are shown in their approximate pressure levels--actual level depends on particular run.

Table 5.2: IMPOSED CHANGES ON MODEL RUNS FOR JUNE CASE

| | 12 - 15 GMT | | 15 - 19 GMT | |
|---|---|---|---|---|
| Pressure | T(deg C) | Q(g/kg) | T(deg C) | Q(g/kg) |
| 500 | 0.0 | 0.0 | -0.8 | 0.0 |
| 525 | 0.0 | 0.0 | -0.4 | 0.0 |
| 550 | 0.0 | 0.0 | 0.0 | 0.0 |
| 575 | -0.6 | +0.3 | +0.8 | 0.0 |
| 600 | -1.8 | +1.2 | +2.0 | 0.0 |
| 625 | -1.2 | +0.6 | +0.8 | -0.4 |
| 650 | -0.9 | +0.3 | 0.0 | 0.0 |
| 675 | -0.6 | +0.3 | +0.4 | -0.4 |
| 700 | -0.6 | +0.3 | +0.8 | -0.8 |
| 725 | 0.0 | 0.0 | +0.4 | -0.4 |
| 750 | +1.2 | 0.0 | 0.0 | 0.0 |
| 775 | +1.2 | 0.0 | 0.0 | 0.0 |
| 800 | +1.2 | 0.0 | 0.0 | 0.0 |
| 825 | +1.2 | 0.0 | 0.0 | +0.4 |
| 850 | +1.2 | 0.0 | 0.0 | +0.8 |
| 875 | +0.9 | -0.3 | 0.0 | 0.0 |
| 900 | +0.6 | -0.9 | 0.0 | 0.0 |

Pressure levels not mentioned had zero changes.

Table 5.3: MODEL RESULTS AT 19 GMT, 6 JUNE

| Run | PH(mb) | TS( C) | QS(g/kg) | PLI( C) | NA | CONDITION |
|---|---|---|---|---|---|---|
| Plain | | | | | | |
| 10-30 | 724 | 30.5 | 12.6 | 4.0 | 0 | S+ |
| 30-30 | 733 | 30.1 | 13.0 | 4.3 | 0 | S+ |
| 30-60 | 745 | 29.7 | 13.2 | 4.4 | 0 | S+ |
| 60-60 | 772 | 28.6 | 14.5 | 5.4 | 0 | S+ |
| Cloud | | | | | | |
| 10-30 | 800 | 27.9 | 13.6 | 4.1 | 0 | S+ |
| 30-30 | 809 | 27.5 | 14.0 | 4.4 | 0 | S+ |
| 30-60 | 820 | 27.1 | 14.3 | 4.6 | 0 | S+ |
| 60-60 | 844 | 26.2 | 15.3 | 5.3 | 0 | S+ |
| Imposed Changes | | | | | | |
| 10-30 | 736 | 31.4 | 12.7 | 4.5 | 0 | S+ |
| 30-30 | 749 | 31.0 | 13.2 | 4.9 | 0 | S+ |
| 30-60 | 761 | 30.5 | 13.4 | 4.9 | 0 | S+ |
| 60-60 | 790 | 29.3 | 14.9 | 6.1 | 0 | S+ |
| Clouds and Imposed Changes | | | | | | |
| 10-30 | 818 | 28.4 | 13.9 | 4.6 | 0 | S+ |
| 30-30 | 829 | 28.0 | 14.3 | 4.9 | 0 | S+ |
| 30-60 | 841 | 27.5 | 14.5 | 4.9 | 0 | S |
| 60-60 | 859 | 26.5 | 15.6 | 5.8 | 0 | S+ |

Run ID is expressed in form: Surface Soil Moisture/Bulk Soil Moisture. PH is pressure level of PBL top. TS is temperature at the top of the surface layer. QS is PBL moisture. PLI is convective instability. NA is negative area (convective instability), in m**2/s**2 (energy/mass). Condition refers to the saturation condition at the top of the PBL: blank = unsaturated, ~S = nearly saturated, S = saturated, S+ = oversaturated.

Table 5.4: SENSITIVITY VALUES FOR 23 GMT, 6 JUNE MODEL RUNS

| Change in: | PH | TS | QS | PLI |
|---|---|---|---|---|
| Factor | | | | |
| Clouds | -33 | -26 | -27 | +10 to -08 |
| Imposed Changes | - 7 | + 9 | - 6 | +44 |
| Clouds and Imposed Changes | -41 | -22 | -35 | +40 |
| Soil Surface Moisture | | | | |
| 10 to 30% | - 5 | - 5 | -12 | +25 |
| 30 to 60% | -11 | -11 | -30 | +73 |
| Bulk Soil Moisture | | | | |
| 30 to 60% | - 5 | - 5 | - 6 | + 6 |

Values are percentage changes of normal variation of parameters, expressed in relation to the maximum change in the plain runs. PH is the pressure level of the top of the PBL, TS is the temperature at the top of the surface layer, QS is the PBL moisture value, and PLI is the convective instability.

Table 5.5: NEGATIVE AREA FOR 30-60 RUN WITH CLOUDS AND IMPOSED CHANGES

| Time | Negative Area (m**2/s**2) |
|---|---|
| 15 GMT | 17.20 |
| 16 GMT | 12.96 |
| 17 GMT | 4.92 |
| 18 GMT | 3.78 |
| 19 GMT | 0.00 |

Negative area is related to needed updraft velocity to reach level of positive buoyancy by relation v = (2*Negative Area)**1/2.

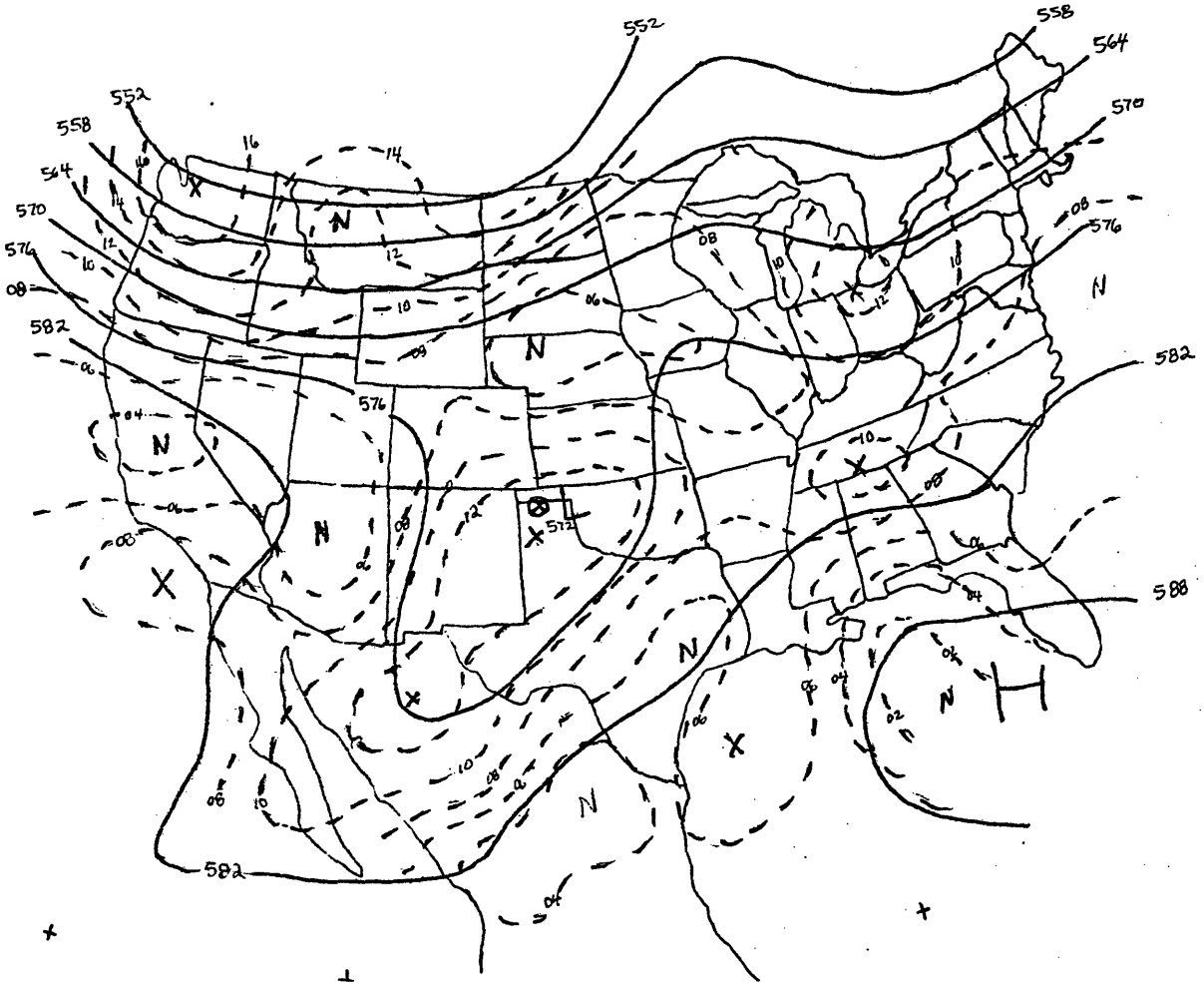


Fig. 5.1 Synoptic-scale 500 mb analysis for 12 GMT, 6 June. Solid lines for heights (dm) and dashed lines for vorticity (10**-5 1/sec).

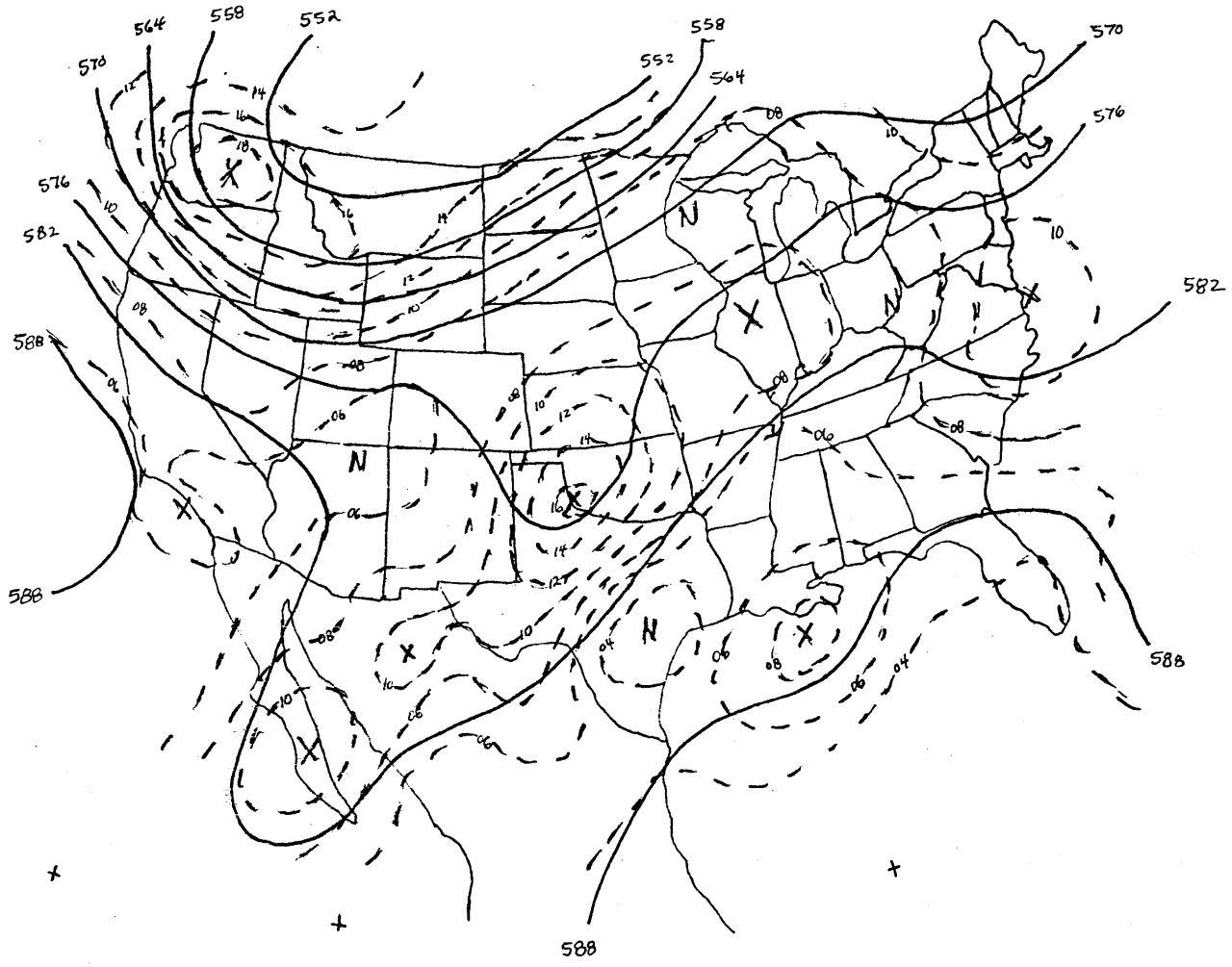


Fig. 5.2 Same as Fig. 5.1 for 00 GMT, 7 June.

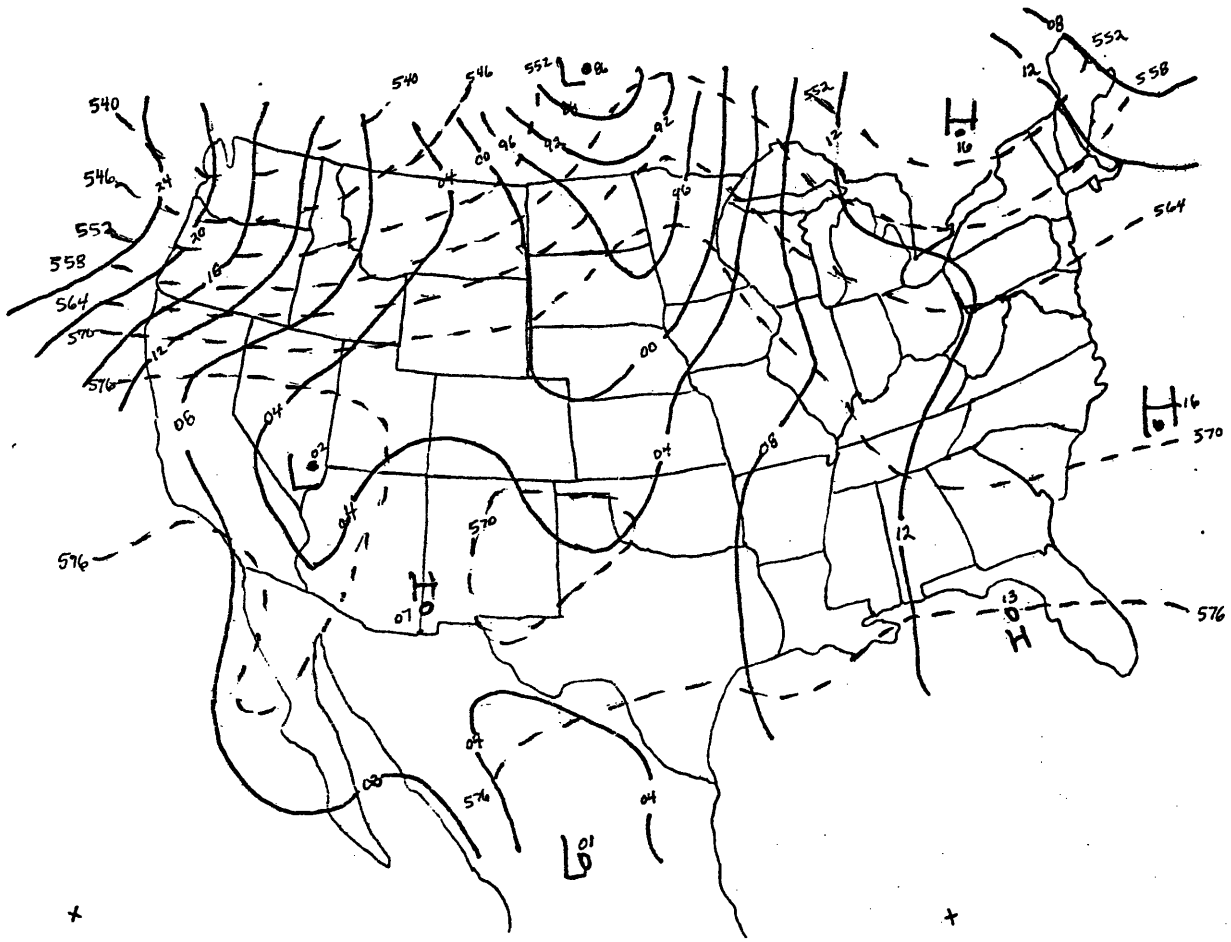


Fig. 5.3 Synoptic-scale surface analysis for 12 GMT, 6 June. Solid lines for sea level pressure (mb) with leading 9 or 10 digit(s) dropped, and dashed lines for 1000 to 500 mb thickness (dm).

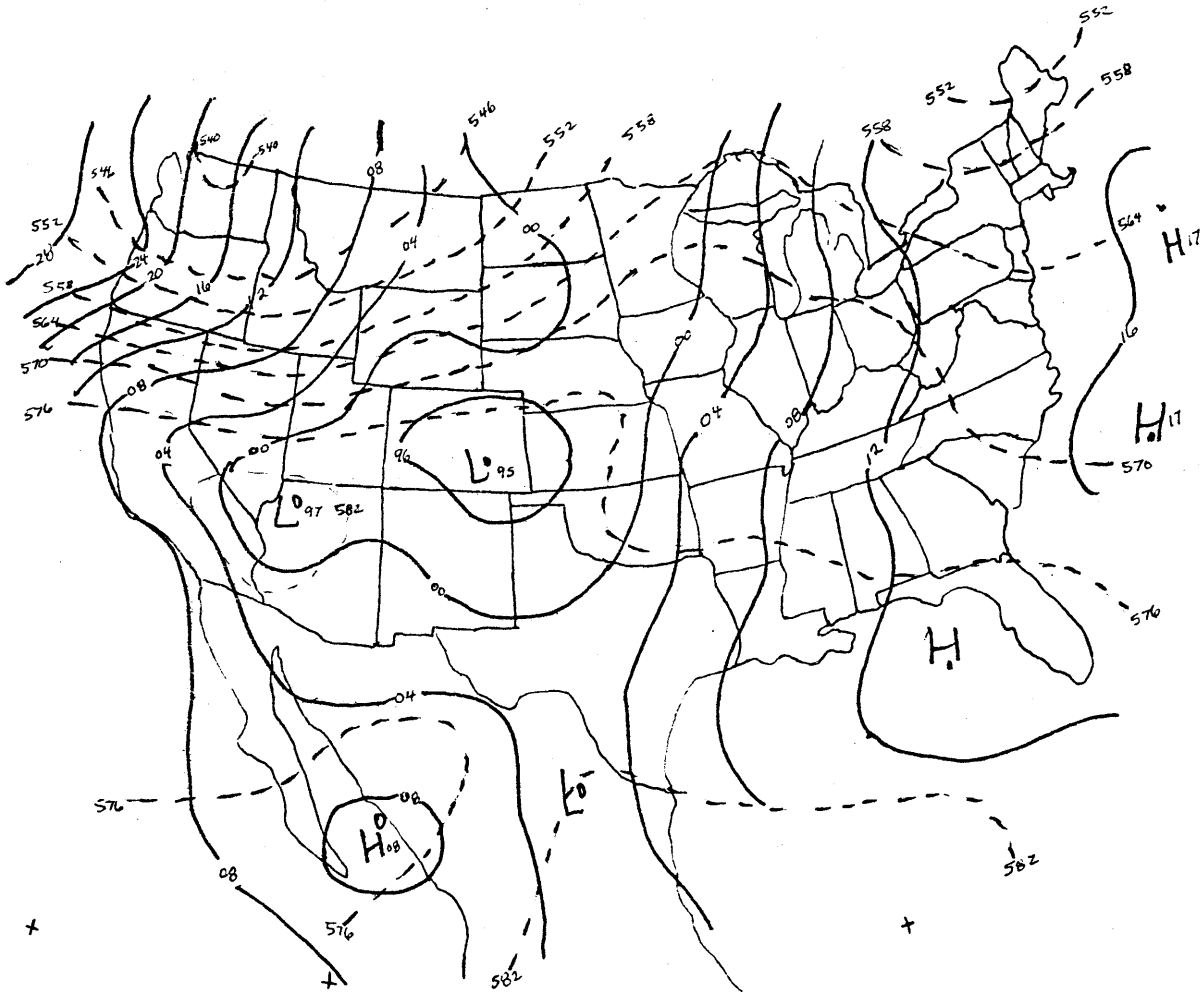


Fig. 5.4 Same as Fig. 5.3 for 00 GMT, 7 June.

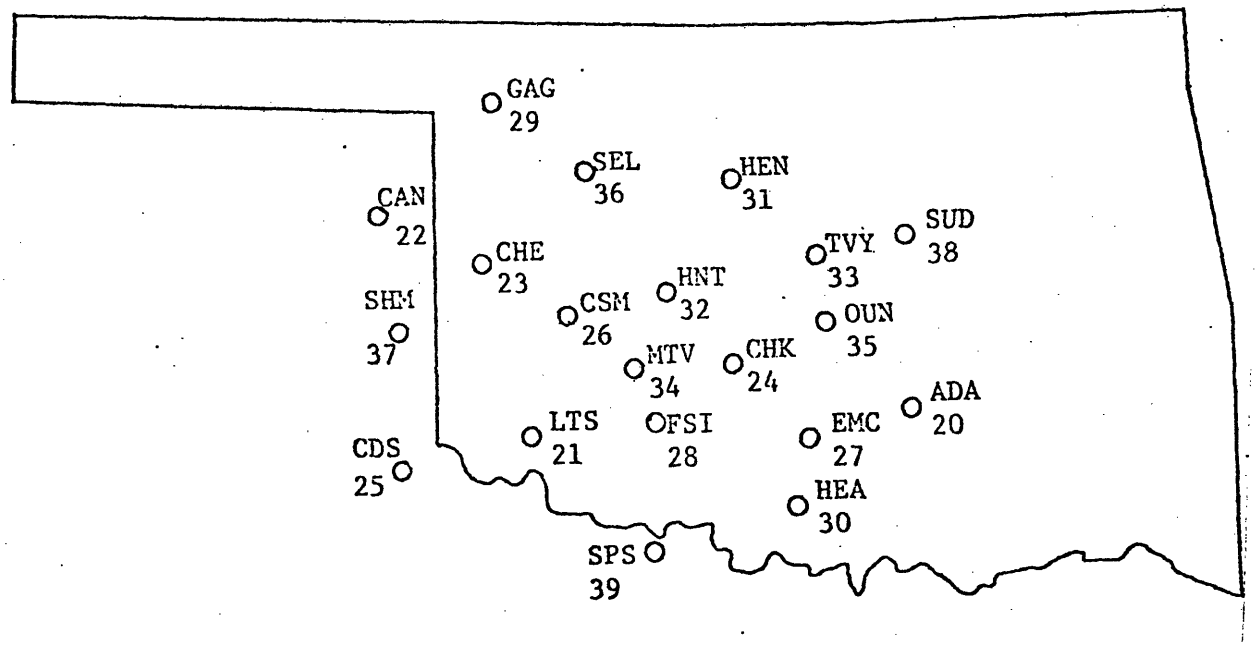


Fig. 5.5 Sounding network for June 6-7 case.

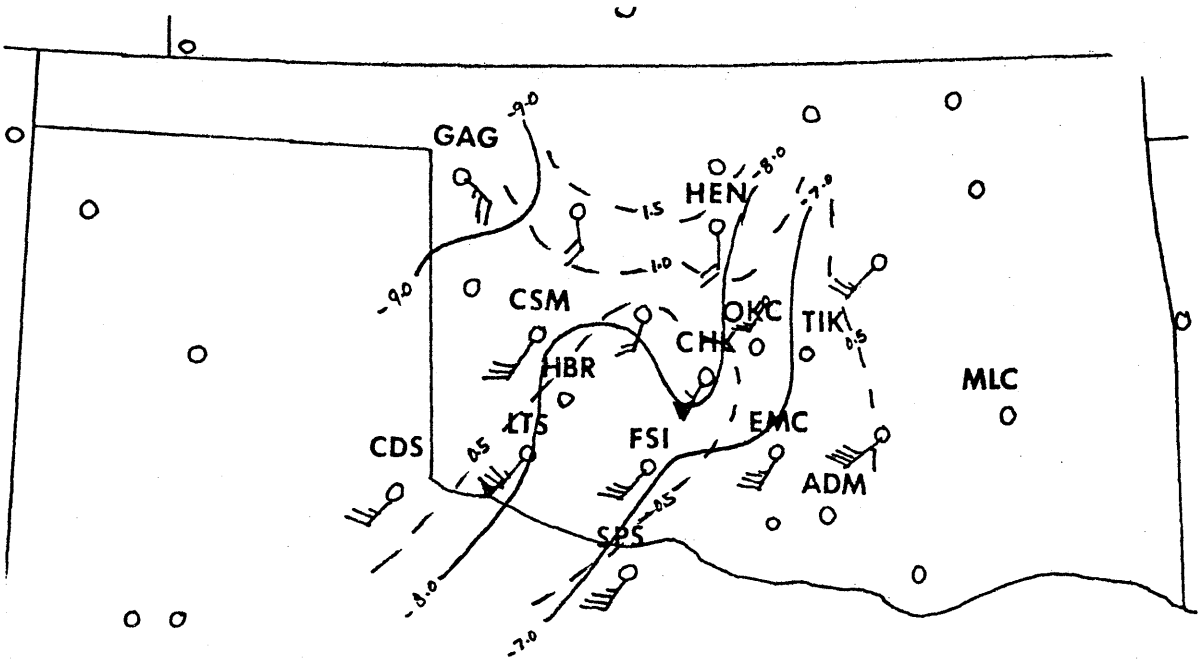


Fig. 5.6 Mesoscale 500 mb analysis for 15 GMT, 6 June. Solid lines for temperatures (deg C) and dashed lines for mixing ratio (g/kg). Wind plotted conventionally (knots).

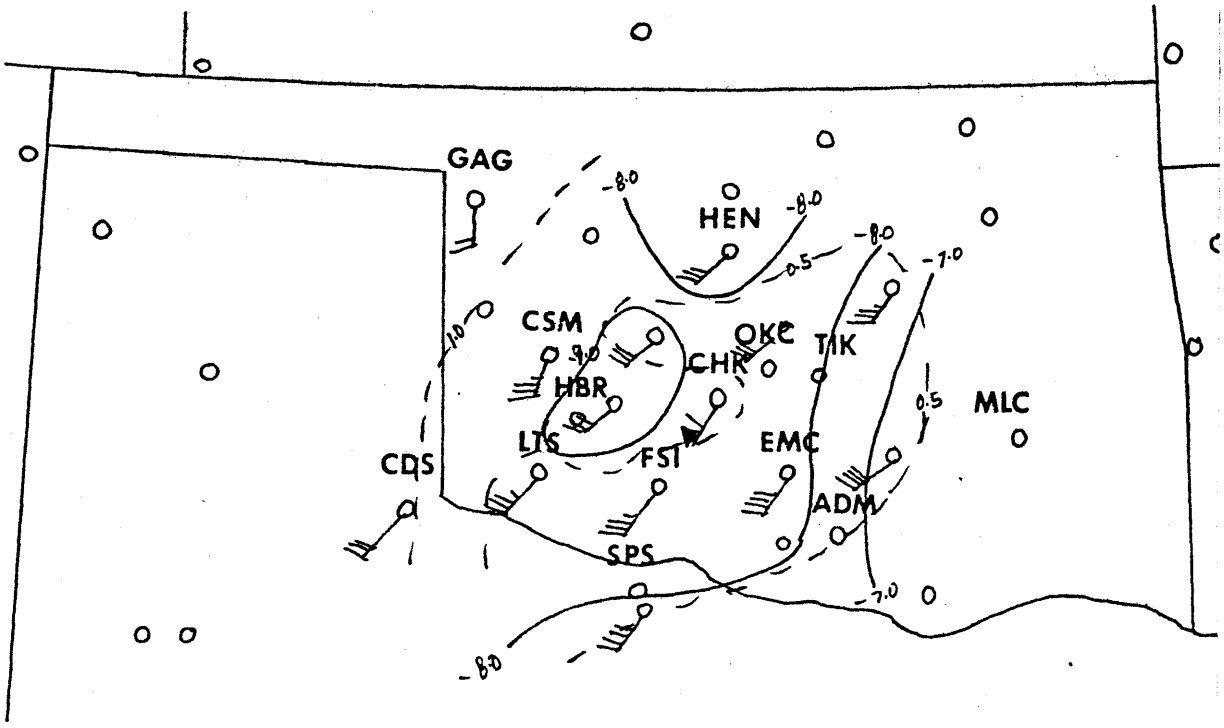


Fig. 5.7 Same as Fig. 5.6 for 18 GMT, 6 June.

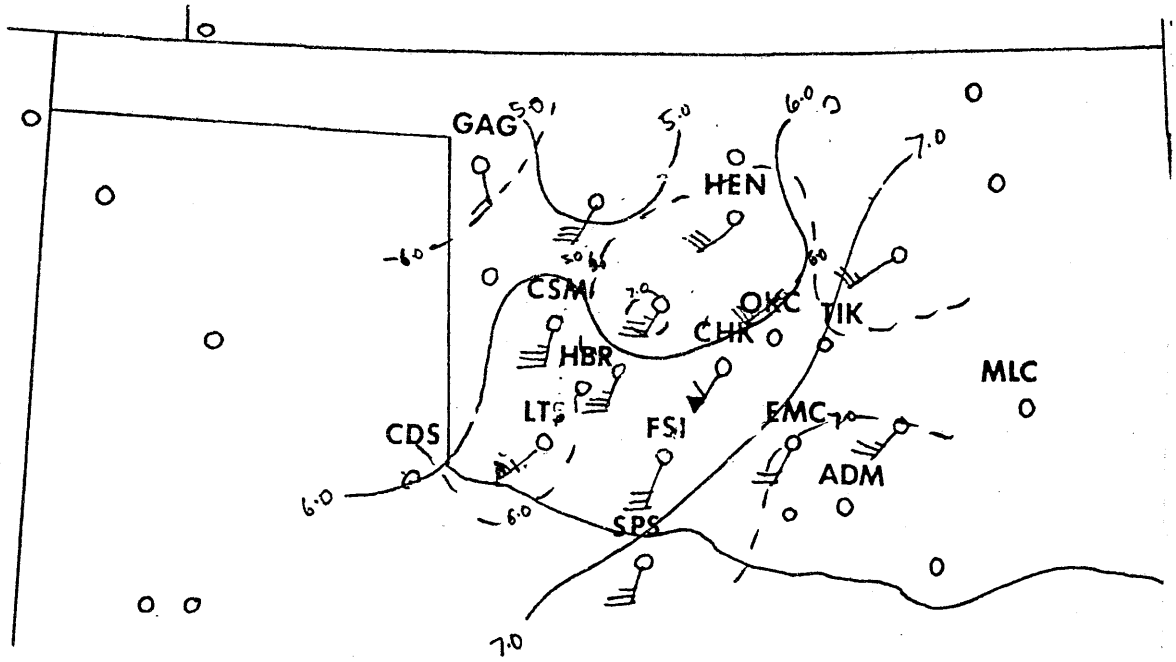


Fig. 5.8 Same as Fig. 5.6 for 700 mb.

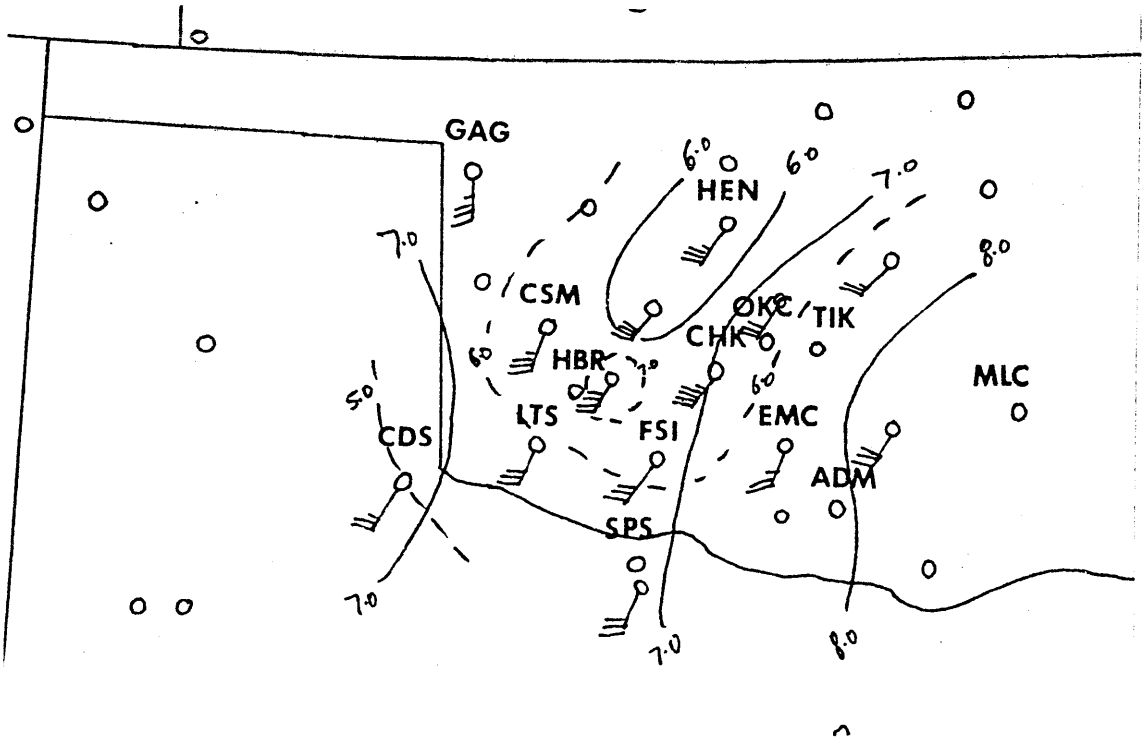


Fig. 5.9 Same as Fig. 5.8 for 18 GMT, 6 June.

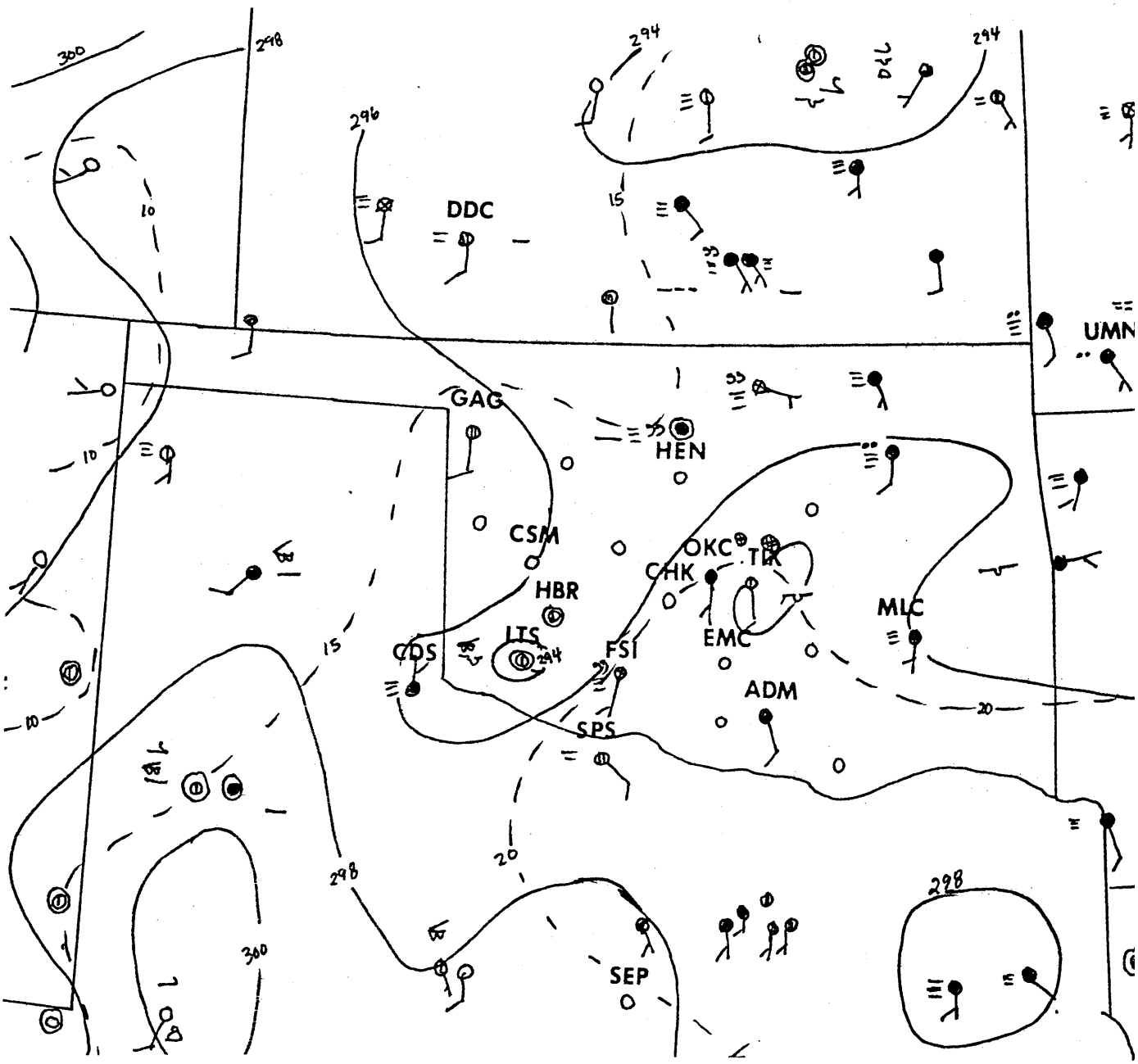


Fig. 5.10 Mesoscale surface analysis for 12 GMT, 6 June. Solid lines are surface potential temperature (K) and dashed lines are dewpoints (deg C). Winds are plotted conventionally (knots). Sky condition is clear (open circle), scattered (single bar), broken (double bar), overcast (filled circle), and obscurred (x in circle). Cloud type is plotted (if available) as is current weather according to conventional synoptic code. Radar echoes are cross-hatched irregularly shaped areas.

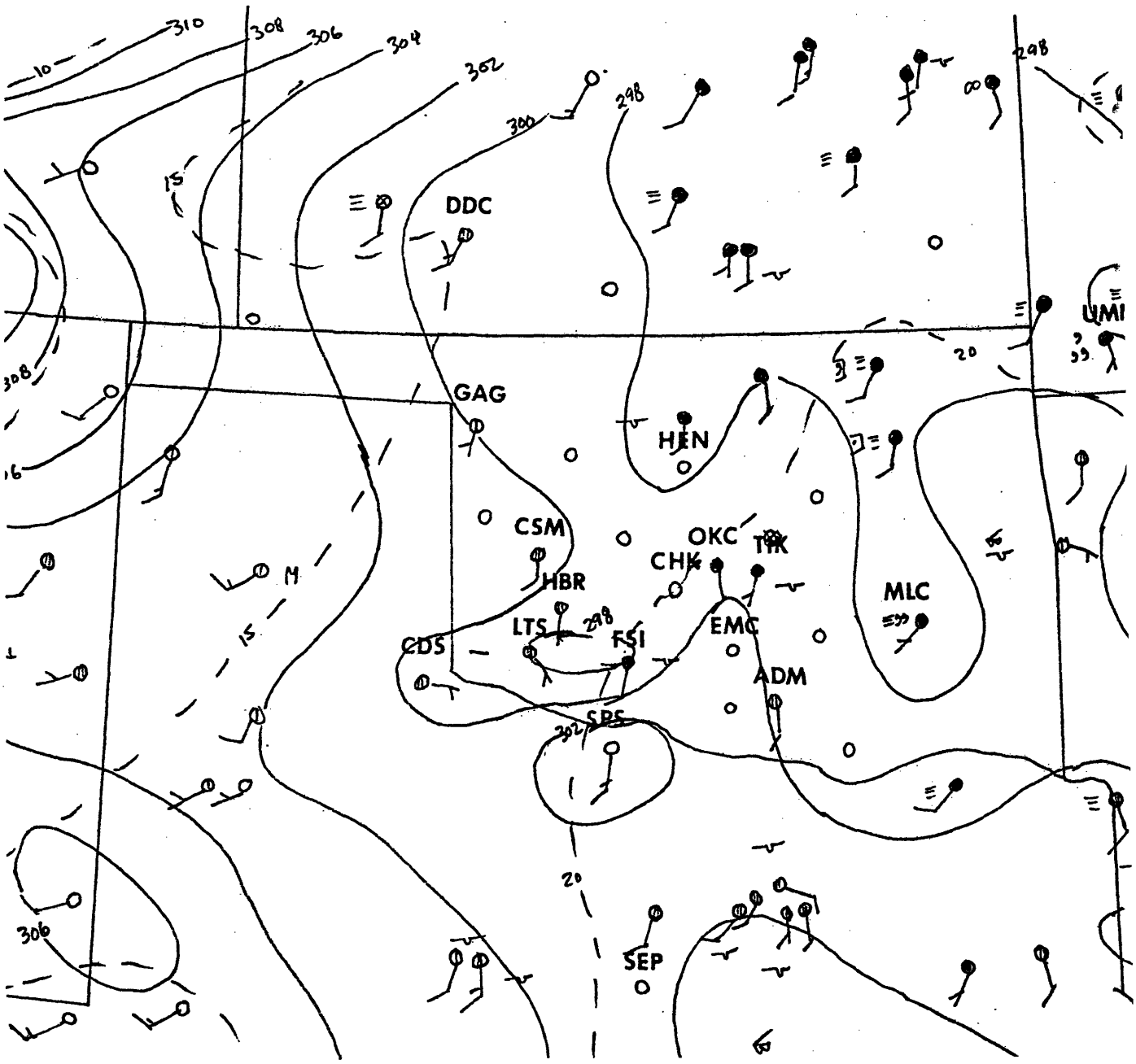


Fig. 5.11 Same as Fig. 5.10 for 15 GMT, 6 June.

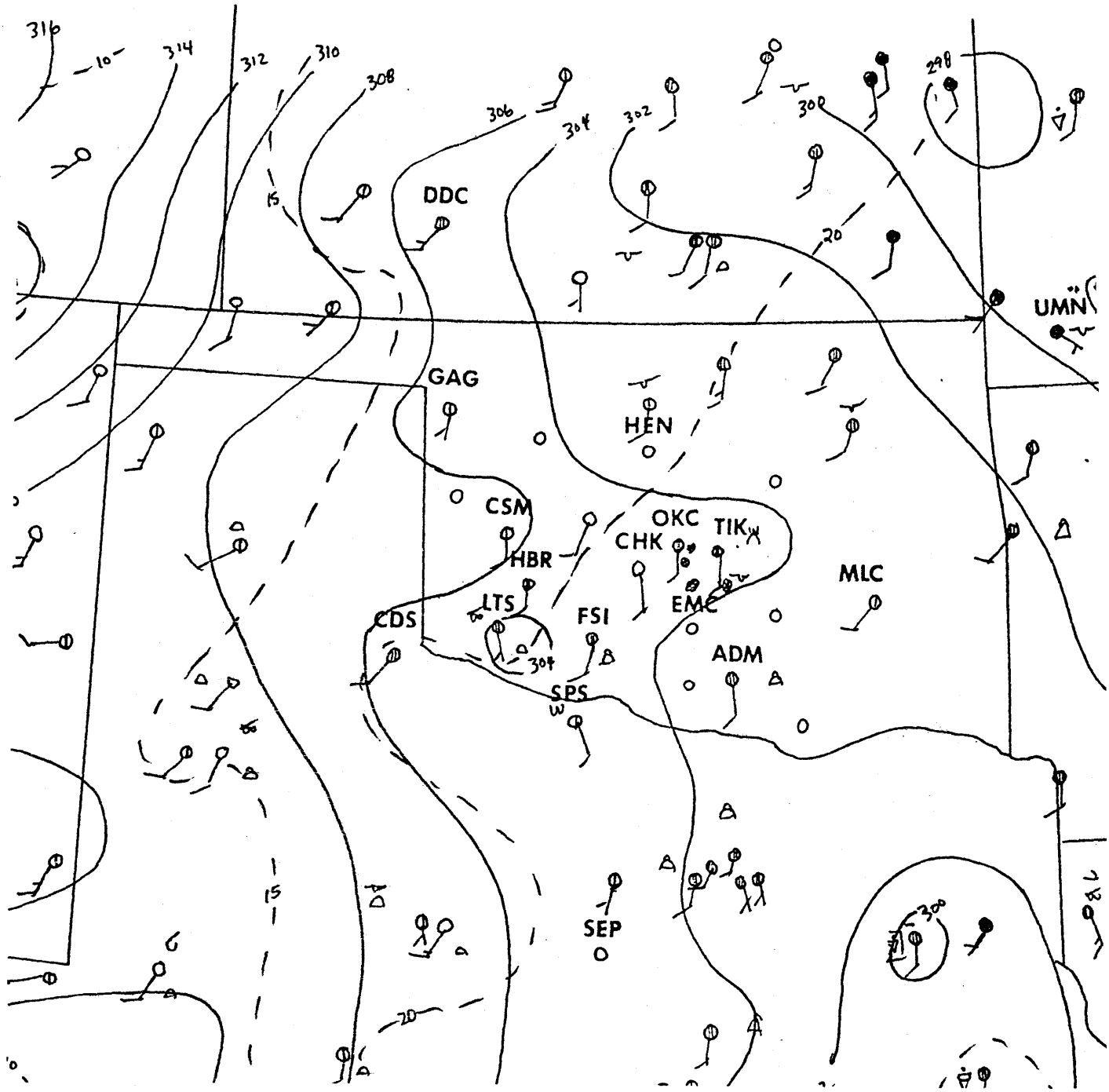


Fig. 5.12 Same as Fig. 5.10 for 18 GMT, 6 June.

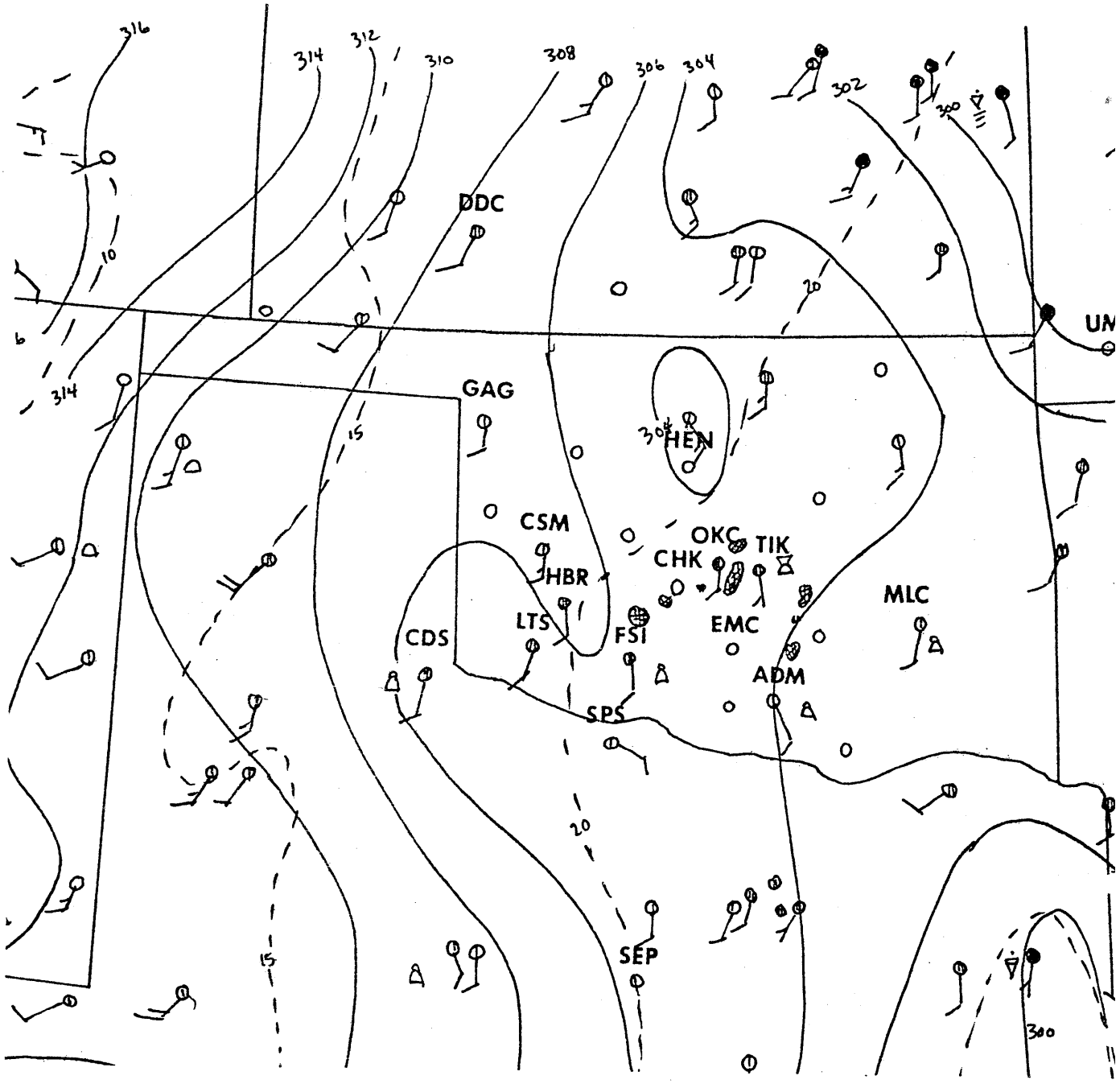


Fig. 5.13 Same as Fig. 5.10 for 19 GMT, 6 June.

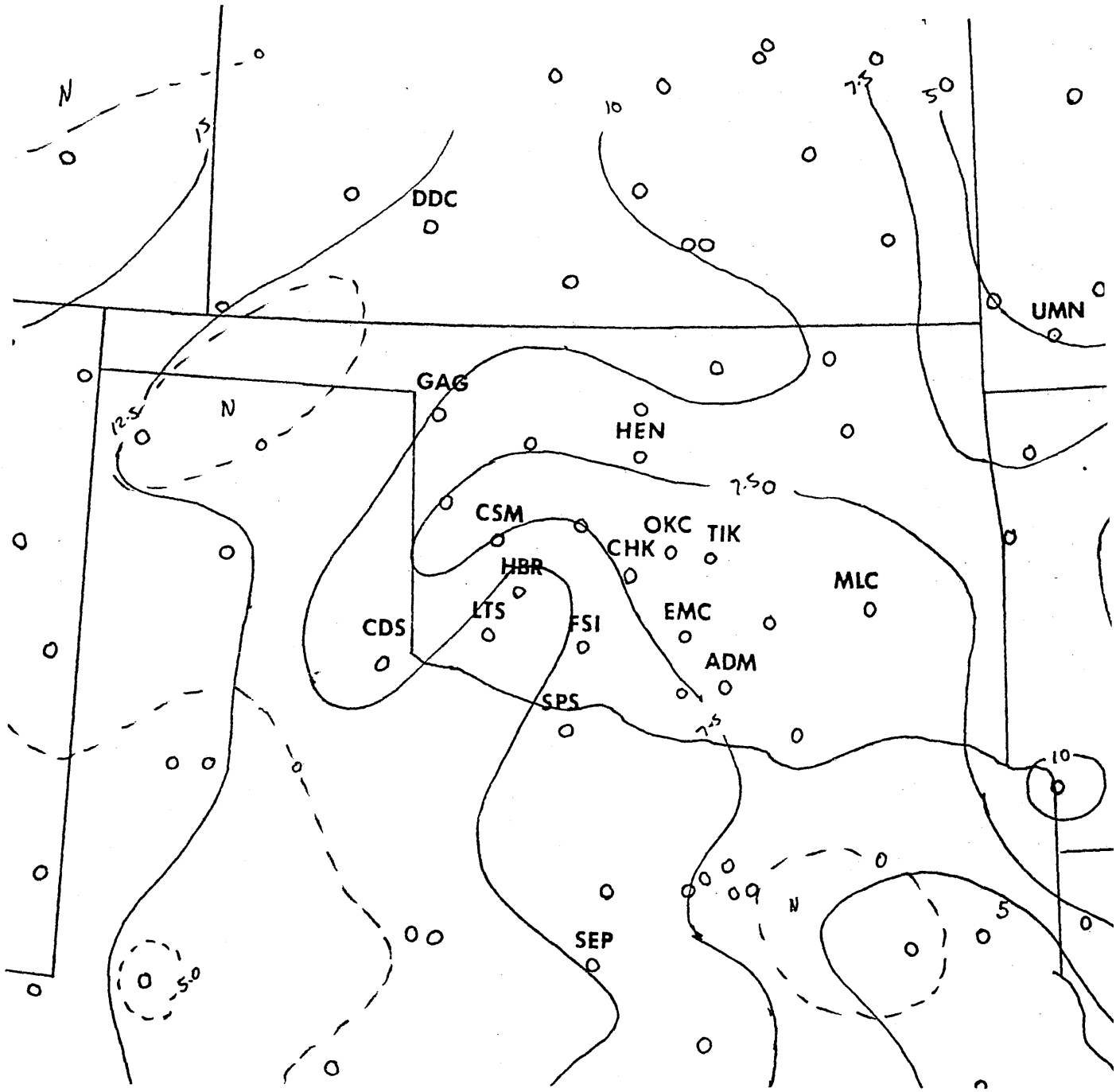


Fig. 5.14 Change of potential temperature and dewpoint between 12 GMT and 19 GMT, 6 June. Solid lines are change in potential temperature (K), and dashed lines are change in dewpoint (deg C).

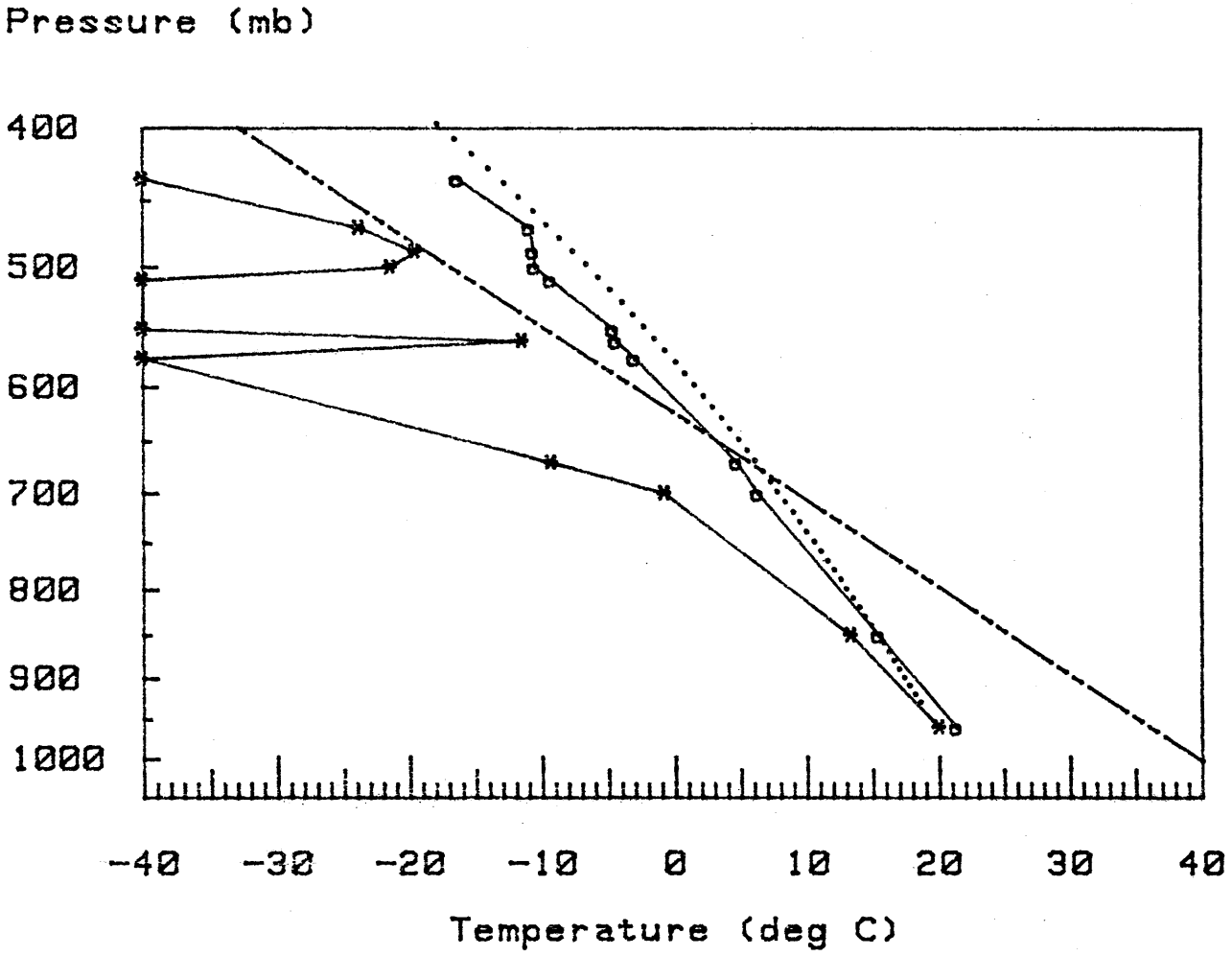


Fig. 5.15 Sounding plotted on a pseudoadiabatic diagram from Oklahoma City, Oklahoma for 12 GMT, 6 June. Solid line connecting dots for temperature (deg C), solid line connecting * for dewpoint (deg C), dash-dotted line for 313 K isentrope, and dotted line showing moist adiabat for mean PBL parcel (or selected parcel if PBL is not well-defined). Dewpoints colder than -40 C are plotted at -40 C.

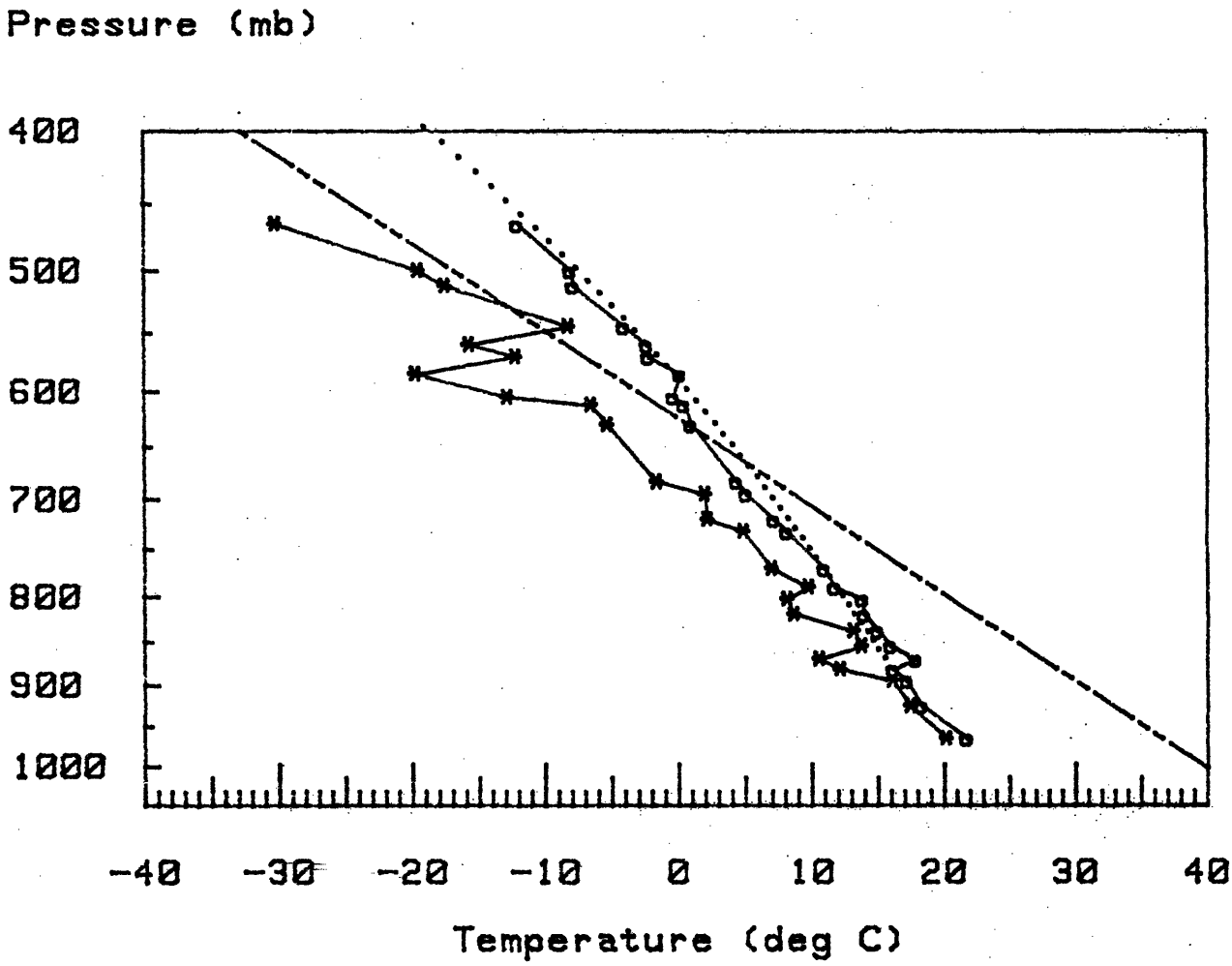


Fig. 5.16 Same as Fig. 5.15 from Hennesey, Oklahoma for 1312 GMT 6 June.

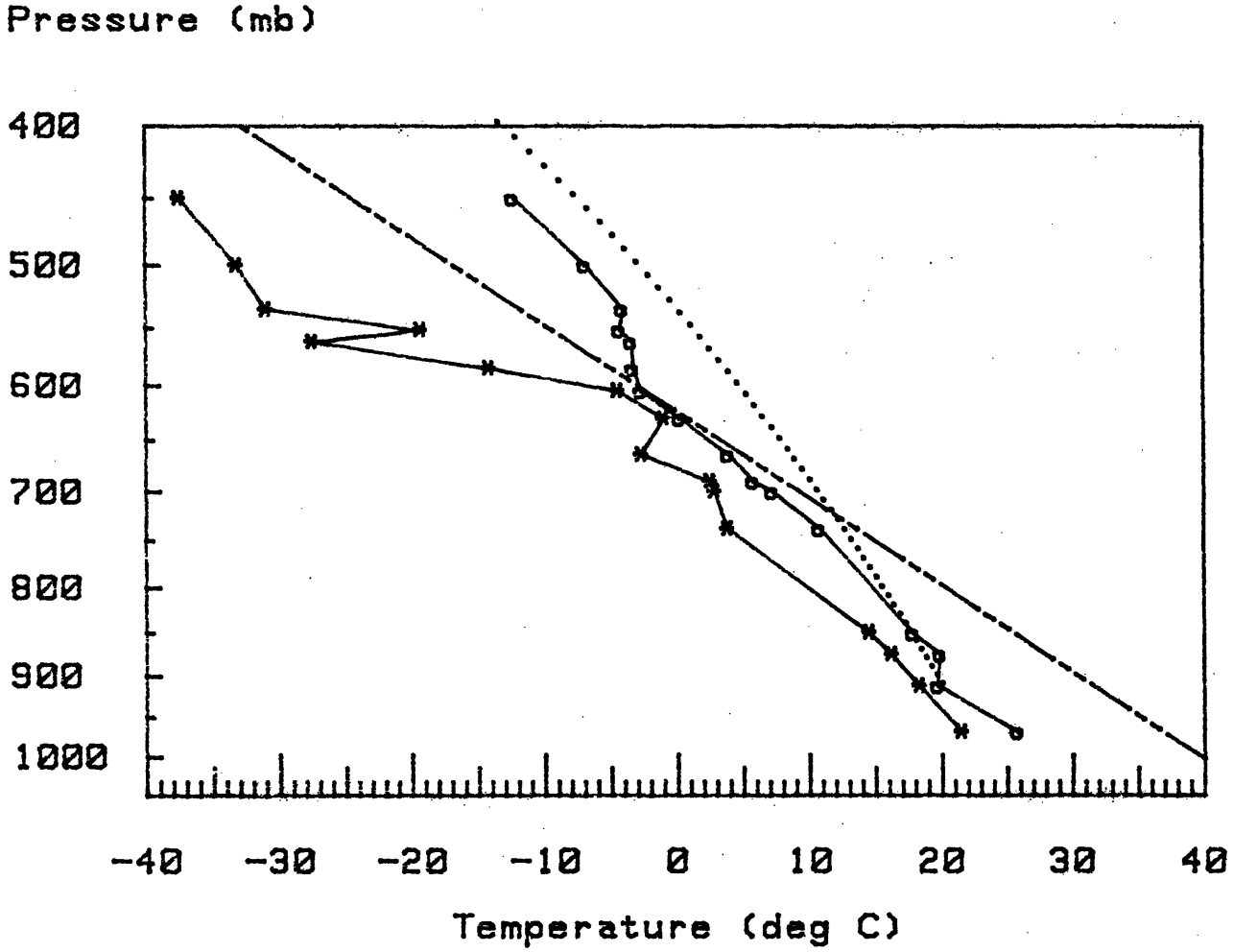


Fig. 5.17 Same as Fig. 5.15 from Elmore City, Oklahoma for 15 GMT, 6 June.

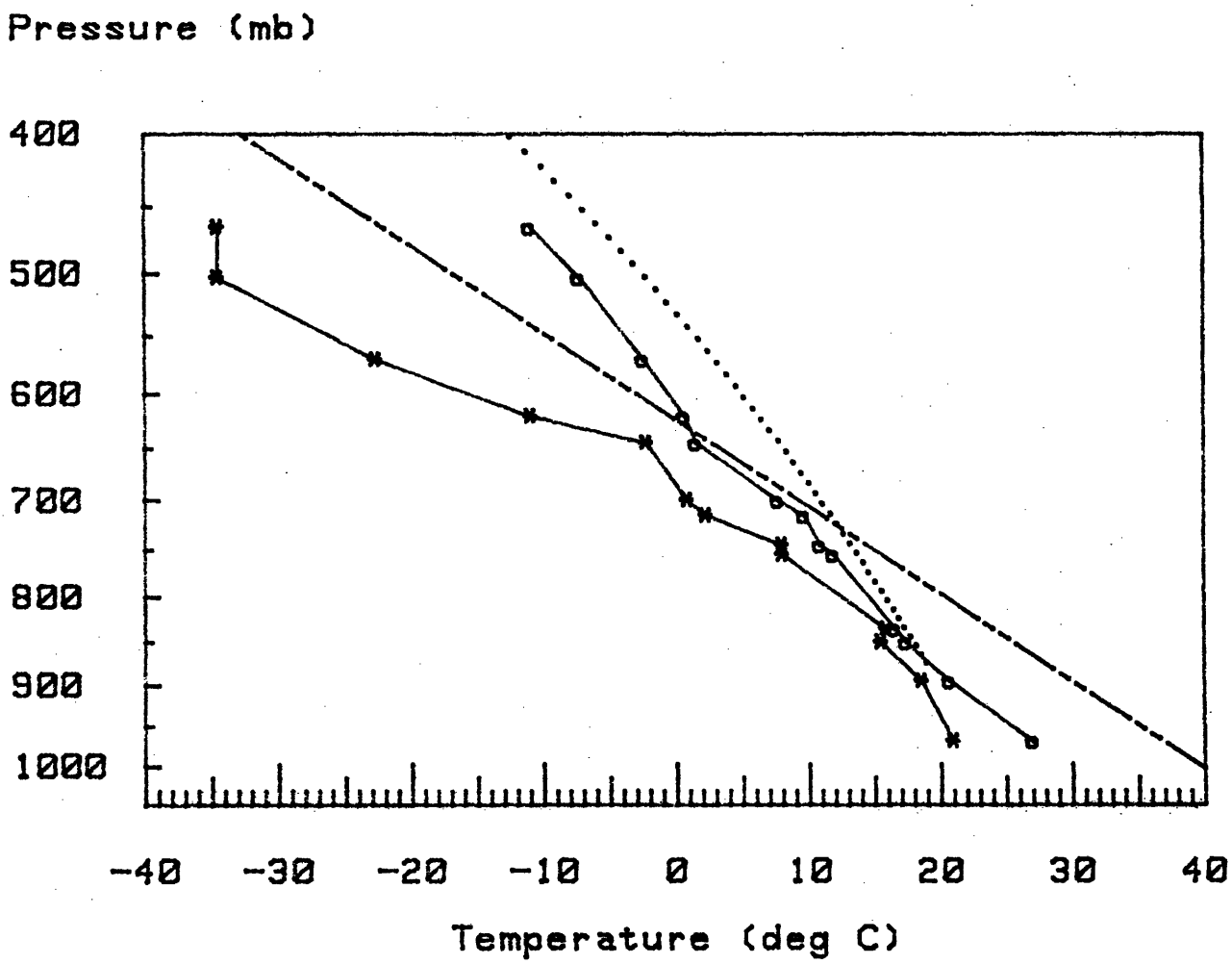


Fig. 5.18 Same as Fig. 5.17 for 18 GMT, 6 June.

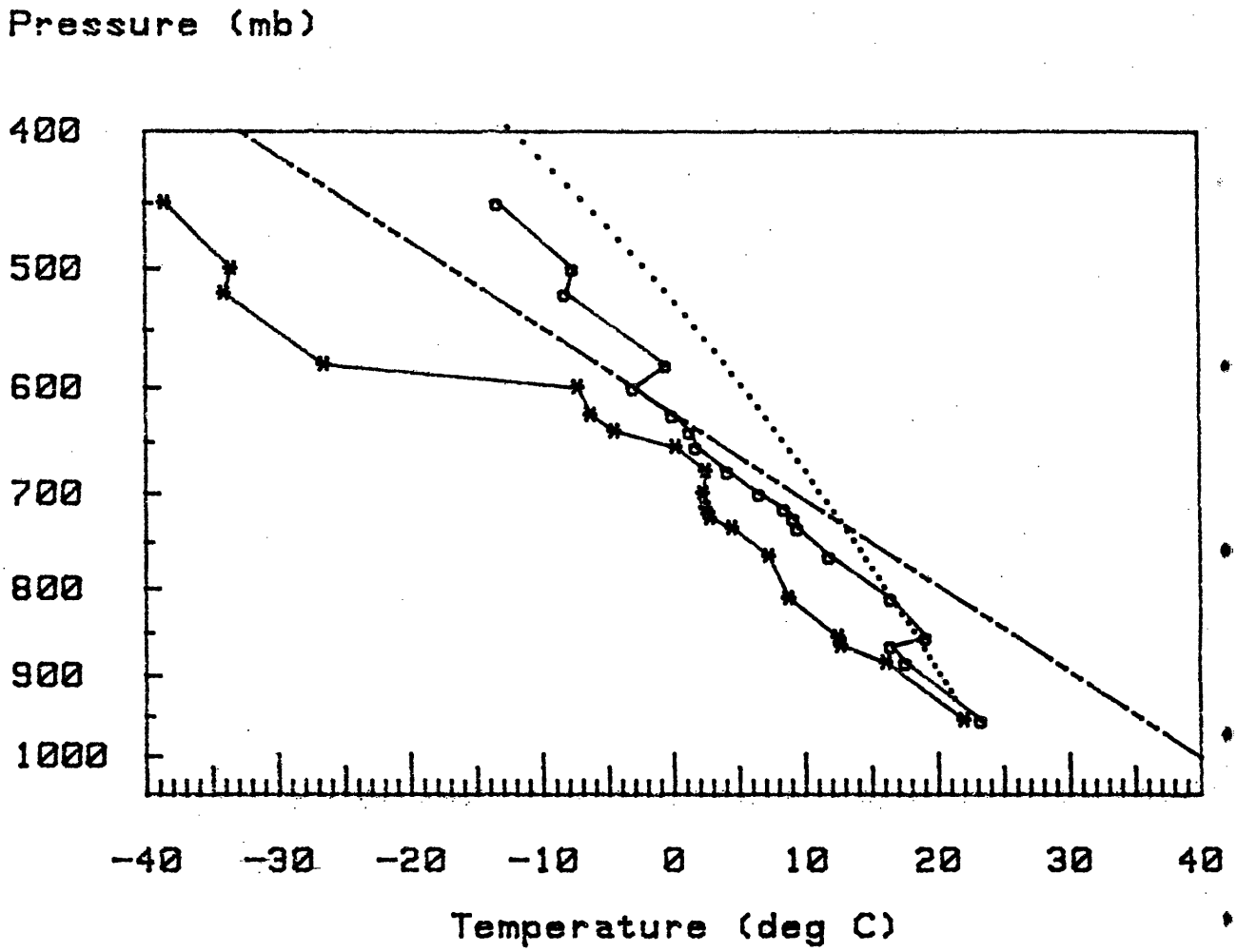


Fig. 5.19 Same as Fig. 5.15 from Fort Sill, Oklahoma for 15 GMT, 6 June.

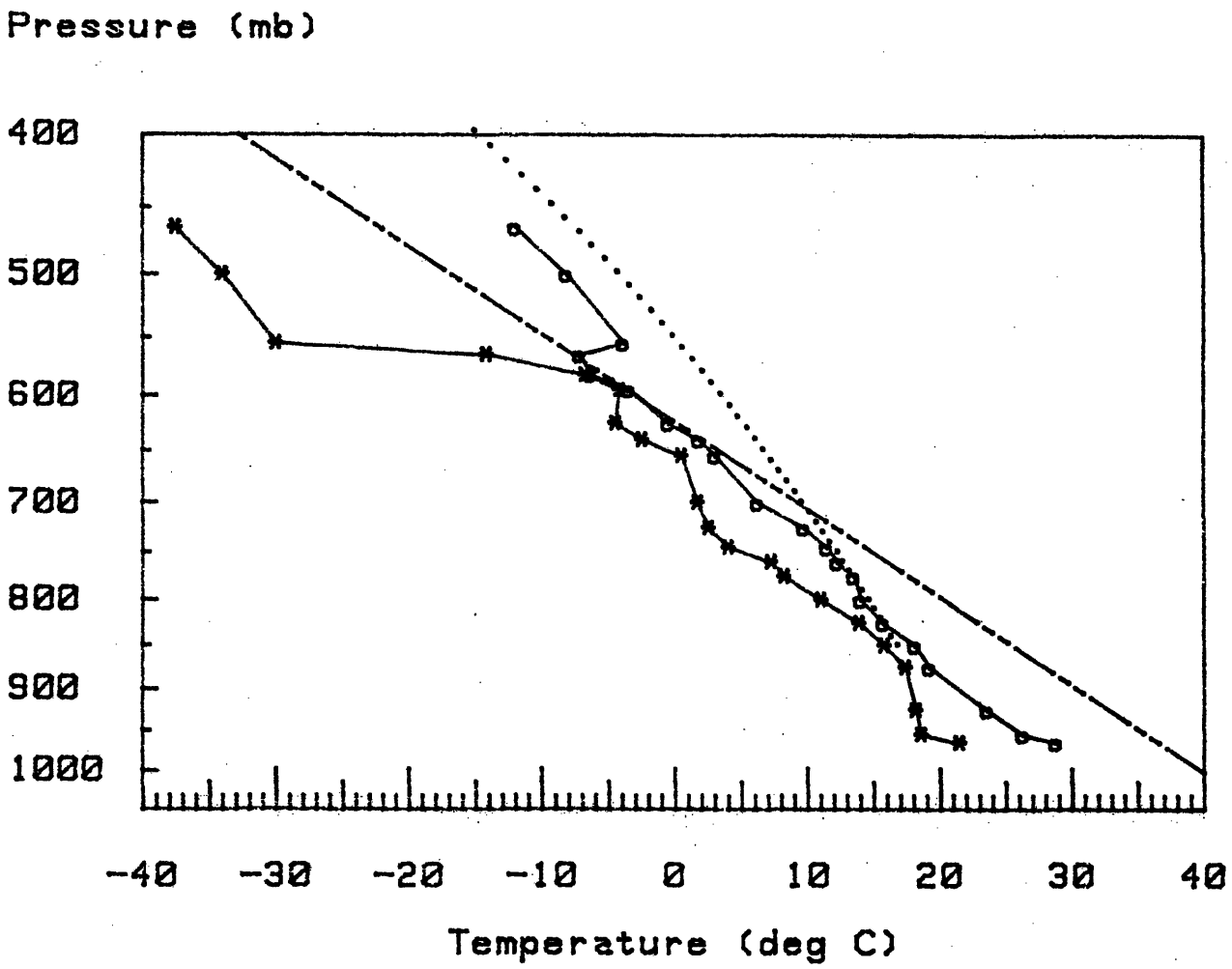


Fig. 5.20 Same as Fig. 5.19 for 18 GMT, 6 June.

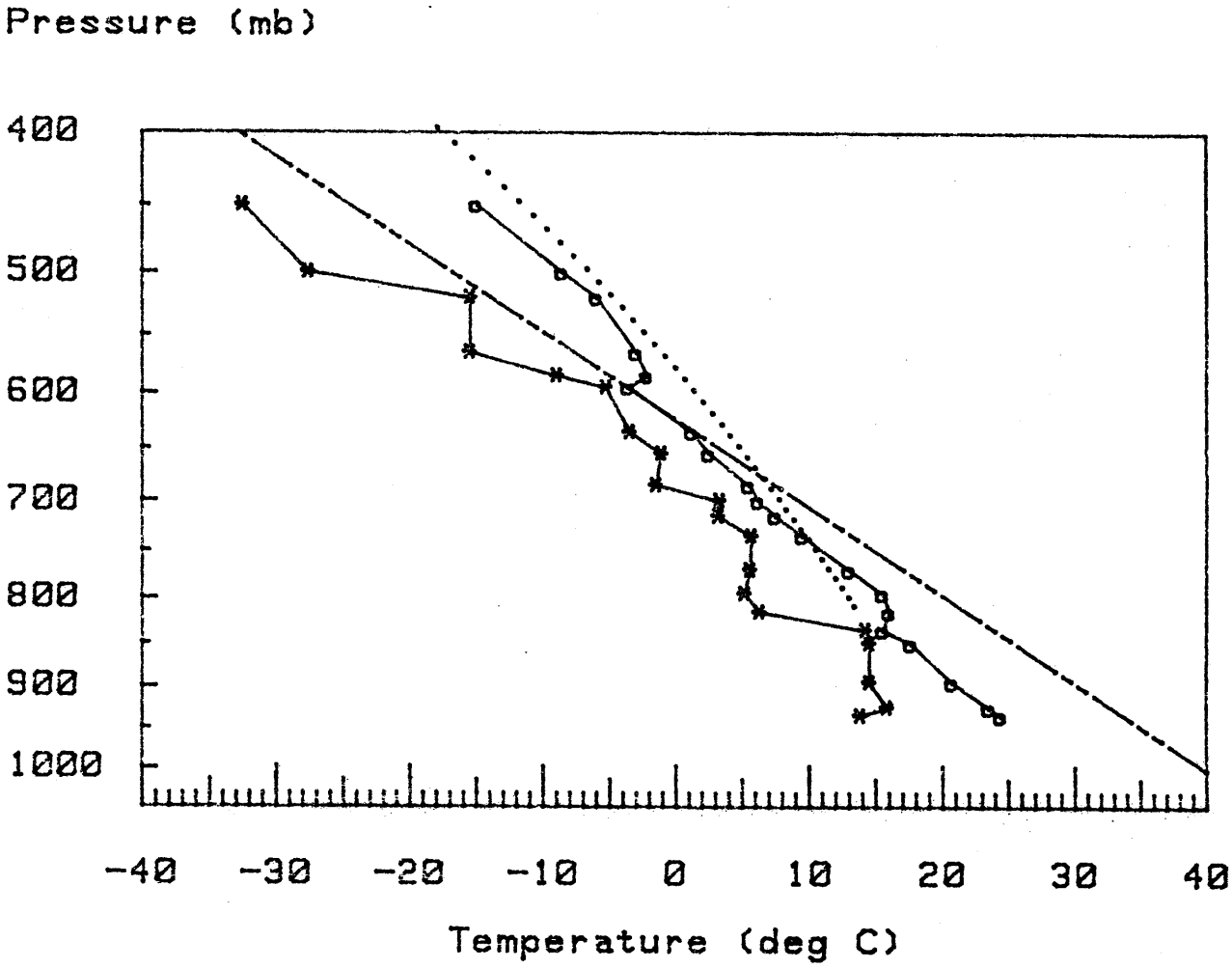


Fig. 5.21 Same as Fig. 5.15 from Clinton Sherman AFB, Oklahoma for 18 GMT, 6 June.

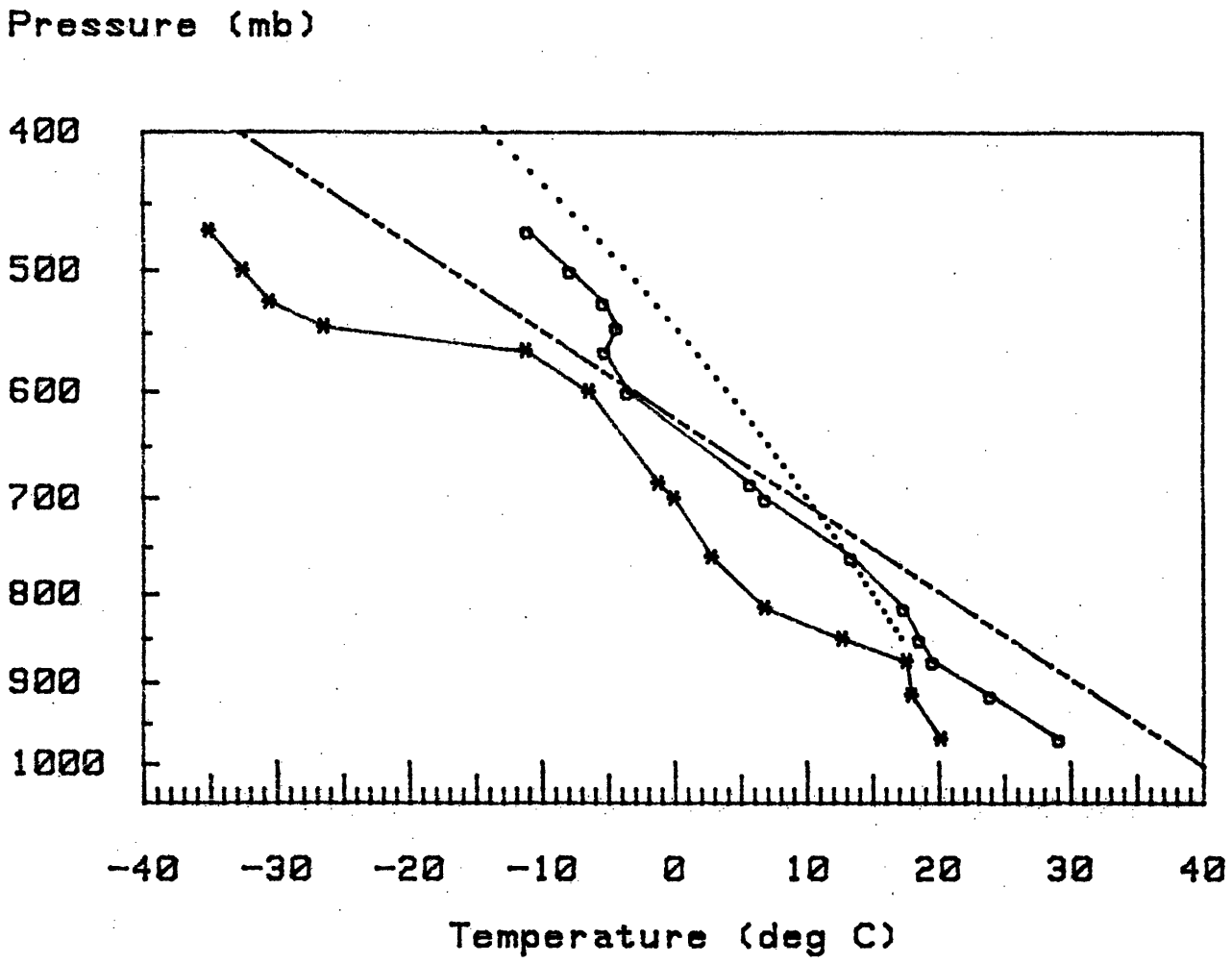


Fig. 5.22 Same as Fig. 5.15 from Wichita Falls, Texas, 17 GMT, 6 June.

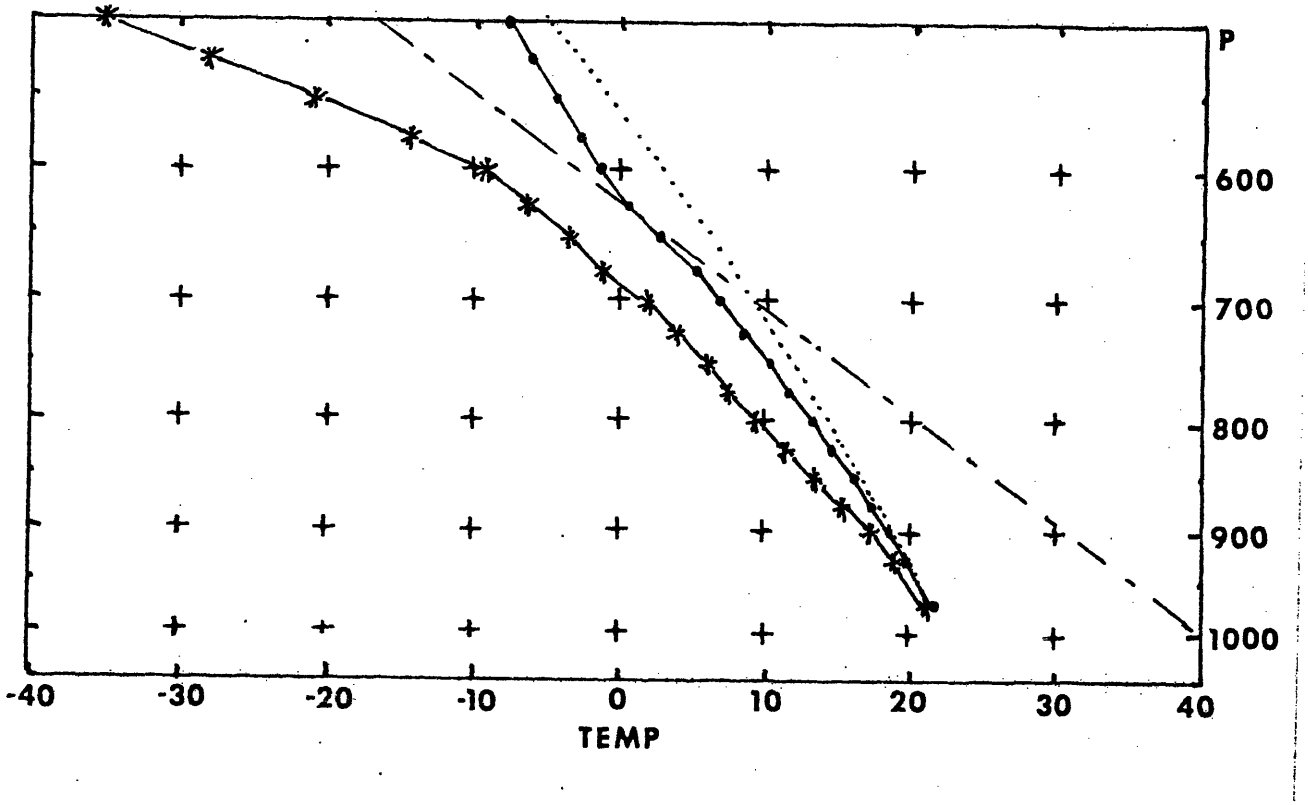


Fig. 5.23 Same as Fig. 5.15 for JUNHYB, 12 GMT, 6 June.

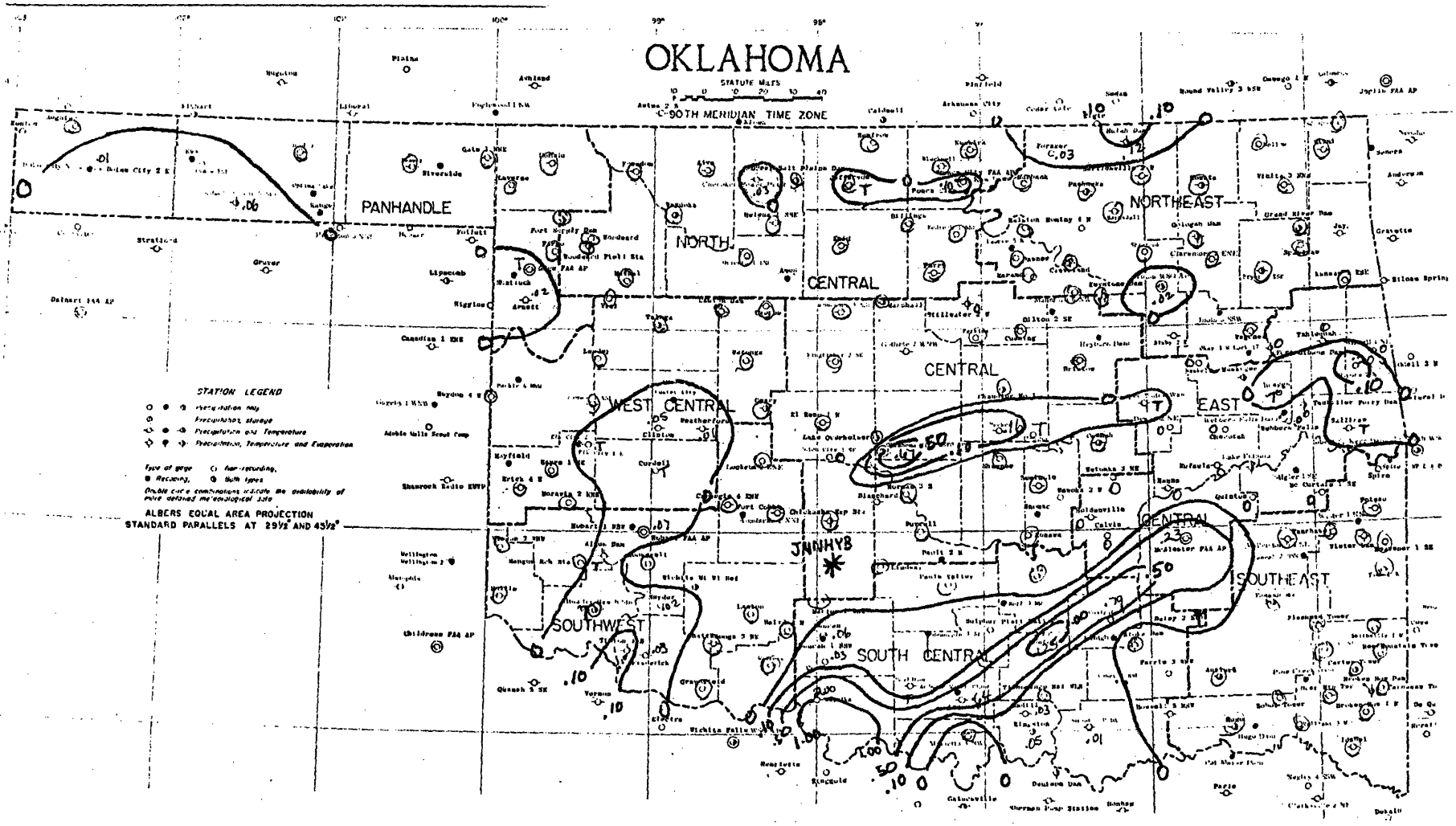


Fig. 5.24 Rainfall for Oklahoma for 5 June in inches. Contours drawn for 0, .10, .50, 1.00 inches.

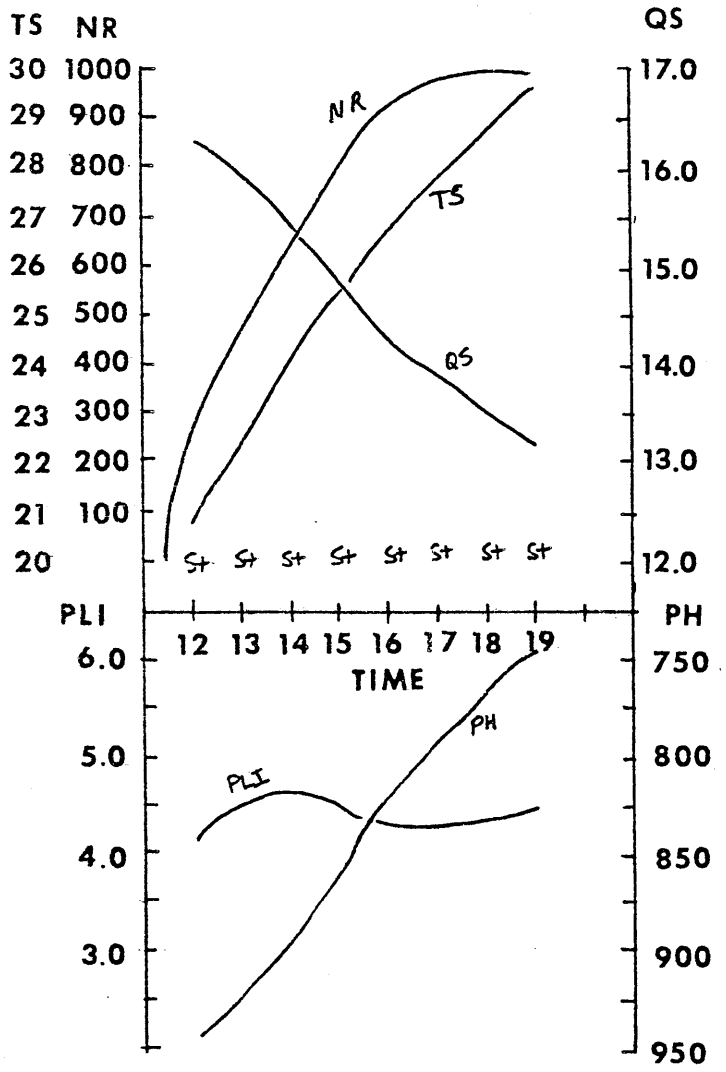


Fig. 5.25 Time variation of model output for JUNHYB sounding, 6 June, 30-60 soil parameters, with no clouds or imposed changes aloft (Plain). NR is net radiation into the surface (mcal/sq cm min), TS is temperature at top of surface layer (deg C), QS is PBL mixing ratio (g/kg), PLI is convective instability (deg C) and PH is pressure at top of PBL (mb). Condition at top of PBL is plotted above time axis: blank = unsaturated, ~S = nearly saturated, S = saturated, and S+ = oversaturated.

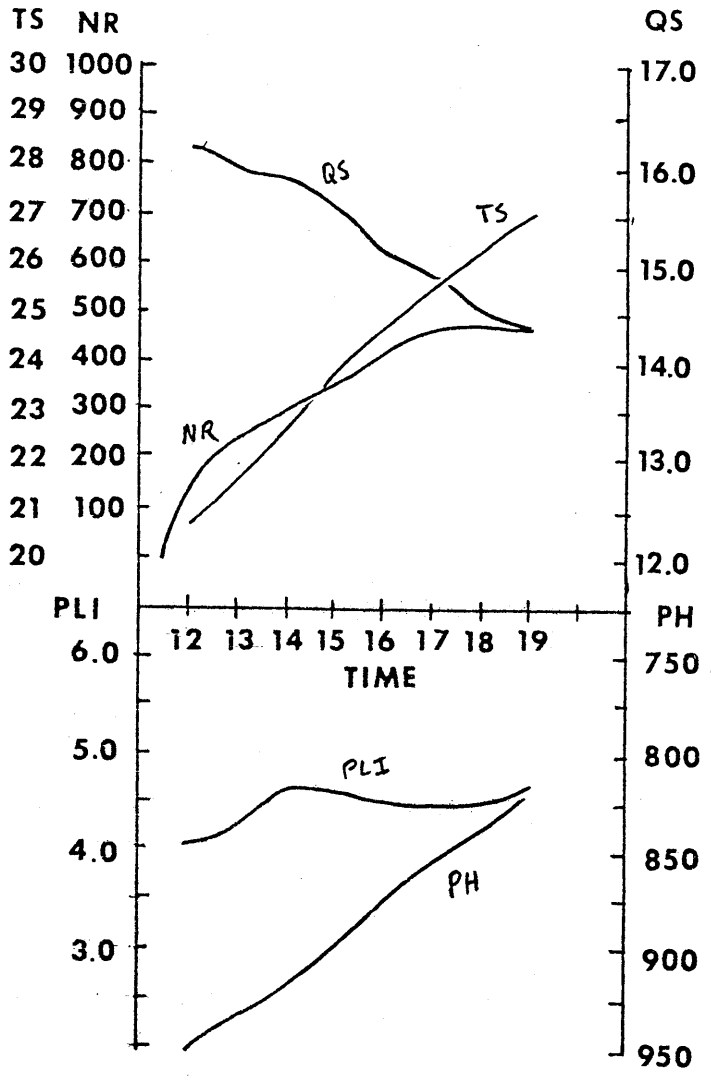


Fig. 5.26 Same as Fig. 5.25 for run with clouds.

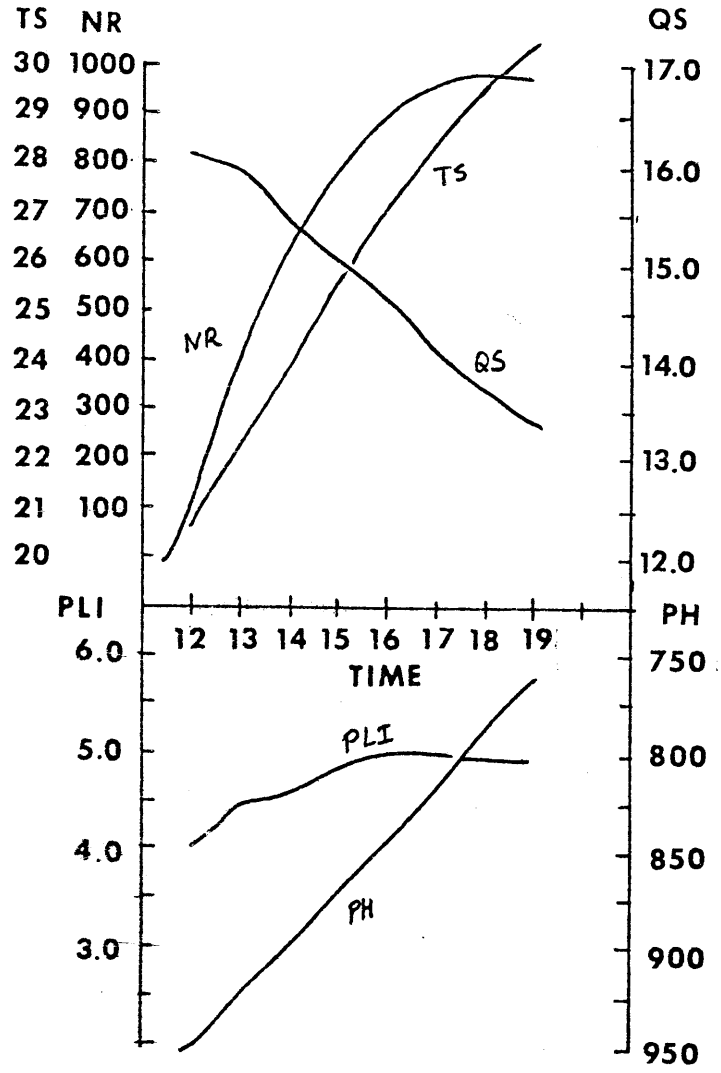


Fig. 5.27 Same as Fig. 5.25 for run with imposed changes aloft.

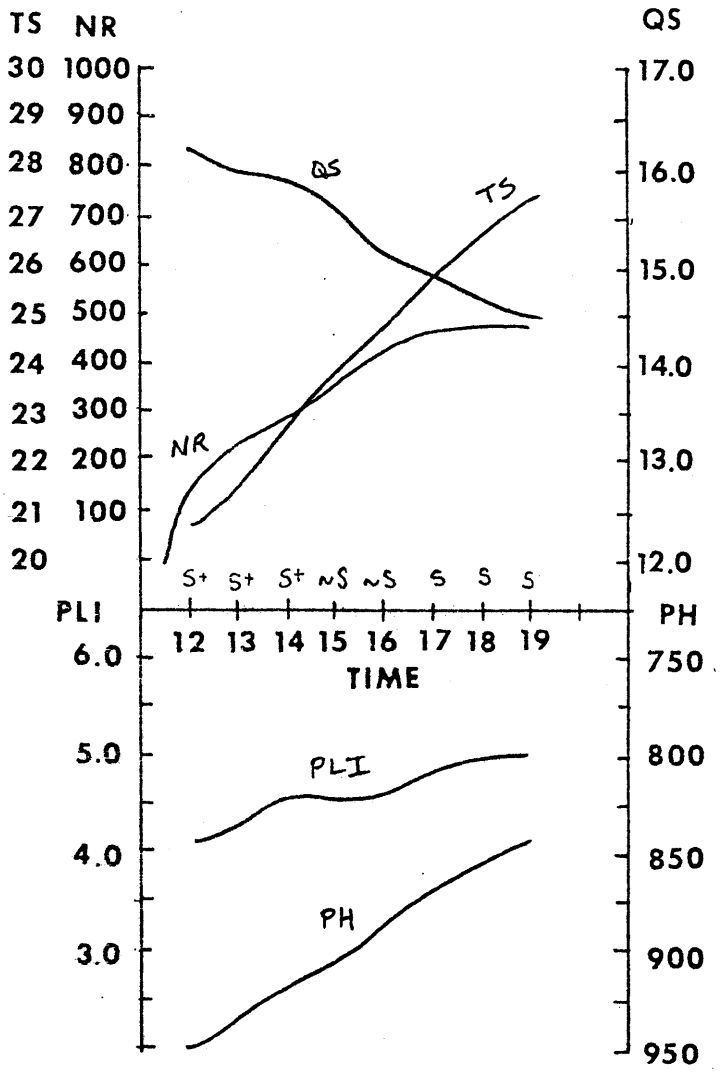


Fig. 5.28 Same as Fig. 5.25 for run with clouds and imposed changes aloft.

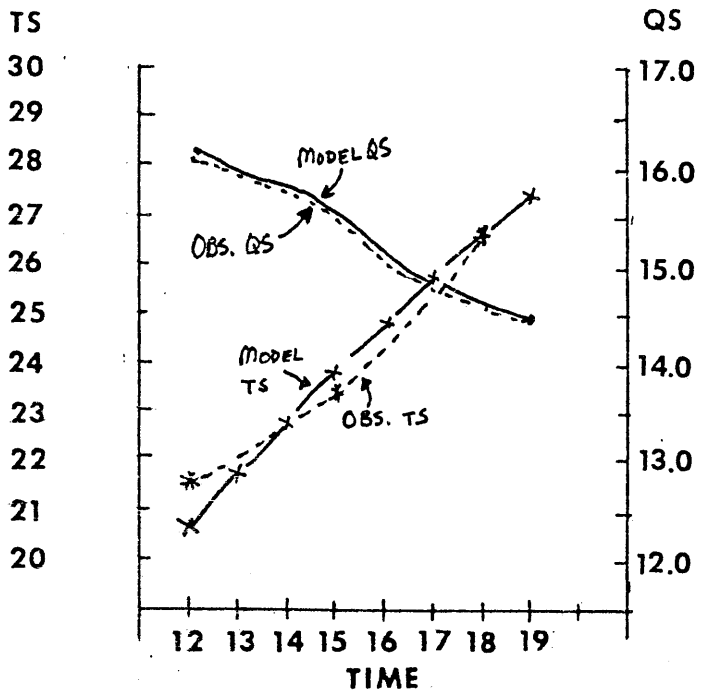


Fig. 5.29 Comparison of TS and QS values from 30-60 model run with clouds and imposed changes aloft with values taken from Elmore City, Fort Sill, and Chickasha, Oklahoma soundings.

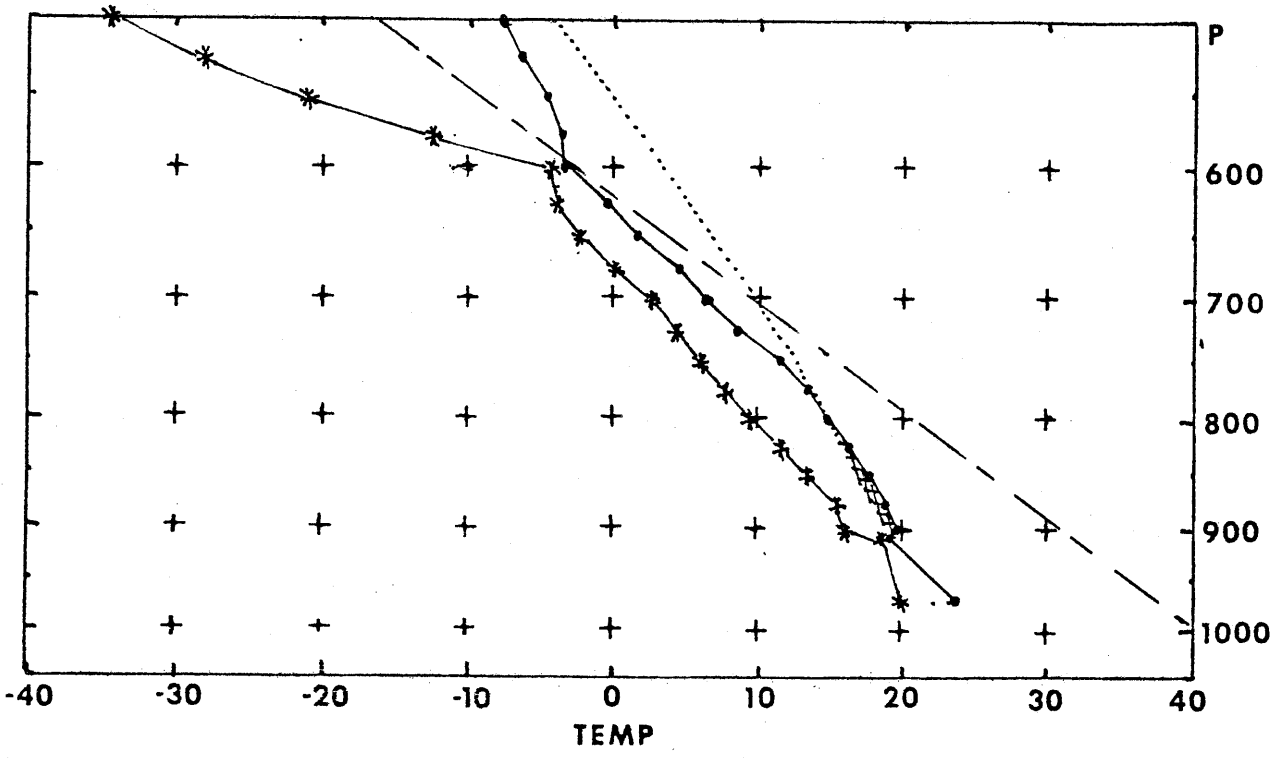


Fig. 5.30 Same as Fig. 5.15 for model output at 15 GMT from JUNHYB initial sounding, 30-60 soil parameters, with clouds and imposed changes aloft. Negative area is cross-hatched.

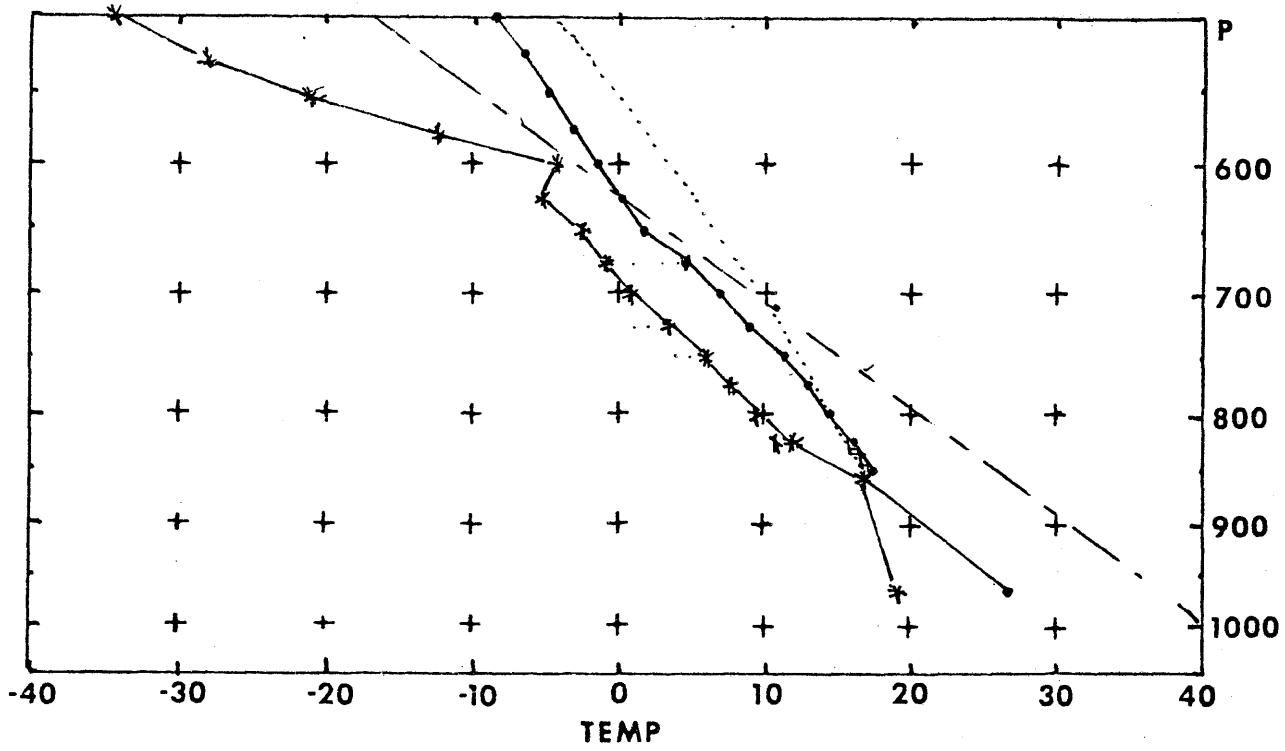


Fig. 5.31 Same as Fig. 5.30 for 18 GMT.

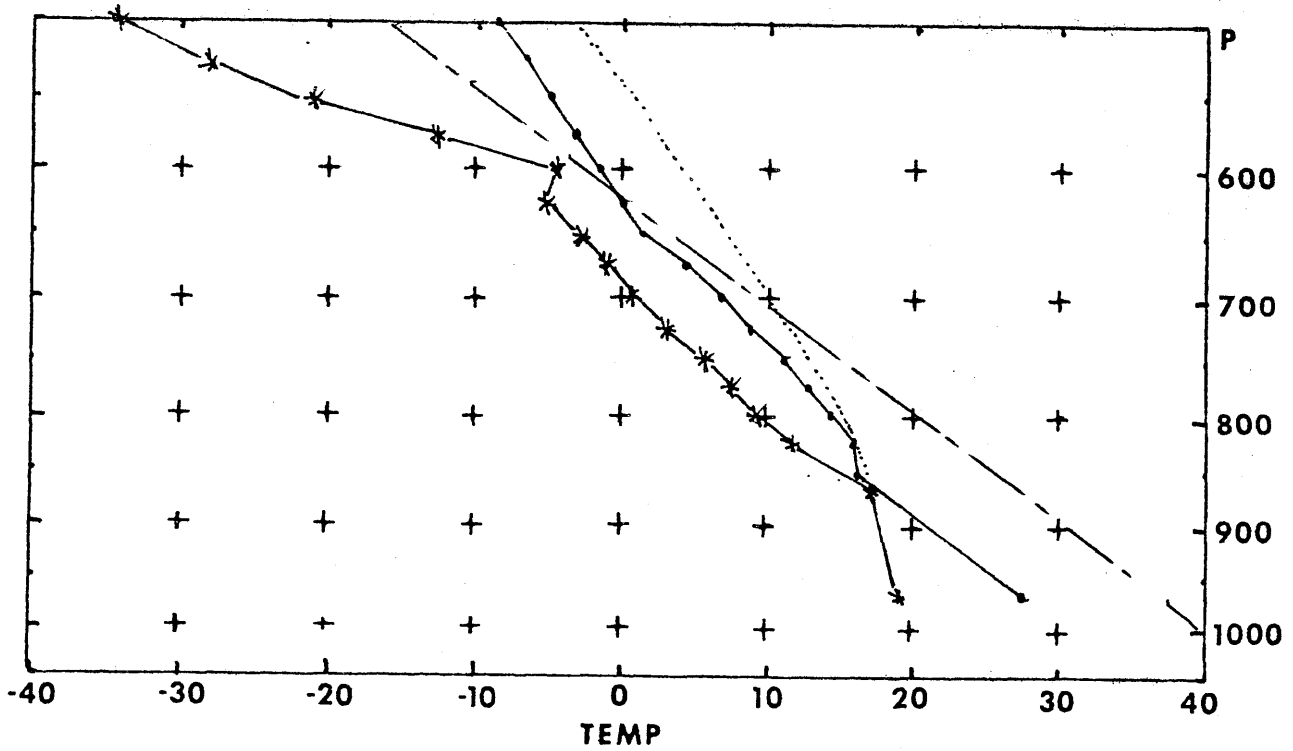


Fig. 5.32 Same as Fig. 5.30 for 19 GMT.

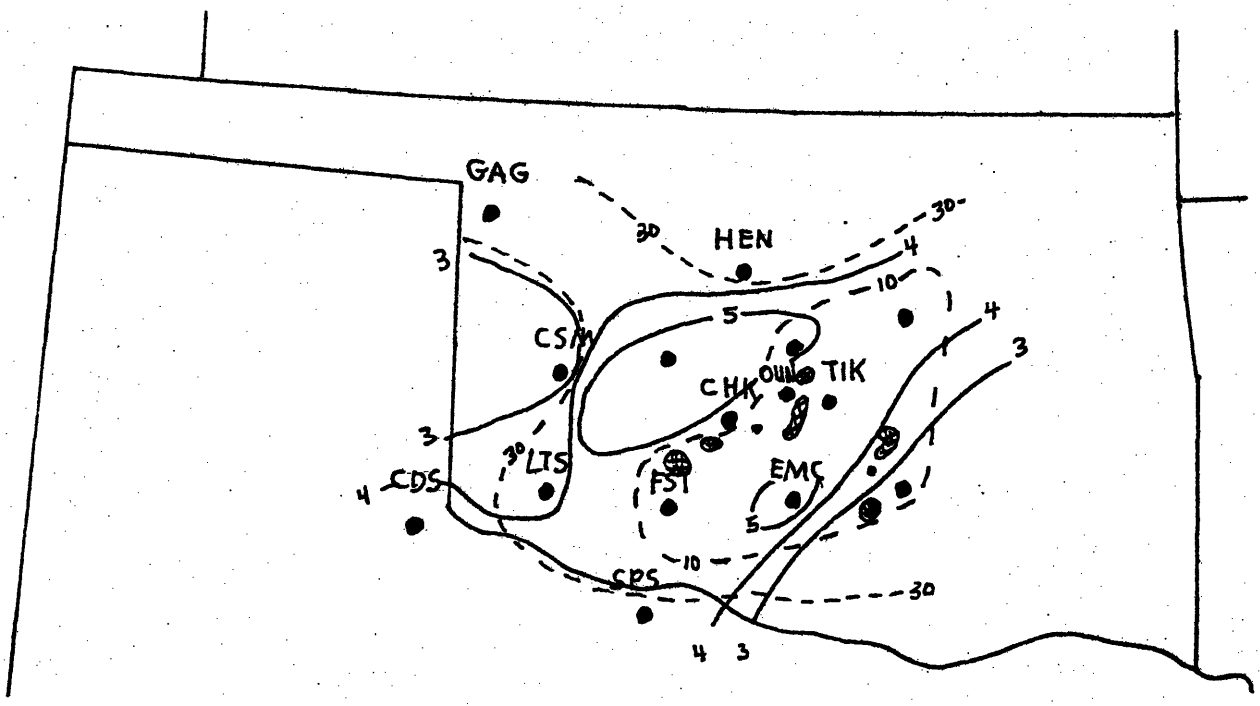


Fig. 5.33 Mesoscale analysis of convective instability (PLI) and convective inhibition (NA) for 18 GMT, 6 June. Solid lines are PLI (deg C) and dashed lines are NA (m**2/s**2). Cross hatching is new radar echoes appearing by 19 GMT.

# CONCLUSIONS

The three cases from SESAME, 1979 were analyzed in detail to determine where and when afternoon convection broke out. The surface and PBL characteristics were delineated as clearly as the data allowed. The model outlined in chapter 2 was used to quantify the various physical factors involved in each case, and the results were tabulated and discussed. They are summarized here.

The model used is one-dimensional, and predicts the evolution of an (assumed) well-mixed boundary layer. It was carefully tested and results were compared with data from O'Neill, Nebraska and model results from Barnard (1977). The model was also compared with data from the April case, at Concordia, Kansas (CNK) and Goodland, Kansas (GLD). The agreement between model output and observations was satisfactory in all cases.

The behavior of the PBL in all three cases was generally as follows. As the PBL heated, it grew in depth, its temperature rose, and the PBL moisture dropped. The PBL grew in depth by entraining dryer, warmer air from the inversion above. Hence the PBL average temperature rose as the PBL rose, and the moisture dropped unless the soil surface was wet enough to supply the needed moisture.

Clouds cut the incident radiation, slowing the heating and PBL growth, and thereby contributing to higher moisture values. Changes aloft tended to be influential as well. Strengthening of the inversion slowed PBL growth, allowing the PBL to heat more from below. Dry advection aloft contributed less moisture from entrainment and gave lower PBL moisture contents.

Soil moisture, especially surface soil moisture influenced the PBL by controlling the surface energy balance. High moisture values gave wetter, shallower, and cooler PBLs. Dry soil PBLs were high, dry and hot.

In each case, the initial conditions were convectively unstable. The 12 GMT data generally showed PLI values which indicated significant instability. The subsequent BLH contributed to an increase in convective instability, but the increase was usually of less magnitude than the initial value. These results suggest that the initial stratification, which was the result of large scale forces, was the most important contributor to convective instability.

Just as the various factors contributed to PBL changes, they exerted influence on the growth of convective instability. The BLH by itself tended to increase the PLI. Individually, the other factors (except soil moisture) almost

always reduced the convective instability. Increased soil moisture in the "plain" runs gave increased PLI values, so that the wettest soil, "plain" run usually had the most convective instability of any of the runs for a given case. The one exception to this was the June case which involved a cloud cover throughout the integration. The "plain" runs actually had the lowest PLI values in the June case.

Convective inhibition responded, generally, in an opposite manner to the soil moisture variation. The dryest soil run often had the least negative area. It was sometimes the case, however, that the most unstable runs also had the least inhibition, when other factors besides BLH were involved. Some of the "clouds only" runs were of this type.

The negative area depends on the three way combination of PBL height, surface temperature (PBL potential temperature), and PBL moisture. An increase in any one parameter, keeping the others the same, gives less inhibition. However, the model changes in response to soil moisture affected all three parameters, in different directions, and in a non-linear way. Increased soil moisture gave higher PBL moisture, but lower PBL height and lower PBL potential temperatures. the magnitudes of the changes depended on details of the sounding, values of soil moisture involved, etc. So the behavior of convective inhibition was very complicated with respect to

soil moisture.

The April and May cases were similar in the sense that clouds were only present during the early morning. This determined the effect clouds had on the growth of convective instability and inhibition. Clouds by themselves tended to reduce the growth of instability by almost 10%. When clouds were added to the runs which included imposed changes aloft, however, the effect of the clouds was to increase the instability. This was true for both April and May cases. The reason for this behavior is as follows. When clouds are added to the model, their effect is to reduce the net radiation, and so reduce the growth of the PBL. When added to the "plain" runs, the reduced growth gave increased PBL mixing ratios but cooler PBLs, and the net result was slightly lower convective instabilities. The imposed changes usually lead to higher growth rates when added to the "plain" runs, and so much dryer PBLs due to the entrainment of dry air aloft. This produced lower PLI values. When clouds were added to the runs with the imposed changes, the result was less growth of the PBL (than the imposed changes only runs), and so higher mixing ratios, but only slightly cooler temperatures in the PBL. The net result of these changes was an increase in PLI due to the higher mixing ratios, although the final values were not as high as in the "plain" runs. Hence the clouds exerted a positive influence on convective instability when added to the

runs with imposed changes.

This non-linear result for both the April and May 23 GMT cases can be stated symbolically in decreasing order of importance:

PLI = Initial conditions + BLH + soil surface moisture + clouds − imposed changes + bulk soil moisture.

The 21 GMT May case symbolic relation is identical except the order of imposed changes and bulk soil moisture is switched. As can be seen, surface soil moisture was very influential on the growth of convective instability under conditions which have only early morning cloudiness. The imposed changes aloft and bulk soil moisture were much less important.

The convective inhibition was more variable in its response. The relation can be stated for the April and May cases as:

NA = Initial conditions − BLH + . . . − Imposed changes + . . .

The order and signs of the other factors were case dependent, and so cannot be generalized without more case studies.

The June case was at least partially cloudy throughout the day, and so its behavior was different from the other two cases. The symbolic relations will not be repeated here. Suffice it to say, however, that the convective instability was reinforced by all of the factors, and the convective inhibition was decreased by all of the applied factors. The imposed changes led to lower boundary layer tops, so the effect was to increase the PBL mixing ratios (less entrainment of dry air) and raise the surface layer temperatures, thereby increasing the PLI. The nature of the imposed changes was special in June too. All of the cases either had imposed changes which led to the creation of an inversion above the PBL, or the initial conditions had an inversion already present. The April and May cases also had changes aloft later in the runs which tended to reduce the strength of the inversion (cooling aloft). The June case did not have this later effect, so the imposed changes had an effect opposite in sign on the PBL evolution.

Many of the runs without clouds grew fast enough to create oversaturation at the PBL top. This suggests that in the real atmosphere, the clouds act as a feedback control mechanism on PBL development. The PBL can grow only fast enough to produce saturation at the PBL top. If the growth speeds up, the cloud cover increases, and slows growth. If the growth is too slow and the PBL top is not saturated, then

the clouds may (depending upon larger scale conditions) thin, until the PBL growth speeds up enough to produce saturation again. This balance between clouds and PBL growth was required to allow the model to simulate the case study outbreaks, even those with only early morning clouds.

The model was able to successfully simulate the outbreak region PBL behavior, especially for the April and June cases. These results indicated that in fact, for weak forcing, the convective inhibition was reduced to very low levels. The convection did not necessarily begin in regions of maximum instability, but seemed to start in the areas of lowest convective inhibition. In the April case, the "simulation" run showed that the inhibition in the outbreak region was only about 16 m**2/s**2 (50-50 run with modified GLD changes and morning clouds, Table 3.6). The analysis of observed values (Fig. 3.42) showed that the convection began in a region of inhibition less than 50, with the nearest observed value being 26. The mesoscale surface analysis (Fig. 3.13) showed that there was convergence in the surface wind field in the outbreak region. The model results and the analysis showed that the negative area was reduced by thermodynamic processes to a minimum value which allowed the available forcing to initiate the convection.

In the May case, the 21 GMT outbreak was strongly linked

to a wind shift line (see Fig. 4.16). Fig. 4.37 showed that the convection began just west of a minimum in inhibition. The "simulation" run for the outbreak (5-70 run with clouds and imposed changes, Table 4.1) had an inhibition of about 13 m**2/s**2, a low value compared with the observations. Again, the thermodynamic processes lowered the inhibition enough to allow the available forcing to initiate the convection.

The 23 GMT outbreak in the May case had less forcing (no obvious wind shift line or convergence at the surface) and the analysis on Fig. 4.40 showed the outbreak occurred in the area of minimum inhibition. The "simulation" run for this outbreak showed inhibition of between 8 and 1 m**2/s**2 (30-30 and 30-70 QCH runs modified for surface temperature advection, Table 4.6). Once again, the convection broke out in a region of minimum inhibition, in this case nearly zero.

In the June case, the pattern was repeated. The analysis on Fig. 5.31 showed the outbreak to be enclosed by the 10 m**2/s**2 line. The "simulation" run showed convective inhibition of zero (30-60 run with clouds and imposed changes, Table 5.3 and also Table 5.5). In this case, the forcing was very weak, and convection did not begin until nearly complete destabilization by thermodynamic processes had taken place. This pattern also occurred in the 10-11 April 1979 SESAME case as analyzed by Sanders (1982). His work showed that the

initial convection began in a region of minimum convective inhibition and modest instability.

The major finding of this thesis is simply stated. Convection requires convective instability, and low values of convective inhibition. When the inhibition can be overcome by the available forcing or trigger mechanisms (21 GMT May case, for example) or the thermodynamic evolution of the PBL reduces the convective inhibition to near zero, the convection will start.

The forecasting of afternoon convection is then, the forecasting of the removal of convective inhibition. This might prove to be a useful forecast aid, but the model used in this research required much labor to produce data simulation runs. Models which use available data such as rainfall amounts, climatological soil data, past weather and possibly satellite data to predict soil moisture would allow operational use of this model. The rest of the input parameters are readily available in real time for forecasting purposes. It would also be possible to use the model in a local mode, allowing local forecast offices to input the soil moisture data they deem appropriate. A third mode of usage would be to run the model with a range of soil moistures, and make a forecast based on the range of output.

PBL behavior is clearly a complicated phenomenon, and is central to the understanding of initiation of convection especially when dynamic forcing is weak or ill-defined. The interaction between PBL variables and the effect on convective instability and inhibition has been quantified for these three cases, but more work is needed before a complete understanding is obtained. Interest in this problem is growing as evidenced by recent work by McCumber and Pielke (1981), Cooper et al. (1982), and Garrett (1982). As the importance and nature of the interractions of these variables becomes better defined, accurate short term forecasting of convective outbreaks will become possible.

## APPENDIX 7.1: Derivation of Radiative Parameterization

The following is taken from Katayama (1972).

### IR RADIATION

The downward flux at level z is

$$IR_d = \int_0^{\infty} \int_{T_z}^{T_\infty} \pi \frac{dB_\nu(T)}{dT} \tau_f\{\ell_\nu(u-u_z)\}dTd\nu + \int_0^{\infty} \pi B_\nu(T_z)d\nu \qquad (A1.1)$$

$$- \int_0^{\infty} \pi B_\nu(T_\infty)\tau_f\{\ell_\nu(u_\infty-u_z)\}d\nu$$

where the second and third integrals correct for the endpoints of the first and

$B_\nu(T)$ = flux of black body radiation of frequency $\nu$, temperature T

$u(z)$ = amount of absorbing medium in the vertical air column from the ground to height z

$\ell_\nu$ = the generalized absorption coefficient

$\tau_f\{\ell_\nu, u\}$ = the transmission function of a slab at frequency $\nu$

Subscripts g, z, $\infty$ represent the ground, height z and the top of the atmosphere respectively. To correct for absorption dependence on pressure, Katayama defines an effective absorber amount

$$u^* = \frac{1}{g\rho_i} \int_{p(z)}^{p_g} q_i \left(\frac{p}{p_{oo}}\right)^{\alpha_i} dp \qquad (A1.2)$$

where $\rho_i$ = density of absorber

$\alpha_i$ = empirical constant

$q_i$ = mixing ratio of absorber

$i$ = absorber identifier

He defines two types of weighted mean transmission functions as follows:

$$\tau(u^*, T) \triangleq \frac{1}{\pi \frac{dB(T)}{dT}} \int_0^\infty \pi \frac{dB_\nu(T)}{dT} \tau_f(\ell_\nu, u) d\nu \qquad (A1.3)$$

$$\tilde{\tau}(u^*, T) \triangleq \frac{1}{\pi B(T)} \int_0^\infty \pi B_\nu(T) \tau_f(\ell_\nu, u) d\nu \qquad (A1.4)$$

where $\pi B(T) = \int_0^\infty \pi B_\nu(T) d\nu = \sigma T^4$

and $\sigma$ is the Stefan-Boltzmann constant.

It is assumed that the total transmission function is a product of the individual transmission functions. The $\tau(u^*, T)$ and $\tilde{\tau}(u^*, T)$ used hereafter will be assumed to be the total transmission functions. Using these mean functions simplifies the equations for the fluxes greatly. (A1.1) becomes

$$IR_d = \pi B_z - \pi B_c \tilde{\tau}(u_\infty^* - u_z^*, T_c) - (\pi B_\infty - \pi B_c)\tau(u_\infty^* - u_z^*, \bar{T}) + \int_{\pi B_z}^{\pi B_\infty} \tau(u^* - u_z^*, \bar{T}) d(\pi B) \qquad (A1.5)$$

where $\pi B_i = \sigma T_i^4$

Similarly, the equation for upward flux at a height z

$$IR_u = \int_0^{\infty}\int_{T_z}^{T_g} \pi \frac{dB_\nu(T)}{dT} \tau_f\{\ell_\nu(u_z - u)\}dT d\nu \quad + \int_0^{\infty} \pi B_\nu(T_z) d\nu \qquad (A1.6)$$

becomes

$$IR_u = \pi B_z + \int_{\pi B_z}^{\pi B_g} \tau(u_z^* - u^*, \overline{T})\, d(\pi B) \qquad (A1.7)$$

These are the equations in the text, 2.4 and 2.5.

Incident Radiation

$S_\infty$, the solar constant is taken to be equivalent to 1.94 Ly/min. The hour angle H is computed from the time of day as compared with the length of day at the particular location. The ground albedo is modified for the sun angle by a method from Wetzel (1972).

$$\alpha_g = \alpha_{go} - \frac{(90 - H)(\alpha_{go} - \alpha_b)}{15} \qquad (A1.8)$$

where H is in degrees

$\alpha_{go}$, $\alpha_b$ limits specified for each site.

$S_o = S_{oo}$ (ZT)(SMOD)

where

ZT = zenith angle, a function of H, day of year

SMOD = correction for the distance to the sun

S is divided into scattered and absorbable parts, 65%

scattered, 35% absorbable. The scattered part is modified for the scattering albedo of the atmosphere,

$$\alpha_s = 0.085 - 0.247 \log_{10}\left(\frac{PG}{1000} \times ZT\right) \qquad (A1.9)$$

where PG = surface pressure (mb)

If clouds are present, the scattering albedo depends on them.

$\alpha_s = 0.54$ Cloud top at or above 600 mb

$= 0.66$ Cloud top below 600 mb

The scattered radiation incident on the ground is modified for multiple reflection between the ground and the atmosphere:

$$GLW_s = 0.651 \cdot S_0 \cdot \left(\frac{1 - \alpha_s}{1 - \alpha_s \alpha_g}\right) \qquad (A1.10)$$

Absorption by water vapor is calculated using the values for effective absorption of H2O as already computed for the IR flux. Fractional absorption for the whole atmosphere down to the level i is:

$$F_i = 0.271 \left(\sum_i \frac{EH2O(i)}{ZT}\right)^{0.303} \qquad (A1.11)$$

where $\sum_i$ is taken from the top of the atmosphere down to level i. Absorption of a given layer is then a function of available radiation and EH2O in the layer.

Any clouds encountered absorb according to their

thickness and height. The cloud tops also reflect some of the absorbable radiation. Any absorbable radiation left at the ground ($GLW_a$) is combined with the scattered radiation to yield the incident solar radiation on the soil. This is modified for the ground albedo to give the ground absorption

$$GAB = (1-\alpha_g)(GLW_s + GLW_a) \qquad (A1.12)$$

The net radiation at the ground is then

$$NR = GAB + IR(Ground) \qquad (A1.13)$$

## APPENDIX 7.2: Derivation of Ekman Layer Similarity Equations

The Ekman layer similarity theory is used to find SH and LH as follows. The equation for PBL wind is (from Arya, 1975)

$$\frac{u V_K}{u_*} = \ln \frac{z}{z_0} + \psi \qquad (A2.1)$$

where

$v_k$ = Von Karman constant

$u_*$ = friction velocity

$z_0$ = roughness length

$\psi$ = structure function

For unstable conditions,

$$\psi = -\ln \frac{h}{L} \qquad (A2.2)$$

So, letting VS = wind speed at z=h, the top of the PBL,

$$u_* = \frac{V_K \, VS}{\ln \frac{h}{z_0}} \qquad (A2.3)$$

The sensible heat flux into the PBL is given by

$$SH = \rho C_p C_\theta u_* \delta\theta \qquad (A2.4)$$

where

$\rho$ = density of air

$c_p$ = specific heat of air

$\delta\theta$ = $\theta$(ground) - $\theta$(PBL)

$$C_\theta = \frac{V_k}{\ln\left(\frac{h}{z_0}\right) - C} \qquad (A2.5)$$

where

$$C = \ln\left(\frac{h}{-L}\right) + 1.0 \qquad (A2.6)$$

which gives

$$SH = \frac{\rho C_p V_k u_* \delta\theta}{\ln\left(\frac{-L}{z_0}\right) - 1.0} \qquad (A2.7)$$

Monin/Obukhov similarity theory defines the M/O length L as:

$$L = \frac{-u_*^3}{V_k \frac{g}{TS} \frac{SH}{\rho C_p}} \qquad (A2.8)$$

where g = acceleration of gravity

TS = surface temperature (air, not ground)

Solving for SH gives

$$SH = \frac{-u_*^3 \, TS \, \rho C_p}{L g V_k} \qquad (A2.9)$$

Equating A2.7 and A2.9, gives

$$\ln\left(\frac{-L}{z_0}\right) - 1.0 = \frac{L g V_k^2 \delta\theta}{-u_*^2 \, TS} \qquad (A2.10)$$

Inserting for $u_*$ from A2.3 and rearranging

$$1.0 - \frac{g \delta\theta}{VS} L \left(\ln \frac{-L}{z_0}\right)^2 - \ln\left(\frac{-L}{z_0}\right) = 0 \qquad (A2.11)$$

For a given $\delta\theta_v$ S this equation is in one variable, L. It is solved by iteration to yield the correct value of L. This value is then inserted in A2.3 to find $u_*$, and L, $u_*$ are inserted in A2.9 to find SH.

Finally, the companion equation for LH is solved

$$LH = \frac{\lambda \rho V_k u_* \delta q}{\ln\left(\frac{-L}{z_0}\right) - 1.0} \qquad (A2.12)$$

where $\lambda$ = latent heat of evaporation

$\delta q = q(PBL) - q(surface)$

q at the surface is found according to Wetzel (1978)

$$q(surface) = q(PBL) + \frac{Gw^2}{2}\left(QSAT - q(PBL)\right) \qquad (A2.13)$$

where QSAT = saturation value of q for ground conditions (TG, PG).

Gw = fractional soil saturation at the surface

APPENDIX 7.3: Derivation of Soil Heat Flux Parameterization

The following is from Bhumralker(1975).

Heat conduction is described by

$$\frac{\partial T_g(z,t)}{\partial t} = \frac{k}{c}\frac{\partial^2 T_g(z,t)}{\partial z^2} \qquad (A3.1)$$

where $T_g(z,t)$ = soil temperature at depth z, time t

$k$ = thermal conductivity of soil

$c$ = volumetric heat capacity

Assume that the surface soil temperature $T_g(0,t)$ is described by

$$TG \overset{d}{=} T_g(0,t) = TBAR + \Delta T_0 \sin(\omega t) \qquad (A3.2)$$

where TBAR = average temperature of the soil, assumed to be invariant with depth

$\Delta T_0$ = amplitude of the variance

$\omega$ = frequency of the variance = $2\pi$/period

The solution of A3.1 is

$$T_g(z,t) = TBAR + \Delta T_0 \exp(-z/d)[\sin(\omega t - z/d)] \qquad (A3.3)$$

where $d = [2k/c\omega]^{1/2}$ = depth at which the amplitude of $\Delta T_0$ is negligible. For an infintesimally thin soil layer, the heat flux into the soil is

$$G(z,t) = -k\frac{\partial T_g(z,t)}{\partial z} \qquad (A3.4)$$

Combining A3.3 and A3.4 gives

$$G(z,t) = \left(\frac{\omega c k}{2}\right)^{1/2} \Delta T_0 e^{-z/d}\left(\sin(\omega t - z/d) + \cos(\omega t - z/d)\right) \qquad (A3.5)$$

## APPENDIX 7.4 Derivation of Ground Variable Equations

The following is from Bhumralker (1975) and Deardorff (1977). Consider a layer of soil from the surface (z=0) to some depth ( =z). The time rate of temperature change for this layer is given by

$$C\,\frac{\partial T_g(z,t)}{\partial t} = -\left[\frac{G(z,t) - G(0,t)}{z}\right] \qquad (A4.1)$$

where c is volumetric heat capacity and all other variables are as previously defined.

$G(0,t)$ = soil heat flux at the surface

$$= NR - SH - LH \qquad (A4.2)$$

$G(z,t)$ = soil heat flux at depth z from Appendix 7.3

$$= \left(\frac{\omega c/K}{2}\right)^{1/2}\left[\gamma/\omega\,\frac{\partial T_g(z,t)}{\partial t} + T_g(z,t) - TBAR\right] \qquad (A4.3)$$

If the approximation is made that

$$T_g(z=1\text{ cm},t) \cong T_g(0,t) = TG \qquad (A4.4)$$

then A4.1 becomes, with A4.2 and A4.3

$$\left[c(=1\text{cm}) + \left(\frac{c/K}{2\omega}\right)^{1/2}\right]\frac{\partial TG}{\partial t} = -HA - \left(\frac{\omega c K}{2}\right)^{1/2}(TG - TBAR) \qquad (A4.5)$$

where $-HA = NR - SH - LH$

Rearranging, gives the equation 2.10 in the text.

$$\frac{\partial TG}{\partial t} = - \frac{HA - \left(\frac{\omega c \rho k}{2}\right)^{1/2} (TG - TBAR)}{c(=1cm) + \left(\frac{c \rho k}{2\omega}\right)^{1/2}} \qquad (A4.6)$$

From Appendix 7.3, d is defined as

$$d = \left(\frac{2k}{c\omega}\right)^{1/2} \quad \text{so} \quad \frac{cd}{2} = \left(\frac{c\rho k}{2\omega}\right)^{1/2} \qquad (A4.7)$$

The denominator of A4.6 can then be written

$$c + \frac{cd}{2} \qquad (A4.8)$$

Let $lcd = c(2cm) + cd$, where $l = \frac{2cm + d}{d}$

for $d = 50$ cm, $l = 1.04$

A4.6 is, then

$$\frac{\partial TG}{\partial t} = \frac{-2HA}{lcd} - \frac{2}{lcd}\left(\frac{\omega c \rho k}{2}\right)^{1/2} (TG - TBAR) \qquad (A4.9)$$

Using A4.7 for the second term, this becomes

$$\frac{\partial TG}{\partial t} = - \frac{2HA}{lcd} - \frac{\omega}{l}(TG - TBAR) \qquad (A4.10)$$

Since $\omega = 2\pi/\tau$, we have with $\tau$ = period

$$\frac{\partial TG}{\partial t} = \frac{-2HA}{lcd} - \frac{2\pi}{l}\frac{(TG - TBAR)}{\tau}$$

$$= - \frac{C_{11} HA}{cd} - C_{12}\frac{(TG - TBAR)}{\tau} \qquad C_{11} + C_{12} \text{ constants}$$

$$(A4.11)$$

Deardorff (1977) suggests that a similar equation be written for soil moisture

$$\frac{\partial WG}{\partial t} = -C_1 \frac{(E-P)}{\rho_w d_i} - C_2 \frac{(WG - WBAR)}{\tau} \qquad (A4.12)$$

where

$\rho_w$ = density of water

$d_i$ = depth of diurnal moisture cycle

E = evaporation

P = precipation

WG = volumetric soil content

WBAR = bulk moisture in soil

$\tau$ = period of diurnal cycle

$C_1$, $C_2$ are constants

Dividing through by field capacity moisture, WMAX and taking $E = LH/\lambda$, P=0

$$\frac{\partial GW}{\partial t} = -C_1 \frac{LH/\lambda}{\rho_w d_1 WMAX} - C_2 \frac{(GW - GWB)}{\tau} \qquad (A4.13)$$

where

GW = WG/WMAX

GWB = WBAR/WMAX

$\lambda$ = latent heat of evaporation

This is the equation used in this model, using (from Deardorff, 1977)

$d_1$ = 10 cm

$\rho_w$ = 1 gm/cm$^3$

$\tau$ = 1 day

$$c_1 = \begin{cases} 0.5 & Gw \geq 75\% \\ 14 - 22.5(Gw - 0.15) & 15\% < Gw < 75\% \\ 14 & Gw \leq 15\% \end{cases}$$

$c_2 = 0.9$

Data for these constants comes from Jackson (1973).

## APPENDIX 7.5: Derivation of Inversion Equations

The following is taken from Zeman and Tennekes (1977). A complete discussion of the equations would be lengthy and unnecessary. It is found in its entirety in the source mentioned above. Briefly, the equations result from consideration of the turbulent energy budget at the inversion. This balances kinetic energy change with buoyant production, turbulent flux divergence, mechanical production, and dissipation. For a convective boundary layer such as will be considered for this model, mechanical production can safely be ignored. Buoyant production is proportional to temperature and heat flux at the inversion. The temperature is modeled already. The sensible heat flux at the inversion is equal to the temperature jump $\Delta\theta$, times the rise of the inversion $\partial h/\partial t$, as proposed by Ball (1960) and Lilly (1968).

$$H_h = \Delta\theta \frac{\partial h}{\partial t} \qquad (A5.1)$$

where $H_h$, ( = sensible heat flux at the inversion) is changed according to Tennekes (1973) where $\partial\Delta\theta/\partial t$ is a function of entrainment of stable air from above, and net sensible heat transfer inside the boundary layer

$$\frac{\partial \Delta\theta}{\partial t} = \gamma \frac{\partial h}{\partial t} - (SH - H_h)/h \qquad (A5.2)$$

The turbulent transfer is parameterized according to Tennekes

(1973). He maintained that the large eddies which transfer most of the kinetic energy scale on h and $w_*$, the inversion height and the convective velocity scale.

$$\text{Turbulent Transfer} = C_f \frac{w_*}{h} \qquad (A5.3)$$

$$w_*^3 = \frac{g}{T_S} SH \cdot h \qquad \text{where } C_f \text{ is an empirical constant}$$

Zilitinkevich (1975) showed that the time rate of change of TKE should be parameterized as

$$= C_t \frac{w_*^2}{h} \frac{\partial h}{\partial t} \quad \text{where } C_t \text{ is an empirical constant} \qquad (A5.4)$$

Part of the dissipation at the inversion scales on h, and can be included with the turbulent flux term. The rest, according to Zeman and Tennekes (1977) can be written as

$$= C_d w_*^2 w_{bv} \quad \text{where } C_d \text{ is an empirical constant} \qquad (A5.5)$$

where $w_{bv}$ = Brunt-Vaisälä frequency in the air above the inversion.

The parameterization is based on a mixing length which depends on the stability above the inversion. Putting A5.3, A5.4 and A5.5 together,

$$C_t \frac{w_*^2}{h} \frac{\partial h}{\partial t} = \frac{g}{T_S} H_h + C_f \frac{w_*}{h} - C_d w_*^2 w_{bv} \qquad (A5.6)$$

Substituting for $\partial h/\partial t$ from A5.1 yields

$$-\frac{g}{Ts} H_h = \frac{w_*^3}{h} \frac{C_f - C_d w_{bv}\left(\frac{h}{w_*}\right)}{1 + \frac{C_t w_*^2 Ts}{g h \Delta\theta}} \qquad (A5.7)$$

Substituting for $w_*$ from A5.3 gives

$$-\frac{H_h}{SH} = \frac{C_f - C_d w_{bv}\left(\frac{h}{w_*}\right)}{1 + \frac{C_t w_*^2 Ts}{g h \Delta\theta}} \qquad (A5.8)$$

which is equation 2.15 in the text.

# REFERENCES

Arya, S.P.S., 1975: Geostrophic drag and heat transfer relations for the atmospheric boundary layer. Quart. J. Roy. Meteorol. Soc., v. 101, pp. 147-161.

Ball, F.K., 1960: Control of inversion height by surface heating. Quart. J. Roy. Meteorol. Soc., v. 86, pp 483-494.

Barnard, J.C., 1977: On the sensitivity of an atmosphere in radiative-convective equilibrium to soil moisture. M.S. Thesis, M.I.T., July, 1977.

Bhumralker, C.M., 1975: Numerical experiments on the computation of ground surface temperature in an atmospheric general circulation model. J. Appl. Meteorol., v. 14, pp. 1246-1258.

Brooks, D.L., 1950: A tabular method for the computation of temperature change by infra-red radiation in the free atmosphere. J. Meteor., v. 7, pp. 313-321.

Businger, J.A., J.C. Wyngaard, Y. Izumi, and E.F. Bradley, 1971: Flux-profile relationships in the atmospheric surface layer. J. Atmos. Sci., v. 28, pp. 181-189.

Caracena, F., R.A. Maddox, L.R. Hoxit, and C.F. Chappell, 1979: Mesoanalysis fo the Big Thompson Storm. Mon. Wea. Rev., v. 107, pp. 1-17.

Carbone, R.E., 1982: A severe frontal rainband. Part I: Stormwide hydrodynamic structure. J. Atmos. Sci., v. 39, pp. 258-279.

Carlson, T.N., R.A. Anthes, M. Schwartz, S.G. Benjamin, and D.G. Baldwin, 1980: Analysis and prediction of severe storms environment. Bull. Amer. Meteor. Soc., v. 61, pp. 1018 to 1032.

Cooper, H.J., M. Garstang, and J. Simpson, 1982: The diurnal interaction between convection and peninsula-scale forcing over south Florida. Mon. Wea. Rev., v. 110, pp. 486-503.

Cotton, W.R., R.L. George, and K.R. Knupp, 1982: An intense, quasi-steady thunderstorm over mountainous terrain. Part I: Evolution of the storm initiating mesoscale circulation. J. Atmos. Sci., v. 39, pp. 328-342.

Darkow, G.L., P.M. Kuhn, and V.G. Suomi, 1958: Surface thermal patterns as a tornado forecast aid. Bull. Amer. Meteorol.

Soc., v. 39, pp. 532-537.

Davis, J.G., and J.R. Scoggins, 1981: The development of convective instability, wind shear, and vertical motion in relation to convective activity and synoptic systems in AVE IV. NASA Contractor Report 3386, contract NAS8-31773.

Deardorff, J.W., 1977: A parameterization of ground surface moisture content for use in atmospheric prediction models. J. Appl. Meteor., v. 16, pp. 1182-1185.

Elsasser, W., 1942: Heat transfer by infra-red radiation in the atmosphere. Harvard Meteor. Stud., No. 6, 105 pp.

Fawbush, E.J., R.C. Miller, and L.G. Starrett, 1951: An empirical method of forecasting tornado development. Bull. Amer. Meteorol. Soc., v. 32, pp. 1-9.

Galway, 1956: The lifted index as a predictor of latent instability. Bull. Amer. Meteorol. Soc., v. 34, pp. 528-529.

Garrett, A.J., 1982: A parameter study of interactions between convective clouds, the convective boundary layer, and a forested surface. Mon. Wea. Rev., v. 110, pp. 1041-1059.

Holle, R.L., and M.W. Maier, 1980: Tornado formation from downdraft interaction in the FACE mesonetwork. Mon. Wea. Rev., v. 108, pp. 1010-1028.

Jackson, R.D., 1973: Diurnal changes in soil water content during drying. Field Soil Water Regime, Soil Sci. Soc. Amer., pp. 37-55.

July, M.J. and R.E. Turner, 1980: A preliminary look at AVE-SESAME IV conducted on 9-10 May 1979. NASA Tech. Mem. (TM-78314). Marshall Space Flight Center, Ala., 51 pp.

Katayama, A., 1972: A simplified scheme for computing radiative transfer in the troposphere. Tech. Rept. No 6, Dept of Met. UCLA. 77 pp.

Koch, S.E. and J. McCarthy, 1982: The evolution of an Oklahoma dryline. Part II: Boundary-layer forcing of mesoconvective systems. J. Atmos. Sci., v. 39, pp. 237-257.

Lettau, H. and Davidson, 1957: Exploring the Atmosphere's First Mile. Pergamon Press, New York, N.Y., volumes I, II.

Lilly, D.K., 1968: Models of cloud-topped mixed-layers under a strong inversion. Quart. J. Roy. Meteorol. Soc., v. 94,

pp. 292-309.

London, J., 1952: the distribution of radiational temperature change in the Northern Hemisphere. J. Meteor., v. 9, pp. 145-151.

McCumber, M.C., and R.A. Pielke, 1981: Simulation of the effects of surface fluxes of heat and moisture in a mesoscale numerical model. 1. Soil layer. J. Geophys. Res., v. 86, pp 9929-9939.

Maddox, R.A., L.R. Hoxit and C.F. Chappell, 1980: A study of tornadic thunderstorms interacting with thermal boundaries. Mon. Wea. Rev., v. 108, pp. 322-336.

Matthews, D.A., 1981: Observations of a cloud arc triggered by thunderstorm outflow. Mon. Wea. Rev., v. 109, pp. 2140-2157.

Miller, D.A., and F. Sanders, 1980: Mesoscale conditions of the severe convection of 3 April 1974 in the east-central United States. J. Atmos. Sci., v. 37, pp. 1041-1055.

Miller, R.C., 1972: Notes on analysis and severe storm forecasting procedures of the Air Force Global Weather Central. Air Weather Service, Tech. Rept. 200(rev.), 102 pp.

Modahl, A., 1979: Low-level wind and moisture variations preceding and following hailstorms in northeast Colorado. Mon. Wea. Rev., v. 107, pp. 442-450.

Moore, (unpublished): The development of a severe weather index for use in a nested grid mesoscale primitive equation model. Report of research at NASA Langley under NASA-ASEE Summer Faculty Fellowship Program, 1979.

Ogura, Y, H.-M. Juang, K.-S. Zhang, and S.-T. Soong, 1982: Possible triggering mechanisms for severe storms in SESAME-AVE IV (9-10 May 1979). Bull. Amer. Meteorol. Soc., v. 63, pp. 503-515.

Raymond, D., and M. Wilkening, 1980: Mountain-induced convection under fair weather conditions. J. Atmos. Sci., v. 37, pp. 2693-2706.

Rogers, C.D., and C.D. Walshaw, 1966: The computation of infra-red cooling rate in planetary atmospheres. Quart. J. Roy. Meteorol. Soc., v. 92, pp. 67-92.

Sanders, F., 1982: The origin and maintenance of the severe thunderstorms of 10 April 1979. Twelfth Conference on Severe Local Storms of the Amer. Meteorol. Soc., January

12-15, 1982, San Antonio, Texas.

Showalter, A.K., 1953: A stability index for thunderstorm forecasting. Bull. Amer. Meteorol. Soc., v. 34, pp. 250-252.

Sun, W.-Y., and Y. Ogura, 1979: Boundary-layer forcing as a possible trigger to a squall-line formation. J. Atmos. Sci., v. 36, pp. 235-254.

Tennekes, H., 1973: A model for the dynamics of the inversion above a convective boundary layer. J. Atmos. Sci., v. 30, pp. 558-567.

Uccellini, L.W., 1975: A case study of apparent gravity wave initiation of severe convective storms. Mon. Wea. Rev., v. 103, pp. 497-513.

Wetzel, P.J., 1978: A detailed parameterization of the atmospheric boundary layer. Atmos. Sci. Paper 302, Colorado State University.

Whiteman, C.D., 1982: Breakup of temperature inversions in deep mountain valleys: Part I. Observations. J. Appl. Meteorol., v. 21, pp. 270- 289.

Williams, S.F., N. Horvath, and R.E. Turner, 1980: A preliminary look at AVE-SESAME II conducted on April 19-20, 1979. NASA Tech. Mem., NASA TM-78280.

Yamamoto, G., 1952: On a radiation chart. Sci. Rept., Tohoku Univ. 3.5 Geophysics, v. 4, pp. 9-23.

Zeman, O, 1975: The dynamics of entrainment in the planetary boundary layer: A study in turbulence modeling and parameterization. Ph.D. Thesis, Penn. State Univ.

Zeman, O, and H. Tennekes, 1977: Parameterization of the turbulent energy budget at the top of the daytime atmospheric boundary layer. J. Atmos. Sci., v. 34, pp. 111-123.

Zilitinkevich, S.S., 1975: Comment on "A model for the dynamics of the inversion above a convective boundary layer". J. Atmos. Sci., v. 32, pp. 991-992.

# ACKNOWLEDGEMENTS

There are many people who have contributed to the research leading to this thesis, as well as the actual preparation of the thesis itself. Firstly, I thank my wife, Beverly, for supporting our family and me, both financially and emotionally throughout this four year project. Without that support, the work would have been impossible.

Secondly, I must thank Professor Sanders for providing the grant money which supported me for so long. I benefitted greatly from the many conferences to which Professor Sanders provided the funds for travel. I am also grateful to my Thesis Committee and to Jane McNabb, for helping me finish at the last possible moment before the end of the first term of 1982-1983.

Thirdly, I express my appreciation to the inhabitants of the 16th Floor for an enjoyable and rewarding residence in Building 54. I especially thank Brad Colman for his friendship, support and companionship.

Finally, I am grateful to Don Grantham of AFGL who allowed me to begin post-doctoral research at AFGL while I finished my thesis at MIT.